

NORTHWESTERN UNIVERSITY

Investigation of Muscle Synergies as a Control Paradigm for Myoelectric Devices

A DISSERTATION

SUBMITTED TO THE GRADUATE SCHOOL
IN PARTIAL FULFILLMENT OF THE REQUIREMENTS

for the degree

DOCTOR OF PHILOSOPHY

Field of Biomedical Engineering

By

Abidemi Bolu Ajiboye

EVANSTON, ILLINOIS

December 2007

Abstract

Investigation of Muscle Synergies as a Control Paradigm for Myoelectric Devices

Abidemi Bolu Ajiboye

A need exists to increase the functionality of myoelectric prostheses without increasing the mental requirement of operation. Implantable myoelectric sensors have made it possible to record multiple muscle activities with high fidelity. Given this high dimensionality of inputs, what is the best way of implementing control? Muscle synergies have been proposed for coordinating the many degrees-of-freedom (DOF) of the neuromotor system. This work aimed to investigate synergies as a viable control paradigm for multi-DOF myoelectric devices with regard to the properties of robustness, scalability, and volitional activation.

First, this work investigated if muscle synergies formed a predictive basis set for muscle coordination patterns associated with a variety of hand postures. Subjects mimed hand postures of the American Sign Language alphabet while electromyographic (EMG) activity was recorded from hand muscles. Non-negative matrix factorization (NMF) showed that a small number of hand postures could establish a robust set of synergies for predicting the EMG patterns of a variety of hand postures.

Second, this work investigated the scaling of muscle synergies in hand grasping at sub-maximal force levels. Subjects performed a force-tracking task using different grasps while EMG was recorded. Statistical and NMF analyses showed that the primary synergies of grasping retained their structures and scaled linearly with grasp force.

Third, this work investigated, through a virtual target reaching task, the volitional control of multiple DOFs using muscle synergies versus single-muscle inputs. It was hypothesized that

users could more intuitively achieve independent and simultaneous control of myoelectric inputs using muscle synergies over single-muscle activations. The results showed that while users were able to independently and simultaneously modulate synergy activations, this control paradigm was statistically no better than one based upon single-muscle inputs.

From these investigations, it is concluded that while muscle synergies exhibit useful properties for control such as robustness, generalizability, and scaling, their practical benefit in a volitional control task is not significantly greater than a single-muscle control paradigm. Results from these investigations also suggest that the method of control implemented by the neuromotor system is not bound by muscle synergies, but rather by a combination of both synergy and single-muscle activations.

Acknowledgements

I want to thank the many people who have in one form or another contributed to my successful completion of the research and writing of this dissertation. I thank my advisor, Dr. Richard Weir, for the many years that he intellectually and personally invested in my development as a researcher and thinker. I am especially grateful for the many times where he saw my open frustrations and “flag pole” moments, and was able to offer helpful insights and directions, even if I didn’t fully appreciate it at the time. He was a tremendous help, and I (and my parents) sincerely thank him. Also, I thank my committee members (Drs. Lee Miller, Sandro Mussa-Ivaldi, Eric Perreault, and Matthew Tresch) for their many ideas and tough questions that made my work much better than what it would have been, were it left to only me. Learning how to answer their many questions and concerns made it much easier for me to be able to find a job, so I am especially grateful. Thank you to all the students and faculty who have over the years shaped my thinking as a scientist and engineer, both practically and philosophically. Special thanks to Todd Farrell and Jon Sensinger, who along with myself, were Dr. Weir’s first doctoral graduate students and who traded ideas back and forth with me on a day-to-day basis. I also thank my many research subjects who were willing to allow me to perform many long and uncomfortable and sometimes painful (but IRB approved) experiments on them, all while maintaining a positive demeanor. They definitely earned their stipends.

I thank my family and friends for their many prayers and support over the years. I thank my parents, Abel and Mary Ajiboye, for their many phone calls and prayers and words of encouragements through the very end of my tenure. Of course, without them I could not be where I am today. I am grateful to them both more than words can express. This doctoral degree is as much theirs as it is mine.

Thank you to the many friends I made while here in Chicago. Thank you specifically for just walking through this phase of life with me, for your faithful encouragements, for the many times of laughter that we had, and for the many hours of unproductive (research-wise) but much needed downtimes. BJ, Jon, Devjani, Lissette, Kiki, Pinata, Gina, Lexyne, Rebecca, Bonnie, Kerice, Andy, Sarah, Todd, James, Venn, Vik, David and Monica, Steve, Carolina and Marcin, and countless others – you are much appreciated.

Finally and most importantly, thank you God. You walked with and sometimes carried me through this chapter of my life. Thank you for surrounding me with friends who were spiritually and emotionally supportive. I'm grateful for the opportunity to have studied amongst some of the best scientists and engineers in this field. I'm grateful for the opportunity and mental capacity to have studied and understood a small piece of your world, and to see your wisdom and purposefulness in all of its complexity.

This work was supported in parts by the National Institute of Health (NIH) Ruth L. Kirchstein Pre-Doctoral National Research Service Award (NRSA) 1 F31 HD49319, and by the National Institute of Health through NIBIB/NICHD Centers under Grant 1 R01 EB01672. Opinions contained in this publication are those of the grantees and do not necessarily reflect those of the NIH.

Contents

Acknowledgements.....	5
List of Figures	12
List of Tables	15
1 Introduction	17
1.1 General Framework.....	17
1.2 Motivation.....	17
1.3 Specific Aims and Hypotheses	21
1.3.1 Aim 1. Muscle Synergies as a Predictive Framework for EMG Patterns of Static Hand Postures.....	21
1.3.2 Aim 2. Muscle Synergies Exhibit Scalability with Increasing Grasp Force.....	23
1.3.3 Aim 3. Independent and Simultaneous Volitional Control of Muscle Synergies	24
1.4 Manuscript Organization.....	26
2 General Background	28
2.1 Introduction.....	28
2.2 Brief History of Pattern Recognition Paradigms for Multifunctional EMG Control	28
2.3 Neuromotor Coordination of Movement through Primitives.....	35
2.3.1 Motor Coordination Investigations involving Cortical Mapping.....	36
2.3.2 Motor Coordination Investigations involving Joint Kinetics and Kinematics	43
2.3.3 Motor Coordination Investigations involving Muscle Synergies	51
2.4 Muscle Synergies as Testable Hypotheses	58
2.5 Conclusion.....	59
3 The Muscle Synergy Model and Parameter Estimation	60

	8
3.1	Introduction.....60
3.2	The Muscle Synergy Model61
3.2.1	General Description61
3.2.2	Estimating the Unknown Parameters64
3.3	Estimating Muscle Synergies: NMF Simulation Analysis.....73
3.3.1	Objective.....73
3.3.2	Methods.....74
3.3.3	Results77
3.3.4	Discussion98
4	Muscle Synergies as a Predictive Framework for EMG Patterns of Static Hand Postures102
4.1	Introduction.....102
4.2	Methods.....105
4.2.1	Subject Information.....105
4.2.2	Electromyography.....106
4.2.3	Tasks and Data Collection110
4.2.4	Data Analysis.....112
4.3	Results119
4.3.1	EMG Pattern Separability and Repeatability – Discriminant Analysis.....119
4.3.2	Descriptive Synergy Analysis.....121
4.3.3	Predictive Synergy Analysis.....125
4.4	Discussion140
4.4.1	Predictive Power of Muscle Synergies140
4.4.2	Structure of Muscle Synergies142
4.4.3	Robustness of Muscle Synergies143

4.4.4	What is the “Correct” Number of Synergies?.....	143
4.4.5	Implications for Myoelectric Control	146
4.5	Conclusion.....	146
5	Muscle Synergies Exhibit Scalability with Increasing Grasp Force	148
5.1	Introduction.....	148
5.2	Methods.....	151
5.2.1	Subject Information.....	151
5.2.2	Maximal Voluntary Grasp Strength	151
5.2.3	Electromyography.....	153
5.2.4	Tasks and Data Collection	154
5.2.5	Data Analysis.....	155
5.3	Results	160
5.3.1	Effect of Fine-Wire Electrodes on Maximal Voluntary Grasp (MVG) Strength	160
5.3.2	Correlation of CP Vector Magnitude to Grasp Force	161
5.3.3	Variance of CP Vector Direction wrt Grasp Force	161
5.3.4	Activations of Muscle Synergies wrt to Grasp Force	162
5.4	Discussion	167
5.4.1	Main Findings	167
5.4.2	Scaling of Activation Coefficients	168
5.4.3	Implications for Myoelectric Control	170
5.5	Conclusion.....	171
6	Independent and Simultaneous Volitional Control of Muscle Synergies.....	172
6.1	Introduction.....	172
6.2	Methods.....	174

	10
6.2.1 Subject Information.....	174
6.2.2 Electromyography.....	175
6.2.3 Tasks and Data Collection	175
6.2.4 Data Analysis.....	182
6.3 Results	186
6.3.1 Individuated Muscles and Estimated Synergies for Control.....	186
6.3.2 Independent Control of a Single DOF	189
6.3.3 Simultaneous Control of Two DOFs.....	194
6.4 Discussion	199
6.5 Conclusion.....	203
7 Conclusions.....	205
7.1 Review of Investigations	206
7.1.1 Muscle Synergies as a Predictive Framework for EMG Patterns of Static Hand Postures.....	206
7.1.2 Muscle Synergies Exhibit Scalability with Increasing Grasp Force.....	207
7.1.3 Independent and Simultaneous Volitional Control of Muscle Synergies	208
7.2 General Conclusions	210
References	211
Appendix A: Muscle Synergy Scalability in Palmar and Tip Hand Grasps	221
Results.....	221
Effect of Fine-Wire Electrodes on Maximal Voluntary Grasp (MVG) Strength.....	221
Correlation of CP Vector Magnitude to Grasp Force.....	222
Variance of CP Vector Direction wrt Grasp Force.....	222
Activations of Muscle Synergies wrt to Grasp Force	223

	11
Discussion	227
Curriculum Vitae	221

Figures

Figure 2.1. Schematic of standard two-site myoelectric prosthesis control.	30
Figure 2.2. Results of neuro-stimulation experiments of (Penfield & Boldrey, 1937).....	38
Figure 2.3. CFFs in spinalized frogs (Bizzi, D'Avella, Saltiel & Tresch, 2002).....	44
Figure 2.4. PCs of Static Hand Postures (Santello et al., 1998).	49
Figure 2.5. Muscle synergies in the EMG response of the frog leg (Tresch et al., 1999).	53
Figure 3.1. Nodal Representation of Muscle Synergy Model	64
Figure 3.2. PCA Sample Data Set and Principal Component (PC) Vectors	68
Figure 3.3. Joint Distributions of ICs and Orthogonal Mixtures	71
Figure 3.4. Effects of varying the number of basis vectors and of using random basis vectors.	80
Figure 3.5. Efficacy of NMF at 25% noise corruption.....	81
Figure 3.6. Original and estimated synergies and sources at 25% noise corruption.	82
Figure 3.7. Effect of noise on NMF estimation of original synergies (i) and sources (ii).	84
Figure 3.8. Effect of noise on NMF estimation of noisy (i) and uncorrupted (ii) data variances.	85
Figure 3.9. NMF behavior on data matrices <i>not</i> constructed using a synergy paradigm.	87
Figure 3.10. Explained variance underestimation results.	90
Figure 3.11. Synergy similarity underestimation results.....	91
Figure 3.12. Source similarity underestimation results.	92
Figure 3.13. Explained variance overestimation results.....	95
Figure 3.14. Synergy similarity overestimation results.....	96
Figure 3.15. Source similarity overestimation results.....	97
Figure 4.1. Electromyography protocol.....	109
Figure 4.2. Mimed letters and numbers of the American Sign Language (ASL) set.	111

Figure 4.3. Sample of recorded EMG signals during miming of ASL postures.....	113
Figure 4.4. Flow chart of descriptive (left) and predictive (right) synergy analyses.	116
Figure 4.5. Representative discriminance matrix for miming of ASL letters and numbers.....	120
Figure 4.6. Complete and cross-validated discriminance percentages for all subjects.....	121
Figure 4.7. Explained variance curve derived from descriptive NMF analysis.	123
Figure 4.8. Variance explained by synergy estimates (all subjects).....	124
Figure 4.9. Recorded EMG patterns vs those estimated by the descriptive NMF model.....	125
Figure 4.10. Explained variance (EV) curves from the predictive synergy analysis.	127
Figure 4.11. Composite results for predictive NMF analysis for one subject.....	128
Figure 4.12. Composite results for predictive NMF analysis for remaining subject population.	129
Figure 4.13. Synergy robustness across 20 random combinations of predictor postures.	131
Figure 4.14. Synergy robustness plots for remaining subject population.	132
Figure 4.15. Synergy robustness across increasing number of predictor postures (1 subject).	134
Figure 4.16. Synergy robustness across increasing number of predictor postures.	135
Figure 4.17. Estimated synergies for each subject (I).....	137
Figure 4.18. Estimated synergies for each subject (II).....	138
Figure 4.19. Estimated synergies for each subject (III).....	139
Figure 4.20. Structure of synergies wrt method of determining control space dimension.....	145
Figure 5.1. Instrumented gauges for grasp force measurements.	153
Figure 5.2. Hand postures and force-tracking task.	155
Figure 5.3. Synergy structures and activation levels for a representative subject.	163
Figure 5.4. Population averaged explained variances of synergies for ASL and force-tracking.	165
Figure 5.5. Population averaged correlations of synergy activations to exerted grasp force. ...	166

Figure 6.1. Four degree-of-freedom field for virtual target reaching task.	179
Figure 6.2. Calculation of linearity error for a given path.	184
Figure 6.3. Individuated muscles and estimated synergies for a representative subject.	188
Figure 6.4. Variance explained by SMP and BSP control methods.	189
Figure 6.5. Average paths of single target activation for a representative subject.	190
Figure 6.6. Error and inefficiency measures for all subjects during individual DOF control.	193
Figure 6.7. Average paths of simultaneous DOF activation for a representative subject.	195
Figure 6.8. Error and inefficiency measures for all subjects during simultaneous DOFs control.	198
Figure 6.9. PLE calculations for perfect simultaneous control and perfect sequential control.	199
Figure A.1. Synergy structures and activation levels for a representative subject.....	224
Figure A.2. Population averaged explained variances of synergies for ASL and force-tracking.	226
Figure A.3. Correlation of synergy activation to exerted grasp force.....	227

Tables

Table 3.1. PCA Sample Data Set.....	67
Table 3.2. One way ANOVA of underestimate simulation results.	93
Table 3.3. One way ANOVA of overestimate simulation results.	98
Table 4.1. Recorded Intrinsic and Extrinsic Muscles of the Hand	108
Table 4.2. Structures of synergies global to the subject population.	139
Table 5.1. Effect of Fine-Wire Electrodes on MVG Strength: Paired T-test Analysis	160

- For Abel, Mary, Bunmi, Seun, Solape, and Grandma Ajiboye



NORTHWESTERN
UNIVERSITY

"Finally, brethren, whatsoever things are true, whatsoever things are honest, whatsoever things are just, whatsoever things are pure, whatsoever things are lovely, whatsoever things are of good report; if there be any virtue, and if there be any praise, think on these things."

Philippians 4:8 – Northwestern University Motto

1 Introduction

1.1 *General Framework*

This manuscript describes the author's investigations of the use of neuromuscular synergies as a potential paradigm for the control of multi-degree-of-freedom (DOF) myoelectric devices. Neuromuscular synergies have been proposed as groups of muscles whose activity levels are neurally coupled and form the basis vectors of complex muscle coordination patterns. Specifically, this work aimed to discover if neuromuscular synergies form a predictive framework for the variety of electromyographic (EMG) patterns observed during the formation of a wide range of hand postures. Secondly, this work aimed to discover if the EMG patterns and synergies underlying multi-digit hand grasping are linearly scaled variants of single characteristic vectors, relative to grasping force level. Finally, this work aimed to investigate the advantages of a neuromuscular synergy based paradigm for real-time control of multi-DOF myoelectric devices. Such a paradigm may be more successful and intuitive for controlling myoelectric devices than the currently implemented single-muscle-based paradigm because it potentially takes advantage of knowledge of the pre-existing neurally coded muscle groupings.

1.2 *Motivation*

As a primary motivation, there is a growing need to add functionality to current commercially available myoelectric prostheses without increasing the mental burden placed on the user. As the number of controllable functions / degrees-of-freedom (DOFs) is increased, the issue of control becomes very significant. This is true particularly in light of the goals of minimizing the

mental burden placed on the user and maximizing the intuitive nature of the control. The current standard paradigm of control in myoelectric systems is to perform a one-to-one mapping (single-input-single-output, or SISO) of each myoelectric input site to each controlled function / DOF. For example, in standard two-site myoelectric prostheses, the electromyographic (EMG) activity from the wrist flexors and extensors are mapped to the closing and opening of the hand, respectively. With the current development of implantable myoelectric sensors, it is now possible to faithfully record focal signals from multiple muscles with high fidelity. Thus the possibilities of controlling a multi-DOF device are potentially increased. Extrapolating this one-to-one mapping control paradigm to a device with multiple controllable DOFs would then require a single myoelectric input site to be tied to each controlled function. With a large number of functions, this would likely place a significant mental burden on the user and make overall control less natural and intuitive.

Current research into control paradigms for myoelectric prostheses has recently focused efforts on investigating pattern recognition algorithms which map individual functions and DOFs to the composite EMG activity pattern observed from all myoelectric input sites. Indeed, some of the author's previous research efforts are within this school of thought (Ajiboye, 2003, Ajiboye & Weir, 2005). The majority of these algorithms focus on extracting multiple parameters from a minimal set of myoelectric input sites and/or characterizing the multiple EMG patterns associated with each controlled function. Such paradigms are advantageous over SISO control methodologies because they minimize the number of required input electrodes and do not require the user to possess conscious individuated control over each myoelectric site. This is a step in the direction of increasing the possibility of intuitive and natural control. However, these control paradigms are limited in that all recognizable EMG patterns must be programmed *a priori*. The addition of new hand postures would require the associated EMG patterns to be

hard-coded into the control system. Thus users would be required to remember as many EMG patterns as there are DOFs to be controlled. This problem would become more pronounced as the number of patterns grows.

The question must be asked of what constitutes natural control of the hand. More specifically, what is the natural way that the intact neuromotor system coordinates the many muscular DOFs to produce the observed postural patterns of the hand? Studies in anatomy, cortical recordings, and other fields have confirmed that the neuromotor system does not exclusively, or possibly even primarily, operate based on a SISO paradigm. Because there are more muscles than controlled joints of the hand, this control problem has been termed “ill-posed”. This is the mathematical equivalent of a system of equations with more variables than equations – there exists an infinite number of solutions unless more constraints are added to the system. Studies of muscle activities during arm reaching, postural standing and perturbations, locomotion, and various reflexes have theorized an additional constraint, namely that muscles are partially grouped together in such a way to constrain their mutual levels of activation. Hence, control becomes modular and is dimensionally reduced. More complex muscle activation patterns are built on these bases of muscle groupings. It is generally agreed that these muscle groupings, termed synergies, are a real phenomenon on some level. What are generally not agreed upon are the compositions and mechanisms of these muscle synergies. It is beyond the scope of this document to attempt to answer this debate fully. This research, however, aims to better understand how knowledge of these natural groupings of muscles can be advantageous in a control paradigm for multifunctional myoelectric prostheses, and specifically how well the muscle synergy model can serve as an EMG recognition algorithm for multiple hand grasp postures. The idea of using muscle synergies as a myoelectric control paradigm has been moderately visited in the past, although in slightly different forms (Finley, Wirta & Cody, 1968,

Taylor & Finley, 1971). The common thread between previous research and this current work is that a control paradigm based upon normal subconscious patterns of synergistic muscle activity would result in prosthesis functions that both appear and are perceived as natural, with little necessary conscious attention from users.

As a secondary motivation, there is a need to better understand the properties of muscle synergies with regard to motor coordination. Namely, if muscle synergies are in fact basic building blocks of more complex muscle patterns, then they should exhibit certain properties. Three of these properties are **low lability**, **scalability**, and **spatial coherence** (Lee, 1984). **Low lability** means that the basis set of muscle synergies is robust and generalizable to different environmental and task conditions. **Scalability** means that the individual muscle activation elements within a synergy should retain the same relative proportion levels with increased activation of the synergy i.e. the structure remains invariant. **Spatial coherence** means that each synergy is driven as a unit, based on an “all-or-none” philosophy. This work investigates these three properties of muscle synergies within the framework of myoelectric control. With regard to low lability, this work examines whether a small set of muscle synergies describing a small set of hand postures is robust and generalizable enough to predict the EMG patterns associated with a wide variety of completely new hand postures. With regard to scalability, this work examines if the muscle coordination patterns and muscle synergies associated with static hand grasp patterns are structurally invariant to grasp force level. Finally, with regard to spatial coherence, this work examines if muscle synergies can be volitionally activated independently and simultaneously as individual units for myoelectric control (i.e. voluntary spatial coherence).

To these ends, the specific aims of the research are as follows.

1.3 Specific Aims and Hypotheses

1.3.1 Aim 1. Muscle Synergies as a Predictive Framework for EMG Patterns of Static Hand Postures

Many investigations have shown muscle synergies to be a viable means of reducing the dimensionality of the muscle coordination problem in motor control. This has been done by demonstrating that a small number of synergies can describe a large percentage of the EMG pattern variability exhibited both within a task and across several tasks. The success of muscle synergies in previous investigations is important, yet inconclusive in that it is not clear if the results reveal information about the control paradigm of the neuromotor system, or only describe characteristics of the observed data. A more powerful assessment of muscle synergies would be to investigate their predictive power with regard to new tasks. Thus, this work investigates whether muscle synergies form a robust lower dimensional *predictive* framework for the EMG patterns of new hand grasp postures. More specifically, this work will answer the following questions.

- How many synergies are needed to complete this lower dimensional predictive framework, and how robust are these synergies?
- How many hand postures are needed to define the muscle synergy set of this framework?
- What is the predictive power of the established framework?

Research participants are instructed to shape the hand into 33 hand grasp postures comprising the static letters and numbers of the American Sign Language (ASL) alphabet while EMG activity is recorded from intrinsic and extrinsic hand muscles. Synergies are determined using a subset of these postures and used to predict the EMG patterns from the unused hand postures.

Working Hypothesis: A reduced set of muscle synergies describing a small set of hand postures can predict the EMG patterns from a wide variety of new hand postures with comparable accuracy.

Alternative Hypothesis: The EMG patterns of new hand postures cannot be accurately predicted using the framework defined by the generative hand posture set. The number of synergies needed to predict new hand postures exponentially grows with an increase in the size of the predicted set.

Implications: Successful prediction of the EMG patterns of new hand postures would suggest that the neuromotor control system possibly uses a system of finite muscle synergies to coordinate the many muscular DOFs associated with control of the hand. Rejection of the working hypothesis, and acceptance of the alternative hypothesis, would suggest that the neuromotor system does not organize and combine synergistic groups as described by the muscle synergy model. Alternatively, each grasp posture may require its own set of synergies for construction, and the total number of synergies may be more than the number of muscles. From the perspective of myoelectric control, acceptance of the working hypothesis would offer the possibility that new untrained movements and positions of the terminal hand device could be constructed through independently and simultaneously controlling combinations of these basis muscle synergies. In contrast, acceptance of the alternative hypothesis would suggest that a control paradigm based upon muscle synergies is not suitable for multifunctional myoelectric control.

1.3.2 Aim 2. Muscle Synergies Exhibit Scalability with Increasing Grasp Force

Redundancy in the neuromotor system potentially allows for multiple modalities of muscle coordination to produce sub-maximal multi-digit hand grasp forces. Hence, the relative proportions of muscle activations could potentially change with different conditions of grasping force level. There are differing views in the literature concerning the paradigm that the neuromotor system uses for muscle coordination to accomplish control of forces in these multi-digit hand grasps. This investigation examines whether the muscle coordination patterns (CPs) used to produce grasps of sub-maximal forces are force-invariant linear scalings of characteristic EMG pattern vectors. The investigation also examines if a simple linear scaling of the associated basis sets of muscle synergies can account for the muscle activities of grasping at varying force levels, or if different synergies are employed at different force levels. Research participants are instructed to perform a force tracking task in which they use power and precision hand grasp patterns to produce the specified force level while EMG activity is recorded from intrinsic and extrinsic hand muscles. The structure and magnitudes of the observed EMG patterns are compared across force levels, as well as the underlying synergy structures.

Working Hypothesis: The muscle coordination patterns (CP) used to produce the same multi-digit grasp at varying isometric grasp force levels are statistically linearly scaled versions of a single characteristic vector. Furthermore, the activation levels of the underlying muscle synergies scale linearly with grasp force.

Alternative Hypothesis: Statistically different muscle coordination strategies are used to produce the same multi-joint grasp pattern at varying isometric force levels. The activation levels of the underlying synergy structure do not linearly scale with grasp force.

Implications: Acceptance of the null hypothesis would imply that the EMG patterns associated with different force levels of grasping are structurally the same and differ only by linear scaling. Furthermore, the scaling of a set of muscle synergies is sufficient for describing grasping at sub-maximal force levels. Rejection of the null hypothesis would suggest that the different force requirements of grasping cause a change in the muscle coordination strategy implemented by the neuromotor system, and hence the aggregate EMG patterns are not simply the result of linearly scaling a fixed set of muscle synergies. From the perspective of myoelectric control, acceptance of the null hypothesis of EMG pattern scalability would imply that muscle synergies could be implemented within a proportional control paradigm, where the scaled activation levels could be used as modulators of functional speed.

1.3.3 Aim 3. Independent and Simultaneous Volitional Control of Muscle Synergies

This investigation aims to address the issue of spatial coherence of muscle synergies. This study examines if muscle synergies can be volitionally activated independently and simultaneously for the purposes of multi-DOF myoelectric control, and specifically with comparison to a single-muscle activation control scheme. Research participants perform a virtual reaching task in a four degree-of-freedom coordinate field, where the positive and negative axes represent the activation levels of four decoupled subject-specific muscle synergies or individual muscles. Participants are instructed to navigate as quickly as possible to

targets within this coordinate field using the instructed synergies or muscles, while attempting to minimize the activities of the undesired synergies and muscles. Subjects perform the same tasks with the addition of a mental load to assess the intuitiveness of each paradigm. Movement error, movement path, and average null space activity are the metrics employed to assess the participants' successes in navigating the synergy and non-synergy fields.

Working Hypothesis: Research participants will be able to demonstrate volitional independent and simultaneous control of muscle synergies. This will be evidenced by higher levels of movement accuracy, path linearity, and less null space activity of the synergy field paradigm than in the non-synergy (i.e. individuated muscle) field paradigm. Furthermore, control using the synergy-based paradigm will be more intuitive than the non-synergy based paradigm due to the natural grouping of muscles by the neuromotor system.

Alternative Hypothesis: Research participants will not be able to volitionally control muscle synergies independently and/or simultaneously for targeting in a four-dimensional environment. The levels of path linearity, effect of mental loading, and null space activity in the synergy field will be statistically indistinguishable from the non-synergy field.

Implications: The ability of research participants to successfully learn to navigate to targets in the synergy field with would suggest that muscle synergies could ultimately be used as a paradigm for myoelectric control. Specifically, each muscle synergy group could be tied to a controlled DOF, and the user would be able to proportionally manipulate that particular DOF independently and/or simultaneously with other DOFs. The inability to navigate the four dimensional field using synergies would ultimately suggest that users cannot volitionally control these groups, and therefore cannot use them within a control paradigm for multi-DOF myoelectric devices. Furthermore, the comparative success of a synergy-based control

paradigm relative to a single-muscle control paradigm would suggest which paradigm is more likely used by the neuromotor system in the muscle coordination of volitional hand movements.

1.4 Manuscript Organization

Chapter 2 (General Background) gives a brief history of the different methodologies of control proposed for myoelectric devices. Also described is background on current literature in the area of motor control that gives philosophical and physiological evidence for the central motor system implementing a synergy-based control for muscle coordination.

Chapter 3 (The Muscle Synergy Model and Parameter Estimation) conceptually and mathematically describes the muscle synergy model. Current literature is presented on how the model parameters are estimated, including a discussion on the inherent assumptions of each estimation technique. Finally, a simulation study of the estimation of the muscle synergy component model parameters, using non-negative matrix factorization (NMF), under varying conditions of noise and over- and underestimation, is presented.

Chapter 4 (Muscle Synergies as a Predictive Framework for EMG Patterns of Static Hand Postures) describes work investigating whether the muscle synergies associated with a small set of hand postures can predict the EMG patterns associated with a wide variety of new hand postures. Much of the current literature has used muscle synergies as a descriptive framework, but few have addressed the issue of predictability and generalizability. This work addresses the first aim, namely the robustness and generalizability of muscle synergies for constructing new hand postures.

Chapter 5 (Muscle Synergies Exhibit Scalability with Increasing Grasp Force) describes work investigating the relationship between muscle coordination strategies and grasp force during multi-joint hand grasping. While some investigations have addressed the issue of global

pattern scaling with respect to precision grasp force, none to the investigator's knowledge have investigated how muscle synergies alter with respect to changes in grasp force of the whole hand. This work addresses the second aim, namely the scalability of muscle synergies.

Chapter 6 (Independent and Simultaneous Volitional Control of Muscle Synergies) describes work investigating if muscle synergies can be volitionally controlled simultaneously and independently for the purposes of myoelectric control. The results of subjects' abilities to reach targets in a four-dimensional synergy field, compared to a non-synergy field, are presented. This work addresses the third aim, namely volitional spatial coherence of muscle synergies.

Chapter 7 (Conclusions) summarizes the findings described in the overall manuscript, and gives direction towards investigations to further augment the findings of this work.

2 General Background

2.1 Introduction

Current commercially available trans-radial myoelectric prostheses are typically controlled by a two-site single-input-single-output (SISO) paradigm for operating a single degree-of-freedom (DOF). The activity of one agonist-antagonist muscle pair, such as the finger flexors (flexor digitorum superficialis) and extensors (extensor digitorum communis) is tied to the control of one motion, such as hand closing and opening. As the number of operable DOFs and functions increases, this SISO control paradigm potentially becomes a limiting factor of control. Extensive research in both the fields of myoelectric control and neuromotor control have aimed to improve upon SISO control algorithms by better understanding how multiple-muscle coordination is achieved by the neuromotor system, and by developing myoelectric pattern recognition and control algorithms that take advantage of patterns of muscle coordination. This chapter presents a review of literature in the fields of myoelectric and neuromotor control concerning the issue of multiple-muscle coordination.

2.2 Brief History of Pattern Recognition Paradigms for Multifunctional EMG Control

The first myoelectric prosthesis was developed by Reinhold Reiter in the 1940s (Reiter, 1948), although popular use in the clinical and commercial environments did not occur until the 1970s. Because the myoelectric signal is a physiologically relevant parameter whose amplitude is monotonically related to the strength of muscle contraction, it can be used as a stable control input for prosthetic control. Most current commercially available myoelectric prostheses

implement two-site control and are single DOF in nature, as shown in Figure 2.1. These two sites are tied to the activities of agonist-antagonist pairs of muscles, and the muscle with the greater activity is usually that which determines the actuated function of the prosthesis. While two-site control has proven successful, this control paradigm is potentially limited when extended to prostheses with multiple controllable functions and DOFs, due to the difficulty of controlling multiple muscles independently of each other. Several different control paradigms, based upon extraction of signal parameters to recognize global myoelectric patterns, have been proposed to address this problem of control of multifunctional prostheses.

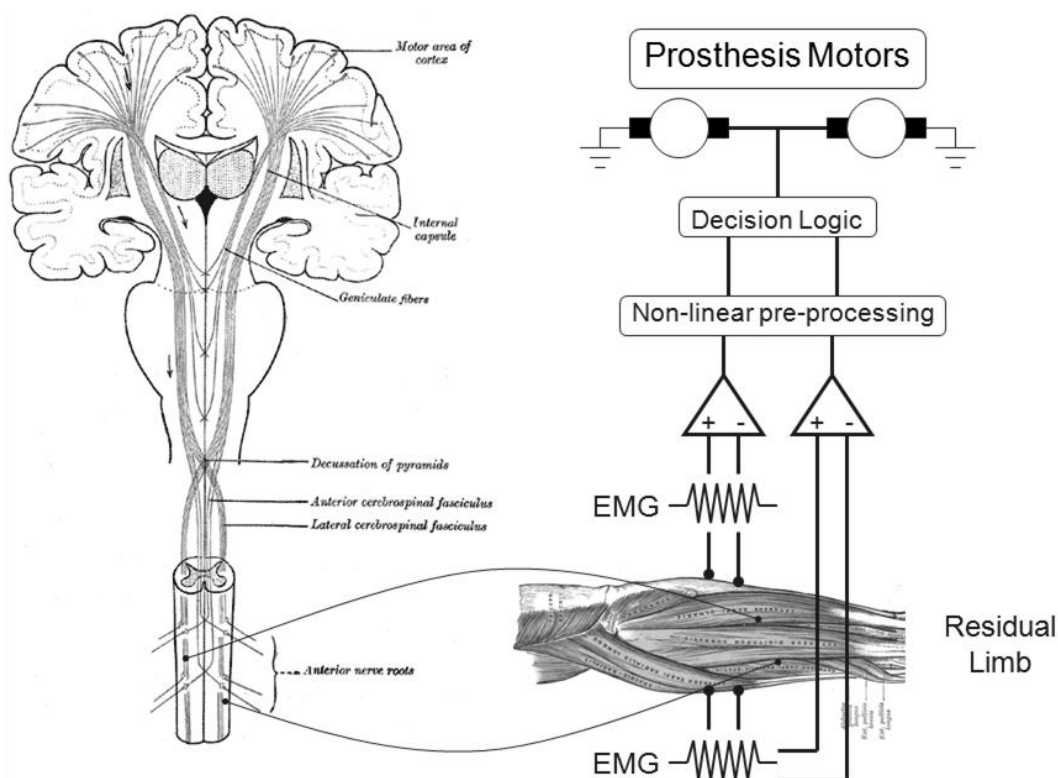


Figure 2.1. Schematic of standard two-site myoelectric prosthesis control.

Efferent signal from the central nervous system cause muscle contractions, which result in electrical activity as a byproduct. This electrical activity (EMG) can be detecting using surface or indwelling electrodes. Standard two-site myoelectric control differentially records EMG from agonist-antagonist pairs and then finds the signal envelope using non-linear techniques such as rectification of root-mean-square. A decision is made on which function the user is attempting to control, and the appropriate motors are driven. In standard two-site control, the decision logic block can be differential, in which the difference in activity drives the appropriate motor, all-or-none in which the most active muscle fully drives the appropriate motor, or a range of other possible decision paradigms.

One paradigm proposed for use in multifunctional myoelectric control has been to model each set of EMG signals associated with specific movements, using their autoregressive-moving-average (ARMA) coefficients (Box & Jenkins, 1970). The underlying hypothesis for these methods was that a repeatable reduced set of parameters (as compared to an infinite set of

possibilities for the signal patterns) characterizing a linear model of the signals would form a database where at least one parameter would be different for each desired motion. This method has been used to distinguish between the muscle coordination patterns associated with resting, loaded flexion of the elbow, and whole hand grasping (Graupe & Cline, 1975). However, the investigators admitted that the proposed paradigm of control would not lend itself to multifunctional simultaneous control. Any system trying to accomplish such would need knowledge of all possible combinations of motions and the associated ARMA coefficients to be effective. In addition, the proposed system was limited in the number of controllable functions it would be able to recognize. Other investigators have extended the work of Graupe & Cline, using more advanced ARMA based and spectral estimation models for discrimination of wrist movements (Doerschuk, Gustafson & Willsky, 1983) and the different articulations of the thumb (Farry, Walker & Baraniuk, 1996). While successful in their own rights, all suffer from the same deficiency in that all combination of degrees-of-freedom would have to first be parameterized to achieve full simultaneous control. The same would have to be done for any new movements to be recognized.

Other investigators have posited that multifunctional myoelectric control is best achieved by extracting large amounts of information from a small set of input signals. In a seminal paper, researchers at the University of New Brunswick suggested that extracting time domain features such as mean absolute value, mean absolute value slope, number of zero crossings, number of slope sign changes, and waveform length from the repeatable first deterministic 300 ms of a pair of EMG signals to operate four distinct classes of movement (Hudgins, Parker & Scott, 1993). Using a standard feed forward multilayer artificial neural network (ANN) for training through back propagation, the investigators were able to distinguish between four classes at a rate of $91.2 \pm 5.6\%$ for normal-limbed subjects and $85.5 \pm 9.8\%$ for amputee subjects. The

benefit of this system was that more functions could be controlled using a small number of myoelectric input sites. However, the work did not address the feasibility of extension of this method to simultaneous control of multifunctional prostheses. Still, other investigators have built upon this work, using these same features (Englehart & Hudgins, 2003), along with “majority voting” schemes, and wavelets as templates for the different muscle coordination patterns associated with movement, to produce continuous classification systems (Englehart, Hudgins & Parker, 2001). The main effort of these proposed paradigms has been to reduce the error rates of classification, rather than to explore control of simultaneous or novel movements.

Another class of paradigms that has been proposed for solving the multifunction control problem is a set of “soft-computing” based schemes such as fuzzy logic, various ANNs (Gallant, Morin & Peppard, 1998), and genetic algorithms (Farry, et al., 1997). Actually, many of these soft-algorithms in conjunction used the feature sets employed by Hudgins et al. Fuzzy logic and fuzzy data clustering based systems which attempt to understand features of muscle coordination in terms of linguistic variables have met varying degrees of success (Chan, et al., 2000, Hussein & Granat, 2002, Karlik, Tokhi & Alci, 2003, Micera, Sabatini, Dario & Rossi, 1999). In fact, much of the current investigator’s previous research was in the use of fuzzy logic systems for recognizing the muscle coordination patterns associated with movements of the wrist and fingers (Ajiboye, 2003, Ajiboye & Weir, 2005). This research reported classification of individual muscle coordination patterns between 94 – 99% for both static and dynamic movements. Again though, the use of such a system in the control of simultaneous and/or novel movements would require a large database of pre-programmed movement combinations.

More recent proposed algorithms for multifunctional myoelectric control have focused on decomposing time domain features of the muscle coordination patterns associated with different limb movements into unique sets of recognizable components. Of particular interest are some

of the efforts based upon Gaussian Mixture Models (GMMs) because they mathematically bear some similarity to the muscle synergy work described in this manuscript. Given a set of N discriminable movements, a set of GMMs $\{\lambda_1 \dots \lambda_N\}$ are constructed from the extracted features of the time series of the EMG patterns. The probability density function (PDF) $p(\vec{x}|\lambda_n)$ of a D -dimensional set of features \vec{x} for a specific movement can be represented by the linear weighted sum of M Gaussian density functions $p_i^n(\vec{x})$, as given in equation 2.1.

$$p(\vec{x} | \lambda_n) = \sum_{i=1}^M w_i^n p_i^n(\vec{x}) \quad (2.1)$$

M is the number of model components to be mixed, $p_i^n(\vec{x})$ is the i^{th} Gaussian density component of model n , and w_i^n is the non-negative weighting coefficient of each component, such that $\sum_{i=1}^M w_i^n = 1$. Each $p_i^n(\vec{x})$ can be thought of as a basis, or building block, Gaussian PDF of $p(\vec{x}|\lambda_n)$. Each $p_i^n(\vec{x})$ is simply a D -dimensional Gaussian function characterized by mean vector $\vec{\mu}_i^n$ and covariance matrix C_i^n , with the form given in equation 2.2. Each GMM is λ_n thus characterized by $\{w_i^n, \vec{\mu}_i^n, C_i^n\}$.

$$p_i^n(\vec{x}) = \frac{1}{(2\pi)^{D/2} |C_i^n|^{1/2}} \cdot \exp \left\{ -\frac{1}{2} \left(\vec{x} - \vec{\mu}_i^n \right)' (C_i^n)^{-1} \left(\vec{x} - \vec{\mu}_i^n \right) \right\} \quad (2.2)$$

Given a set of muscle coordination patterns for training, parameters for the set of GMMs can be estimated by expectation-maximization algorithms (Akaho & Kappen, 2000). Given a novel data stream and associated extracted time domain features \vec{x} , the mixture model λ_n which best models the new data vector is determined to be that of the most probable movement. Gaussian mixture models have shown success rates of up to 96% for distinguishing between six distinct classes of upper-limb movements, using either auto-regressive and/or time domain feature sets

for \vec{x} (Chan & Englehart, 2003, Huang, Englehart, Hudgins & Chan, 2005). While the GMM as implemented by these investigators still suffers from the limitation of having to develop a set of parameters for every conceivable set of simultaneous and/or novel movement, *it does point in the promising direction of viewing complex movements as built upon simpler sub-movements, which can be used as a basis for recognizing these more complex movements.*

All the efforts described briefly above have the underlying goal of trying to reduce the error rates of classification while increasing the number of movements to be classified. None of the proposed paradigms, however, address the issue of simultaneous control of multiple functions / DOF or of novel movements. The Gaussian mixture model approach does offer some promise because it regards the features of complex movements to be combinations of those of simpler movements, i.e. movement primitives. This hierarchical approach of using movement primitives for multifunctional myoelectric control has been previously suggested in literature, although not fully investigated. Engineers have reported success of control of the Utah/MIT Dextrous Hand (UMDH) using a programming language called HPL (Hand Programming Language) that describes hand manipulation tasks through functional motor primitives (Speeter, 1990). Control of hand tasks was successfully achieved through the concatenation and linear combination of these motor primitives. Although explicitly a robotic application, the success of the Utah/MIT Dextrous Hand in using motor primitives to control hand manipulation does suggest promise for myoelectric applications. Consequently, a better understanding of the control paradigms by which the central and peripheral nervous systems (CNS / PNS) perform muscle coordination through movement primitives may give insight into designing better prosthesis control algorithms.

Motor primitives can be thought of as bases functions or fundamental building blocks of movement that give a hierarchical structure to a particular system. This idea is quite evident

when one examines the structure of language. In linguistics, if sentences are thought of as signals to be transmitted, then words can be thought of as the primitives of language, with letters of the alphabet being units of individuated control. All communication is hierarchically built upon these language primitives. In the same way, biological systems may be organized in similar fashion, with the relationship between movement primitives and larger movements paralleling the relationship between letters and words and sentences. In the next section, literature in the area of motor control is reviewed that speaks to idea that muscle coordination for complex movements is based upon the combination of motor primitives.

2.3 Neuromotor Coordination of Movement through Primitives

Two major viewpoints have been held that attempt to explain how the central nervous system (CNS) controls and coordinates the many degrees-of-freedom of the neuromuscular system. The first viewpoint is based upon individuated motions and stresses the uncoupled control of individual joints and muscles to generate the necessary kinetics and kinematics of movement (Soechting & Lacquaniti, 1989). This viewpoint is largely based upon early work that involved cortical stimulation of the primary motor cortex (M1) area that seemed to indicate a point-to-point somatotopic mapping of hand control. This viewpoint is best illustrated by the homunculus (Penfield & Boldrey, 1937, Penfield & Rasmussen, 1950) and simiusculus (Woolsey, Erickson & Gilson, 1979, Woolsey, et al., 1952) diagrams, which have been considered to be textbook standards and are both seemingly characterized by a strict somatotopic organization of motor control. Researchers have recently argued against his viewpoint, stating that it does not account for the current body of evidence from neuro-stimulation experiments (Lemon, 1988, Schieber, 1990). The second viewpoint postulates that because of the inherent redundancies in the neuromuscular system, motor control is an “ill-posed” problem. As a result the neuromotor

system coordinates the many degree-of-freedom through the use of fundamental control primitives of movement to produce more complex movements (Bernstein, 1967, Bernstein, 1971, Sherrington, 1906). These fundamental control primitives would serve to both constrain the neuromotor system so that the problem of coordination would thus be well-defined, and serve to potentially increase the efficiency of control. In the following sections, the experimental evidence for and against movement primitives is reviewed from the areas of cortical stimulation, investigations into the coordination of joint kinematics and kinetics, and investigations of coordination of muscle patterns.

2.3.1 Motor Coordination Investigations involving Cortical Mapping

For years, the homunculus and simiusculus have been the textbook standard in the field of neuroscience in terms of their suggested mappings of the M1 motor cortex. These diagrams were the result of early cortical stimulations to the M1 area, and upon initial inspection, seemed to indicate a strict point-to-point somatotopic (discrete organization) mapping of the hand (Figure 2.2). It was thought that specific areas of the brain represented control of specific parts of the hand, and that these areas were both non-overlapping and organized to represent the anatomical medial to lateral progression of the controlled digits. The strictest homunculus diagram even suggested that the mediolateral ribbon of M1 served to divide control of the thumb and index finger from the middle, ring, and pinky fingers (Schieber, 2001). These diagrams initially led some researchers to believe a viewpoint of hand coordination that is based upon individuated control of joints and muscles. A more in-depth analysis of both Penfield & Boldrey's and Woolsey et. al's work shows that a strict point-to-point somatotopic map is not consistent with their independent results. For example, Figure 2.2(A) shows that control of the thumb and little finger, represented by Roman numerals I and V respectively, can be elicited

from both the medial and lateral sections of the cortex. Figure 2.2(B) shows even more explicitly the overlapping regions of the motor cortex that control various limbs and muscles. Woolsey's results in particular show that a single stimulation point could produce movement in several fingers of the hand. Hence, it seems that the hand is not somatotopically organized in the primary motor cortex area.

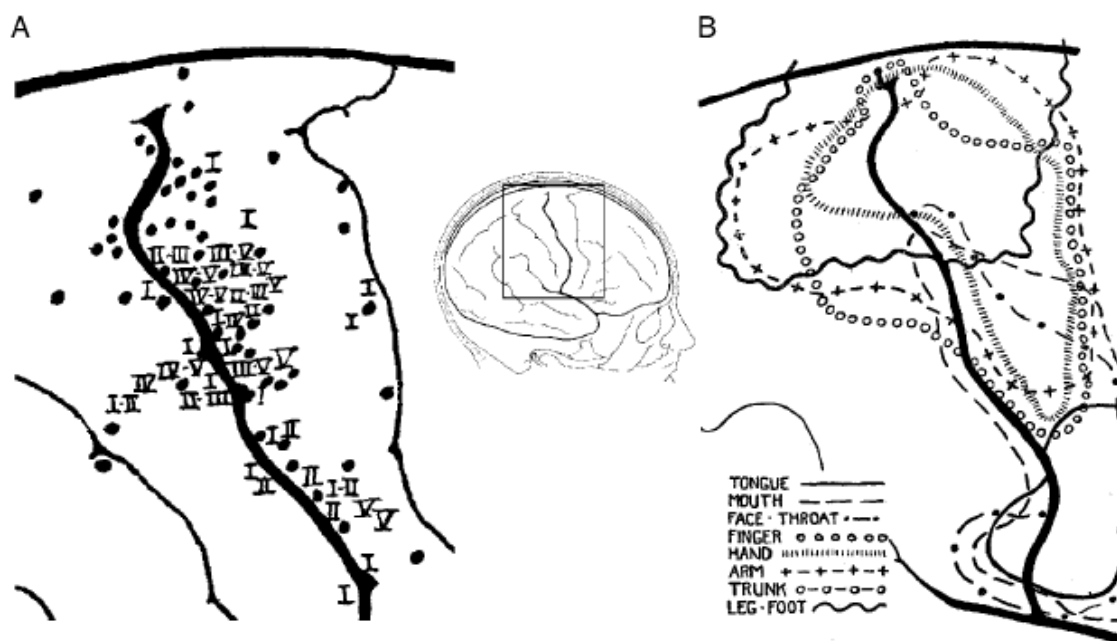


Figure 2.2. Results of neuro-stimulation experiments of (Penfield & Boldrey, 1937).

A) Roman numerals represent stimulation sites that elicited finger movements. Thumb through little finger are represented I – V, respectively. Black dots are stimulation sites that elicited movement from all digits. It can be observed that there are medial and lateral representations for both the thumb and little finger, in addition to several sites that controlled multiple fingers. The theory of a strict somatotopic (i.e. discrete organization) ordering of motor control is not consistent with these results. B) The outlines show the total areas where movements of fingers, entire hand, and proximal arm were elicited through neuro-stimulation. Observed is that there are not discrete areas. Instead, major overlap of areas is the prevailing trend, and suggests an alternative method to motor control, such as synergistic or pattern based, rather than individuated joint or muscle based control (Schieber, 2001).

It has been suggested that there are at least six major constraints on a strict somatotopic organization of the primary motor cortex (Schieber, 2001). First, an individual muscle seems to be controlled by convergent outputs to its spinal motoneuron pool from large territories of the M1 cortex. Second, the outputs of single neurons in the M1 cortex diverge to innervate motoneuron pools of multiple muscles. Third, horizontal interneuronal connections prevent

motor cortex sites from acting completely independent of each other. Fourth, a distributed activation pattern is observed when movement occurs at even one joint, and hence, the activation is not organized in anatomical order. Fifth, trauma induced or temporary inhibitor induced partial inactivation of the M1 area generally results in weakness of the overall hand instead of individual digits. Sixth, the observed plasticity of the cortical area during initial learning or rehabilitation learning implies that regions are not discretely hard coded to control specific joints or muscles. These physiological constraints seem to indicate that there is a limit to the potential somatotopic organization of hand control. Hence, the evidence seems to suggest a distributed organization of hand function. More recent investigations have been performed to demonstrate evidence to this end. Specifically, technological advancements in cortical stimulation, where more focal intracortical microstimulations in the M1 have been performed, have enabled more in-depth and accurate studies (Gould, Cusick, Pons & Kaas, 1986, Sato & Tanji, 1989) than those of Penfield & Boldrey and Woolsey et. al. The results have been consistent with an organizational map of limb control that shows evidence of significant overlap and little evidence of a strict somatotopic organization of M1.

Technological advances in neural recording techniques have also aided in understanding cortical organization. Studies have investigated individuated flexion and extension of the fingers and wrist in two rhesus monkeys while recording from individual M1 neurons. The authors reported that many neurons were related to multiple individuated movements, stressing the divergence constraint on somatotopic organization. Furthermore, reconstruction of the neuronal spatial distribution of the M1 hand area showed that active neurons for each individuated movement was over a large portion of the cortical area (Schieber & Hibbard, 1993). This stressed the convergence constraint on somatotopic organization. Also observed was that the spatial activation groups significantly overlapped between the thumb and medial and lateral

digits. A more recent study (Poliakov & Schieber, 1999) reported similar results. Specifically, the authors were investigating whether or not there was evidence for neuronal clustering during individuated finger movements of three rhesus monkeys, and whether or not these clusters were related to activation of specific muscle groups, movement involving specific joints, or other features of the movement. Using a cluster analysis technique, the authors reported that they observed little evidence that neurons clustered into functional subgroups based upon concrete or abstract features of movement. Hence, they concluded that control of individuated finger movements was more likely accomplished through the activation of a diverse population of neurons dispersed throughout the M1 area. Other researchers have performed similar studies of neuronal clustering and have found some evidence that the activity of neurons cluster into functional discrete groups, and that the activity of each group was correlated to the activity of a distinct group of muscles (i.e. muscle synergies), rather than individual muscles (Holdefer & Miller, 2002).

Investigations into motor cortex impairment induced either through an injury or a neural inhibitor have also been used to examine organization of individuated finger control in the M1 area. Schieber examined records of several stroke patients who exhibited impaired movements of fingers. He reported that of the nine patients whose impairments were restricted to hand function, five exhibited uniform impairment of all five digits, three exhibited more severe impairment in the thumb and index as compared to the middle, ring, and pinky fingers, and one had more severe impairment in the ring and pinky fingers as compared to the thumb and index fingers. None of the cases exhibited impairment of one and only one digit, nor did any of the cases exhibit impairment of the second, third, and fourth digits as compared to the thumb and fifth digits (Schieber, 1999). This led the investigator to conclude that there may be evidence of a broad somatotopic organization (thumb and index finger control vs. middle, ring, and pinky

finger control) that is overlaid onto the distributed activation of neurons during individuated finger movements. Similarly, another study examined long term loss of individuated finger motions in subjects with pure motor hemiparesis, where again the affected area was primarily limited to the motor cortex. Specifically of interest was whether or not damage to the cortex area equally affected the ability of the digits to move independently. The investigators reported that the middle, ring, and pinky fingers as a group seemed to exhibit impaired individuation more than the thumb or index fingers, with the index exhibiting slightly more impaired individuation than the thumb (Lang & Schieber, 2003). Inhibitor induced impairment of the motor cortex have also produced similar results. Researchers have discovered that an injection of gamma-aminobutyric acidA (GABAA) -agonist muscimol, a neural inhibitor, into precise and select areas of the M1 cortex area resulted in the significantly reduced ability of monkeys to perform independent finger movements and whole hand grasping motions (Brochier, Boudreau, Pare & Smith, 1999). Other researchers have as well found that intracortical injection of a neural inhibitor produced distributed inactivation and weakness in overall hand control instead of specific joints. They suggest that if the motor cortex were somatotopically organized as is generally accepted, then precisely placed inhibitor injections would produce weakness and inactivity in individual joints and fingers. Rather, since they found that each finger could be affected by inhibitor injection at several points in the motor cortex, hand control must be distributed within the M1 area (Schieber & Poliakov, 1998).

In summary, there seems to be a significant amount of evidence to suggest that the primary motor cortex is not characterized by a strict point-to-point somatotopic organization. In addition, the mapping is not spatially organized i.e. control of medial and lateral body parts is not necessarily regulated to medial and lateral parts of the M1 area, respectively. Furthermore, this lack of organization suggests that strictly controlling individual joints and/or muscles

independently is not the strategy of choice by the motor cortex. Rather, control of these parameters seems to be overlapping and dispersed throughout the M1 area. Of their own simiusculus diagram, Woolsey et. al stated,

“It must be emphasized...that this diagram is an inadequate representation of the localization pattern, since in a line drawing one cannot indicate the successive overlap which is so characteristic a feature of cortical representation...” (Woolsey et al., 1952).

and Penfield and Rasmussen, commenting on their homunculus diagram, stated,

“A figurine of this sort cannot give an accurate indication of the specific joints in which movement takes place, for in most cases movement appears at more than one joint simultaneously.... It is a cartoon of representation in which scientific accuracy is impossible” (Penfield & Rasmussen, 1950).

This wealth of evidence has thus led many investigators to conclude that the peripheral and central constraints of the neuromotor system suggest a pattern based means of coordination for the many degrees-of-freedom of the hand, potentially for the purposes of simplifying control (Schieber & Santello, 2004).

2.3.2 Motor Coordination Investigations involving Joint Kinetics and Kinematics

2.3.2.1 Evidence from Spinalized Frog Experiments

Researchers have investigated motor coordination by examination of the kinetics and kinematics that result from the various muscle coordination patterns of movement. In a series of experiments, several researchers have examined the role of the spinal motor system in the construction of complex movements in the frog both through experimental and modeling studies (Loeb, et al., 2000). (Bizzi, Mussa-Ivaldi & Giszter, 1991) and (Giszter, Mussa-Ivaldi & Bizzi, 1993) investigated the organization of the spinal circuitry in frogs whose spinal cord had been disconnected from the brain stem. The frog's ankle was locked in various positions as individual sections of the spinal cord were subjected to micro-stimulation. Isometric forces at the ankle were recorded at these different positions to construct a force field (Figure 2.3). These force fields were characterized by an equilibrium point to which all of the forces converged. This point is where there would be zero recorded forces in both force vector components, and it would be the final ankle position were the leg free to move. Of interest is that the authors reported that despite varying several parameters of micro-stimulation, there were only a small number of these convergent force fields (CFFs), presumably resulting from the small number of basis muscle synergies. Some of their preliminary studies showed that these CFFs could be combined to produce the CFFs resulting from simultaneous micro-stimulation of two sites. They concluded that these CFFs could be viewed as fundamental movement primitives that the CNS uses to construct complex motor behaviors. (Mussa-Ivaldi, Giszter & Bizzi, 1994) showed that linear vector summation could be applied to these movement primitives to explain the CFFs observed during simultaneous micro-stimulation of two sites, with the predicted and actual

results having a high coefficient of similarity. The authors expressed surprise that a linear combination could be applied to explain the complex nonlinearities that characterize neuronal and kinematic activity.

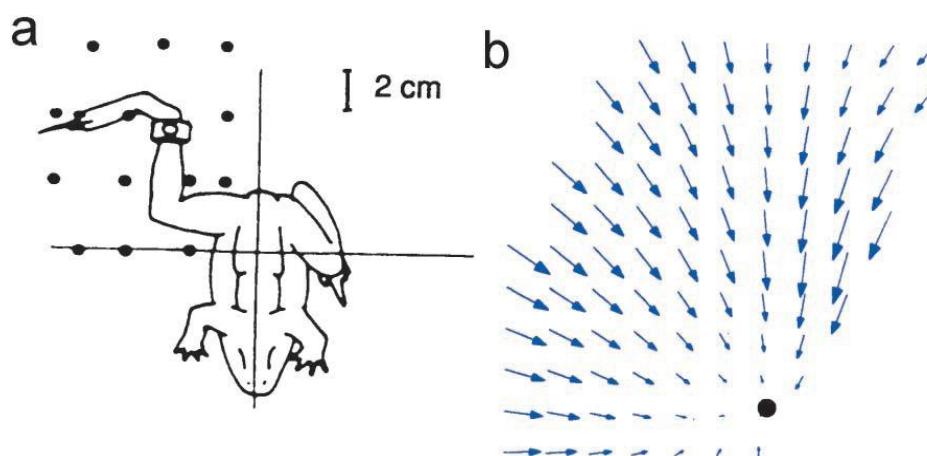


Figure 2.3. CFFs in spinalized frogs (Bizzi, D'Avella, Saltiel & Tresch, 2002).

Isometric forces were measured at the ankle while the spinal cord was micro-stimulated. The result is a force field, where all forces converge to an equilibrium point. This point is where there are no recorded forces at the ankle and would be the ankle position were the frog leg free to move. It was reported that only a small number of these CFFs were observed despite varying various parameters of stimulation. The authors conclude that these CFFs may be viewed as a primitive of motor control. Further investigations revealed that the CFFs induced by single micro-stimulation points can be vectorially combined to produce CFFs resulting from simultaneous micro-stimulation of two independent points (Mussa-Ivaldi et al., 1994).

Other investigators extended this analysis to supraspinal systems, hypothesizing that the supraspinal systems also generate motor outputs based upon these convergent force field motor primitives, and that these CFFs can also be linearly combined to produce more complex motor behaviors (d'Avella & Bizzi, 1998). Force field data were collected while stimulation was applied to the vestibular afferents of frogs and principal component analysis (PCA) was used to investigate whether or not the dimensionality of the resultant CFFs could be reduced. The

authors reported that the dimensionality could be reduced to a small number of movement primitives to explain the variety of observed force field patterns, and that this reduction suggested that the supraspinal systems may activate and linearly combine the same movement primitives that were observed during direct spinal stimulation. Other researchers examined force field primitives in frogs performing voluntary limb behaviors. These investigators showed that force fields observed during the wiping reflex of the frog could be explained by a force field summation paradigm. Furthermore, they showed that when an obstacle was introduced to obstruct this wiping reflex, the frog demonstrated a correction response whose force field was superimposed over the original force field. Hence, the correction response did not alter the integrity of the original response, but was rather summed with it. Hence, real limb behaviors and even on-line corrections could be explained by linear interactions between these force field movement primitives (Kargo & Giszter, 2000).

In summary, evidence suggests that both the circuitry of the spinal and supraspinal systems seem to construct complex motor behaviors through the use of movement primitives. These researchers have shown that these movement primitives could be represented as convergent force fields, which presumably are the force vectors resulting from the muscle synergy primitives interacting with the limb mechanics. Furthermore, these CFFs can be combined using vector summation to explain the observed force fields of more complex behaviors. These results are consistent with the notion that the biological system prefers to construct new and more complex skills on top of previously learned and simpler skills (Mussa-Ivaldi & Solla, 2004). Much of this work is also reviewed in greater detail elsewhere (Bizzi, Tresch, Saltiel & d'Avella, 2000, Tresch, Saltiel, d'Avella & Bizzi, 2002).

2.3.2.2 *Evidence from Experiments in Hand Kinematics*

In addition to the neural circuitry constraints that are implicit in the proposed CFF models, other researchers have hypothesized that there exist parallel biomechanical constraints. With regard to the control of hand functions, the many biomechanical degrees-of-freedom allow for performing of both gross grasping functions and more highly complex movements. Many of these more sophisticated movements are characterized by great articulation of the digit joints and a seemingly high level of individuated finger movements. However, research has shown that digit movement is not strictly individuated, even when an attempt is made to move just one instructed digit. This observation has been quantified in rhesus monkeys through introducing the individuation and stationarity indices (Schieber, 1991). The individuation index is a normalized measure of the degree that other digits moved during the movement of a particular instructed digit, and the stationarity index is a normalized measure of the degree that a specific digit remained unmoved during the movement of a particular instructed digit. Schieber found that wrist movement was highly individuated from digit movements in both flexion and extension. Of the digits, the thumb and index fingers proved to be the most individuated in both flexion and extension, while the middle, ring, and little fingers showed the least amount of individuation. Generally, flexion was more individuated than extension in all digits. The stationarity analysis showed the thumb and wrist to exhibit the least movement when they were not instructed, while the second through fifth digits exhibited comparable levels of stationarity. High values of both individuation and stationarity for the thumb, index finger, and wrist suggested that they were more individually controlled as compared to the middle, ring, and little fingers. However, no digit had perfect individuation or stationarity indices, indicating that control of no digit was completely isolated from all others. These results are consistent with much of

the results from analysis of cortex impairments (Lang & Schieber, 2003, Schieber, 1999). Other investigators have confirmed these results in human subjects, and in addition, showed that the digits of the dominant and non-dominant hands had comparable levels of individuation and stationarity, with the exception of the thumb (Hager-Ross & Schieber, 2000). The thumb showed greater independence on the dominant hand. The lack of complete independent control of digits is even seen during exercises where it would be imagined that perfect independence would be required, such as during typing (Soechting & Flanders, 1997). This overall lack of digit independence has led many researchers to investigate the possibility that postural synergies in the form of joint co-variations, while naturally having some origin in the anatomical structure, may also have some origin in the neural circuitry.

Investigators have examined the existence of postural synergies in the static hand postures that characterized fifty-seven different objects (Santello, Flanders & Soechting, 1998). Subjects were instructed to mime hand shapes that would be used to grasp these objects, while fifteen joint angles were recorded. These objects ranged in the hand shapes and sizes they typically bring to mind for adequate grasping, and the authors, using a discriminant analysis technique (Johnson & Wichern, 1992, Santello & Soechting, 1998), verified that the elicited hand shapes were in fact different. A cursory analysis showed that not all joint angles were independent, but some seemed to linearly co-vary. This was verified using a statistical technique known as principal component analysis (PCA), which serves to reduce the dimensionality of the number of controlled variables in the system (Glaser & Ruchkin, 1976). The authors found that the first three principal components (PCs) explained 90% of the data variance, with the first two explaining 84%. This led them to conclude that the fifteen degree-of-freedom system could be approximated by control of two or three degrees-of-freedom (i.e. PCs), where each PC (i.e. postural synergy) was a description of a pattern of joint co-variation (Figure 2.4). The first PC

seemed to control flexion of all metacarpal phalangeal (MCP) joints, some flexion of all proximal interphalangeal (PIP) joints, adduction of all MCP joints, and thumb external rotation and adduction. The second PC seemed to control extension of all MCP joints and flexion of all PIP joints, and similar thumb control as the first PC. Overall hand positions were then approximated as a weighted combination of these two synergies. Other researchers have performed similar analyses on data from subjects signing twenty-six letters of the American Sign Language (ASL) alphabet. This was of interest because signing generally requires more individuated finger movement than grasping. It was found that the dimensionality of the hand could be reduced to four effective postural principle components that explained 80% of the data variability. Furthermore, using these four PCs, they could accurately classify all twenty-six signed letters at a rate of 86.6% (Jerde, Soechting & Flanders, 2003). Other researchers also found that four PCs could explain >80% of data variance during signing of the ASL alphabet, and that four PCs explained >90% of data variance during grasping of real objects (Weiss & Flanders, 2004). They did not comment, however, on the similarities between the four PCs used for spelling versus grasping.

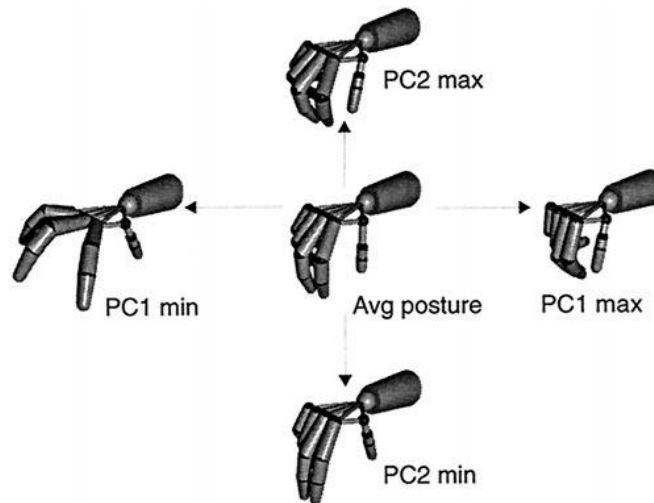


Figure 2.4. PCs of Static Hand Postures (Santello et al., 1998).

A study of prehensile patterns used in grasping 57 everyday objects revealed that >80% of the variance observed between all grasp patterns could be explained by the first two principal components (PC_1 and PC_2). These PCs represent deviations from the average hand posture, and are characterized by flexion/extension or abduction/adduction of the mcp, pip, and thumb joints.

Researchers have investigated whether or not dynamic hand postures can be explained by simpler kinematic movement primitives. It has been established that the shape of the hand during flight is distinctly affected by the shape and size of the intended object to be grasped, and that the hand gradually molds in-flight to the object's contour (Santello & Soechting, 1998). Researchers have examined whether or not this temporal gradual shaping could be explained by a set of kinematic movement primitives i.e. postural synergies (Mason, Gomez & Ebner, 2001). Joint kinematics were recorded while subjects reached-to-grasp sixteen objects that varied in size and concavity. Using a singular value decomposition (SVD) analysis (Hendler & Shrager, 1994), the authors were able to reduce the kinematic data into a linear combination of orthogonal postural synergies which they termed eigenpostures. These eigenpostures were

constant but their weights were modulated in time. The investigators found that the first three PCs (eigenpostures) explained 99.5% of the variance, with the first PC accounting for 97.3%. This first eigenposture was characterized by a generally open grasp with all the joints slightly flexed, and proved to be very similar for all subjects, regardless of the subject's hand size or the size of the grasped shape. The major result of this work was that eigenpostures (i.e. postural synergies) were invariant to object concavity and size, and could be used to describe the entire reach-to-grasp motion. This result was verified in a similar study of monkey grasps (Mason, Theverapperuma, Hendrix & Ebner, 2004). However, the major shortcoming of this work is that while the objects did vary in concavity and size, they by and large all required the same power grasp hand pattern. It is therefore no surprise that many of the eigenpostures were similar for the different objects and subjects. (Santello, Flanders & Soechting, 2002) addressed this issue by using objects that required hand shapes that visually differed in more than just size. Furthermore, they allowed their kinematic primitives to vary with time, as opposed to forcing them to be static and allowing the weighting coefficients to be time modulated. Santello et al. found that despite varying the shape and size of the objects and varying the conditions of the reach-to-grasp (from memory versus sight), two time varying synergies could explain >75% of the observed data variance. Finally, postural synergies have been used to describe joint coordination pattern involved not just in grasping, but also in dynamic object manipulations. Subjects were instructed to perform various object manipulation tasks such as turning the page of a book, crumpling a sheet of paper, manipulating Chinese balls, and fishing through a set of keys. Joint angles were recorded using a Cyberglove, and PCA was used to assess the covariance structure of the joint angles. The results of this investigation demonstrated the joint covariances could also be explained by a set of dimensionally reduced synergies, although the dimension for hand manipulation was more than twice that reported for hand grasping by

Santello et al. (Todorov & Ghahramani, 2004, Todorov & Jordan, 2002). These authors suggested that the extracted synergies showed a high level of task specificity, rather than being global enough for general hand posture construction.

The referenced investigators have concluded that the overall body of work in this area provides evidence for several ideas. First, that the CNS does simplify the control of complex motions, and specifically hand control, through the use of simpler movement primitives – in this case, eigenpostures. Second, that the CNS does not control individual joints, but rather controls several joints, as evidenced by the fact that eigenpostures did not affect individual joints. Finally, they suggested that the dynamic acts of reach-to-grasp and object manipulation, and not just static hand grasp patterns, could be described by these postural movement primitives.

2.3.3 Motor Coordination Investigations involving Muscle Synergies

Muscle synergies have been proposed as a way of explaining how the CNS coordinates the many neuromuscular degrees-of-freedom involved in any movement (Bernstein, 1971). Specifically, it was a way of reducing the number of variables required to be controlled (Loeb et al., 2000). Lending credibility to this idea are some investigations which have shown evidence that muscle patterns and synergies are potentially encoded in the activity of neurons in the M1 motor cortex (Holdefer & Miller, 2002, Kakei, Hoffman & Strick, 1999). However, some studies have presented evidence against a synergy paradigm for muscle coordination. Presented here is evidence from studies on both sides of the muscle coordination debate.

2.3.3.1 Evidences for a Muscle Synergy Paradigm

A series of studies have examined the use of muscle synergies by the frog CNS in constructing the complex motor responses of the hind limb to a cutaneous stimulus. These

studies defined a muscle synergy to be a group of muscles in which the activation levels of all muscles were specified together, although not necessarily to the same activation level. Hence, there would exist predetermined patterns of co-activation, as specified by the CNS. The investigators hypothesized that an individual muscle could belong to several synergistic groups, and that its total activation level would be a weighted linear sum of the activation levels specified for each synergy. Furthermore, they proposed that any observed pattern of electromyographic (EMG) activity could be explained by a linear combination of this finite set of synergy groups, as described by equation 2.3.

$$m_j^{obs} \approx m_j^{pre} = \sum_{i=1}^N c_{ij} w_i \quad c_{ij}, w_i \geq 0 \quad (2.3)$$

m_j^{obs} is the j^{th} muscle's observed EMG pattern, m_j^{pre} is the j^{th} predicted EMG pattern, c_{ij} is the weighting coefficient of the i^{th} muscle synergy in the j^{th} EMG response, N is the number of muscle synergy groups, and w_i is the activation pattern of the i^{th} muscle synergy. The authors applied a cutaneous scratch as a stimulus to fourteen different points on the frog hind limb and recorded the EMG responses. Using computational analysis, they established four muscle synergies that could describe all recorded muscle patterns of the frog hind limb. They found that a linear combination of the derived synergies and associated weights were able to explain a large amount of the variance observed in the muscle activation patterns. Furthermore, they observed that these synergies were quite similar across each frog, although the precise weighting differed from frog to frog (Tresch, Saltiel & Bizzi, 1999). They concluded that their work provided further evidence that the central nervous system constructs complex motor behaviors using combinations of muscle synergies instead of attempting to independently control individual muscles.

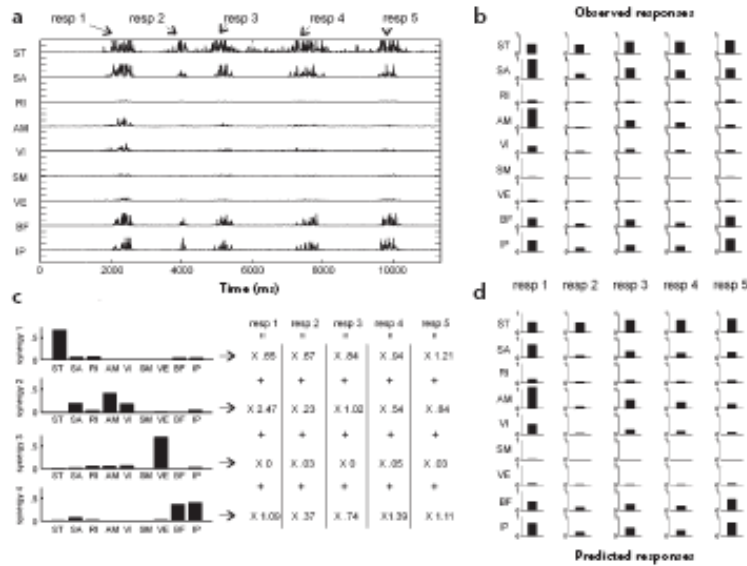


Figure 2.5. Muscle synergies in the EMG response of the frog leg (Tresch et al., 1999).

A) Five EMG responses evoked during cutaneous stimulation of the frog hind limb. B) Averaged observed responses. C) Computational analysis resulting in four muscle synergies and associated weights. Each synergy is a group of muscles with preset relative activation levels. These synergies are combined using a weighted linear sum. D) The predicted EMG responses based upon the determined muscle synergies were very similar to the observed responses (average $r^2 = 0.90 \pm 0.03$).

Other investigators extended Tresch et. al's hypothesis to propose that the activation of the muscle synergies were not only modulated in amplitude, but also in time, such that the new system could be expressed by equation 2.4.

$$m_j^{obs} \approx m_j^{pre} = \sum_{i=1}^N c_{ij} w_i (t - t_i) \quad c_{ij}, w_i \geq 0 \quad (2.4)$$

m_j^{obs} is the j^{th} muscle's observed EMG pattern, m_j^{pre} is the j^{th} predicted EMG pattern, c_{ij} is the weighting coefficient of the i^{th} muscle synergy in the j^{th} EMG response, N is the number of

muscle synergy groups, w_i is the activation pattern of the i^{th} muscle synergy, and t_i is the time delay of synergy onset (d'Avella, Saltiel & Bizzi, 2003). Furthermore, the combination of the independently amplitude modulated and time shifted synergies could represent all generated patterns of myoelectric activity during frog kicking. In this case, a synergy was defined as a group of muscles and their corresponding activation time courses. In examining the kicking behavior in frogs, the three resulting synergies and associated activation time courses and amplitude modulations explained roughly sixty-five percent of the variance present in the data. They reported that randomly generated time-varying synergies explained roughly nineteen percent of the data variance, thereby suggesting that significant information is contained in the synergies they observed. This study was extended to show that many of these time modulated synergies were shared by several activities of the frog hind limb (jumping, swimming, and walking), although there appeared to be some others that were activity specific. The total number of synergy groups that could explain all behaviors was still small (d'Avella & Bizzi, 2005). Furthermore, these muscle synergies have been shown to be largely robust to afferent stimuli, only changing their levels of activation but not their inherent structures (Cheung, d'Avella, Tresch & Bizzi, 2005).

One argument against global muscle synergies has been that they could potentially be highly dependent on the analyzed tasks and thus have no independent existence (Buchanan, Almdale, Lewis & Rymer, 1986). To fully establish global muscle synergies, all possible tasks of the neuromotor system would have to be included within the synergy analysis. To address this problem of task dependency, a set of investigators attempted to evoke muscle synergies directly using stimulation of the frog spinal cord. They believed that any resultant muscle synergies were hard-coded in the spinal circuitry. These researchers reported that their approach resulted in seven synergies that, when linearly combined, could explain ninety-one percent of the

variance observed in the EMG patterns (Saltiel, et al., 2001). The investigators concluded that this work presented more evidence that the intact CNS combines simple discrete elements to generate complex motor behaviors, thereby reducing the controlled number of degrees-of-freedom.

Finally, muscle synergies have been shown to be able to describe other tasks of the neuromotor system such as automatic responses to postural perturbations in cats and in humans (Ting & Macpherson, 2005, Torres-Oviedo, Macpherson & Ting, 2006), voluntary shifts of center-of-pressure during standing (Krishnamoorthy, Latash, Scholz & Zatsiorsky, 2003), and the control of fast-reaching arm movements (d'Avella, Portone, Fernandez & Lacquaniti, 2006). One study of particular interest investigated the role of muscle synergies in coordinating muscles of the hand during object grasping and performing a sign language task (Weiss & Flanders, 2004). These investigators showed that their six dimensional hand posture control problem could be described by a three dimensional set of muscle synergies at 80% explained variance, and a four dimensional set at 90% explained variance. While the reduction in control dimensionality is not very impressive, especially given that only six muscles were originally considered, the results still do suggest that a muscle synergy paradigm could account for coordination of muscle activities during hand tasks. A more central shortcoming of this study, and perhaps of several of the studies in the muscle synergy literature, is that the extracted muscle synergies have only been shown to *describe* many of the observed muscle patterns. Hence, it is a possibility that the synergies are specific to the observed tasks, and a different set of synergies could have been extracted if a different set of tasks were observed. A more glaring possibility is that the success of the descriptive synergy paradigm may be a result of fitting the model to the data. Both of these possibilities leave open the possibility that the extracted

muscle synergies are not robust and generalizable, and hence suggest the need for a more complete approach of discerning the role of muscle synergies in control applications.

2.3.3.2 Evidences against a Muscle Synergy Paradigm

Some studies have suggested that the concept of muscle synergies is not physiologically based, or at best it is an artifact of the biomechanical constraints of the neuromotor system. The majority of these studies came to this conclusion due to a lack of finding consistent spatial and/or temporal relationships between any two muscles given a wide variety of tasks and/or conditions. Many of these studies assumed a synergy model that required a restrictive coupling of the activities of any two muscles, rather than the synergy models described above, where the activity of any given muscle could be simultaneously affected by multiple synergies (Ting & Macpherson, 2005).

Buchanan and colleagues performed a study in which three normal human subjects were required to exert isometric torques about the elbow in several different directions and at various magnitudes. EMG activities were recorded from the biceps brachii, brachialis, and brachioradialis. First, these researchers reported that no muscle acted in isolation for any given direction of applied force. Second the three-dimensional EMG pattern remained constant and by and large scaled linearly with increasing torque magnitude, suggesting that there existed a stereotypical pattern of muscle activation for each direction. However, when comparing spatial patterns of activity between different directions of applied torque, there was little evidence of consistent patterns of co-activation between any two muscles. Rather, the directional dependency of the co-activation patterns suggested that any observed synergies were specific to the task biomechanical requirements, rather than existing independently as constructs of the neuromotor system (Buchanan et al., 1986).

Another study by Soechting and Lacquaniti seemed to suggest similar results. In their study, the correlations of four to six elbow and shoulder muscles were analyzed both during responses to force perturbations in various directions, and during various volitional arm movements (drawing a circle, star, figure eight, etc...). A cross-correlation analysis revealed to what extent the activities of the recorded muscles were temporally coupled. The results of this study indicated that there was no consistent temporal coupling of any two muscles across the multiple tasks and parameters. The authors concluded that the strictest definition of a muscle synergy (i.e. that investigated by Buchanan) was incongruent with their results. They did consider the possibility that the activity of a given muscle could be simultaneously affected by multiple synergies, but suggested through a PCA analysis of their data that there would not be a significant decrease in the dimensionality of the control problem to warrant a synergy construct. The investigators finally concluded that a synergy paradigm is not necessary to reduce the control dimensionality of upper-arm movements in the muscle domain, but may do so with respect to limb kinematics (Soechting & Lacquaniti, 1989).

A study by Maier and colleagues investigated the spatial and temporal coupling of hand muscles during a fingertip endpoint force production task. Subjects matched a specified force with the index fingertip while EMGs were recorded from up to fifteen muscles controlling the thumb and fingers. Spatial and temporal correlation analyses produced similar results to that of Buchanan and Soechting, namely that there were very few instances of the activities of any two muscles being strictly coupled in either the spatial or time domain across the examined force levels. However, because the authors did find some coupling, they concluded that the muscles for hand control were not fully independent of each other. However, they were also not governed by a fixed coupling control paradigm (Maier & Hepp-Reymond, 1995b).

The aforementioned studies in this section have all concluded that the strictest definition of a muscle synergy, namely two or more muscles whose relative spatial or temporal activities are fixed, is incongruent with the data from their experiments. While this may be true, it is the current author's belief that this strictest definition of a muscle synergy is too limiting. Based upon other work described above, it is suggested that the model of Tresch et al. and colleagues may offer more insight and usefulness for coordination of muscles.

2.4 Muscle Synergies as Testable Hypotheses

One of the main criticisms against the muscle synergy concept is that it has seldom been formalized and tested against a falsifiable hypothesis, and when it has, the results have been mixed at best. Much of the above work that presents evidence for the muscle synergy model goes about showing the existence of synergies through a descriptive mechanism i.e. the synergies describe some large percentage of data from which they were observed. The underlying thread for these presented works can be summarized by the neuromotor synergy hypothesis, which states that "low-level, neurally based patterns significantly constrain intentional actions" (Lee, 1984). To thoroughly test this hypothesis though, a prescriptive framework must be established by muscle synergies. Lee (1984) formalized several testable properties of a prescriptive framework of neuromotor synergies (i.e. muscle synergies). The first is that synergies should be robust and reliable (i.e. exhibit **low lability**), regardless of changing input parameters and task requirements. Second, muscles within a synergy should maintain the same relative activation levels with **scaling** of the synergy. Third, synergies should be **spatially coherent**, meaning that they should be activated in an all-or-none fashion. Several of the discussed investigations have investigated the scaling property, and indirectly the spatial coherence property. The property of low lability has not been properly addressed by the

descriptive frameworks reported in the literature, particularly for hand control. These three properties, and specifically their implications with regard to myoelectric control, form the framework for the investigations presented in the remaining of this manuscript.

2.5 Conclusion

In summary, a wealth of literature has provided evidence that a dimensionally reduced set of motor primitives in the form of muscle synergies can form a descriptive framework for a wide variety of motor tasks, such as locomotion, postural stability, and hand grasping. Not many of these studies though address issues necessary for muscle synergies to form a prescriptive framework. Doing so would add more credibility to the neuromotor synergy hypothesis as a framework of motor control. This prescriptive framework is also of importance to myoelectric control. The current research state-of-the-art control paradigms are EMG pattern recognition paradigms that require a priori programming of the individually and simultaneously controlled postures and degrees-of-freedom. A myoelectric control scheme based upon a prescriptive muscle synergy paradigm would potentially allow for controlling of new hand postures and positions and simultaneous degrees-of-freedom. In the remainder of this manuscript, the author describes his investigations towards this end.

3 The Muscle Synergy Model and Parameter Estimation

3.1 Introduction

The control of movement by the central nervous system (CNS) has been termed an ill-posed problem because of the biomechanical and neuromuscular redundancies in the anatomical structure (Bernstein, 1967). There is seemingly an infinite number of solutions and variable configurations of the degrees-of-freedom that could accomplish any desired movement goal. This problem of redundancy is particularly illustrated in the control of the human hand, which has over twenty-seven bones and over thirty extrinsic and intrinsic multi-joint muscles (Gray, 1973) to control twenty-two anatomical degrees-of-freedom (DOFs). This is the mathematical equivalent of a system of equations that has more variables than constraints. For this system to be uniquely solvable, more constraints must be introduced. Likewise, for the hand to be fully controllable by the neuromotor system, more constraints must be added. There is a long held view that the motor control system imposes these constraints in the form of neuromotor synergies (Sherrington, 1906). Furthermore, by actualizing control in the space defined by the smaller number of synergies instead of the much greater number of individual DOFs, the CNS potentially reduces the complexity of the motor control problem. These synergies serve as fundamental building blocks of movement, and are manifested in muscle activation, joint kinetics and kinematics, reflex activation, and other domains of control. There is yet to be a consensus concerning in which domain these synergies are directly operative. In this chapter and in the remainder of this document, the discussion of neuromotor synergies is limited to the domain of coordination of muscle activation, and will henceforth be referred to as muscle synergies.

Several methods, some of which include non-negative matrix factorization (NMF), independent component analysis (ICA), and principal component analysis (PCA), have been proposed to assess the number and composition of the muscle synergies related to a motor task. This manuscript focuses primarily on the use of NMF for assessing muscle synergies. In the remainder of this chapter, the muscle synergy model (MSM) will be described, along with several algorithms and their underlying assumptions for determining the unknown parameters of the model. Also described are computer simulations designed to test the efficacy of the model under varying conditions of noise and over- and underestimation of the number of muscle synergies.

3.2 The Muscle Synergy Model

3.2.1 General Description

Consider a closed environment that contains n signal sources $h_i(t)$ ($i = 1..n$) and m receivers $v_j(t)$ ($j = 1..m$) at some distances w_{ij} from the sources. Assuming no nonlinear interaction terms, each receiver records a signal that is some linear weighted combination of the source signals, with the weightings determined by the distance between each receiver and source. The recorded signals can be expressed as a system of equations as shown in equation 3.1 and written in shorthand as shown in equation 3.2, which leads to the matrix expression shown in equation 3.3.

$$\bar{v}_j(t) = w_{1j}\bar{h}_1(t) + w_{2j}\bar{h}_2(t) + w_{3j}\bar{h}_3(t) + \dots + w_{nj}\bar{h}_n(t) \quad \forall i \quad (3.1)$$

$$\bar{v}_j = \sum_i w_{ij}\bar{h}_i \quad \forall j \quad (3.2)$$

$$V = W \times H, \quad \text{where}$$

$$V_{m \times o} = \begin{bmatrix} \bar{v}_1(t) \\ \bar{v}_2(t) \\ \vdots \\ \bar{v}_m(t) \end{bmatrix}, W_{m \times n} = \begin{bmatrix} w_{11} & w_{21} & \cdots & w_{n1} \\ w_{12} & \ddots & & w_{n2} \\ \vdots & & \ddots & \vdots \\ w_{1m} & \cdots & \cdots & w_{nm} \end{bmatrix}, H_{n \times o} = \begin{bmatrix} \bar{h}_1(t) \\ \bar{h}_2(t) \\ \vdots \\ \bar{h}_n(t) \end{bmatrix} \quad (3.3)$$

The data matrix \mathbf{V} is of size $m \times o$, where m is the number of receivers and o is the number of data observations. The data observations can be temporal (hence $v(t)$), or they can be spatially independent observations, in which case t is the observation index. The distance matrix \mathbf{W} is of size $m \times n$, where n is the number of signal sources, and w_{ij} represents the weight of signal source i on receiver j . The source matrix \mathbf{H} is of size $n \times o$, and serves as the input to the system. Like \mathbf{V} , these inputs can be temporal in nature or spatially independent observations. All that is observable about the system are the signals recorded by the receivers. In other words, only the parameters of \mathbf{V} are known; \mathbf{W} and \mathbf{H} are unknown. The number of receivers m is not necessarily equal to the number of sources n , as illustrated by the following example.

Consider a scenario in which two individuals are having a conversation. The listener serves as the receiver and the speaker serves as a signal source. In addition to the speaker, there are other speakers in the room who also serve as signal sources. The listener picks up signals from all sources, and the resultant heard signal is some weighted combination of the signals from each of the sources. This scenario is known as the classic ‘‘Cocktail Party Problem’’ (Cherry, 1953, Haykin & Chen, 2005). In this situation, even though the received signal is an aggregate of signals from several different sources, the auditory system is able to reconstruct the original source signals, and specifically the signal from the desired speaker, with high fidelity (Cherry, 1953). With several listeners in the room, each listener then acts of one of the m receivers, and the problem is exactly that as described by equations 3.1 – 3.3.

The muscle synergy model proposes that coordination of muscle activation operates in much the same way as the “Cocktail Party Problem”. In this case, the muscles are the receivers, with the recorded electromyographic (EMG) signals represented in the data matrix \mathbf{V} . The source signals \mathbf{H} are the neural inputs to the motor system. The matrix \mathbf{W} represents the activation level of each muscle as determined by each signal source. Together, the relative activation level of all muscles as specified by a single source is termed a muscle synergy (i.e. each column in matrix \mathbf{W}). Hence, the total activation level of each muscle is determined by summing the products of each pair of each specified activation level in each synergy and the input from each source (equation 3.2). Figure 3.1 illustrates a nodal representation of the muscle synergy model. As with the receivers in the “Cocktail Party Problem”, only the signals at the muscles are observable. Both the neural inputs and the muscle synergies are unknown to the outside environment (i.e. the electromyographer). Estimating these parameters is the subject of the remainder of this chapter.

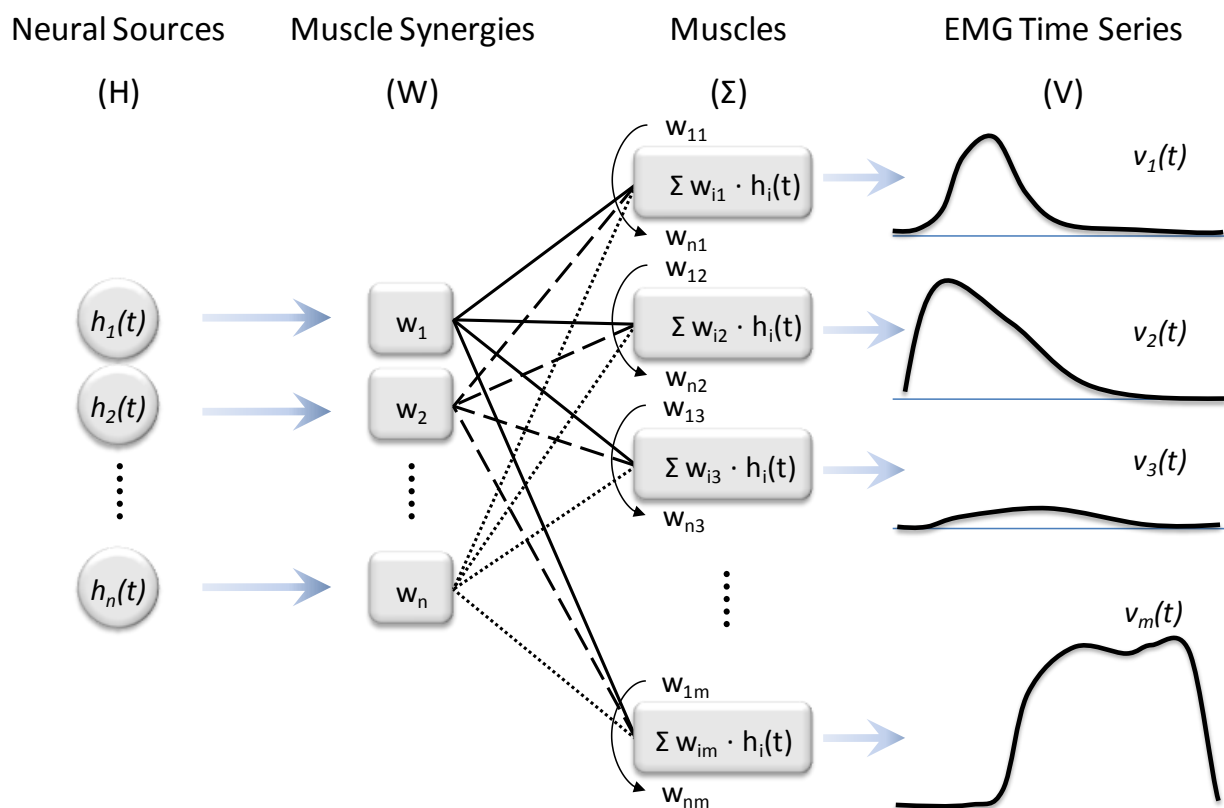


Figure 3.1. Nodal Representation of Muscle Synergy Model

Neural input sources (H) send command signals which act as multipliers to each muscle synergy (W), which are then summed to produce the observed EMG activities (V).

3.2.2 Estimating the Unknown Parameters

Because both the neural inputs and the muscle synergies of the model are not directly observable, estimation of these parameters has commonly been termed blind source separation (BSS) (Jutten & Herault, 1991, Muller, Vigario, Meinecke & Ziehe, 2004). The terminology cannot be strictly applied to the muscle synergy model because the classical BSS problem makes some assumptions (specifically statistical source independence) that are not necessarily held by the synergy model. Several methods have been proposed to address the problem of

discerning the synergies \mathbf{W} and the source signals \mathbf{H} . Three of these approaches and their underlying assumptions are briefly described.

3.2.2.1 *Principal Component Analysis*

Principal component analysis (PCA) (Hyvarinen, Karhunen & Oja, 2001) is a statistical analysis method for data reduction that is typically used in applications such as image compression and computer-based facial recognition (Smith, 2002). Given an $m \times o$ (m variables, o observations) data matrix \mathbf{V} of independent observations, PCA aims to discern the underlying n common factors (variables) of the data set, where $n < m$. If the m variables contain redundant information and are correlated, the data can be expressed in the reduced n -dimensional factor space instead of the original m -dimensional variable space, thereby accomplishing feature extraction and dimensionality reduction. The data representation in the m -dimensional space is a weighted linear combination of the data representation in the n -dimensional space.

As with the muscle synergy model, a PCA analysis only assumes knowledge of the data matrix \mathbf{V} and hence the m -dimensional space – the analysis is blind to the n -dimensional space. PCA determines the n -dimensional space by assuming that the n factors are uncorrelated and hence not redundant (i.e. orthogonal). Given two variables X and Y , their covariance $\mathbf{C}_{X,Y}$ is defined by equation 3.4. A positive covariance means generally that as X increases, Y increases and vice versa. A negative covariance means generally that as X increases, Y decreases and vice versa. A covariance of zero means that the two variables are uncorrelated. Given m variables, a symmetrical covariance matrix is then defined by equation 3.5. The covariance values that make up the diagonal of the matrix are the variances of each respective variable.

$$s_{X,Y}^2 = \frac{\sum_{i=1}^n (x_i - \bar{X})(y_i - \bar{Y})}{n-1}, \quad \text{where } \bar{X} = \frac{\sum_{i=1}^n x_i}{n}, \quad \bar{Y} = \frac{\sum_{i=1}^n y_i}{n} \quad (3.4)$$

$$\mathbf{C} = \begin{bmatrix} s_{1,1}^2 & s_{1,2}^2 & \dots & s_{1,m}^2 \\ s_{2,1}^2 & \ddots & & s_{2,m}^2 \\ \vdots & & \ddots & \vdots \\ s_{m,1}^2 & \dots & \dots & s_{m,m}^2 \end{bmatrix} \quad (3.5)$$

The n -dimensional factor space is determined by the eigenvectors of the covariance matrix \mathbf{C} of the zero-mean data. In reality, because \mathbf{C} is $m \times m$, there are actually m eigenvectors, and associated with each eigenvector is an eigenvalue that determines how much of the data variance is explained by that corresponding eigenvector. So while all m eigenvectors are needed to explain 100% of the data variance, a high percentage of the data may be able to be explained by n eigenvectors, with the unexplained variance potentially resulting from noise. Thus with PCA, both dimensionality reduction and factor separation is achieved.

One property of the set of eigenvectors is that they are orthogonal. Hence, applying PCA to the muscle synergy model would make the assumption that the muscle synergies are orthonormal (i.e. orthogonal and unit length) vectors and hence uncorrelated. This is illustrated by the following example. Consider the artificial two-dimensional data set of the activity from two muscles M_1 and M_2 as given by Table 3.1. The data is zeroed with respect to each variable and the covariance matrix \mathbf{C} and associated eigenvectors (columns of \mathbf{W}) and eigenvalues (λ) are given in equation 3.6.

Table 3.1. PCA Sample Data Set

M_1	7.3	3.2	8.5	1.2	5.4	8.4	3.8	8.2	4.7	5.7	9.3	4.4	1.7	7.4	4.2	2.7	5.2
M_2	3.3	1.8	4.0	0.7	2.0	3.6	2.4	4.6	2.7	3.5	4.1	2.3	0.8	3.2	1.8	1.9	2.7

$$C = \begin{bmatrix} 6.146 & 2.5878 \\ 2.5878 & 1.2447 \end{bmatrix}, \quad W = \begin{bmatrix} PC_2 & PC_1 \\ 0.3952 & -0.9186 \\ -0.9186 & -0.3952 \end{bmatrix}, \quad \lambda = \begin{bmatrix} 0.1313 \\ 7.2594 \end{bmatrix} \quad (3.6)$$

Even though there are two eigenvectors (i.e. principal components, or PCs), the data can very nearly be approximated by using only the second eigenvector (PC_1), since it explains roughly 98% (7.26 of 7.39) of the data variance, while the first eigenvector (PC_2) explains only 2% (0.13 of 7.39) of the data variance. Hence the data observed by the two “receivers” (variables M_1 and M_2) is thus almost completely explained by one “source” (factor PC_1). Plotting the data and the principal component vectors (Figure 3.2) shows that PC_1 indeed explains the majority of the data variance. In this trivial two-dimensional example, PC_1 is the vector that points in the direction of the best-fit line (i.e. direction that explains the most amount of variance), and PC_2 is the vector that points in the direction of the best-fit line once PC_1 has been removed (i.e. direction that explains the second most amount of variance).

As previously mentioned, the principal components found by PCA are restricted to being orthonormal and hence uncorrelated. There does not seem to be a physiological basis for why a restriction of orthonormality must be imposed on the muscle synergies. If this restriction is imposed however, it is of benefit to go a step further and add the restriction of statistical independence, which is different and much stronger than non-correlation. While PCA cannot address the issue of statistical independence, independent component analysis (ICA) does so.

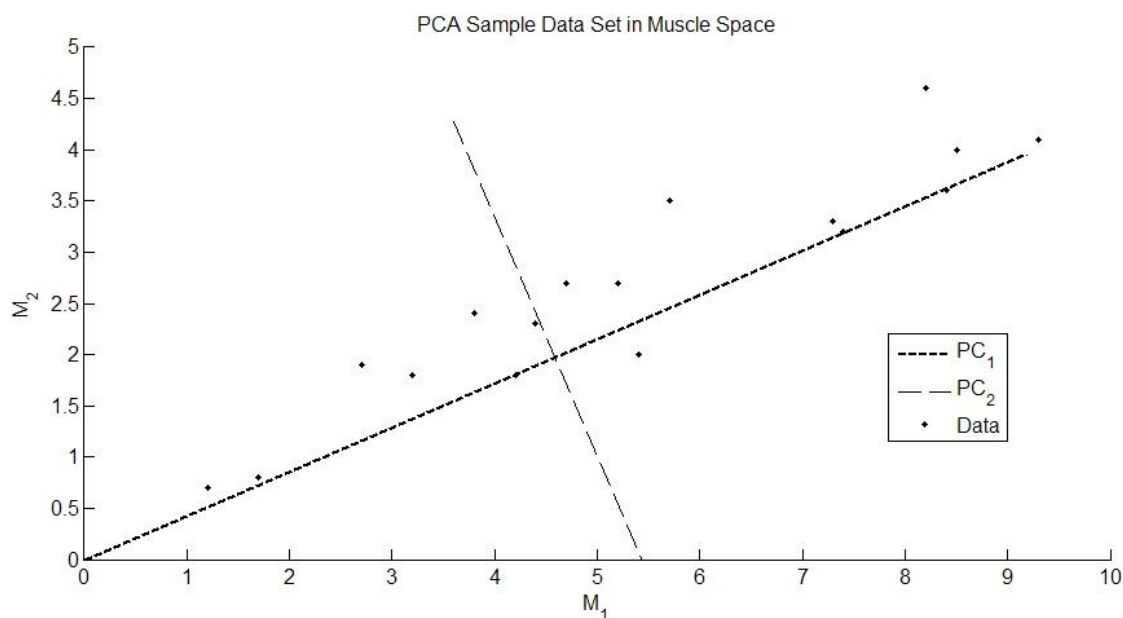


Figure 3.2. PCA Sample Data Set and Principal Component (PC) Vectors

While two principal components (PCs) are needed to explain 100% of the data variance, the first (PC_1) explains roughly 98% of the data variance. Hence, the data can be represented solely by PC_1 with little loss of information. Hence, PC_1 is the predominant underlying factor, or “source” that determines the activity recorded from muscles M_1 and M_2 . Because PC_1 and PC_2 are orthogonal, they form a new coordinate space in which the data can be represented, by way of coordinate transformation.

3.2.2.2 Independent Component Analysis

Independent component analysis, or ICA (Comon, 1994, Hyvarinen et al., 2001, Hyvarinen & Oja, 2000) is the classic method of solving the blind source problem. It is similar to PCA in that it attempts to express the original data set in another reduced coordinate space by means of a transformation matrix. It differs from PCA in that the independent components are statistically independent, which is a stronger criterion than PCA’s non-correlation criterion. Hence, ICA first assumes statistical independence. Generally speaking, a set of variables are statistically independent if knowledge about the value of one variable gives no information about the value

of the others. Strictly speaking, a set of variables are statistically independent if and only if the joint probability density function can be expressed as a simple product of the individual probability density functions (Hyvarinen et al., 2001). This is mathematically expressed by equation 3.7.

$$p(y_1, y_2, \dots, y_n) = p(y_1)p(y_2)\dots p(y_n) \quad (3.7)$$

Secondly, ICA assumes that at most one of the independent components (ICs) has a Gaussian distribution. The reason for this is illustrated in Figure 3.3. Take for example two independent uniformly distributed sources h_1 and h_2 . Their joint distribution is illustrated in Figure 3.3(i), and the joint distribution of the mixed signals v_1 and v_2 is illustrated in Figure 3.3(ii), where v_1 and v_2 are the results of applying an orthogonal mixing matrix \mathbf{W} to the sources h_1 and h_2 (i.e. $\mathbf{V} = \mathbf{WH}$). The joint distribution of h_1 and h_2 shows that they are indeed uncorrelated and independent, because knowledge of the value of one variable gives no knowledge of the the value of the other. The joint distribution of v_1 and v_2 shows that they are uncorrelated but dependent, because the value of one variable limits but does not fully explain the value of the other (e.g. at the extremes). Conversely, take two independent Gaussian distributed sources h_1 and h_2 . Their joint distribution is illustrated in Figure 3.3(iii), and the joint distribution of the mixed signals v_1 and v_2 is illustrated in Figure 3.3(iv), where v_1 and v_2 are the results of applying the same orthogonal mixing matrix \mathbf{W} to the sources h_1 and h_2 (i.e. $\mathbf{V} = \mathbf{WH}$). The joint distribution of h_1 and h_2 shows that they are indeed uncorrelated and independent, while the joint distribution of v_1 and v_2 shows that they are also uncorrelated and independent. Hence, ICA cannot distinguish between the original independent components and an orthogonal transformation of them because they have the same joint distribution (Hyvarinen & Oja, 2000).

Thirdly, ICA assumes that the number of mixed signals is the same as the number of independent signals (i.e. \mathbf{W} is a square matrix). Hence, ICA does not perform dimensionality reduction. In the event that it is necessary, dimensionality reduction can first be performed by methods such as PCA, followed by an ICA analysis. This is commonly referred to as ICAPCA (Tresch, Cheung & d'Avella, 2006).

While it seems logical and physiologically appropriate to impose independence as a restriction on the neural input sources modulating the activation of each synergy, it does not seem physiologically appropriate to restrict the distribution of the neural inputs to be non-Gaussian. In the event that several neural inputs were Gaussian, ICA would fail to identify them. While ICA is limited in this fashion, non-negative matrix factorization (NMF) is not because it only imposes a restriction of positivity on both the neural inputs and muscle synergies.

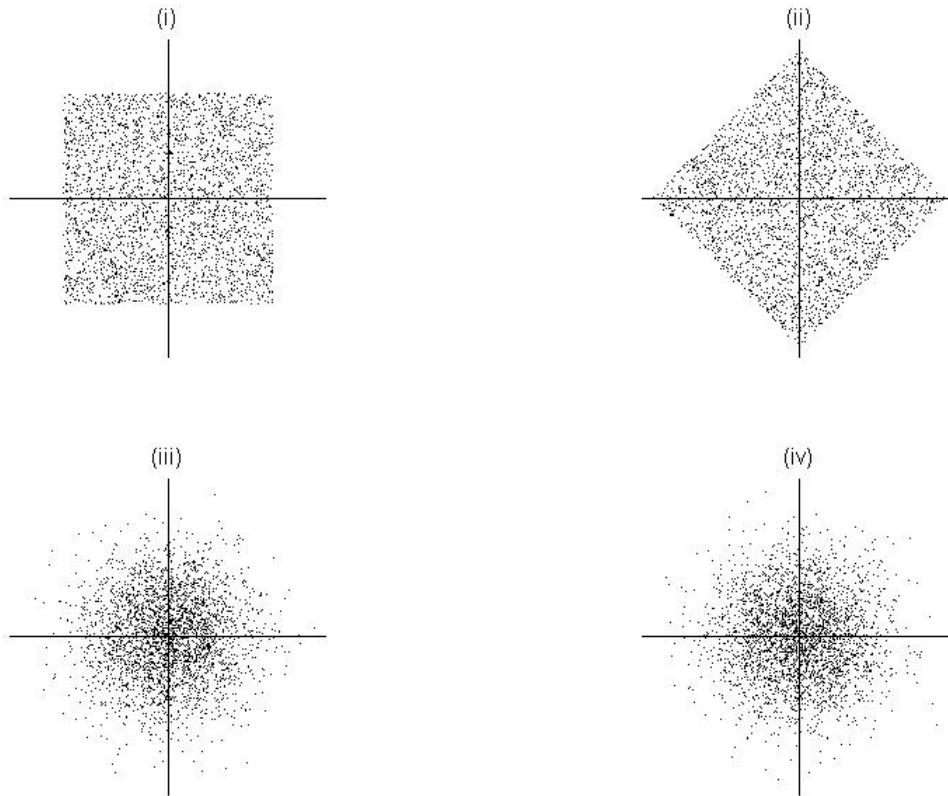


Figure 3.3. Joint Distributions of ICs and Orthogonal Mixtures

ICA can only estimate a pair of Gaussian independent sources up to an orthogonal transformation. This is because the joint distribution for a pair of Gaussian sources is the same as when an orthogonal transformation is applied. Hence, ICA only allows at most one of the independent sources to be Gaussian. (i) The joint distribution for a pair of uniformly distributed independent sources. (ii) The joint distribution of an orthogonal transformation of the uniform sources. (iii) The joint distribution for a pair of Gaussian distributed independent sources. (iv) The joint distribution of an orthogonal transformation of the Gaussian sources.

3.2.2.3 *Non-negative Matrix Factorization*

Non-negative matrix factorization (NMF) is similar to the aforementioned PCA and ICA techniques in that it tries to express recordable data as a weighted linear summation of a set of basis vectors. NMF differs, however, in its philosophy and interpretation of these basis vectors. Each basis vector in both PCA and ICA is a holistic representation of the data, typically

constituting some level of variance accounted for that is not reproduced by the other basis vectors. Because these vectors can be additive or subtractive, their physical representations are not always intuitive. In NMF each basis vector is a parts-based representation of the data, corresponding to discernable physical components of the data, in contrast to the holistic eigenvector bases of PCA and ICA (Lee & Seung, 1999). For example, in the realm of facial recognition, a PCA or ICA analysis would reveal basis vectors, with each being an additive or subtractive holistic representation of the face, and referred to as an “eigenface”, whereas the basis vectors of an NMF analysis would correspond to the variants of a specific part of the face, such as a mouth or nose (Lee & Seung, 1999, Turk & Pentland, 1991).

The goal of NMF is, given a data matrix \mathbf{V} , to find positive valued matrices \mathbf{W} and \mathbf{H} , such that $\mathbf{V} = \mathbf{WH}$. \mathbf{W} and \mathbf{H} are initialized to random estimates, and a cost function is defined to determine the efficacy of these estimates. The goal of NMF is to then optimize the cost function with respect to these estimates. Several cost functions have been proposed in literature, including the Euclidean distance norm (Equation 3.8). A gradient search algorithm can be used to determine \mathbf{W} and \mathbf{H} (Tresch et al., 1999), although it is potentially slow. The iterative update rules expressed in equation 3.9 have been shown to monotonically minimize the Euclidean distance cost function, and appropriately converge \mathbf{W} and \mathbf{H} (Lee & Seung, 2001).

$$\|\mathbf{V} - \mathbf{WC}\|^2 = \sum_{ij} (V_{ij} - [\mathbf{WC}]_{ij})^2 \quad (3.8)$$

$$\begin{aligned} W_{n+1} &= W_n * \frac{V \times C_n^T}{W_n \times C_n \times C_n^T} & C_{n+1} &= C_n * \frac{W_n^T \times V}{W_n^T \times W_n \times C_n} \\ W_{n+1}(a) &= \frac{W_{n+1}(a)}{\text{norm}(W_{n+1}(a))} & \forall \text{ columns 'a'} & \end{aligned} \quad (3.9)$$

where ' $*$ ' is element-wise matrix multiplication,
' $/$ ' is element-wise matrix division,
' \times ' is standard matrix multiplication.

As mentioned earlier, NMF differs from PCA and ICA in that the basis vectors determined by NMF are positive parts of the whole, rather than holistic non-intuitive elements. Equally as important, NMF does not make any restrictions on the statistical distributions of the basis vectors, unlike ICA. Furthermore, dimensionality reduction is equally accomplished with NMF as with PCA. As a result, we move forward in the remainder of this document using NMF to estimate the parameters of the muscle synergy model.

3.3 Estimating Muscle Synergies: NMF Simulation Analysis

3.3.1 Objective

NMF has been used extensively in the literature to analyze EMG data for the purpose of determining basis vectors (i.e. muscle synergies) to adequately represent underlying structure present in the observed data. Studies such as the analysis of frog hind limb reflex responses (Tresch et al., 1999), investigations of natural motor behaviors in lower level vertebrate (d'Avella & Bizzi, 2005, d'Avella et al., 2003) and the role of sensory feedback (Cheung et al., 2005), and the analysis of automatic neuromotor responses to postural perturbations (Ting & Macpherson, 2005, Torres-Oviedo et al., 2006), have all assumed that the muscle synergies discerned by NMF are inherent and physiologically appropriate to the data, rather than simply a result of matrix manipulation and data fitting. It is this assumption that is addressed by the simulations described in the remainder of this section. To this end, these simulations specifically aim to investigate

- how the robustness of NMF in estimating both the synergies and sources is affected by varying the dimensionality of the basis vector space,
- how well a set of random synergies can be used to explain a data matrix constructed by a set of known synergies,
- how the estimates are affected by additive noise to the system,
- how well a random data matrix, not generated by a synergy paradigm, can be explained by a set of synergies and sources, and
- how the determined synergies and sources are affected by over- and underestimation of the number of basis vectors.

Recent literature has extensively examined the performance of NMF, along with other algorithms, in varying scenarios of noise level and distribution (Gaussian versus signal-dependent), source signal distribution, and source signal correlation (Cheung & Tresch, 2005, Tresch et al., 2006). The simulations described here do not reproduce the work described in recent literature, but rather seek to augment it to increase the breadth of knowledge concerning the behavior of NMF, and to establish confidence in the algorithm for future analysis of experimental data.

3.3.2 Methods

For all simulations, data sets were generated consistent with $\mathbf{V} = \mathbf{WH} + \boldsymbol{\eta}$, where \mathbf{V} is the $m \times o$ EMG data matrix, \mathbf{W} is the $m \times n$ synergy matrix, \mathbf{H} is the $n \times o$ input source matrix, and $\boldsymbol{\eta}$ is a noise component. A known set of n synergies, each of dimension $m \times 1$ and of exponential distribution with a mean of 1, were randomly generated along with a set of n signal sources, each of dimension $1 \times o$ ($o = 200$ observations) and also of exponential distribution with a mean of 1. Exponential distributions were chosen because it is generally consistent with the observed

distributions of experimental data (Tresch et al., 2006). Before construction of the data matrix \mathbf{V} , each synergy in \mathbf{W} was normalized to be a unit vector.

3.3.2.1 Effect of Varying the Number of Basis Vectors

The robustness of NMF was investigated with respect to varying the number of synergies n used to construct the data matrix $\mathbf{V} = \mathbf{WH}$. n was allowed to range from 1 to m , the number of muscles in the system ($m = 11$). For each n , a random \mathbf{V} matrix was constructed from random \mathbf{W} and \mathbf{H} matrices. \mathbf{V} was then corrupted with varying amounts of noise η , as is later described. Starting with new random estimates of \mathbf{W} and \mathbf{H} (henceforth referred to as \mathbf{W}_{est} and \mathbf{H}_{est}), the update rules in equation 3.9 and the cost function in equation 3.8 were used to determine final estimates of the original \mathbf{W} and \mathbf{H} matrices. Convergence of the NMF algorithm was determined to be when the absolute change in the cost function was less than a tolerance $\varepsilon = 0.0001$ for more than twenty (20) consecutive iterations. The maximum number of iterations allowed was 20000. Twenty (20) trials were performed for each n . Reported is the efficacy of the NMF algorithm to determine the original synergy and source matrices under the varying condition of total number of original basis vectors.

3.3.2.2 Effect of Random Synergies

To assess the risk of the NMF algorithm returning random synergy and source matrices while still explaining a large portion of the data variance, simulations with random synergies were run on the data matrices generated in 3.3.2.3. Specifically, random synergy and source matrices \mathbf{W}_{random} and \mathbf{H}_{random} were generated, and \mathbf{H}_{random} was updated in accordance to equation 3.9 while \mathbf{W}_{random} was not updated. Parameters of convergence were the same as described in

3.3.2.1. This resulted in estimated data matrices $\mathbf{V}_{est_random} = \mathbf{W}_{random}\mathbf{H}_{est_random}$, which were compared to the original data matrices \mathbf{V} .

3.3.2.3 *Effect of Additive Noise*

The simulations described in sections 3.3.2.1 and 3.3.2.2 were performed under varying conditions of noise, subject to $\mathbf{V}_{noisy} = \mathbf{WH} + \boldsymbol{\eta}$, where $\boldsymbol{\eta}$ is the noise component. Specifically, $\boldsymbol{\eta}$ was a Gaussian distributed zero mean white noise signal, with the standard deviation allowed to discretely range between 0 and 100% of the standard deviation of the data matrix \mathbf{V} . The overall noise power of the corrupted signals is reported, and was calculated as $1-r^2$, where r^2 is the fraction of the variance of the corrupted data set \mathbf{V}_{noisy} explained by the unadulterated data matrix \mathbf{V} (Cheung & Tresch, 2005). Reported is the efficacy of the NMF algorithm to determine the original synergy and source matrices under the varying condition of noise magnitude.

3.3.2.4 *NMF Behavior on Non-Synergy-based Random Data Matrices*

A legitimate question to ask is whether NMF finds inherent structure in data or whether NMF creates artificial structure where none is present. To answer this, $m \times o$ ($m = 11$, $o = 200$) data matrices were randomly generated *without* using a synergy construction paradigm. The uncorrelated data values were selected from an exponential distribution. NMF was used to estimate synergy and source matrices that would best explain the data, and the propensity of NMF to create structure where none existed, at varying levels of noise corruption, was assessed by comparing the original random data matrices \mathbf{V} to the estimated data matrix \mathbf{V}_{est} .

3.3.2.5 *Effect of Over- and Underestimating the Number of Basis Vectors*

Finally, the effects of over- and underestimating the total number of synergies were investigated. The previously described simulations were carried out knowing the correct

number of synergies to estimate for the data matrix \mathbf{V} . However, this luxury is not afforded when analyzing experimental data – the correct number of basis vectors is not known. To examine the effects of over- and underestimation, random data matrices were constructed from a set of n known synergies and sources, corrupted with Gaussian noise of magnitude 25%, and NMF was used to estimate the original synergies, allowing the total number of synergies in each estimate to range between 1 and m ($m = 11$), the number of muscles in each synergy. The similarity of the original to estimated synergies and sources, along with the variance explained by the estimates, is reported.

3.3.3 Results

For each trial, similarities were assessed between the original synergies and sources and the estimated synergies and sources. The normalized dot product (NDP), shown in equation 3.10, was used to compare \mathbf{W}_{est} to \mathbf{W} , while the r^2 metric was used to compare \mathbf{H}_{est} to \mathbf{H} and \mathbf{V}_{est} to \mathbf{V} , where $\mathbf{V}_{est} = \mathbf{W}_{est}\mathbf{H}_{est}$. r^2 is the fraction of the variance of the original data set \mathbf{V} explained by the estimated data matrix \mathbf{V}_{est} .

$$NDP_{AB} = \frac{\bar{\mathbf{A}} \cdot \bar{\mathbf{B}}}{|\bar{\mathbf{A}}| \cdot |\bar{\mathbf{B}}|} \quad (3.10)$$

Original and estimated synergies were linked using a best-match algorithm in which the NDP was calculated for all combination original/estimate pairs. The pair with the highest NDP was deemed a match, and the process repeated until all estimated synergies were matched with an original synergy. The estimated and original sources were matched in accordance with the matching of the estimated and original synergies.

3.3.3.1 Effect of Varying the Number of Basis Vectors

Figure 3.4 (Estimate Plot: square symbol) shows the results of the NMF analysis on uncorrupted synergy-based data matrices \mathbf{V} . Reported for each number of synergies are the mean and one standard deviation of the similarities (NDP) between the original and estimated synergies (i), the mean and one standard deviation of the similarities (r^2) between the original and estimated sources (ii), and the mean and one standard deviation of the similarities (r^2) between the original and estimated data matrices (iii). There is a statistically significant monotonic decrease ($p < 0.01$) for the average similarity of the synergies as the total number of basis vectors is increased, along with an increase in the standard deviation of the similarities (i). Analysis of the source estimates also shows a statistically significant monotonic decrease ($p < 0.01$), and an even greater concavity in the curve of source number versus r^2 similarity (ii). Generally, it seems that NMF does a better job of estimating the synergy matrices \mathbf{W} than the source matrices \mathbf{H} (note the difference in the scale of the two graphs). Even with the discrepancies between the estimated and original synergy and source matrices, 100% of the data variance can still be explained given a high number of synergies. Actually, at all synergy levels, 100% of the data variance can be explained (iii). This is naturally because the original data set was left uncorrupted prior to analysis, and hence this particular simulation scenario represents the trivial case. For comparison, the same set of graphs are displayed for a 25% noise corruption level in Figure 3.5, and an example of a set of six original synergies and sources and their corresponding estimates are illustrated in Figure 3.6. While the same monotonic trend exists in the comparisons of synergies and sources, the variance explained by the estimated data set compared to the original clean and corrupted data sets have opposite monotonic trends as the number of synergies is increased. **The greater the number of**

synergies in the original construction, the less variance of the clean data set is explained, while the more variance in the corrupted data set is explained. The effect of additive noise on the estimation results are more thoroughly reported in 3.3.3.3.

3.3.3.2 *Effect of Random Synergies*

To determine if the NMF algorithm could find a corresponding source matrix for any synergy set and explain 100% of the data variance in \mathbf{V} , \mathbf{W}_{est} was held constant while \mathbf{H}_{est} was updated. Figure 3.4 (Random Plot: triangle symbol) shows the results of the NMF analysis. There appears to be a general increasing trend in the average similarity of the random synergies to the original synergies with an increase in the number of synergies. In contrast, there appears to be a general decreasing trend in the average similarity of the estimated pseudo-random sources to the original sources with an increase in the number of synergies. A two-sampled t-test revealed that for an uncorrupted data matrix \mathbf{V} , the similarities of the resultant synergies and sources from the NMF analysis (square symbol) to the original synergies and sources were statistically significantly greater than the similarity of the random synergies and pseudo-random sources (triangle symbol) ($p < 0.05$) at all number of synergies, except when the number of original synergies was one. The variances explained by the NMF estimates were also statistically significantly greater than that explained by the pseudo-random estimates at all number of synergies ($p < 0.05$). **These results suggest that the synergies and sources found by NMF represent structure inherent to the data, rather than being meaningless constructs and a simple result of statistical fitting of the data.** The effect of additive noise on these significance results is reported in 3.3.3.3.

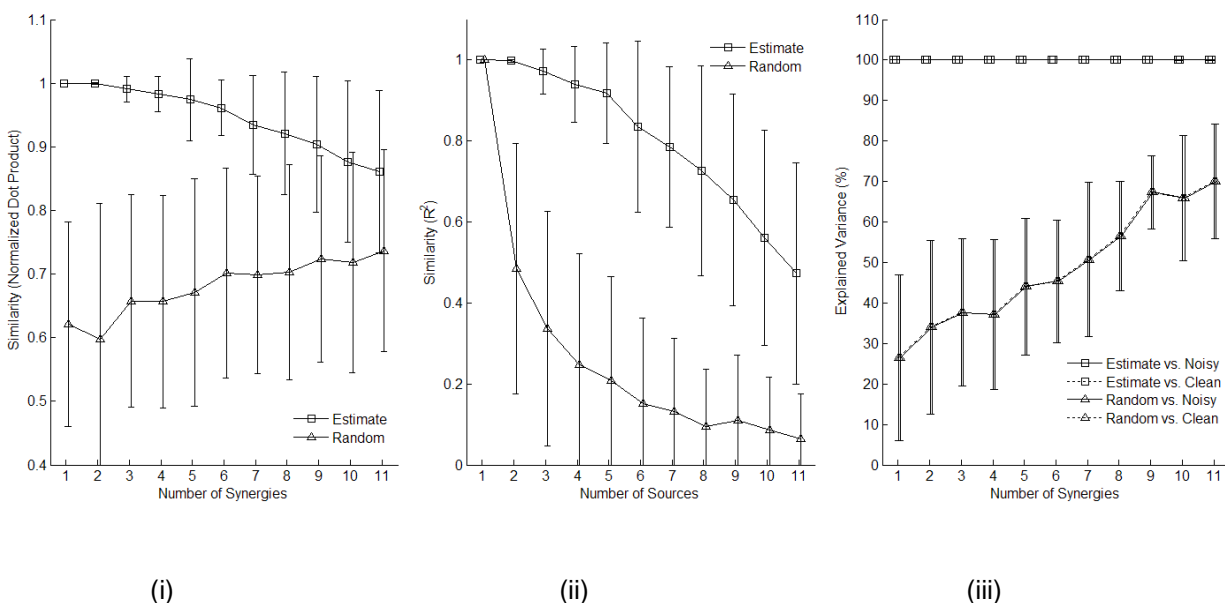


Figure 3.4. Effects of varying the number of basis vectors and of using random basis vectors.

The efficacy of NMF was investigated as the number of synergies used to construct the original data matrix was systematically increased. The similarity of the estimated synergies, the estimated sources, and the overall explained variance of the estimates are reported (square symbol). As the number of synergies increased, the average similarity of the estimates to the original synergies monotonically decreased (i), as did the average similarity of the estimates to the original sources ($p < 0.01$) (ii). Despite the discrepancy in the estimates at the higher number of synergies, 100% of the data variance was still explained by the estimates (iii). This however is a result of the fact that the original data was left uncorrupted, hence representing the trivial case. The effect of noise corruption on the estimates and variance explained is reported in 3.3.3.3. The ability to use pseudo-random synergies and sources to explain the data was also investigated (triangle symbol). The estimate similarities were statistically significantly greater than that of the pseudo-random synergies and sources ($p < 0.05$), suggesting that the results of the NMF analysis do not construct meaningless synergies and sources, but rather the deciphered synergies and sources represent structure inherent to the data.

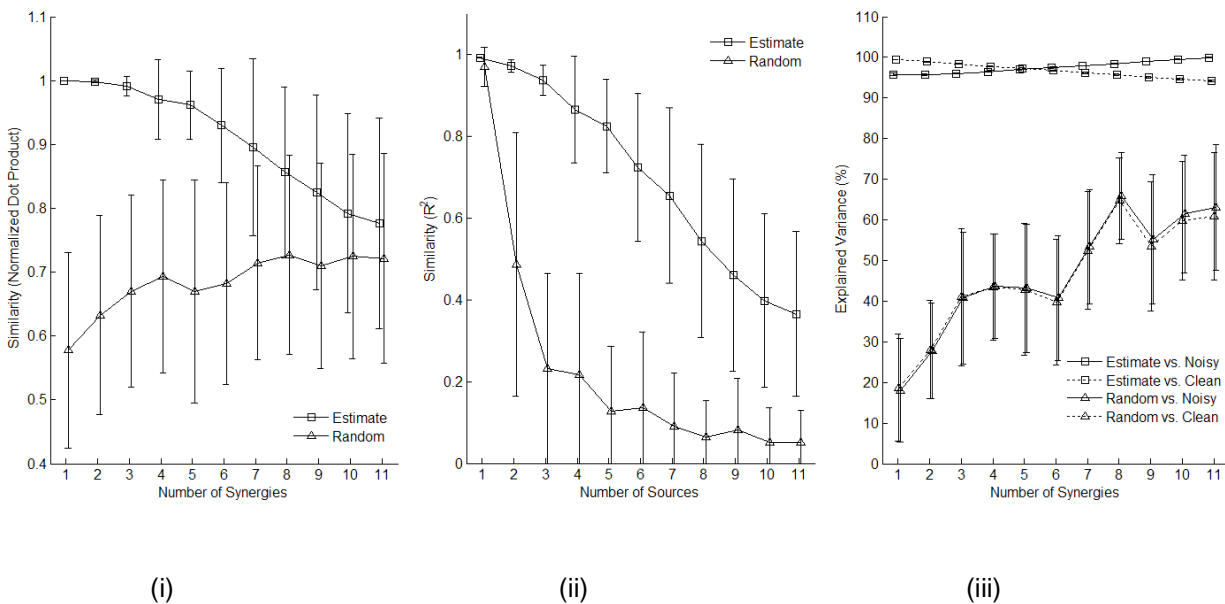


Figure 3.5. Efficacy of NMF at 25% noise corruption.

The results of applying NMF to data corrupted at a noise level of 25% are similar to that of uncorrupted data. There is still a monotonically decreasing trend for the similarities of both the estimated synergies and sources with increasing number of basis vectors. Of note is that as the number of basis vectors is increased, there is an increase in variance explained of the corrupted data, but a decrease in the variance explained of the uncorrupted data.

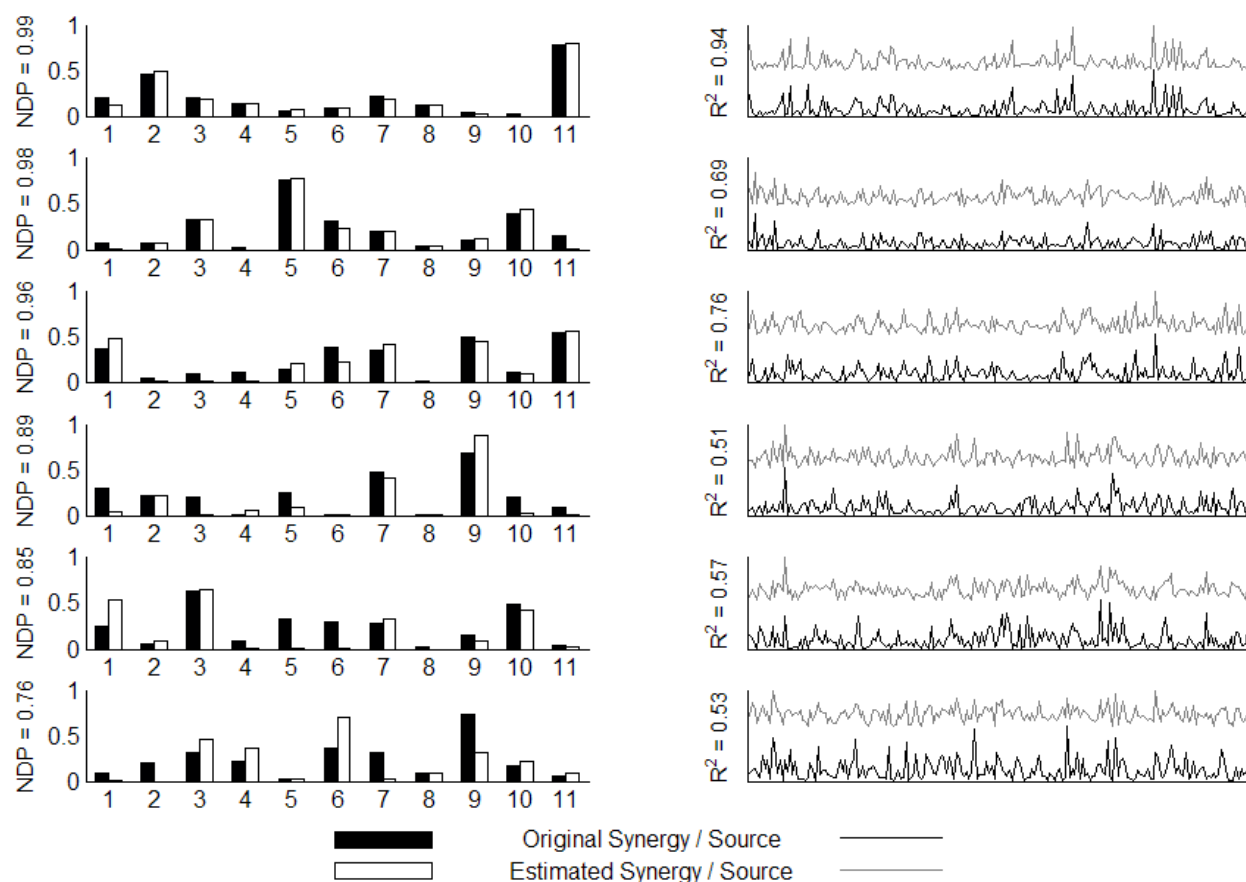


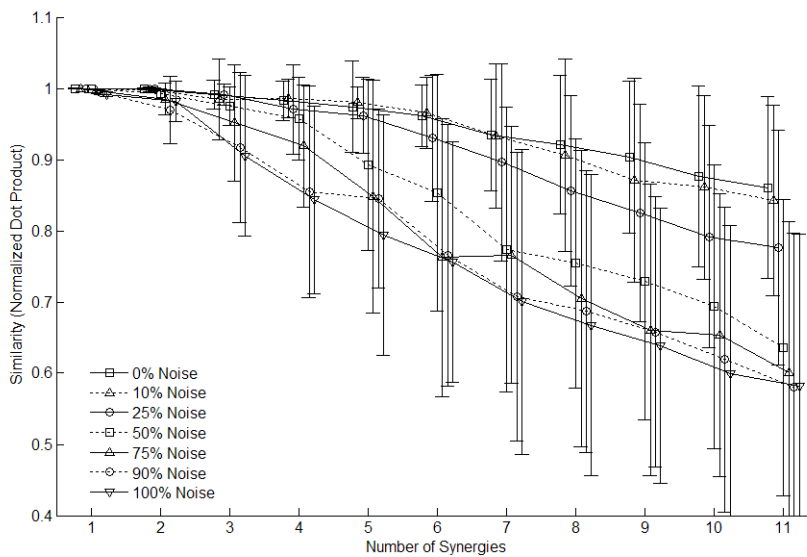
Figure 3.6. Original and estimated synergies and sources at 25% noise corruption.

Illustrated are the original and estimated synergies and sources from an NMF analysis of data originally constructed with six basis vectors and corrupted by 25% Gaussian noise. NMF was able to discern several of the synergies (left column) with high fidelity, primarily the first four, and to a lesser extent the last two. NMF was less successful in discerning the original sources (right column). Original and estimated synergies and sources were matched using a best-match algorithm described in the text. Similarity values (NDP and R^2) for each matched pair are displayed vertically oriented on the y-axis. R^2 of V_{est} relative to uncorrupted V was 96.93%.

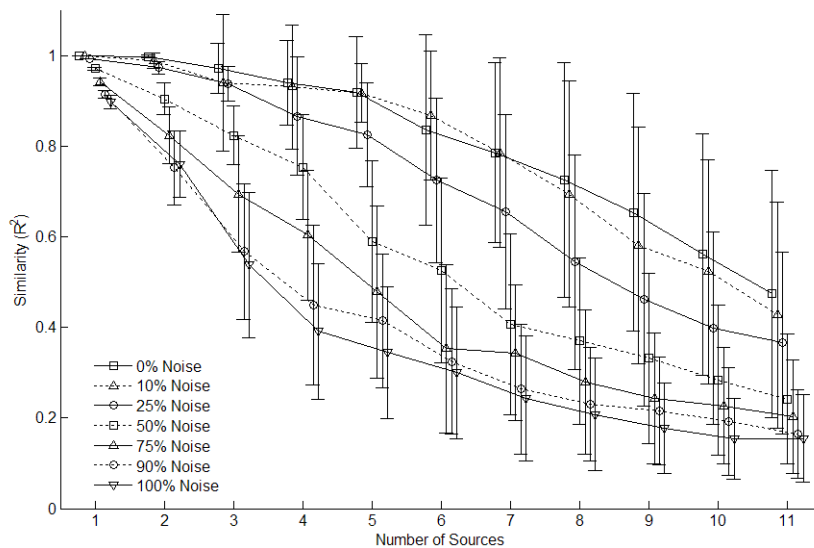
3.3.3.3 Effect of Additive Noise

The two previous sections primarily reported the ability of NMF to decipher the original synergies and sources of an uncorrupted EMG data matrix V . Clearly this represents the trivial

case because real biological data suffers from noise corruption of internal and external origins. It is more interesting and informative to investigate the ability of NMF to decipher the original synergies and sources of a corrupted EMG data matrix V . Figure 3.7 reports the effect of noise on the similarities of the estimated synergies and sources to the original synergies and sources, and Figure 3.8 reports the effect of noise on the variance explained in the corrupted and uncorrupted data sets by the estimates. As expected, increasing the amount of noise corruption of the original data matrix was detrimental to estimating the original synergies and sources at all number of synergies, as evidenced by the slope of the curves getting more and more negative with increasing noise. The same decreasing monotonic trend was exhibited at all levels of noise, where increasing the number of synergies used to construct the data decreased the overall similarity of the estimated to the original synergies and sources. Interestingly, as the number of synergies increased, the variance of the corrupted data explained by the NMF estimates monotonically increased to 100%, regardless of the noise level and the discrepancies in the synergies and sources. In contrast, the variance explained of the original clean data monotonically decreased for increasing noise level and synergy number. **These results suggest that while NMF is capable of finding synergies that explain 100% of the data variance regardless of noise level, it is not of benefit to do so because there comes a point when it is the noise that is being explained, rather than the underlying uncorrupted data. A 100% explanation of the data variance may be more indicative of noise fitting, particularly in higher dimensional data sets. In such a case, the deciphered synergies and sources can very well be significantly dissimilar to the authentic synergies and sources.**



(i)



(ii)

Figure 3.7. Effect of noise on NMF estimation of original synergies (i) and sources (ii).

For each noise level, an increase in the number of basis vectors negatively affected the ability of NMF to correctly identify the original synergy and source matrices. An increase in the noise magnitude used to corrupt the data was increasingly detrimental to NMF's ability to discern the original synergy and source matrices.

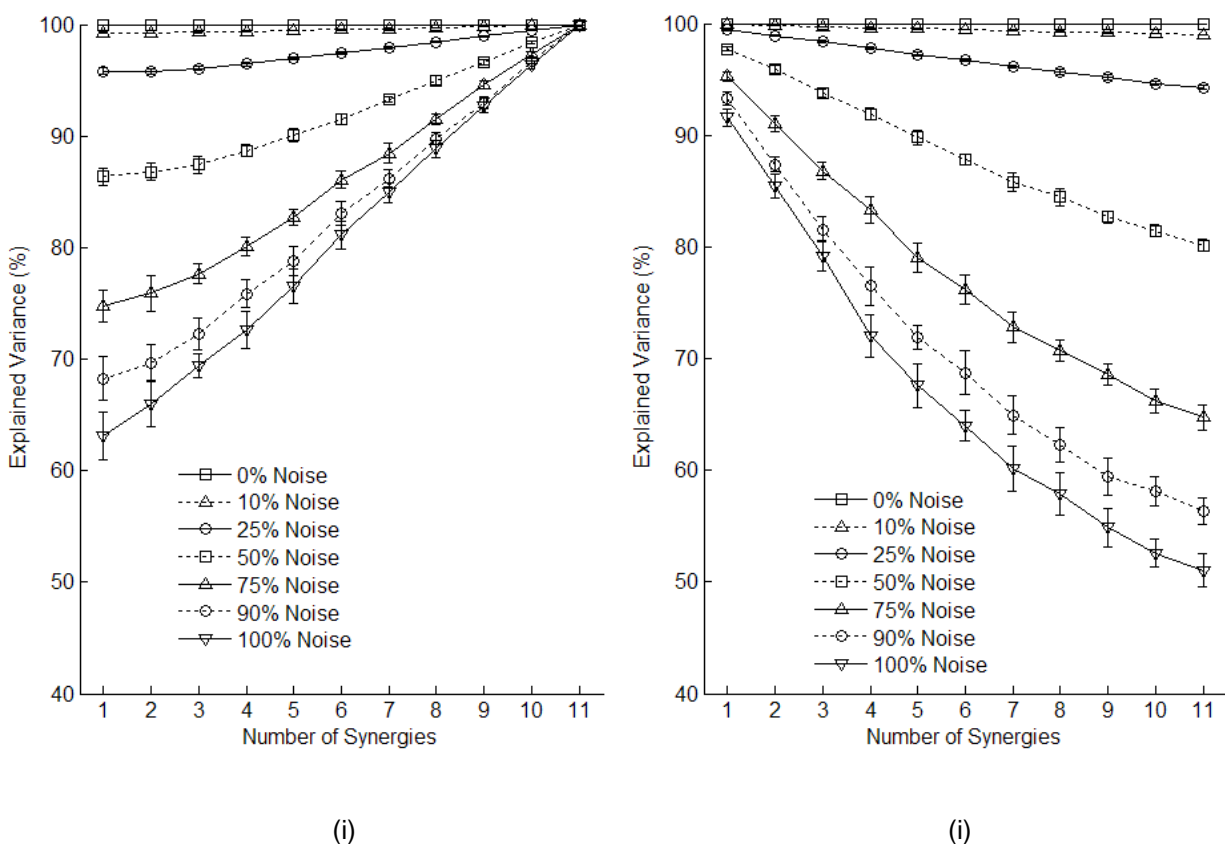


Figure 3.8. Effect of noise on NMF estimation of noisy (i) and uncorrupted (ii) data variances.

The effect of noise on the total noisy (i) and uncorrupted (ii) data variance explained by the NMF estimates is plotted versus number of synergies. For all noise levels, increasing the number of synergies increased the variance explained of the noisy data set, but decreased the variance explained of the uncorrupted data set. Interestingly, at all noise levels, 100% of the variance of the noisy data was explained using the maximum number of synergies, whereas this explained the least amount of variance of the uncorrupted data. This observation suggests that in low dimension-space data sets, NMF is able to tease out the structure in data, even at high levels of noise corruption. However, higher dimension-space data sets seem to be more negatively affected by noise.

3.3.3.4 NMF Behavior on Non-Synergy-based Random Data Matrices

Figure 3.9 reports the behavior of NMF on data matrices that were *not* constructed using a synergy-based paradigm. Varying amounts of noise were added to these matrices and NMF

was used to assess if any lower dimensional structure could be created. The figure shows the amount of variance of the original uncorrupted data sets that was explained by the data set as estimated by the resultant NMF basis vectors and corresponding inputs. It is of note that even in the uncorrupted data sets (0% noise), the dimensionality of the data sets could not be reduced below the original eleven (11) degrees-of-freedom without significantly affecting the variance explained. **This suggests that in a data set without inherent lower-dimensional structure, NMF will not artificially create this lower dimensional structure.** Rather, all degrees-of-freedom will be needed to adequately describe the data, in effect meaning that lower-dimensional basis vectors were not present in the data.

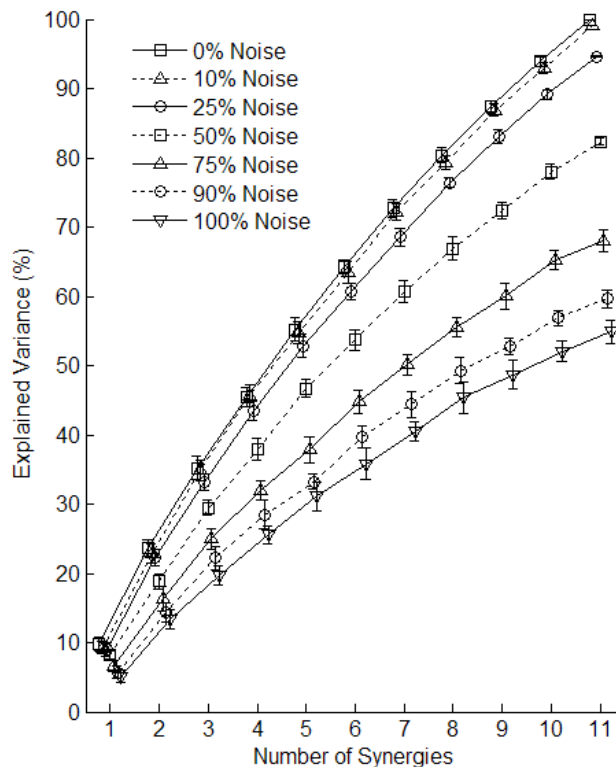


Figure 3.9. NMF behavior on data matrices *not* constructed using a synergy paradigm.

On data matrices not constructed from a synergy-based paradigm, there is little to no reduction of the control space dimensionality. Almost the full dimensionality of the muscle space is necessary to explain the majority of the data variance. This suggests that NMF parts-based approach will not artificially create synergy basis vectors where none exist in the data. Rather, the reduced dimensionality space of the NMF estimates synergies represents actual structure of the data.

3.3.3.5 Effect of Over- and Underestimated the Number of Basis Vectors

As previously mentioned, the above simulations, while informative, have an inherent advantage in that the number of basis vectors for estimation is known a priori to the analysis. This however is not the case when analyzing experimental data, which then creates the possibility of over- or underestimating the number of basis vectors. The effects of under- and

overestimating the number of basis vectors are reported in Figure 3.10 – Figure 3.12 and Figure 3.13 – Figure 3.15, respectively.

In Figure 3.10 – Figure 3.12, each group of bars represents the results of NMF underestimations of data matrices constructed from the specified number of original synergies. For example, in Figure 3.10, the sixth group of bars (labeled '6' on the x-axis), represents the resultant explained variances of the NMF analyses assuming one, two, three, four, five, and six basis vectors, as specified by the legend. As expected, Figure 3.10 shows that for each group of estimations, the explained variance of the original data set monotonically increased as the actual number of basis vectors used to construct the data matrix was approached. The similarities of the underestimated synergies to the original synergies are reported in Figure 3.11. The k estimated synergies were matched to the best k of n ($k < n$) original synergies, and the average similarities of the estimates to the originals were computed on those k synergies. Likewise, the similarities of the k estimated sources were directly matched to k of n original sources, and the average similarities are reported in Figure 3.12. A cursory analysis of the synergy similarities revealed that for a lower number of original synergies, the average similarity generally increased as the number of estimated synergies increased. With a higher number of original synergies, this monotonic trend was instead parabolic, with the correct estimate of the number of synergies actually producing a lower average similarity than some incorrect estimates. A cursory analysis of the source similarities showed that for a low number of sources, the trend is monotonically increasing with an increase of the number of estimated sources in each group, but is parabolic for larger number of sources. A one-way analysis of variance (ANOVA) with a subsequent multiple pairs test revealed to what extent the observed differences in explained variance, synergy similarity, and source similarity between underestimates and actual estimates were statistically significant. Statistical significance within

each group is determined by the 95% confidence intervals (CI) for the differences between explained variance, synergy similarity, and source similarity for each pair of estimated versus actual number of synergies. The intervals that do not include zero are considered to represent statistically significant differences while those that include zero represent statistically insignificant differences. For example, the 95% CI of the estimated variance difference of estimating 4 synergies when there are actually 5 synergies is (-4.17%, 1.50%). Because this interval includes zero, there is no statistically significant difference between the explained variances when estimating 4 versus 5 synergies when the actual number of synergies is 5. However, the 95% CI of the estimated variance difference of estimating 3 synergies when there are actually 5 synergies is (-6.76%, -1.09%). Because this interval does not include zero, there is a statistically significant difference between the explained variances when estimating 3 versus 5 synergies when the actual number of synergies is 5. Table 3.2 reports, for each actual number of synergies, which estimated synergies produced a statistically significant detriment to the explained variance, synergy similarity, and source similarity. Particularly for a lower number of synergies, the average explained variance and source similarity were less robust to underestimation, sometimes being significantly affected by underestimation of even one or two basis vectors. The average synergy similarity however, was more robust to the problem of underestimation, sometimes even not being significantly affected by underestimation of even two or three basis vectors.

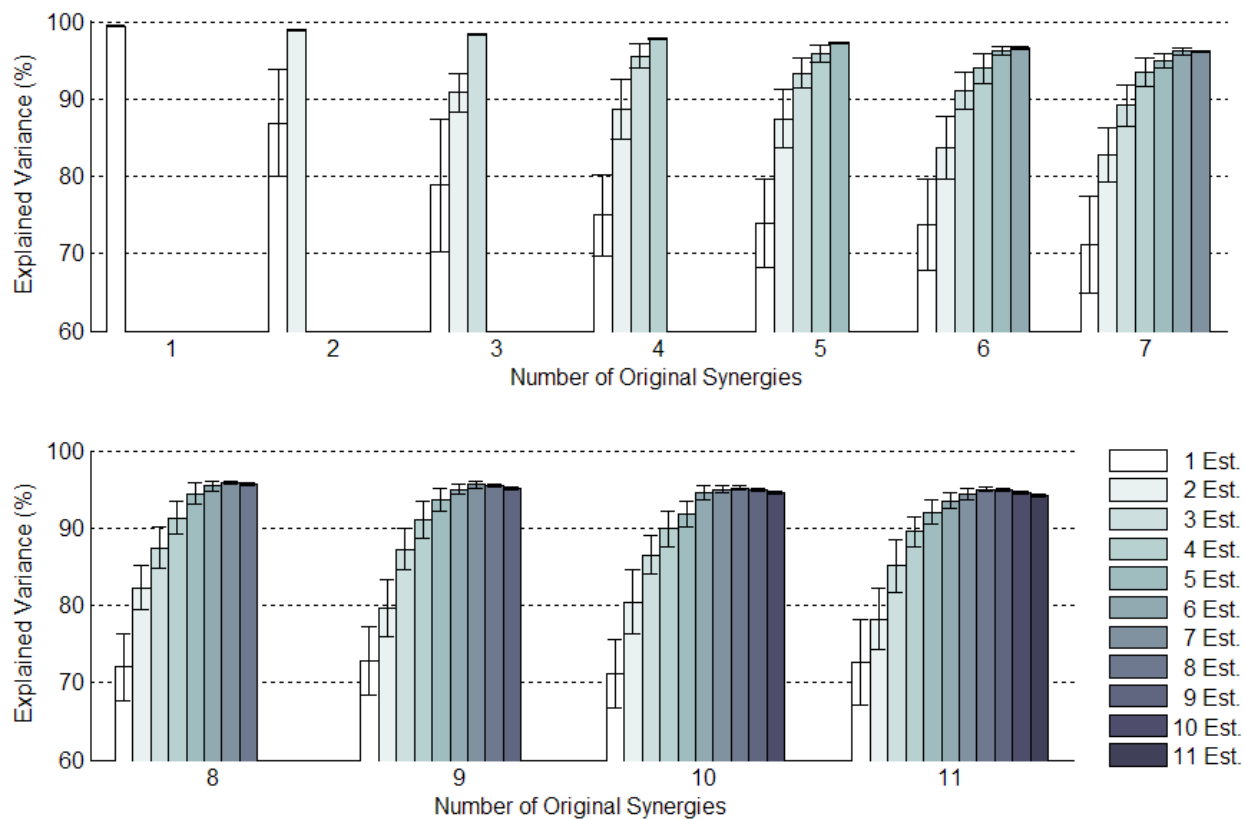


Figure 3.10. Explained variance underestimation results.

Data matrices were constructed from randomly generated exponential synergy / source matrix pairs, using $k = 1..11$ original synergies (x-axis). For each data matrix, NMF was used to underestimate the data matrix using $i = 1..k$ synergies. As the number of estimated synergies approached the actual number of synergies in the system, the variance explained by the NMF estimates steadily increased, although at higher level synergies, there was a slight decrease. One-way ANOVA revealed that for a larger number of synergies, the explained variance was robust to adverse effects of underestimations of even up to four synergies, while for a smaller number of synergies, the explained variance was only robust for one or two underestimations.

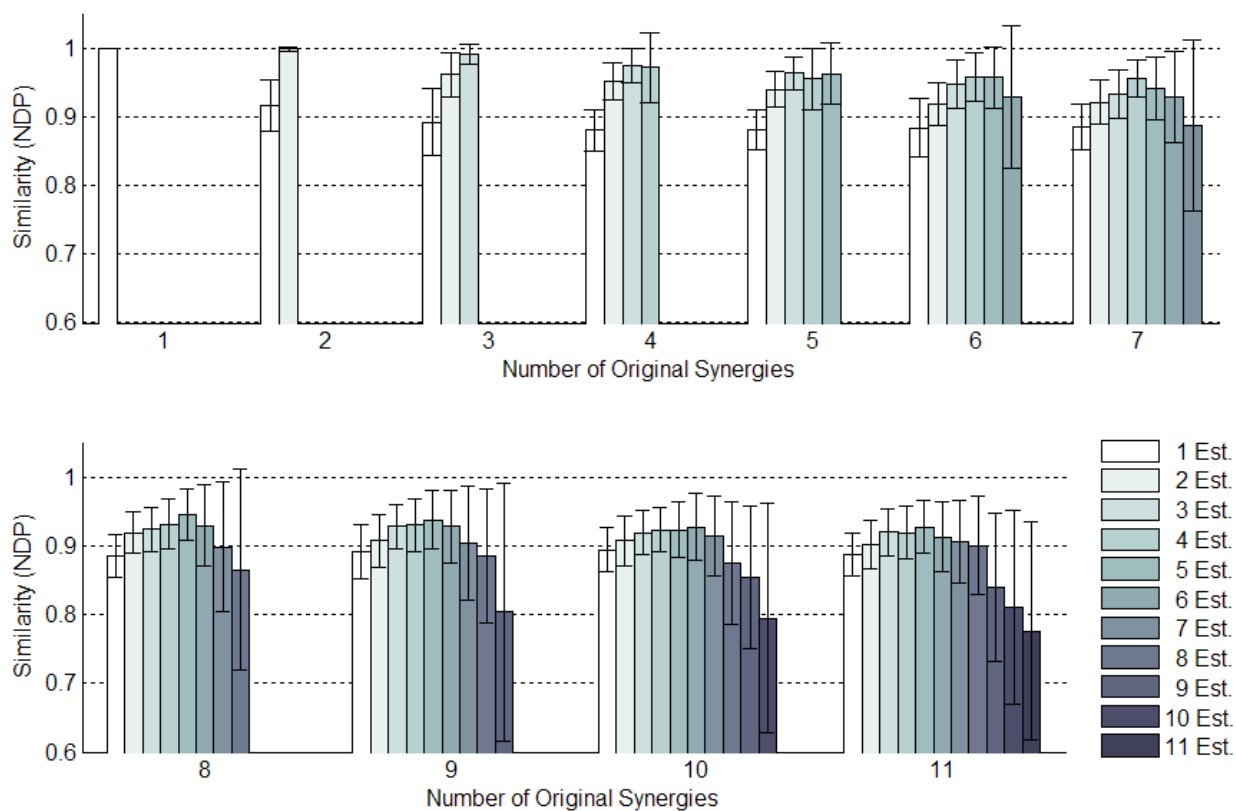


Figure 3.11. Synergy similarity underestimation results.

For each set of underestimations, the k estimated synergies were best-matched to the n original synergies (see text for details). The average similarity of the matched synergies is reported as the normalized dot product (NDP). A one-way ANOVA revealed that the similarity of the estimated to the original synergies was generally robust to negative effects of underestimation. With a higher number of original synergies, the average similarity was lower because, while several of the synergies were well matched, others were poorly estimated, decreasing the overall average similarity and increasing the standard deviations.

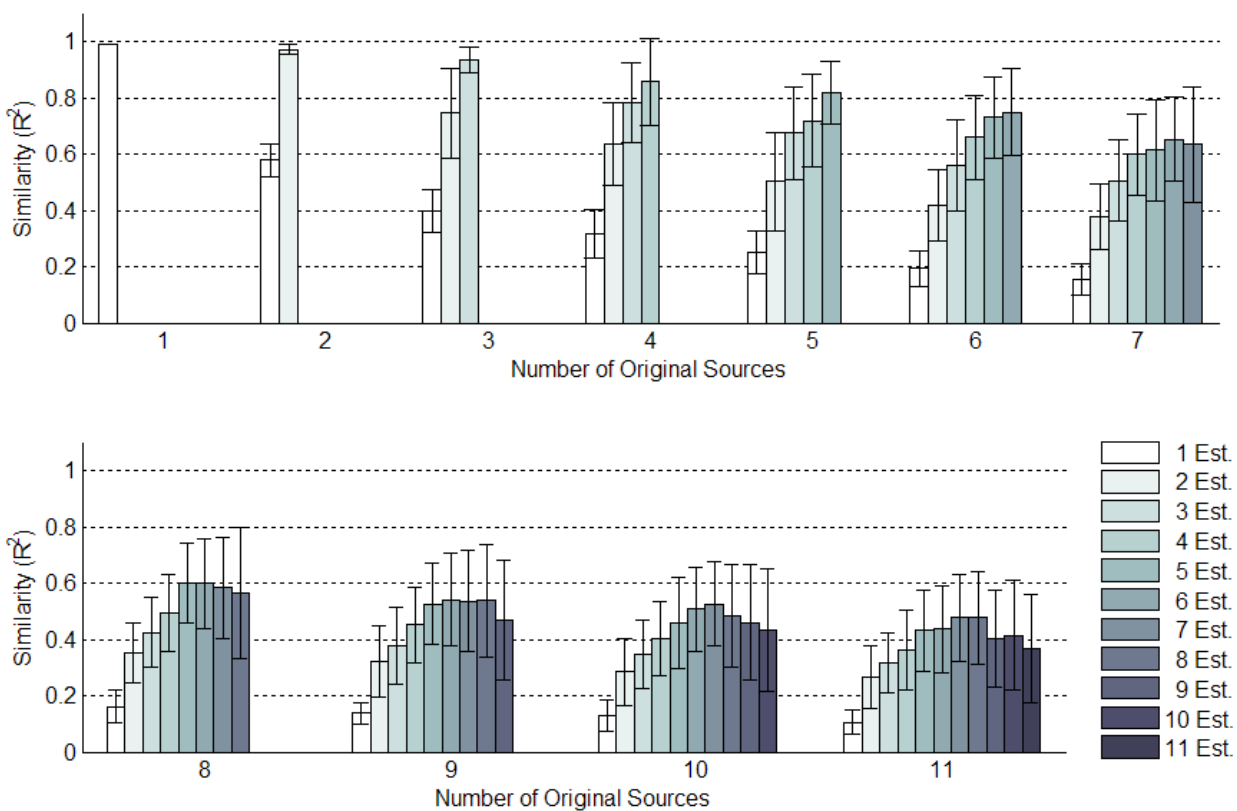


Figure 3.12. Source similarity underestimation results.

Sources were matched according to the results of best-matching the synergies. Similar to the effects of underestimation on the synergies, average source similarity was more robust at higher a higher number of original synergies than at a lower number of original synergies. At the lower number of synergies, dissimilarities do seem to be a direct result of underestimation, whereas with a higher number of synergies, dissimilarities seem to be more so a result of simply having a large number of basis vectors.

Table 3.2. One way ANOVA of underestimate simulation results.

# of Actual Synergies	<i>Underestimates Showing Statistically Significant Decrease in Explained Variance ($p < 0.05$)</i>	<i>Underestimates Showing Statistically Significant Decrease in Synergy Similarity ($p < 0.05$)</i>	<i>Underestimates Showing Statistically Significant Decrease in Source Similarity ($p < 0.05$)</i>
2	1	1	1
3	1, 2	1, 2	1, 2
4	1, 2	1, 2	1, 2, 3
5	1, 2, 3	1, 2	1, 2, 3, 4
6	1, 2, 3	1	1, 2, 3, 4
7	1, 2, 3	–	1, 2, 3
8	1, 2, 3, 4	–	1, 2, 3
9	1, 2, 3, 4	–	1, 2, 3
10	1, 2, 3, 4, 5	–	1, 2, 3
11	1, 2, 3, 4	–	1, 2

In Figure 3.13 – Figure 3.15, each group of bars represents the results of NMF overestimations of data matrices constructed from the specified number of original synergies. Overestimation did not have a large effect on the variance of the original data set explained by the NMF estimates; all overestimations still explained roughly between 95% and 100% of the data variance. The similarity of the estimated synergies to the original synergies did not seem to be largely affected as well by overestimation of one or to synergies, although greater overestimations did significantly affect the estimated synergy structures. The similarity of the sources was greatly affected by overestimating the total number of synergies by three or more. A one-way ANOVA with a subsequent multiple pairs test helped to quantify to what extent the differences were statistically significant. The statistically different pairs are reported in Table 3.3. This analysis revealed that there seemed to be a statistically significant detriment of explained variance with any overestimation of a one-synergy system. A closer analysis revealed that the upper and lower bounds of the 95% CI of the differences were on the order of

one thousandth of a percent. The ANOVA also revealed that the differences found in the similarity of synergies had 95% CI upper and lower bounds on the order of 0.02 (not percent – this is a unit normalized dimensionless metric). In contrast, the 95% CI upper and lower bounds for the source similarity differences ranged from on the order of 0.1 to 0.5 (not percent – this is a unit normalized dimensionless metric).

In summary, the under- and overestimation simulations revealed that underestimation is problematic in terms of explaining the variance of the full data set, whereas this is not an issue in overestimation. Neither under- nor overestimations of a small magnitude significantly negatively impaired NMF in discerning the underlying basis vectors. Both under- and overestimation were equally detrimental to determining the underlying sources. So while NMF is robust in determining basis vectors, its behavior in regard to discerning their respective time modulated weights is more erratic in the presence of significant over- and underestimation.

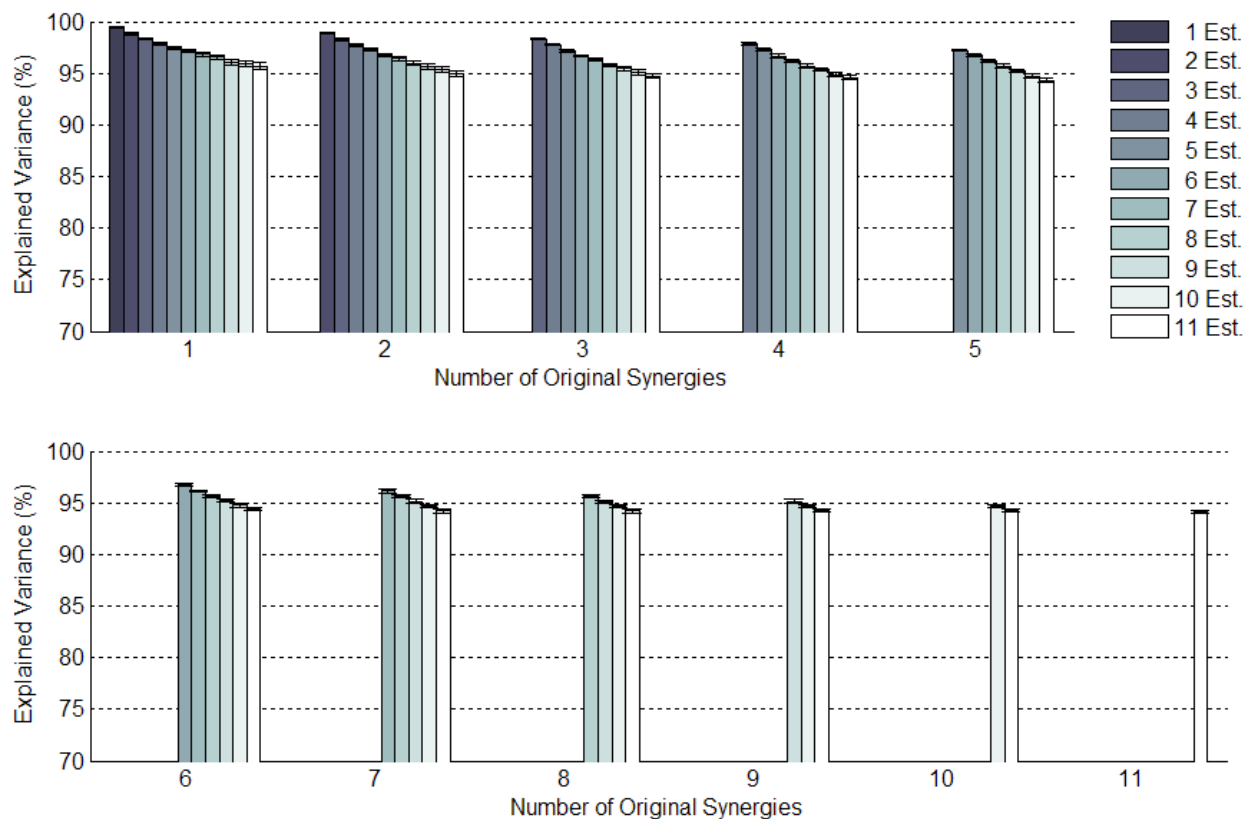


Figure 3.13. Explained variance overestimation results.

Data matrices were constructed from randomly generated exponential synergy / source matrix pairs, using $k = 1..11$ original synergies (x-axis). For each data matrix, NMF was used to overestimate the data matrix using $i = k..11$ synergies. As the number of estimated synergies diverges from the actual number of synergies in the system, the variance explained by the NMF estimates systematically decreases, with minimal variance. A one-way ANOVA revealed that for a given number of original synergies, any overestimation produced a statistically significant detriment to the variance explained by the estimates, although the actual differences between adjacent overestimates were relatively small.

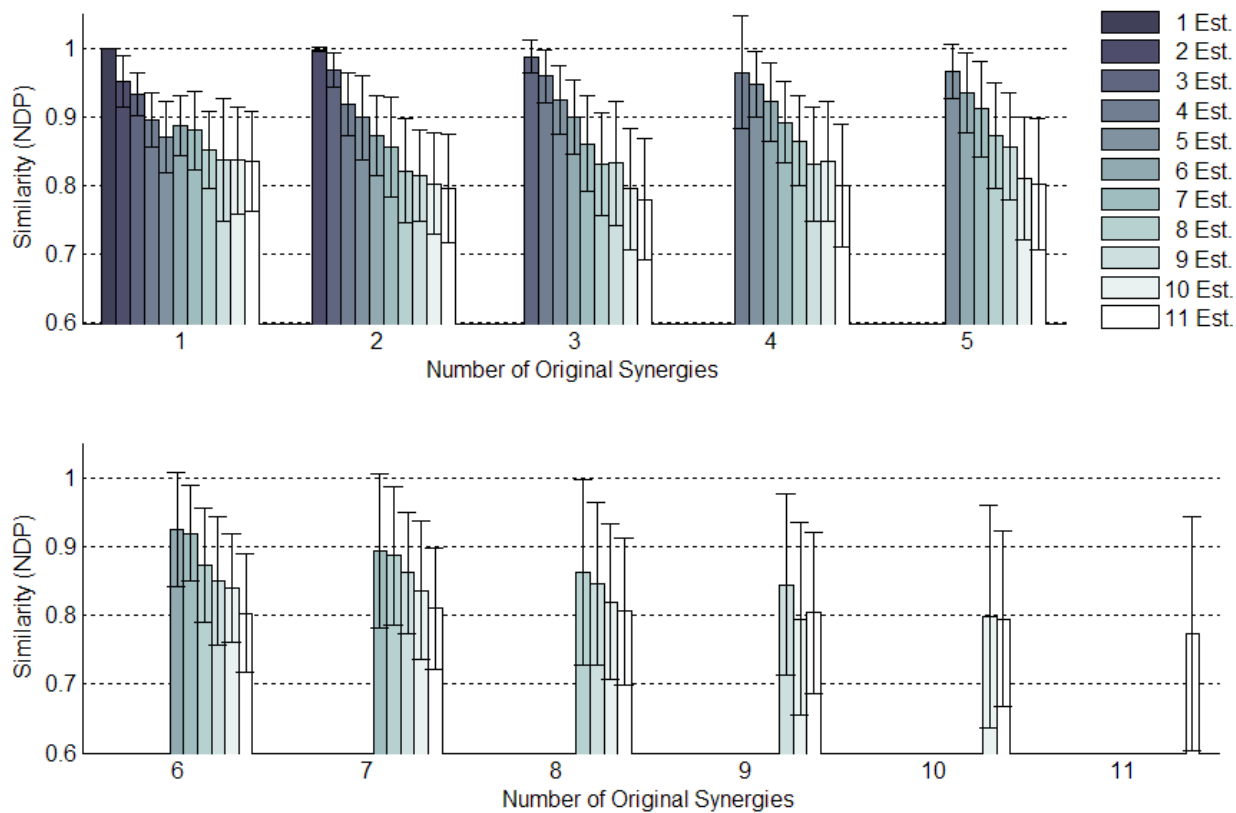


Figure 3.14. Synergy similarity overestimation results.

Overestimation resulted in a steady decrease in the average similarity of the estimated to original synergies. A one-way ANOVA showed that statistically significant difference existed as a result of overestimation of two or more synergies for any value of original number of synergies.

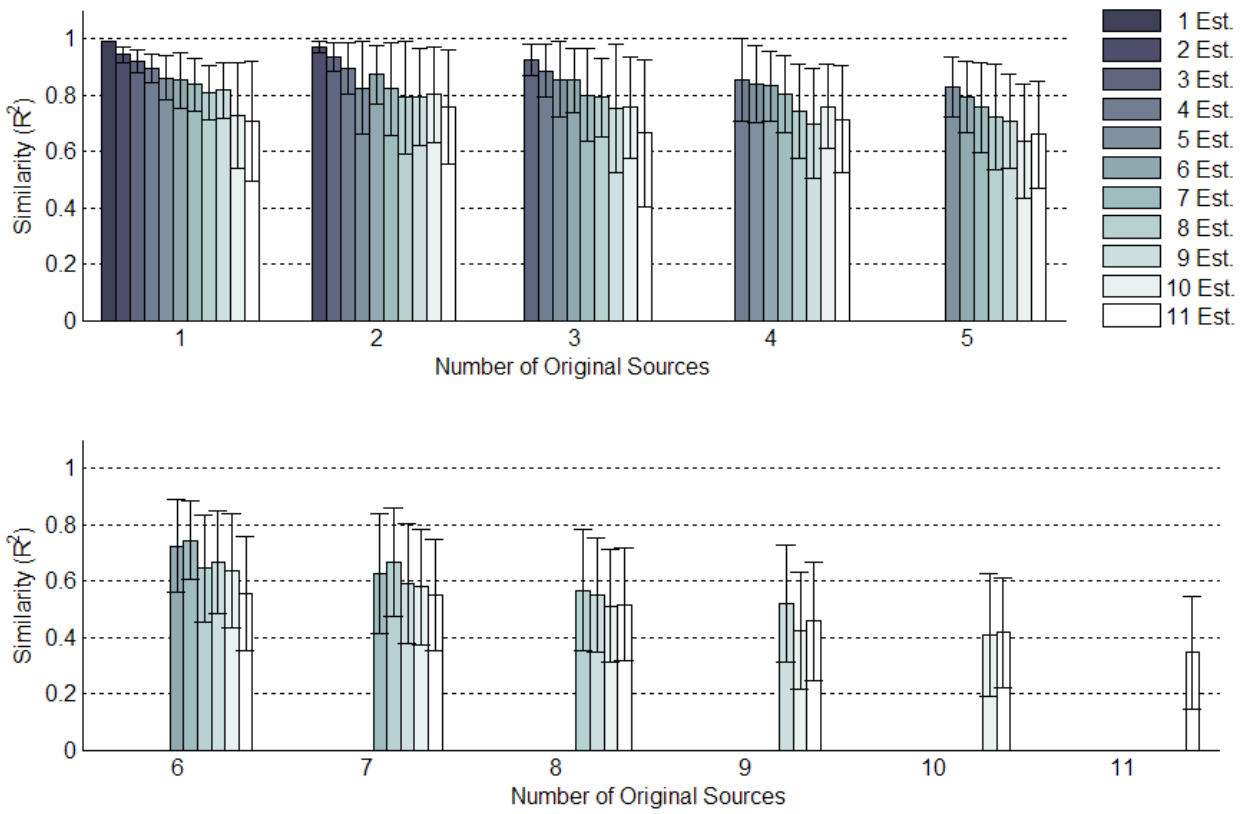


Figure 3.15. Source similarity overestimation results.

Sources were less affected by small overestimation than the synergies. According to the ANOVA analysis, the average source similarity was not statistically significantly affected by overestimations of up to about three synergies.

Table 3.3. One way ANOVA of overestimate simulation results.

# of Actual Synergies	Overestimates Showing Statistically Significant Decrease in Explained Variance ($p < 0.05$)	Overestimates Showing Statistically Significant Decrease in Synergy Similarity ($p < 0.05$)	Overestimates Showing Statistically Significant Decrease in Source Similarity ($p < 0.05$)
1	2, 3, 4, 5, 6, 7, 8, 9, 10, 11	3, 4, 5, 6, 7, 8, 9, 10, 11	5, 6, 7, 8, 9, 10, 11
2	3, 4, 5, 6, 7, 8, 9, 10, 11	4, 5, 6, 7, 8, 9, 10, 11	5, 6, 7, 8, 9, 10, 11
3	4, 5, 6, 7, 8, 9, 10, 11	5, 6, 7, 8, 9, 10, 11	7, 8, 9, 10, 11
4	5, 6, 7, 8, 9, 10, 11	6, 7, 8, 9, 10, 11	8, 9, 10, 11
5	6, 7, 8, 9, 10, 11	6, 7, 8, 9, 10, 11	7, 8, 9, 10, 11
6	7, 8, 9, 10, 11	8, 9, 10, 11	8, 10, 11
7	8, 9, 10, 11	10, 11	11
8	9, 10, 11	10, 11	–
9	10, 11	10, 11	10, 11
10	11	–	–

3.3.4 Discussion

The described simulations have investigated the efficacy of non-negative matrix factorization (NMF) in determining the underlying parts of a data matrix of the form $\mathbf{V} = \mathbf{WH} + \boldsymbol{\eta}$, where \mathbf{V} ($m \times o$) is the EMG data matrix, \mathbf{W} ($m \times n$) are the time-invariant muscle synergies (basis vectors), \mathbf{H} ($n \times o$) are the time modulated neural inputs (weighting coefficients), and $\boldsymbol{\eta}$ is a noise component. In the simulation investigating the effect of the original number of basis vectors on the estimations, increasing the number of basis vectors had an adverse effect on both the synergy and source estimations, but not on the variance of the original data set that was explained by the estimates. A question arises as to how NMF could perform poorly on the source estimates and yet still perfectly explain the data set, particularly with a large number of basis vectors. One can imagine a simple case in which \mathbf{V} consists of $m = 11$ muscles, is constructed from $n = 11$ synergies, and is then estimated assuming 11 synergies. In such a

situation, assuming zero noise corruption, the data could easily be explained by having each synergy / source pair be correlated to the activity of one and only one muscle. Hence, each synergy would be a unit vector directed along each respective axis in the muscle space, and each source would be the activity modulation of each respective muscle. As a result, there would be no reduction of system dimensionality, and in effect, no synergies. While this scenario is unlikely, it is mathematically possible. This hypothetical scenario, however, raises the question as to whether or not the synergies found by NMF are unique. Because NMF essentially functions by an iterative search algorithm (Lee & Seung, 2001), it is possible that the algorithm could end up in a local minimum instead of the global minimum, thereby potentially producing slight variations in the discerned synergies and sources. However, it has been reported in the literature that NMF produces consistent results when the data matrix consists of at least 50 – 100 responses (Tresch et al., 1999). **Hence, the slight variations are negligible assuming enough data observations.** Furthermore, when working with experimental data, NMF is repeatedly performed on the same data set under the same estimation conditions (number of basis vectors, criteria of convergence, etc...), and the estimate pair that produces the largest explained variance is deemed to be the global minimum (d'Avella et al., 2003).

Two simulation investigations addressed the fundamental question of whether or not the parts-based method of analysis is finding structure inherent to data or rather mathematically creating artificial structure. Directly speaking, are muscle synergies actually present in EMG data or are they the result of clever, albeit useful, matrix manipulations? First, fixed random synergies (W) and the corresponding estimated sources (H_{est}) were used to try to explain data constructed from known synergies and sources. **The fact that a source matrix could not be found for any synergy matrix to adequately explain the data suggests that the synergy / source matrix pairs are specific to the data set and not simply an artificial construct.**

Furthermore, finding synergy / source matrix pairs in experimental data would then lead to the conclusion that these matrix pairs have physiological origin and meaning, rather than being just an abstract mathematical concept. This statement is bolstered by the fact that when random data matrices were generated *without* using a synergy paradigm, the data matrix could not be reduced to a lower dimensional basis vector space i.e. the same number of dimensions were needed to construct the synergy space as was the muscle space. **Thus a data matrix constructed by synergies cannot be explained by any arbitrary synergy set, and NMF will not create lower dimensional synergies for a data matrix that has none.**

One continual question in any parts-based analysis is how to determine the appropriate number of basis vectors. The current practice is to determine this number empirically, performing the estimations assuming one, two, three, and up to m synergies, where m is the original dimensionality of the problem. Plotted against m is the variance (r^2) explained by the estimates, and a knee of the curve is determined, such that the addition of more synergies does not add significant information to the estimates. Rather the additions may simply explain corruption in the data (d'Avella et al., 2003, Ting & Macpherson, 2005, Tresch et al., 1999). Other studies have addressed this question in greater detail (Tresch et al., 2006). The contributions of these simulations, and specifically the analyses of over- and underestimation, have been to quantify to what extent synergies are preserved by NMF in the presence of improper estimation of the number of basis vectors. The finding that synergies are generally similar, even if over- and underestimation occurs by two synergies, is consistent with what has been reported in literature (Tresch et al., 2006). The importance of correctly estimating the number of synergies / sources, however, is underlined by the results showing the significant detriment over- and underestimation have on estimating the structure of the sources, and, with specific regard to underestimation, the overall data matrix.

Overall, the described simulations, in addition to the results of current literature, have shown NMF to be a useful tool in discerning actual structure in data matrices, and to be a suitable tool for analyzing experimental data. The limits of NMF, specifically with regard to source estimation, and its behavior in the presence of noise, are thus noted and are taken into consideration in the analyses of the experimental data of the experiments described in this manuscript.

4 Muscle Synergies as a Predictive Framework for EMG Patterns of Static Hand Postures

4.1 Introduction

The issue of muscle coordination is central to the control of multifunctional myoelectric prostheses. Much of the current research in the control of multifunctional myoelectric trans-radial prostheses has been focused on recognition of global muscle coordination patterns associated with specific movements. Many of these techniques have involved extracting time and frequency domain feature sets from the EMG signals (Hudgins et al., 1993), and using artificial neural networks (Gallant et al., 1998), fuzzy logic systems (Ajiboye & Weir, 2005, Chan et al., 2000), linear discriminant analyzers, Gaussian mixture models (Chan & Englehart, 2003, Huang et al., 2005), and the like to differentiate these parameter patterns one from another. While these approaches have achieved varying amounts of success, they are all dependent on a priori knowledge of the global muscle coordination patterns associated with specific movements. Hence new movements have to be pre-programmed before they can be recognized and controlled. A more versatile paradigm of control would be one in which a larger set of complex movements and muscle coordination patterns could be constructed from a lower dimensional set of basis coordination patterns. The work described in this chapter is part of a larger effort investigating the use of muscle synergies as a potential control paradigm of myoelectric trans-radial prostheses.

The central nervous system's (CNS) coordination of the many neuromuscular degrees-of-freedom (DOFs) associated with performing a task has been termed an ill-posed problem

because of the biomechanical and neuromuscular redundancies in the anatomical structure (Bernstein, 1967). It has been suggested in the literature that the CNS coordinates musculature to build complex motor patterns based upon an arguably finite set of fundamental control modules. These control modules, when combined sequentially or in parallel, produce the wide range of observable patterns of movement (Mussa-Ivaldi & Solla, 2004). Indeed, this idea is not new and has been postulated since the turn of the twentieth century (Bernstein, 1967, Bernstein, 1971, Sherrington, 1906) – only the nomenclature and proposed physiological manifestations have changed. Most recently, and directly applicable to myoelectric control, is the idea of fundamental muscle coordination patterns, termed muscle synergies (Bernstein, 1971, Tresch et al., 1999). Muscle synergies (i.e. groups of muscles whose activation levels are together specified) are an attractive idea because empirical evidence suggests that muscle patterns are potentially encoded in the activity of neurons in the M1 motor cortex (Holdefer & Miller, 2002, Kakei et al., 1999). Furthermore, muscle synergies have been shown to form the bases of complex muscle coordination patterns involved in activities such as kicking, swimming, and jumping of frogs (Bizzi et al., 2002, Cheung et al., 2005, d'Avella & Bizzi, 2005, d'Avella et al., 2003, Saltiel et al., 2001, Tresch et al., 1999, Tresch et al., 2002), postural standing and muscle responses to postural perturbations (Ting & Macpherson, 2005, Torres-Oviedo et al., 2006), and human arm movements (d'Avella et al., 2006, Soechting & Lacquaniti, 1989).

Specifically regarding hand control, several studies have presented evidence that postural activity associated with a wide variety of hand postures could be described by a kinematic synergy framework. Studies in typing (Soechting & Flanders, 1997), hand shaping for tool use (Santello et al., 1998), dynamic posture formation (Mason et al., 2001, Mason et al., 2004), and miming of the American Sign Language (ASL) alphabet (Jerde et al., 2003) have reported that the high dimensional kinematics of the hand can be described by a lower dimensional set of

basis postures, which are combined to produce the more complex joint positions. To the author's knowledge only one major study to date has examined similar synergistic-based dimensionality reduction paradigms with regard to the EMG activities associated with hand postures. This particular study aimed to describe the hand postures associated with the ASL alphabet and with grasping of everyday objects with a low-dimensional set of muscle synergies, and to align these muscle synergies with postural synergies of the hand (Weiss & Flanders, 2004). The investigators reported that the six-dimensional EMG patterns associated with the hand postures for grasping everyday objects could be described at a rate of 80-90% by a three or four dimensional set of muscle synergies.

One shortcoming of many of the studies reported in the muscle synergy literature is that though a basis set of synergies describe the observed data sets, there is little compelling evidence to suggest that the extracted muscle synergies have real physiological significance and hence are more than just a description of the observed data. Plainly speaking, these results have shown that muscle synergies form a *descriptive* framework for the EMG patterns observed during a set of tasks, but they do not explore if these synergies can form a *predictive* framework for a brand new set of tasks. Demonstrating a predictive framework is a more powerful assertion, and would more strongly suggest that muscle synergies are a reasonable control paradigm both for motor control by the CNS, and for myoelectric control. The investigation of whether or not muscle synergies form a predictive framework for a wide variety of hand postures would suggest that the synergies are robust and generalizable. Robustness and generalizability have been articulated by other investigators as necessary testable hypotheses for validation of the muscle synergy concept. Hence the aim of this work is **to investigate if muscle synergies form a robust lower dimensional framework for the**

prediction of the EMG patterns of new static hand postures. Specifically, the following questions will be answered.

- How many synergies are needed to complete this lower dimensional predictive framework, and how robust are these synergies?
- How many hand postures are needed to define the muscle synergy set of this framework?
- What is the predictive power of the established framework?

Working Hypothesis: A reduced set of muscle synergies describing a small set of static hand postures can predict the EMG patterns from a wide variety of new static hand postures with comparable accuracy.

Alternative Hypothesis: The EMG patterns of new hand postures cannot be accurately predicted using the framework defined by the generative hand posture set. The number of synergies needed to predict new hand postures exponentially grows with an increase in the size of the predicted set.

4.2 Methods

4.2.1 Subject Information

Seven healthy research subjects (one woman, six men, age 29.1 ± 11.0 yrs), all of which were self-described right-hand dominant, participated in this study. No subject had known history of any neuromuscular disorders. Subjects were obtained from a diverse population at the Rehabilitation Institute of Chicago and Northwestern University, and efforts were made to be consistent with the demographics of the Chicago area. All subjects gave informed consent to the procedures as approved by the Northwestern University Office for the Protection of

Research Subjects (NUOPRS) Institutional Review Board. Subjects are referred to by their Subject ID number (SID₁₋₇).

4.2.2 Electromyography

4.2.2.1 Hardware for EMG Data Collection

All EMG data was recorded using a Noraxon (Phoenix, AZ) Telemetry 2400R System™. The sixteen channel system includes a wireless transmitter-receiver system with an adjustable internal gain up to 2000 (transmitter: 2, receiver: 1000), a bandwidth of 20 – 1000 Hz, and an internal sampling rate of 3000 Hz. The analog signal from the receiver was then fed through a 12-bit A/D board, and digitally sampled at 3000 Hz. The data was recorded and visualized using an in-house custom built virtual instrument interface in National Instruments (Austin, TX) LabVIEW Developer's Environment ver 7.2. Raw EMG was saved in a standard ASCII file for further processing.

4.2.2.2 Selection of Recorded Muscles

Given that both intrinsic and extrinsic muscles participate in the control of the hand, it would be ideal to record from all involved muscles to best characterize muscle activity during the various hand postures. However, the muscular characterization of hand posture was limited to eight extrinsic and five intrinsic hand muscles / muscle groups. The chosen extrinsic muscles were *flexor digitorum superficialis (FDS)*, *flexor digitorum profundus (FDP)*, *extensor indicis proprius (EIP)*, *extensor digitorum communis (EDC)*, *extensor digiti minimi (EDM)*, *extensor pollicis longus (EPL)*, *flexor pollicis longus (FPL)*, and *abductor pollicis longus (APL)*. The chosen intrinsic muscles were *abductor pollicis brevis (APB)*, *flexor pollicis brevis (FPB)*, *opponens pollicis (OP)*, *abductor digit minimi (ADM)*, *flexor digit minimi (FDM)*, and *first dorsal*

interosseus (FDI). Table 4.1 lists these muscles and their biomechanical functions, and shows their anatomical locations. The activity of the extrinsic muscles and that of *FDI* were recorded using intramuscular electrodes, while the activities of the remaining muscles were recorded using standard bipolar Ag/AgCl surface electrodes. The choice of selected muscles and selected recording methods were for two reasons. First, subject comfort was of great importance, as was minimizing subject pain caused by the large number of needle sticks required by the protocol (a minimum of nine fine-wire placements). Second it has not been quantitatively shown how the placement of surface and, more so, fine-wire needles affect hand shape and grasping. However, it seems reasonable to assume that there is an effect, and the effect would possibly be greater if needle electrodes were placed in the intrinsic muscles as compared to the extrinsic muscles. Thus, intramuscular recording was limited to the extrinsic hand muscles. Since the hand is a small space and the intrinsic muscles are small, there existed a risk of cross-talk information by using surface electrodes in lieu of intramuscular fine-wire electrodes. In light of the high probability of cross-talk between neighboring muscles, ***abductor pollicis brevis (APB)*, *flexor pollicis brevis (FPB)*, and *opponens pollicis (OP)*** were considered to be one muscle group (TE – thenar eminence) for the purposes of these investigations, and were recorded as such. Likewise, ***abductor digit minimi (ADM)* and *flexor digit minimi (FDM)*** were considered to be one muscle group (HTE – hypothenar eminence) and were recorded as such.

Table 4.1. Recorded Intrinsic and Extrinsic Muscles of the Hand

	Muscle	Function
EXTRINSICS	flexor digitorum superficialis (FDS)	flexes 2 nd phalanx of fingers (at PIPs); continued contraction flexes 1 st phalanxes (at MCPs) and wrist
	flexor digitorum profundus (FDP)	flexes terminal phalanx (at DIP); continued contraction flexes other phalanxes and wrist
	extensor indicis proprius (EIP)	extension of index finger (independent of other fingers)
	extensor digitorum communis (EDC)	finger extension; abduction of index, ring, and little fingers, and to a lesser extent, the wrist
	extensor digit minimi (EDM)	extension of little finger
	extensor pollicis longus (EPL)	extension of 2 nd phalanx of thumb (at IP)
	flexor pollicis longus (FPL)	flexes 2 nd phalanx of thumb (at IP); continued contraction flexes 1 st thumb phalanx
	abductor pollicis longus (APL)	thumb abduction; extension of 1 st thumb phalanx (at MCP); wrist abduction
INTRINSICS	flexor pollicis brevis (FPB)	flexes and adducts the thumb
	abductor pollicis brevis (APB)	abducts the thumb to form right angle with palm
	opponens pollicis (OP)	flexes the thumb metacarpal bone
	first dorsal interosseus (FDI)	abducts the index finger from the midline of the hand
	flexor digiti minimi (FDM)	flexes the little finger
	abductor digit minimi (ADM)	abducts the little finger and flexes the proximal phalanx

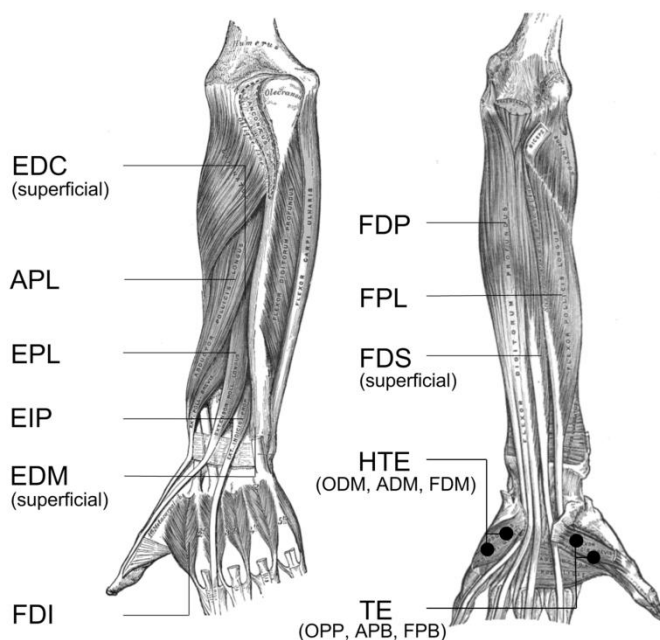


Figure 4.1. Electromyography protocol.

EMG signals were recorded from eleven extrinsic and intrinsic muscles. Intramuscular (fine-wire) EMGs were recorded from FDP, FDS, EDC, EDM, EIP, EPL, APL, FPL, and FDI. Surface EMGs were recorded from TE (consisting of the intrinsic thumb muscles) and HTE (consisting of the intrinsic pinky finger muscles). Needle electrode placements were verified using low current electrical stimulation.

4.2.2.3 Surface and Fine-Wire Electrode Placements

All muscles in the subjects' dominant arms were initially located by palpation while subjects performed selected hand test maneuvers designed to primarily contract the muscle of interest. These test maneuvers were referenced from standard clinical electromyography (Perotto & Delagi, 2005) and anatomy (Gray, 1973) texts. After marking the insertion sites with a non-indelible marker, a standard disposable thirty-seven gauge monopolar tungsten probing needle was used to refine insertion locations and to determine the appropriate insertion depth. Visual and audio feedback of the firing of motor units was sometimes used to aid in location of the muscle sites. Bipolar fine-wire electrodes (inter-electrode distance on the order of 2 mm) were

then inserted mid-muscle belly using Basmajian's single needle technique (Basmajian & Stecko, 1962), and in accordance with the electromyography text. Electrode placements were verified by observing the expected kinematic responses to low current electrical stimulation. Standard surface electrodes were placed over the thenar (TE) and hypothenar (HTE) intrinsic hand muscle groups.

4.2.3 Tasks and Data Collection

Subjects were seated upright in a comfortable chair with the dominant arm and wrist supported. Wrist movement was not restricted. Subjects were instructed to shape their dominant hand into each of thirty-three static letters and numbers of the American Sign Language (ASL) set (Figure 4.2). Dynamic letters 'J' and 'Z' were omitted, along with the number '0', which was visually the same as the letter 'O'. During the electromyography phase of the study (prior to data collection), subjects familiarized themselves with the hand positions of the ASL set so that they would be consistent in performing the hand postures during the data collection phase. Published literature has suggested that this learning phase gives ample time for subjects to learn to produce consistent hand postures congruent with that of fluent ASL spellers (Jerde et al., 2003, Weiss & Flanders, 2004).



Figure 4.2. Mimed letters and numbers of the American Sign Language (ASL) set.

Subjects shaped their hand into each of thirty-three static letters and numbers of the ASL set. Static letters were only used in the experiment protocol. Hence, the letters 'J' and 'Z' were omitted from the study. Also, the number '0' was omitted because it was visually the same as the letter 'O'. Letters were presented to subjects in randomized order.

Initiated by an audio cue, subjects were shown on a computer screen the letter and hand position to replicate. Subjects had eight seconds to create and hold the specified hand posture. Subjects typically took one to two seconds to create the posture, and then held it for the remaining six to seven seconds. At the end of the eight second period, the visual aid was cleared and an audio cue instructed the subjects to return to the rest position. The next letter was presented after a two second rest period. This rest period served to washout any potential effects the previous hand posture may have on the motor strategy used to produce the next hand posture. Subjects were instructed to only apply as much force necessary to maintain the hand in the given posture, and specifically were instructed to not co-contract their muscles beyond this required level. Hence, the hand position and force level of posture was self-

selected by each subject. The investigator monitored subjects' performances for consistency of hand positions with the visual aid. The presentation order of the ASL set was completely randomized so as to remove any effects that order could potentially have on the muscle coordination patterns used to produce the hand postures. Each subject completed seven trials of miming the full ASL set, with a five minute break given in between each trial to minimize the possibility of fatigue. EMG activities were recorded from the eleven aforementioned muscles during the entire phase of ASL miming. Time, ASL letter, and EMG voltages were saved to an ASCII file for later processing.

4.2.4 Data Analysis

4.2.4.1 Pre-processing

All EMG signals were filtered using a sixth-order Butterworth bandpass with [low, high] cutoff frequencies of [30, 600] Hz, and a second-order Butterworth notch filter with [low, high] cutoff frequencies of [59.5, 60.5] Hz. To only capture the static phase of each mimed ASL posture, only the portions of EMGs from $t = 2.5$ sec to $t = 5$ sec per posture were used for the remaining analyses (Figure 4.3). The root-mean-square (RMS) values of the resulting signals were computed over this range of static miming. This RMS value was used as the representative EMG activity for each muscle. The RMS values were normalized relative to the resting and maximum activities of the respective muscles observed during maximal voluntary contraction (MVC) tests, such that all resultant muscle activities ranged between zero and one. Each miming of posture was represented as an eleven-dimensional vector in normalized muscle space, with each dimension corresponding to one of the recorded muscles. Hence each full trial of a set of mimed postures was represented as a data matrix $V_i \{i = 1..7\}$ of dimension 11×33

(*muscles x number of postures*). The full data matrix V of recorded activity for each subject was thus of dimension 11×231 .

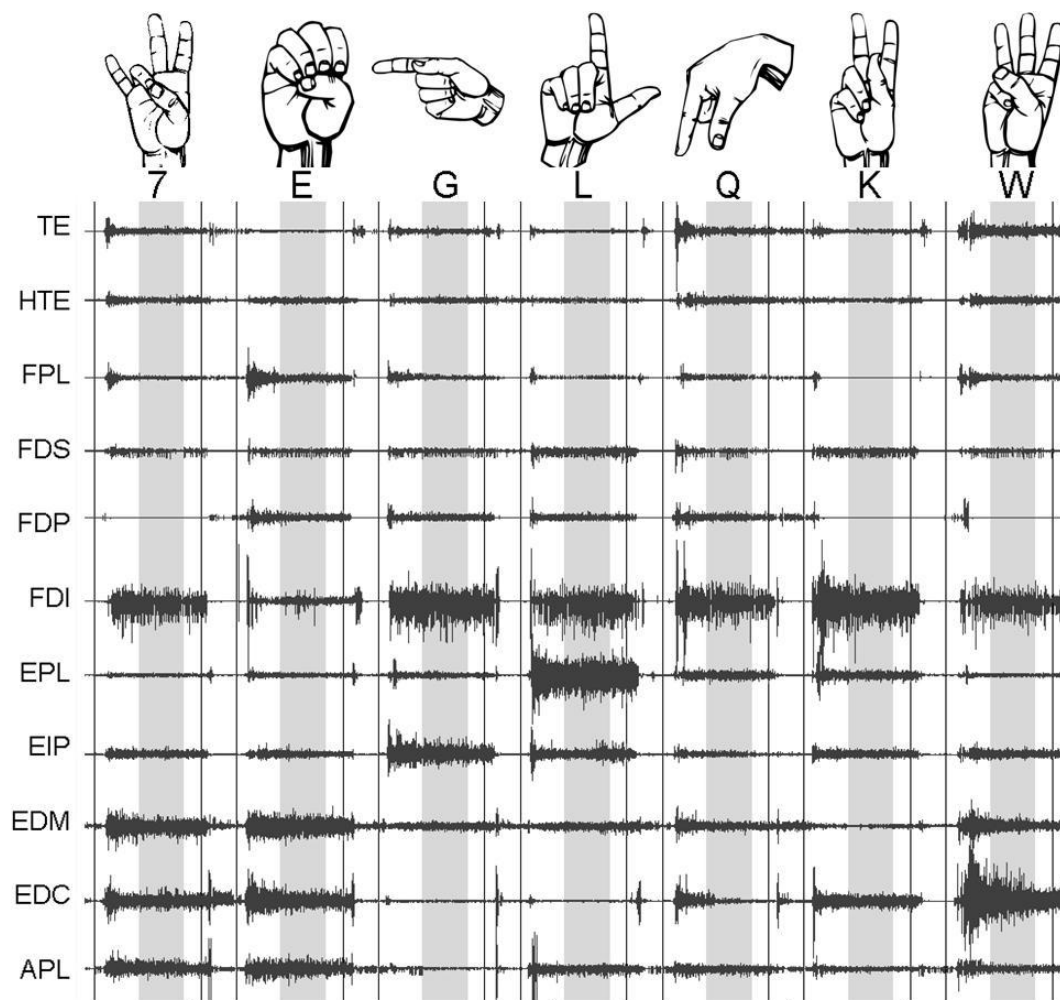


Figure 4.3. Sample of recorded EMG signals during miming of ASL postures.

Subjects formed and held the instructed postures for 8 seconds, but only the steady state portion from $t = 2.5$ sec to $t = 5$ sec was analyzed. The thirty-three postures were presented in random order within each trial, with a total of seven trials. Recorded EMGs were bandpass and notch filtered, and the normalized RMS was calculated as the representation of muscle activity during the analyzed time frame.

4.2.4.2 EMG Pattern Separability and Repeatability – Discriminant Analysis

A discriminant analysis (Santello et al., 1998, Santello & Soechting, 1998) was first performed to assess how distinct the EMG patterns associated with each posture were from one another, and consequently, how repeatable they were between trials. This analysis represents the data in multidimensional muscle space and finds linear discriminant functions that serve to maximize the ratio of the inter-group to intra-group variances, for the purposes of maximally separating the data (Balakrishnama & Ganapathiraju). In this work, discriminant analysis was implemented in two stages: first using all data points, and then second using a leave-one-out cross-validation method. It is this second implementation that tests the validity of the discriminant groups by assessing the accuracy of classifying each posture in the proper group. Reported for each subject are the classification accuracies using stage one (complete implementation) and stage two (cross-validation implementation).

4.2.4.3 Descriptive Synergy Analysis

Non-negative matrix factorization (NMF) was used to determine a set of dimensionally reduced basis vectors that could describe the full thirty-three letter, 7 trial EMG data matrix \mathbf{V} of dimension 11×231 . The descriptive NMF algorithm is described in detail in section 3.2.2.3 and illustrated in Figure 4.4 (left hand side). Briefly, estimates of the synergy (\mathbf{W}_{est}) and source (\mathbf{H}_{est}) matrices are determined by beginning with random estimates and then updating the estimates using equation 3.9. Updating continues until an optimality criterion, in this case the Euclidean distance norm (equation 3.8) of the difference between the recorded data matrix (\mathbf{V}) versus the estimated data matrix ($\mathbf{W}_{est} \times \mathbf{H}_{est}$), is constant within a specified $\epsilon = 1e-5$ for $s = 20$ consecutive iterations.

Given a specified number of synergies n to estimate, the full data matrix (\mathbf{V}) was randomly split into generation (\mathbf{V}_{gen}) and cross-validation (\mathbf{V}_{val}) sets such that five trials of each posture were in the generation set and two were in the cross-validation set. Synergy ($\mathbf{W}_{n,gen}$) and source ($\mathbf{H}_{n,gen}$) estimates were derived from the generation data set. $\mathbf{W}_{n,gen}$ was then applied to the validation data set to generate $\mathbf{H}_{n,val}$, where the update rules of equation 3.9 were applied to $\mathbf{H}_{n,val}$ but not $\mathbf{W}_{n,gen}$. To assess how much information was actually contained in the calculated synergies represented by $\mathbf{W}_{n,gen}$, the cross-validation data (\mathbf{V}_{val}) was also analyzed using a randomly generated exponentially distributed synergy matrix $\mathbf{W}_{n,rnd}$. $\mathbf{W}_{n,rnd}$ was also not updated while the corresponding $\mathbf{H}_{n,rnd}$ was updated according to equation 3.9. For each set of $\{\mathbf{V}, \mathbf{W}_{gen}, \mathbf{H}_{gen}\}$ matrices, the overall accuracy of the estimates was quantified by the variance explained of the original data set \mathbf{V} by the synergy and source estimates. The metric of explained variance chosen is the standard coefficient of determination r^2 , which ranges from 0 (i.e. 0% explained variance) to 1 (i.e. 100% explained variance). For a given number of synergies n , the descriptive synergy analysis was run 50 times, and the trial that returned the greatest variance explained of \mathbf{V}_{val} was the selected trial.

With experimental data, the correct number of synergies is unknown. Hence, the descriptive synergy analysis described above was performed with the estimated number of synergies n allowed to range from 1 to 13, resulting in an explained variance (EV) curve that related explained variance to number of estimated synergies. The correct number of synergies was determined to be the knee of this curve i.e. the point at which estimating additional synergies did not significantly explain more of the data variance. Specifically, this was determined to be the smallest n such that a linear fit of the EV curve, from n to 13, had a residual mean square error less than $5e-5$. Reported for each subject are the number of estimated synergies and the variance explained by the synergy set.

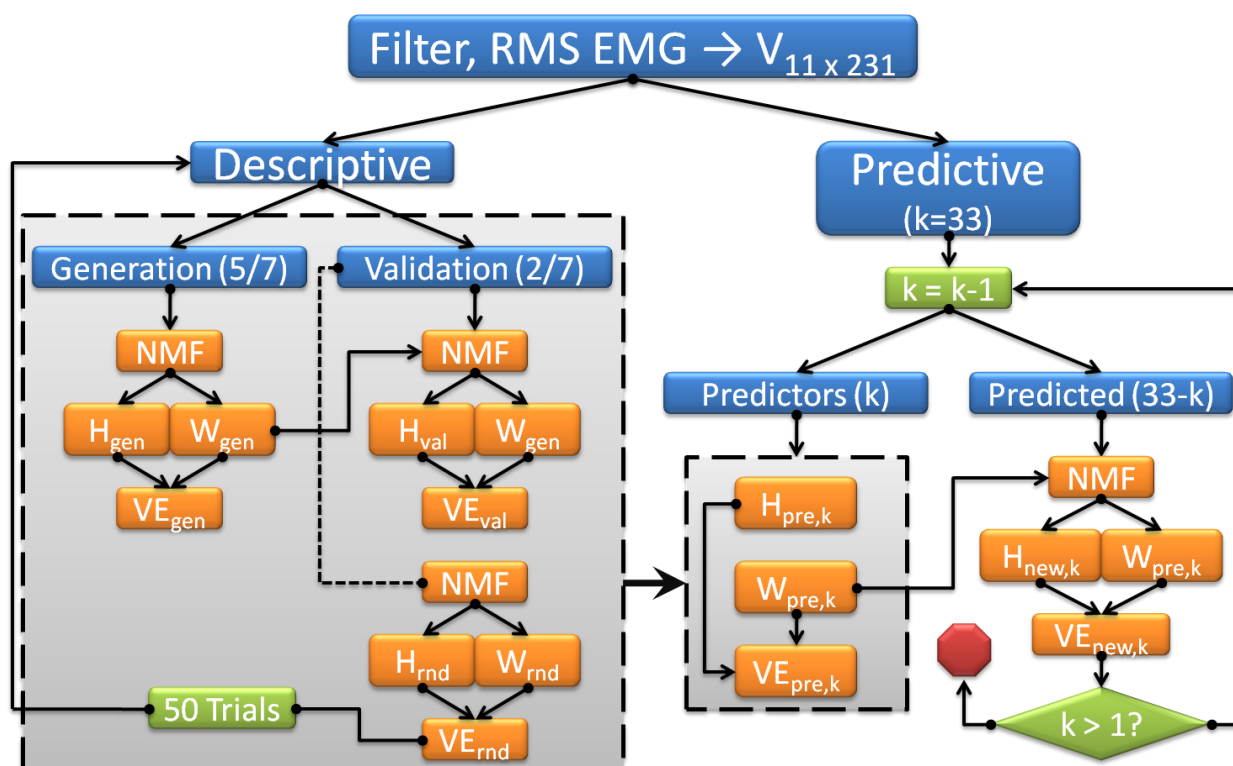


Figure 4.4. Flow chart of descriptive (left) and predictive (right) synergy analyses.

The non-negative matrix factorization (NMF) model was used to estimate the synergies of the EMG patterns associated with ASL miming in both a descriptive and a predictive framework. In the descriptive framework, all postures were used to estimate synergies, and the synergies were cross-validated. In the predictive framework, the data was split into postures that served as predictors vs those that were predicted. Synergies were estimated using the predictors, and the resultant estimates were used to predict the EMG patterns of the predicted postures. The ratio of predictor vs predicted postures was systematically varied from 32:1 to 1:32, in an effort to deduce how many postures were necessary to form the full predictive framework.

4.2.4.4 Predictive Synergy Analysis

The descriptive synergy analysis serves to investigate if a dimensionally reduced set of basis synergies can *describe* the entire set of observed EMG patterns in miming of the ASL postures.

This analysis is consistent with what has been presented in much of the motor control literature. While necessary and informative, the results of the descriptive synergy analysis may be in part due to a simple fitting of the observed data. An analysis investigating the *prediction* of the EMG patterns of new hand postures would be more powerful in discerning the validity of muscle synergies as a viable paradigm for EMG pattern recognition and myoelectric control. To this end, a predictive synergy analysis (Figure 4.4, right hand side) was performed.

Initially NMF analysis was used to determine the basis set of muscle synergies that could describe the EMG patterns of $k = 32$ predictor postures. Given 33 total postures and k predictor postures, there are $\binom{33}{k}$ different combinations of sets of predictor postures. Descriptive NMF analysis was applied to these predictor sets, which proceeded as described in section 4.2.4.3, resulting in $\mathbf{W}_{pre,k}$ and $\mathbf{H}_{pre,k}$, and a corresponding explained variance of $VE_{pre,k}$. The resultant n synergies of $\mathbf{W}_{pre,k}$ were then used to predict the EMG patterns of the set of predicted postures. Specifically, NMF was applied to the EMG patterns of the predicted ASL posture set, with only $\mathbf{H}_{new,k}$ updated according to the described NMF rules, while $\mathbf{W}_{pre,k}$ was held constant. The actual EMG data matrix of the predicted postures was then compared to the predicted EMG data matrix $\mathbf{V}_{new,k} = \mathbf{W}_{pre,k} \times \mathbf{H}_{new,k}$, resulting in a variance explained value $VE_{new,k}$ (i.e. r^2) that was the measure of the predictive success of the synergy framework defined by $\mathbf{W}_{pre,k}$.

The above methodology was performed for $k = 32$ predictor postures down to $k = 1$ predictor posture. The number of combinations of predictor versus predicted postures exponentially increases from $k = 32..16$ predictor postures, and then exponentially decreases from $k = 16..1$ predictor posture. The actual number of possible combinations C is given by equation 4.1.

$$C = \sum_{k=1}^{32} \binom{33}{k} = \sum_{k=1}^{32} \frac{33!}{k!(33-k)!} \approx 8.59 \times 10^9 \quad (4.1)$$

Given the time necessary to process NMF on both the predictor and predicted EMG sets, it was unfeasible to run all combinations. Hence out of all possible combinations of k predictors, twenty were randomly selected as representative sets. The set which explained the most variance of the predicted EMG postures was chosen as the representative set. Reported for each representative set are the numbers of synergies necessary to form the predictive framework, the variance explained of the predicted EMG postures, and the variance explained of the predicted EMG postures by a set of random synergies. Also reported is the minimum number of synergies, and hence predictor postures, necessary to form an adequate predictive framework for all thirty-three of the ASL postures. This minimum number of synergies was determined as that corresponding to the minimum number of postures which could explain greater than 90% of the variance in the predicted EMG posture set.

The robustness of the estimated predictive synergies was investigated, both within combination sets of the same number of predictor posture, and across combination sets of differing numbers of postures. Given a number of predictor postures k , 20 of $\binom{33}{k}$ were chosen for analysis. Hence the choice of postures could determine the structure of the estimated synergies. Furthermore, increasing k could potentially alter the structure of the estimated synergies. To assess the robustness of synergies between different predictor sets, the estimated synergy sets were ordered using a best-matching algorithm. The degree of matching between any two synergies was quantified using the normalized dot product, given in equation 4.2. Synergies were linked using a best-match algorithm in which the NDP was calculated for all pairs between two sets of estimates. The pair with the highest NDP was deemed a match, and the process repeated until all synergies were linked that were matched above random chance.

$$NDP_{AB} = \frac{\bar{A} \cdot \bar{B}}{|\bar{A}| \cdot |\bar{B}|} \quad (4.2)$$

Finally the robustness of synergies across the subject population was examined. Each subject's predictive synergy framework could be composed of exclusively subject specific synergies. Alternatively, there could be one synergy framework with high predictive power for all subjects. Still, each subject's predictive framework could be composed of both general population and subject-specific synergies. To assess this, the best-match algorithm was used to align synergies across the subject population.

4.3 Results

4.3.1 EMG Pattern Separability and Repeatability – Discriminant Analysis

Discriminant analysis revealed that the EMG patterns associated with the thirty-three mimed ASL letters and numbers were discernable and repeatable across several trials. The average discriminance percentages (i.e. classification accuracies) for the complete and cross-validation data sets were $81.8 \pm 3.6\%$ and $64.7 \pm 5.3\%$, respectively. Discriminance matrices (actual postures vs. predicted postures) for a representative subject are shown in Figure 4.5, and the discriminance percentages for all subjects are shown in Figure 4.6. Discriminance was greater than chance ($1/33$), and many of the incorrect classifications were between posturally and visually similar letters, such as between the number '2' and letters 'U' and 'V', and between the number '6' and the letter 'W' (see Figure 4.2).

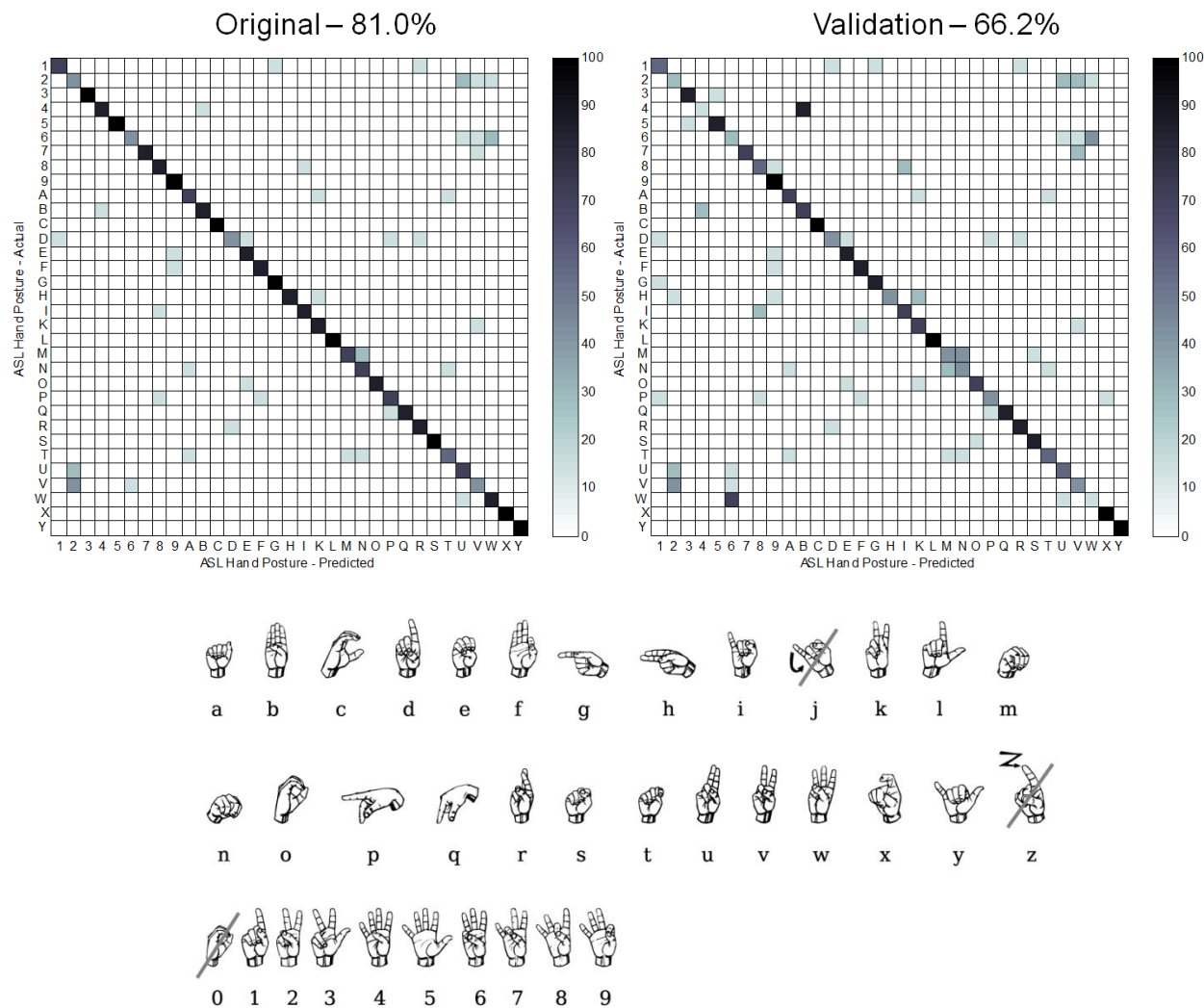


Figure 4.5. Representative discriminability matrix for miming of ASL letters and numbers.

The discriminability matrices (top) show that the EMG patterns for the thirty-three mimed ASL letters were distinct and repeatable across several trials. The two discriminability matrices show the discernability of the EMG patterns for a representative subject. The actual mimed letter is the column axis, and the predicted classification is the row axis. Perfect discriminability would be represented by a solid black diagonal surrounded by all white boxes. The majority of the inability to discriminate the mimed postures showed up when trying to discriminate an 'M' from an 'N', a '2' from a 'U' or 'V', and a '6' from a 'W'. Visually these letters (bottom) are quite similar (see Figure 4.2), and so the discriminability inability is not surprising. Overall though, the discriminability levels for both the complete and cross-validation data sets are significantly greater than chance (1/33).

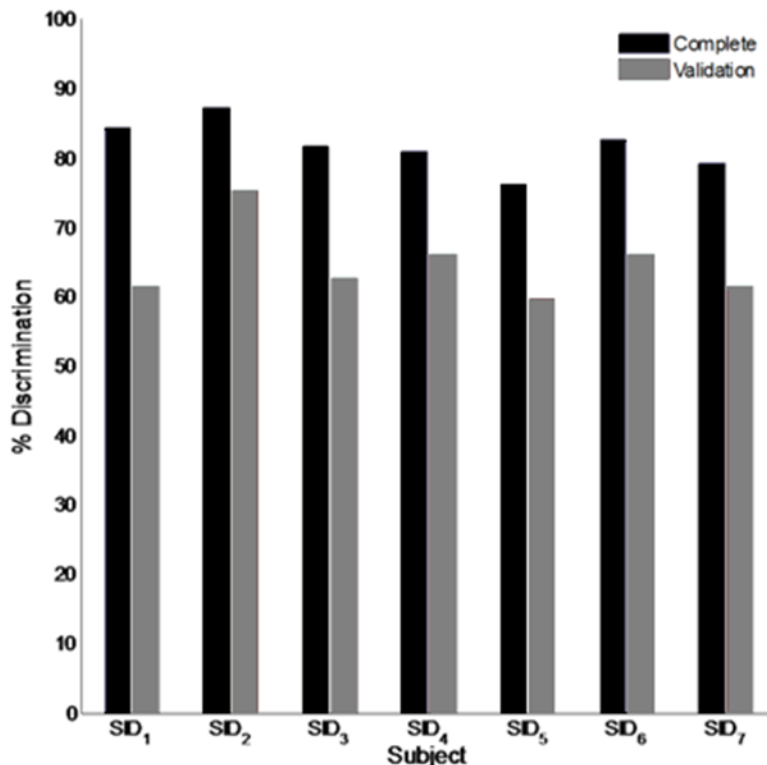


Figure 4.6. Complete and cross-validated discriminance percentages for all subjects.

The EMG patterns associated with the ASL letters were discernable and repeatable across the subject population.

4.3.2 Descriptive Synergy Analysis

Figure 4.7 shows an explained variance curve derived from NMF analysis of the EMG patterns recorded during miming of the ASL postures for a representative subject. For this subject, the set of EMG patterns associated with the full set of mimed ASL letters could be described by 8 synergies, a reduction in dimensionality from the original 11-dimensional muscle set. These sets of 8 synergies accounted for on average $97.4 \pm 0.0\%$ of the variance in V_{gen} and $97.0 \pm 0.0\%$ of the variance in V_{val} . In contrast, the random synergy sets only accounted for

44.3 \pm 15.4% of the variance in V_{val} , suggesting that the synergies estimated from the V_{gen} data set contained significant information about the EMG patterns in V_{val} , and hence the high explained variance was not completely the result of data fitting. These high levels of explained variance were found across the entire subject population. The average number of synergies necessary to describe the full ASL posture set across the subject population was 8.3 \pm 1.3. Figure 4.8 reports the average explained variance for V_{gen} , V_{val} , and the random synergy sets for each subject, and shows that for a representative subject, the original EMG patterns were faithfully recreated by the descriptive NMF model.

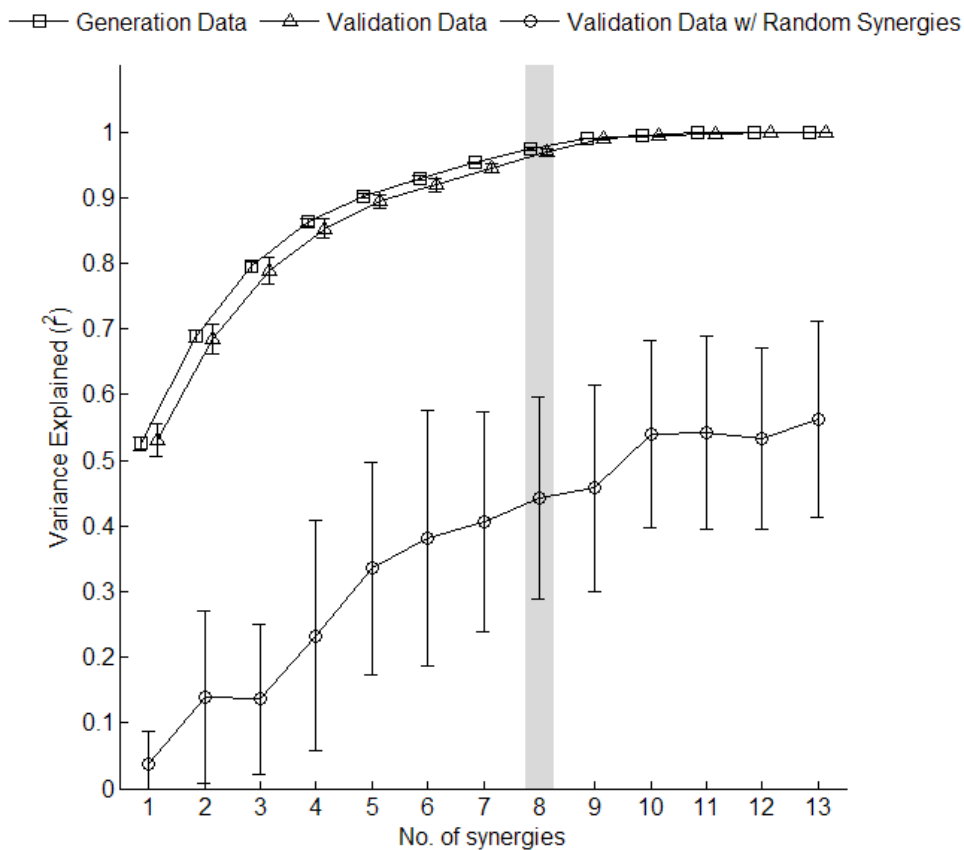


Figure 4.7. Explained variance curve derived from descriptive NMF analysis.

Synergies were estimated from $n = 1..13$ using non-negative matrix factorization (NMF). NMF was applied to the generation data set, and the estimated synergies were validated using a cross-validation data set. To assess how much information was contained in the estimated synergies, the cross-validation set was estimated using random synergies as well. The variance explained by the estimates relative to the investigated data set was calculated for all estimates. Clearly, there is significant information contained in the original synergy estimates, as seen by the fact that the random synergy curve (circle) is significantly less at all estimated synergies. The cross-validation curve (triangle) is on par with the generation curve (square), suggesting that the calculated muscle synergies are robust across multiple trials of posture miming. The correct number of synergies (highlighted in gray) was determined to be that point in the cross-validation curve in which the addition of more synergies did not significantly increase the amount of explained variance, based upon the mean-square-error of a linear fit.

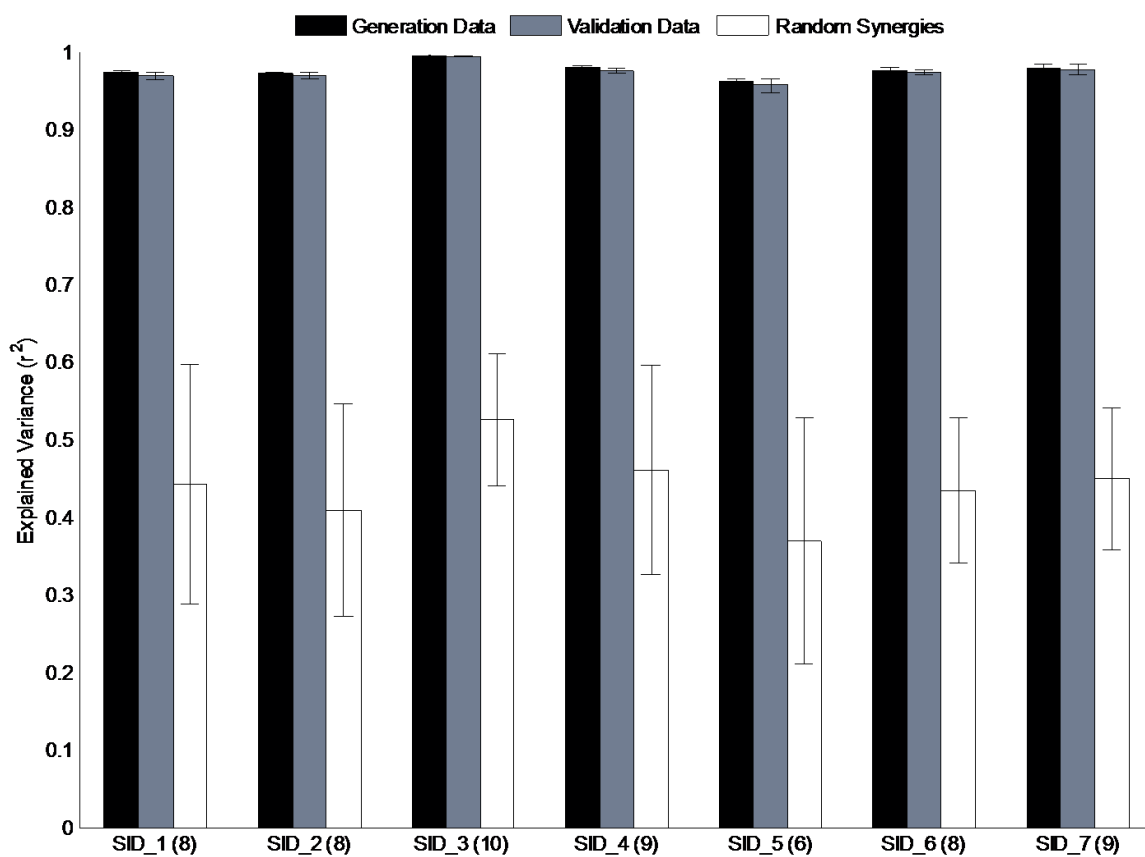


Figure 4.8. Variance explained by synergy estimates (all subjects).

The variance explained using the cross-validation data was on par with that from the generation data. Using random synergies to explain the cross-validation data resulted in significantly lower r^2 values, suggesting that the extracted synergies contained significant information. For each subject, the number of extracted synergies is shown in parentheses.

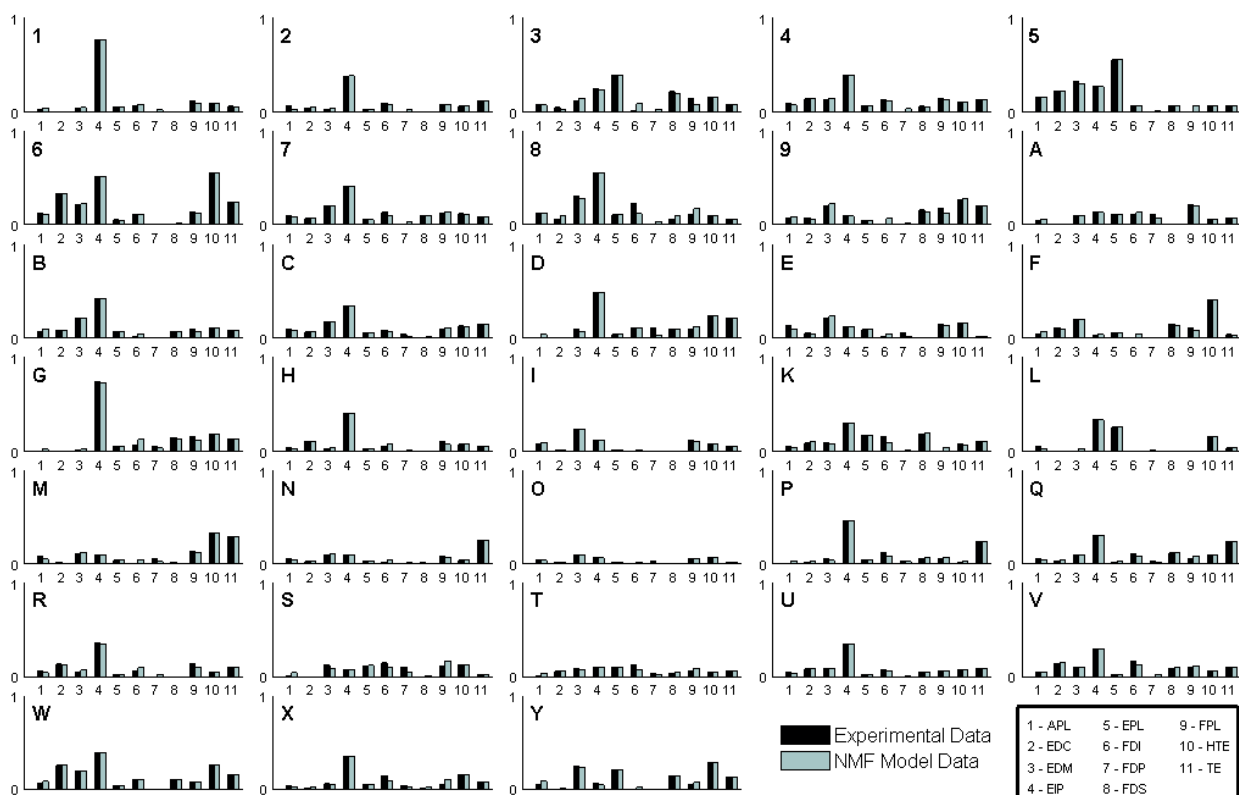


Figure 4.9. Recorded EMG patterns vs those estimated by the descriptive NMF model.

The synergies and sources estimated by the descriptive NMF model were able to faithfully recreate the EMG patterns experimentally observed during miming of the static ASL letters and numbers.

4.3.3 Predictive Synergy Analysis

Figure 4.10 shows a subset of the explained variance curves resulting from the predictive NMF analysis for one characteristic subject. As with the rest of the subject population, as the number of predictor postures increased from 1 to 32, the predictive power of the synergy framework increased i.e. the explained variance of the new predicted ASL postures increased. The number of synergies needed to define this predictive framework increased as well. However, a threshold was reached, where increasing the number of predictor postures did not

increase the number of synergies needed to define this predictive framework, nor did it significantly increase the variance explained of the new predicted hand postures. This is illustrated in Figure 4.11, which shows data from one representative subject. As the number of postures to be predicted increased from 1 to 20, and hence number of original predictor postures decreased from 32 to 13, the overall predictive power of the estimated synergies remained relatively constant and above 90%, and the number of estimated synergies held constant at 8. However, the predictive power began to significantly diminish with greater increase in the number of predicted postures, and consequently a decrease in the number of original predictor postures and the number of estimated synergies. The knee, chosen as the smallest number of original postures that still established a predictive synergy framework greater than 90%, was 13 postures, corresponding to 8 synergies. Figure 4.12 shows similar plots for the remaining subjects. For the entire subject population, the average minimum number of original postures necessary to establish a 90% predictive synergy framework was 10.9 ± 1.7 , corresponding to 7.9 ± 1.7 synergies. This compares to the 8.3 ± 1.3 synergies found across the subject population from the descriptive NMF analysis of all 33 ASL postures.

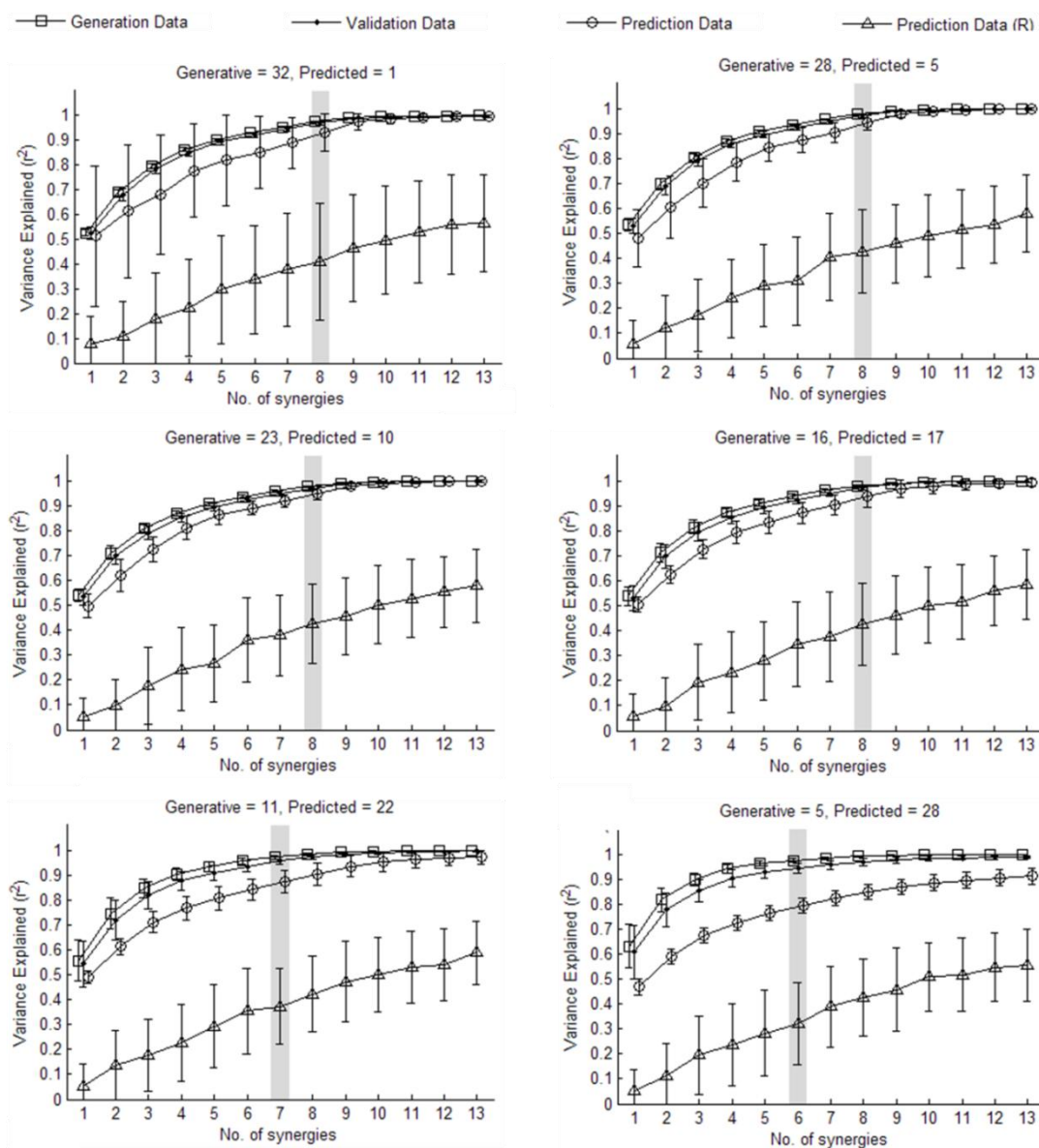


Figure 4.10. Explained variance (EV) curves from the predictive synergy analysis.

Synergies were estimated and validated ('□' and '•' curves) using the generative (predictor) ASL postures. The EMG patterns of new ASL postures were predicted using both the estimated synergies ('○' curve) and randomly generated synergies ('△' curve). The knee was determined based upon the validation curves, and is highlighted in gray. As the number of postures used to define the predictive synergy framework increased, naturally the number of synergies needed increased, as well as the explained variance of the predicted set. However, there was no significant increase in predicted EV past a threshold of 13 generative postures (8 synergies) for this particular subject.

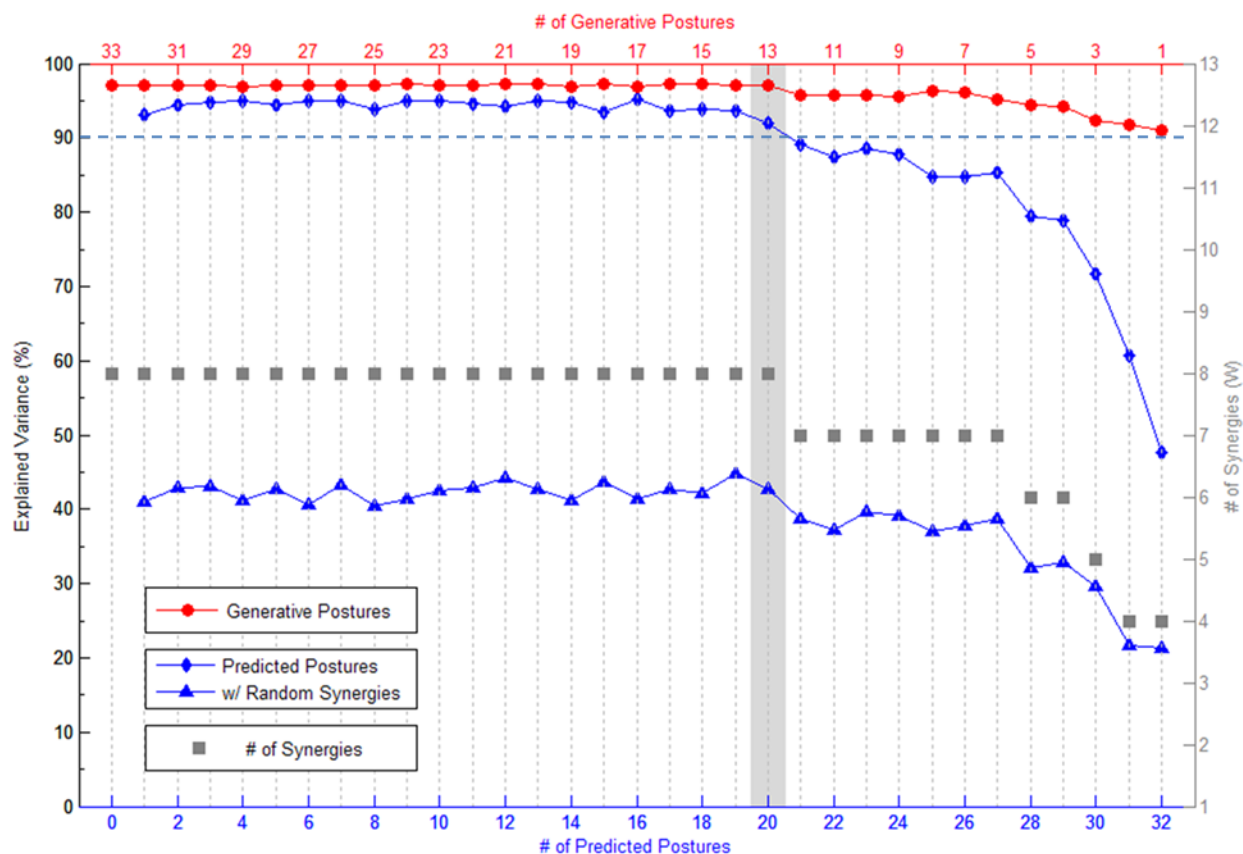


Figure 4.11. Composite results for predictive NMF analysis for one subject.

Each line curve represents a separate phase of the predictive NMF analysis performed on one characteristic subject. The line curves illustrate the variance of the EMG data sets of the predictor ('●' curve, left y-axis, top x-axis) and predicted ('◆' and '▲' curves, left y-axis, bottom x-axis) ASL postures explained by the estimated synergies, and the corresponding number of estimated synergies ('■' plot, right y-axis). The plots are aligned such that the n synergies used to estimate k generative postures were the same used to predict $33-k$ predicted postures. Generally, above a threshold of a certain number of generative (i.e. predictor) postures, the predictive power of the estimated synergies did not significantly increase. A knee was chosen such that the estimated synergies had a predictive power of at least 90%. The knee for this subject was 13 generative postures, corresponding to 8 synergies. For comparison, the predictive posture of 8 random synergies was approximately 40%.

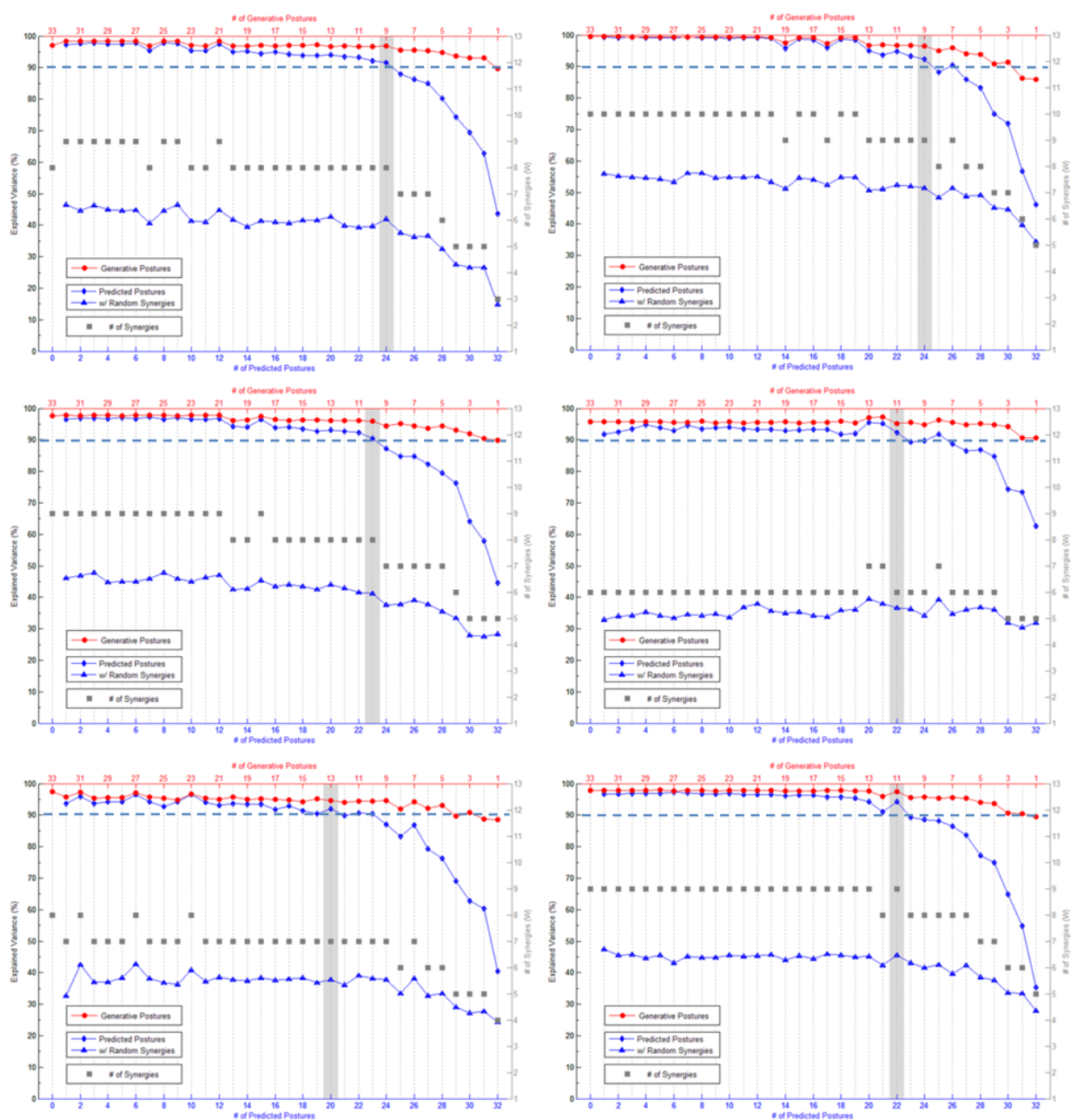


Figure 4.12. Composite results for predictive NMF analysis for remaining subject population.

The average number of postures needed to establish a predictive synergy framework of 90% across the subject population was 10.9 ± 1.7 , corresponding to 7.9 ± 1.7 synergies. The knees for each subject (minimum 90% predictive power) are highlighted in gray.

The robustness of the synergies found at the knee for each plot in Figure 4.11 and Figure 4.12 was examined both across combinations involving the same number of generative (i.e. predictor) postures, and across combinations involving varying numbers of predictor postures. Figure 4.13 shows the robustness of one subject's estimated predictive synergies across the 20 different randomly selected predictor sets. Robustness was quantified by the normalized dot product (*NDP*). The figure shows that the majority of synergies exhibited low lability across the different combinations of predictor posture sets. Average *NDP* for the estimated synergies across the different combination sets ranged from $S = 0.85$ to 0.99 , compared to an expected value of $S = 0.14 \pm 0.11$ for random synergies. Similar plots for the remaining six subjects are shown in Figure 4.14. Overall, within each subject, estimated synergies were generally robust to different predictor combinations.

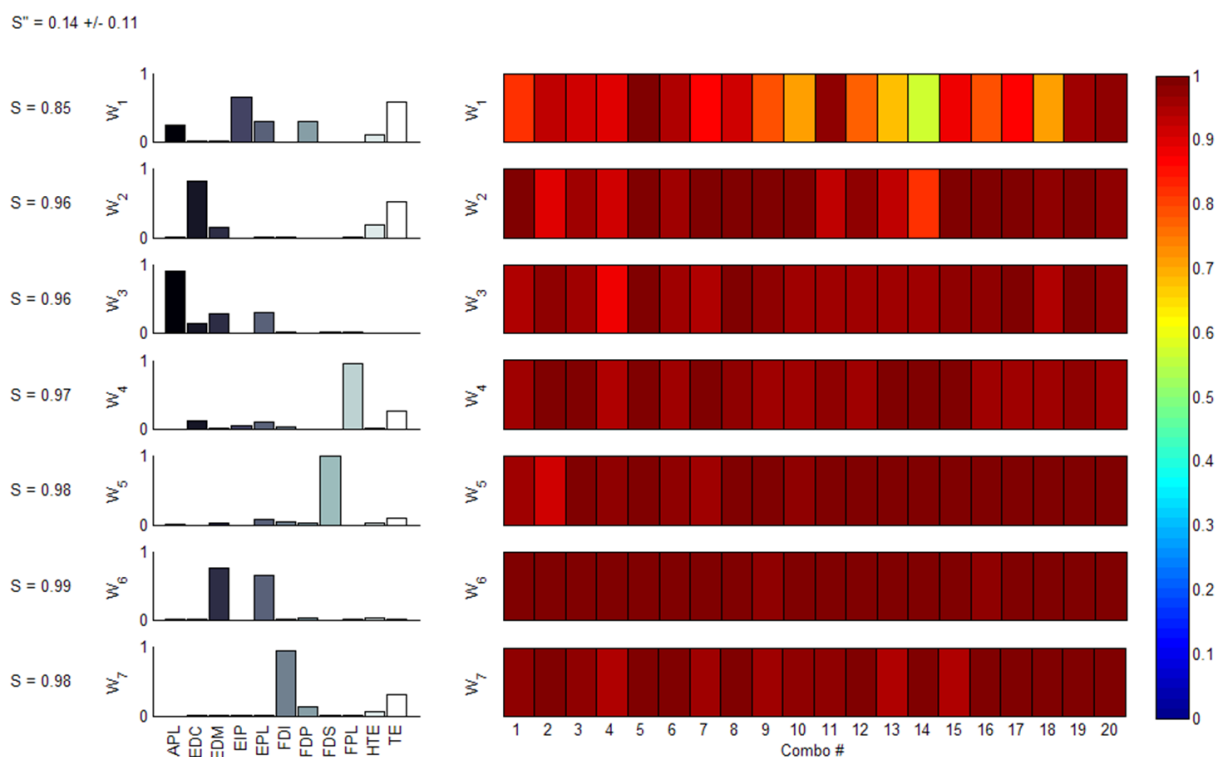


Figure 4.13. Synergy robustness across 20 random combinations of predictor postures.

The estimated synergies for one subject (bar plots, left column), and their robustness (right color plots). Robustness (i.e. similarity) was assessed across the 20 different randomly selected combinations of predictor postures, and quantified using the normalized dot product (*NDP*), which ranged from 0 (no similarity – dark blue) to 1 (perfect similarity – dark red). The majority of synergies were highly robust despite the different combinations of selected predictor postures, as evidenced by the majority of the blocks on the right representing *NDPs* close to 1. Actual robustness values for each synergy are shown on the far left as an *S* value. All robustness values were significantly greater than expected by random chance ($S'' = 0.14 \pm 0.11$).

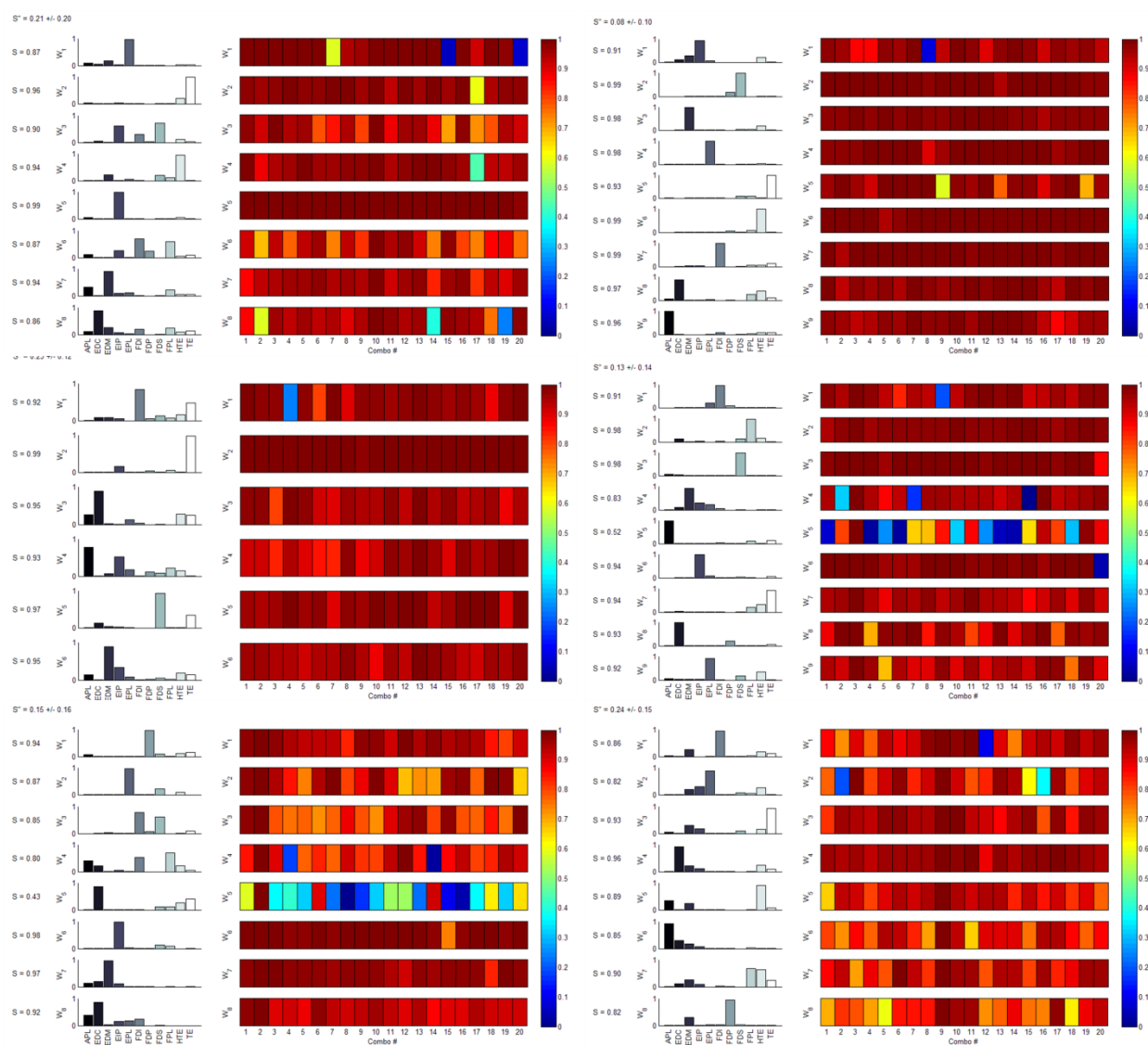


Figure 4.14. Synergy robustness plots for remaining subject population.

The effect of the number of predictor postures on the robustness of the estimated synergies was also quantified using the normalized dot product (*NDP*). The synergies estimated at the knees (gray-shade) of the plots in Figure 4.11 and Figure 4.12 were compared to the synergies estimated at all other points. Figure 4.15 shows for one characteristic subject the robustness of

the estimated predictive synergies, relative to increasing the number of postures used to define the predictive framework. Again, the estimated synergies by and large proved highly robust to increasing the number of postures used to generate the synergies of the predictive framework.

Adding additional postures did not change the structure of existing synergies. Rather the same synergy structures were maintained, or new synergies were added to the framework. Figure 4.16 shows similar plots for the remainder of the subject population. Again demonstrated is the robustness of the synergy structures in the midst of increasing the number of predictor postures.

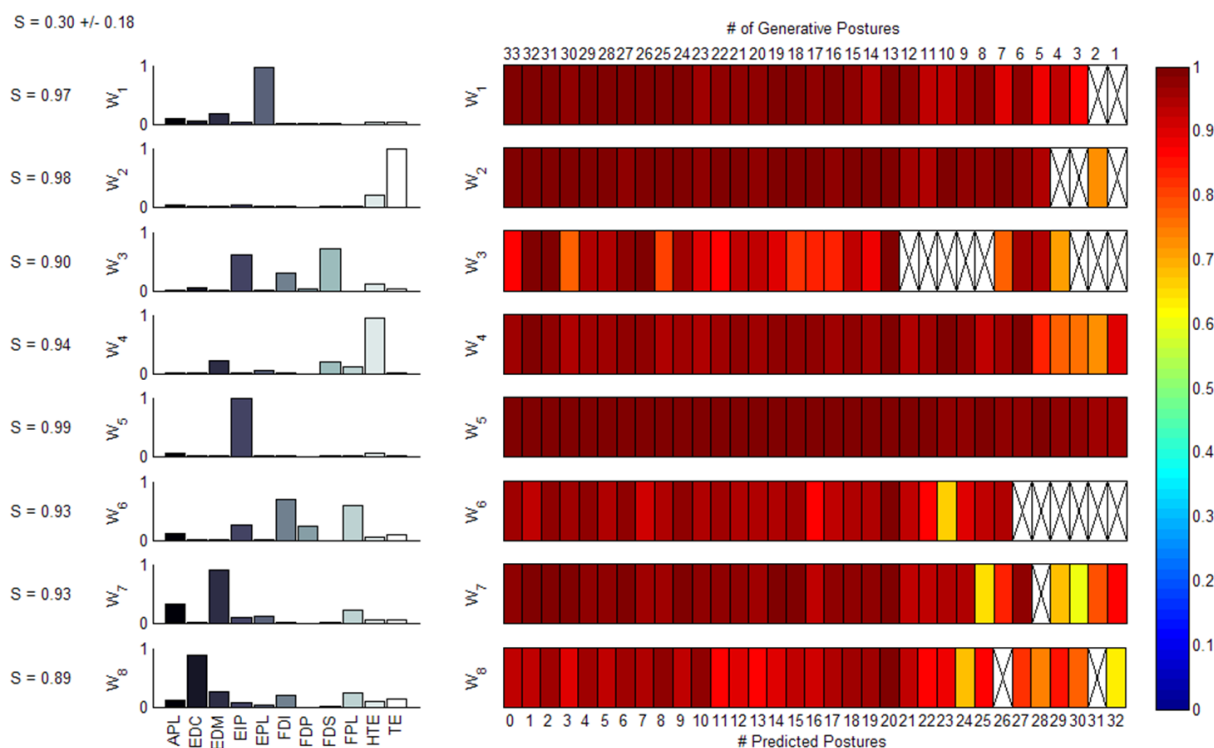


Figure 4.15. Synergy robustness across increasing number of predictor postures (1 subject).

Increasing the number of postures used to estimate the synergies of the predictive framework by and large did not alter the structure of the existing synergies. Rather, the synergies proved robust to adding additional postures, or the addition of new postures simply added new synergies to the existing predictive framework. An 'X' means that the synergy did not match another synergy in that compared set above random chance.

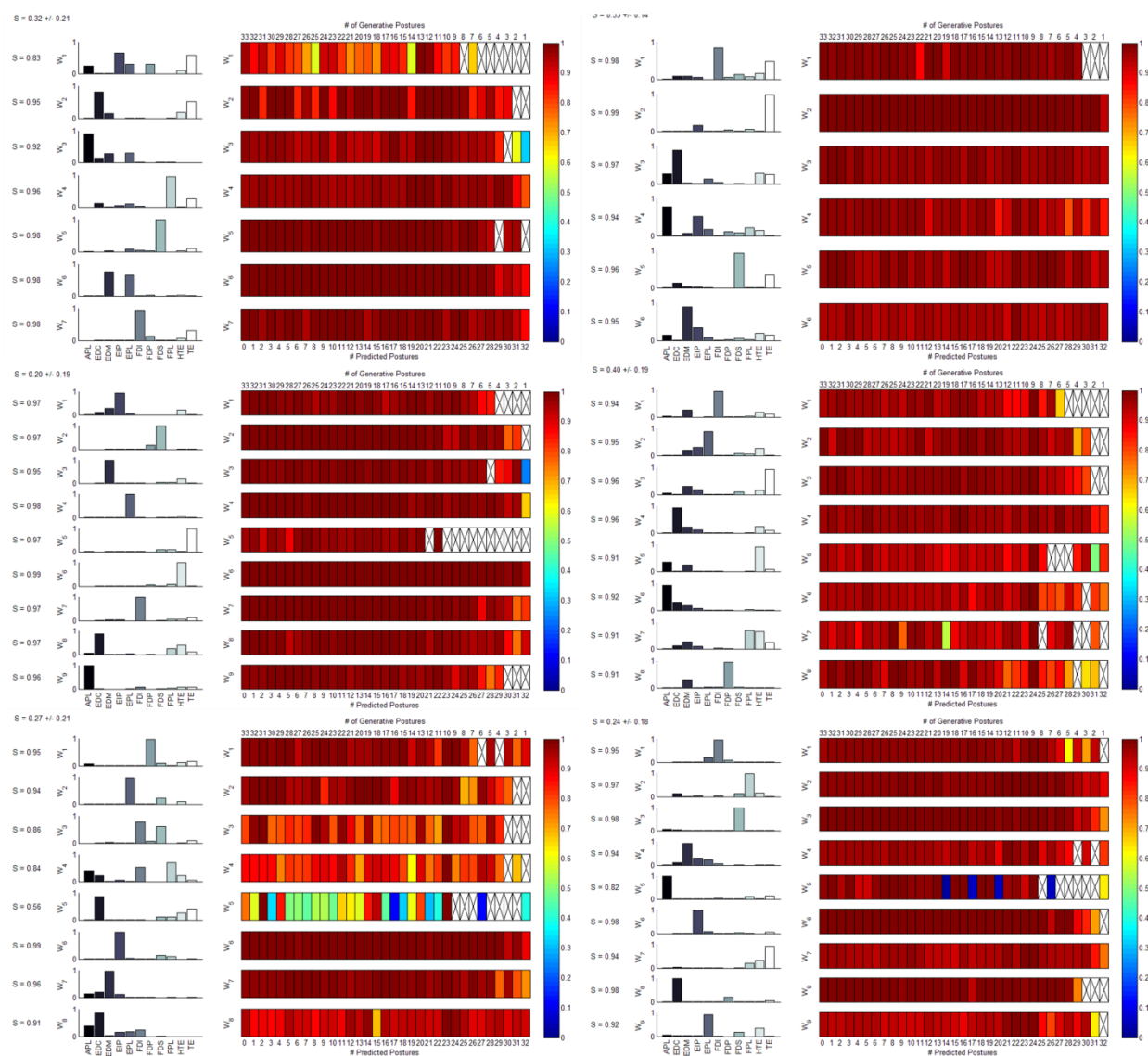


Figure 4.16. Synergy robustness across increasing number of predictor postures.

Finally, the similarity of the synergy structures across the subject population was examined. The estimated synergies for each subject were aligned using the described best-match algorithm, based upon the normalized dot product, to determine if subjects exhibited the same predictive synergy framework, if each subject had a separate synergy framework, or some

combination of the two. The threshold for similarity was two standard deviations above the similarity of randomly exponentially distributed synergies. These synergies are shown in Figure 4.17 – Figure 4.19. Many synergies (W_1 , W_3 , W_4 , W_5 , W_6 , W_7 , W_9 , and W_{11}) were general enough to exist across the majority of the subject population, while many others only showed up in individual subjects. Examining the structure of these synergies shows that the general population synergies were sparser than the subject-specific synergies, and were usually dominated by one muscle, with some subject-dependent minor residual activity from peripheral muscles. Synergy W_1 primarily governs the activity of FDI, synergy W_3 primarily governs the activity of FDS, synergy W_4 primarily governs the activity of EDM and to a lesser extent EIP, synergy W_5 primarily governs the activity of APL, synergy W_6 primarily governs the activity of EIP, synergy W_7 primarily governs the activity of the intrinsic TE group and to a lesser extent the intrinsic HTE group, synergy W_9 primarily governs the activity of EPL, and synergy W_{11} primarily governs the activity of EDC balanced with the activities of TE and HTE intrinsic groups. While these non-subject-specific synergies were not exhibited by all subjects, some of the observed subject-specific synergies were slight variants of these population synergies. The structures of the non-subject-specific synergies are summarized in Table 4.2. It should be noted that several individuals did exhibit subject-specific synergies that represented balanced activation of two or more muscles, such as W_{12} and W_{13} of SID₃.

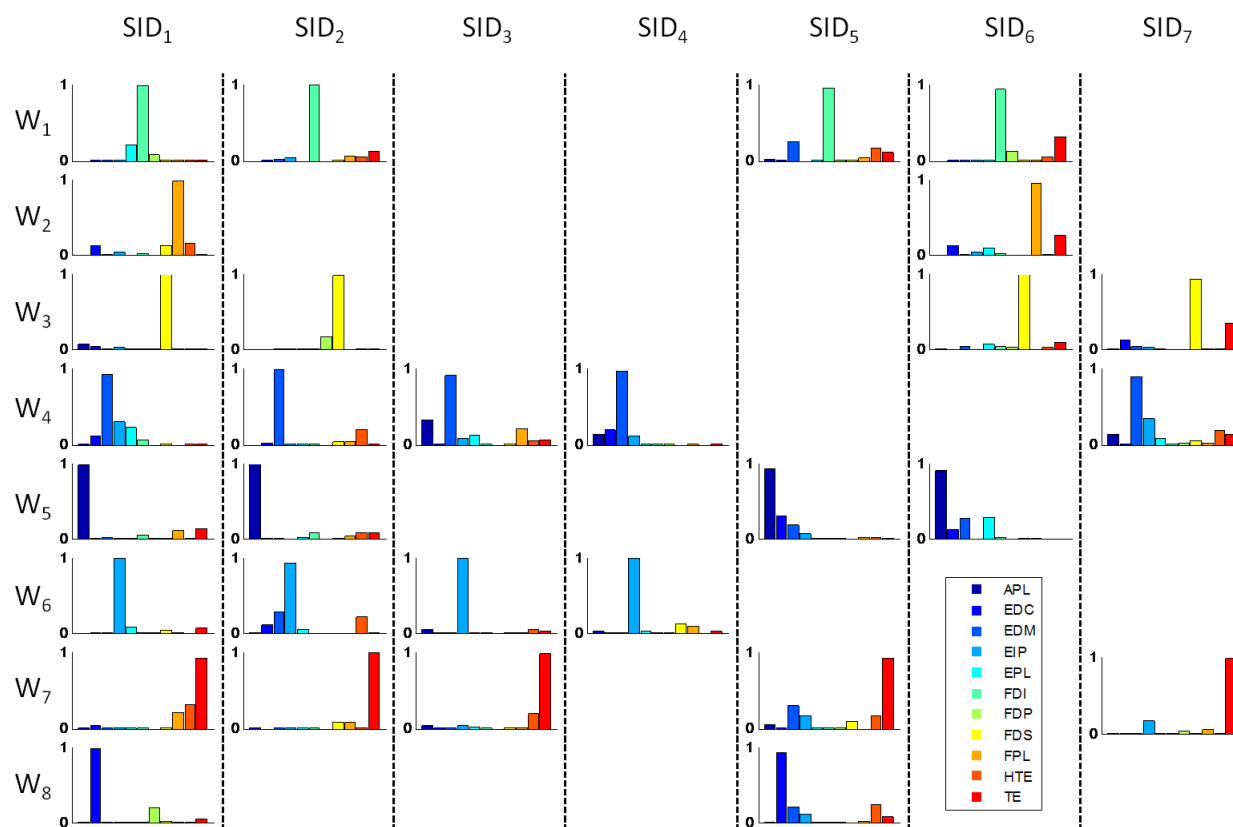


Figure 4.17. Estimated synergies for each subject (I).

The estimated synergies defining the predictive framework for each subject are shown in each of the seven columns. The synergies were aligned to determine which synergies were shared across the population versus which were subject-specific. Many synergies, such as W_1 , W_3 , W_4 , W_5 , W_6 , W_7 , and W_9 and W_{11} (Figure 4.18) were exhibited across the predictive frameworks of several subjects, while others such as $W_{15} - W_{23}$ (Figure 4.18, Figure 4.19), seemed to be specific to the coordination patterns of individual subjects.

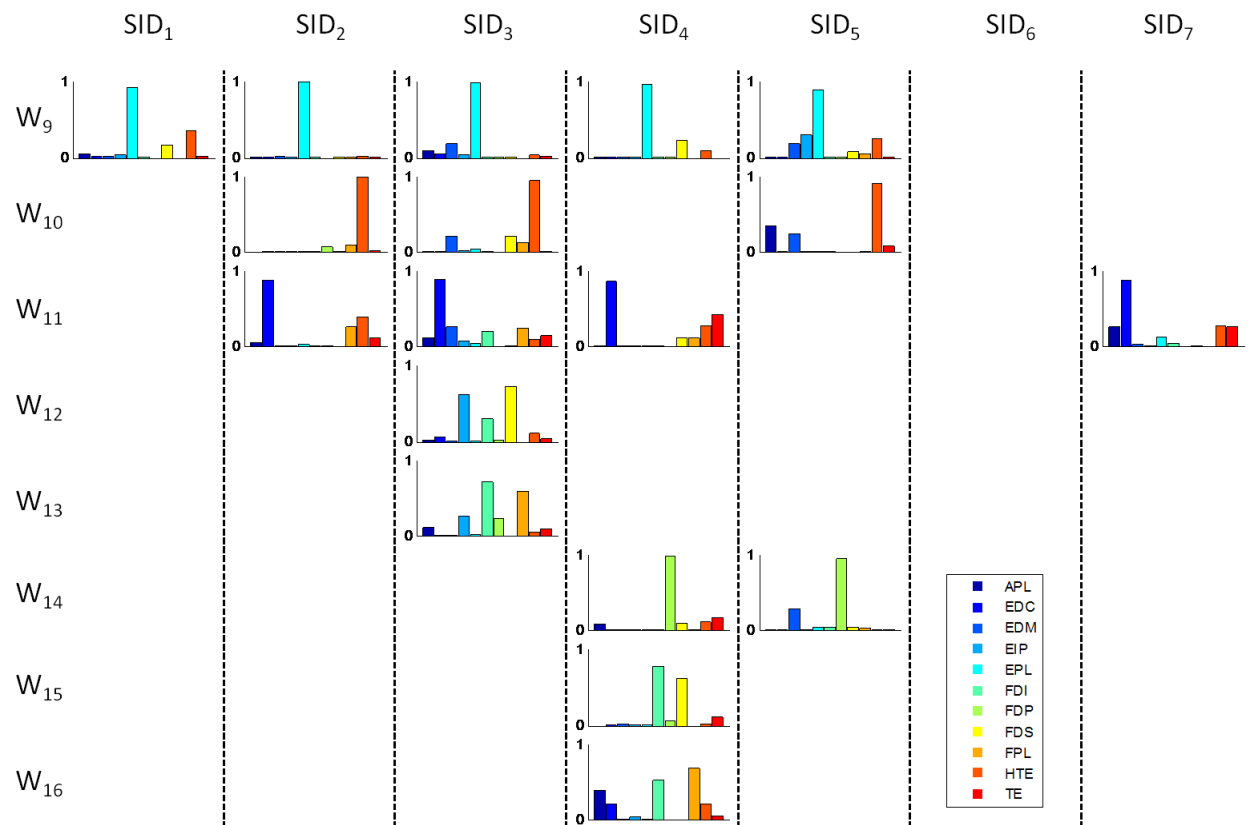


Figure 4.18. Estimated synergies for each subject (II).

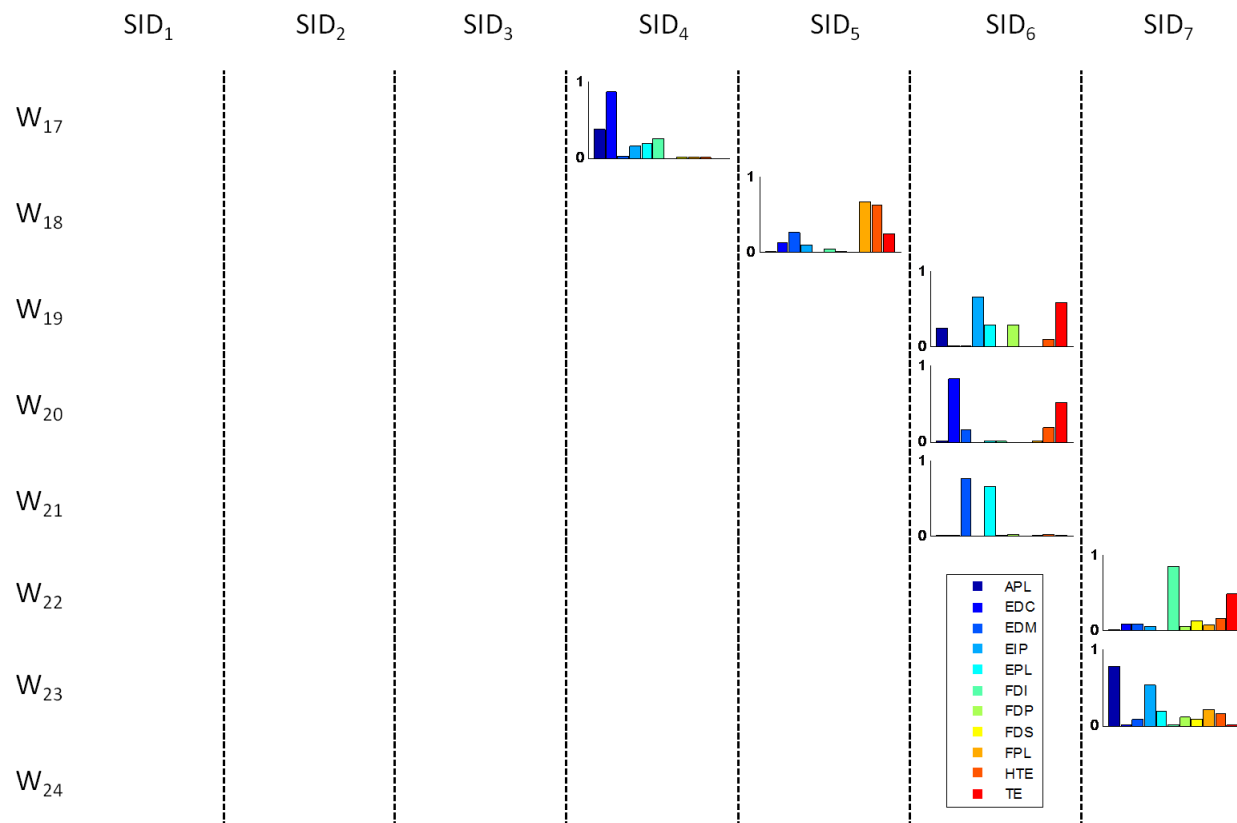


Figure 4.19. Estimated synergies for each subject (III).

Table 4.2. Structures of synergies global to the subject population.

Synergy	# Subjects	Primary Muscle Components
W ₁	4	FDI
W ₃	4	FDS
W ₄	5	EDM (and EIP to a lesser extent)
W ₅	4	APL
W ₆	4	EIP
W ₇	5	TE (and HTE to a lesser extent)
W ₉	5	EPL
W ₁₁	4	EDC (and TE and HTE to a lesser extent)

4.4 Discussion

This work has investigated the power of a muscle synergy framework in predicting the EMG patterns of new static hand postures. To the author's knowledge, only one major study (Weiss & Flanders, 2004) has examined the concept of muscle synergies as a dimensionality reduction paradigm for the production of a wide variety of hand postures. Their investigation showed that a six-dimensional coordinate muscle space could be reduced to a three to four dimensional coordinate muscle synergy space, while describing 80-90% of the variance observed in the EMG data associated with grasping and ASL spelling. While informative, this study failed to make a compelling case that the new framework established by their extracted synergies was useful within a physiological control paradigm. The efficacy of this framework in predicting new hand postures, which speaks to their robustness and generalizability, is a testable and necessary hypothesis given the accepted definition of muscle synergies (Lee, 1984). However, it was not explored in their work. In short, the work of Weiss & Flanders established that muscle synergies can form a *descriptive* framework for a wide variety of known hand postures. The results of the current work described in this manuscript demonstrate that muscle synergies are robust and generalizable enough to *predict* the EMG patterns of new hand postures.

4.4.1 Predictive Power of Muscle Synergies

The nature of muscle synergies, as the concept has been presented in literature, is that they serve to reduce the dimensionality of the problem of muscle coordination. Hence the muscle coordination patterns associated with a wide variety of intentional tasks could be solely composed of these motor primitives. On one extreme, the neuromotor system could use a small set of synergies to construct all possible intentional tasks. On the other extreme, every

possible intentional task could have its own set of governing synergies for muscle coordination. Given this second extreme, however, the dimensionality of control would exponentially increase with the addition of new tasks, contradicting one of the main advantages of the synergy concept. Hence, it seems more likely that, should synergies be a viable means of coordination, a small set of synergies would be able to account both for existing and new tasks. Therefore, predictive power is a necessary property of muscle synergies.

The results of this study show that 90% predictive power of new static hand tasks could be achieved with an average of as few as 11 static hand postures and 8 muscle synergies. 80% *predictive* power required on average 7 muscle synergies, reduced from 11 original dimensions. This is in contrast to the Weiss study that required 4 muscle synergies for 80% *descriptive* power, reduced from 6 original dimensions. Of interest is that for all subjects, the predictive power of the muscle synergy framework reached an asymptote past the critical number of postures. The addition of new postures to the generative (predictor) set did not increase the overall predictive power of the framework. This, along with the fact that the predictive power with respect to the new hand tasks was comparable to that of the original hand tasks, suggests that each static hand task does not require its own set of synergies. Rather, a limited set can account for these new postures. Furthermore, as shown in Figure 4.11 and Figure 4.12, the number of synergies did not significantly increase past this critical number. Hence, the extracted synergies were not posture specific, but rather contained information pertinent to the construction of the EMG activity of these new hand postures. Had this not been true, the predictive power of the extracted synergies would have been on par with those of random synergies, also shown in Figure 4.11 and Figure 4.12. This conclusion is in agreement with that of other researchers, who have shown that task-independent muscle synergies can be elicited from stimulating various sites within the frog spinal cord (Saltiel et al., 2001).

4.4.2 Structure of Muscle Synergies

The synergies extracted from the mimed hand postures show that, within any given subject, a muscle can belong simultaneously to multiple synergies. This is consistent with the muscle synergy model, and what has been observed in other muscle coordination studies of standing, locomotion, and grasping (d'Avella et al., 2003, Ting & Macpherson, 2005, Tresch et al., 1999, Weiss & Flanders, 2004). Of interest is that the majority of synergies that were found to be shared amongst the subject population were very sparse in nature. Each of the non-subject-specific synergies (8 out of 23) seemed to primarily control the activity of an individual muscle. It seems thus that these synergies (actually not synergies but individuated muscles) may form a basic low-level paradigm of individuated muscle control that is common to the general population. Higher-level paradigms of control involving synergies that co-activate multiple muscles may then be more subject-specific, depending on the neuromuscular architecture of each individual. This possible hierarchy of control is in congruence with what has been proposed based upon cortical mapping studies, namely that there may be a level of somatotopic individuated control of the degrees-of-freedom of the hand superimposed over the distributed activation of neurons that coordinate multiple DOF (Schieber, 1999). What is clear is that both types (individuated control vs synergy based control) exist and are utilized within an individual subject for predicting the EMG patterns of a wide variety of hand postures. This may explain why other studies have reported what seems to be flexibility in the synergistic activities of two or more muscles (Macpherson, 1991, Maier & Hepp-Reymond, 1995b). Depending on the task, low-level individuated control may be more pronounced than high level coordinated synergy control, and vice-versa.

4.4.3 Robustness of Muscle Synergies

By using varying combinations of the possible $\binom{33}{k}$ sets of k predictor postures to estimate the predictive synergy framework, the robustness of the synergies to varying hand posture requirements was examined. The majority of estimated synergies were remarkably stable despite different postures being included in the predictor set. This suggests that the estimated synergies were by and large not highly dependent on which postures are used to estimate them, giving more credence to their task-independence. There were two subjects, however, who each seemed to exhibit a single unstable synergy, in that the appearances of the synergies were dependent on which postures were included in the predictor set (Figure 4.14). This seems to suggest that there are some synergies that were posture dependent, whereas the majority of synergies seem to be shared by a large number of the hand postures. The estimated synergies also showed robustness to the addition of postures to the predictor set. Adding new postures to the predictor set could have maintained the current synergy framework, augmented the current synergy framework by simply adding new synergies (increasing the dimensionality), or entirely altered the structure of some of the synergies in the current framework. The fact that the synergy framework of subjects was not significantly altered in structure with the addition of new postures, as evidenced by the high similarity values in Figure 4.15 and Figure 4.16, further suggests that they are task independent, and not highly labile in the presence of new task demands.

4.4.4 What is the “Correct” Number of Synergies?

One of the major unresolved issues in dimensionality reduction problems is determining the appropriate number of underlying uncorrelated dimensions. A wide variety of methods have

been employed in the literature, including that used in this investigation (mean square error of a linear fit), and thresholding at an arbitrarily decided value. The methodology of deciding the “correct” number of synergies has the potential of affecting the structures of the estimated synergies and hence the results of these investigations. Take for example the subject whose explained variance curve is shown in Figure 4.7. Using the linear fit method, eight synergies were found to define the reduced dimensional space. However, using a threshold of 90%, as is sometimes used in other investigations, the dimensionality of the synergy space becomes 6D. Using an 80% threshold, as was used in the Weiss and Flanders’s study, the dimensionality is reduced to 3D or 4D. Figure 4.20 shows how the number and structures of the synergies change depending upon the chosen method for estimation of the underlying dimensionality. While many of the synergies retain their structure, several disappear or become less sparse with a decrease in the cutoff threshold. Thus, by decreasing the threshold, the synergy sets resemble groups of muscle activation more than individuated muscle control. However, there is no real justification for choosing an arbitrary cutoff of 80% or even 90%. It seems that the linear fit approach is a more systematic method of deciding the number of synergies because it determines the point at which more synergies do not significantly add to the explained variance. Thus, even though the synergies estimated using this method are more sparse and resemble control of individuated muscles, this is arguably a better representation of the control scheme implemented by the motor system.

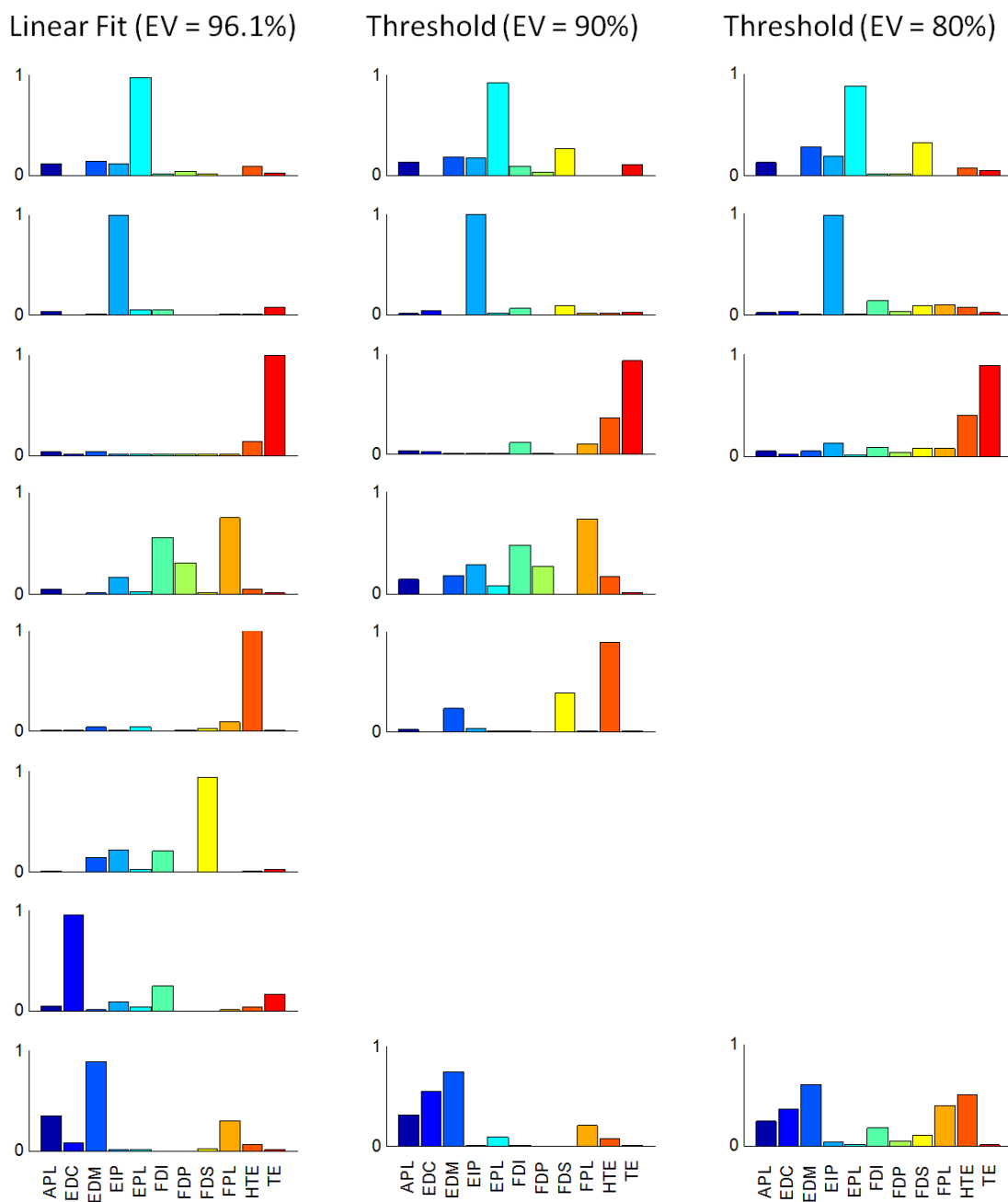


Figure 4.20. Structure of synergies wrt method of determining control space dimension.

The number of synergies and the structure of the synergies were partially dependent on the method used to estimate the “correct” number of synergies.

4.4.5 Implications for Myoelectric Control

As stated in the introduction, one of the primary motivations for investigating muscle synergies as a paradigm of myoelectric control is that it would negate the need of programming the EMG patterns of all possible hand postures into the control architecture. Rather, using a known and finite basis set of controllable muscle coordination patterns, more complex EMG patterns and hence movements could be controlled. What this investigation has done is show that the EMG patterns of new hand postures can be composed from a basic set of muscle synergies. The activation of each of these synergies could potentially be tied to the control of a particular degree of freedom, and the individual could then control the prosthesis by volitionally activating individual synergies. The issue of whether individuals can volitionally and accurately control individual synergies is addressed in a subsequent chapter. However, first showing that new untrained hand postures could be constructed from a static set of finite synergies is necessary for the implementation of a synergy-based control paradigm.

4.5 Conclusion

Muscle synergies have been proposed as a means of control of the motor system to coordinate the many neuromuscular degrees-of-freedom. While many studies have shown that muscle synergies can form a *descriptive* framework for a large number of tasks, this study has shown that, using a small number of hand postures, synergies can form a *predictive and robust* framework for a wide variety of hand postures. Furthermore, the synergy structures remain relatively constant with the addition of new hand postures. The sparseness of some of the synergies common to the subject population suggests that the neuromotor system may use a

dualistic approach for control, rather than exclusively synergies or individual muscles, depending on the task requirements.

Muscle synergies have potential for use in myoelectric control because these simple building blocks of muscle coordination could be used to build more complex muscle coordination patterns and hence more complex movements. This investigation has shown that the EMG patterns of new complex hand postures can be accurately produced from a small finite set of static robust muscle synergies. Future work stemming from this investigation includes demonstrating that individuals can accurately control these synergies for myoelectric control. This issue is explored in a subsequent chapter of this manuscript.

5 Muscle Synergies Exhibit Scalability with Increasing Grasp Force

5.1 Introduction

Understanding how the central nervous system (CNS) coordinates the many degrees-of-freedom (DOFs) associated with performing a task has been a long-standing problem in the area of motor control. This issue of coordination has been termed “ill-posed” because of the biomechanical and neuromuscular redundancies in the anatomical structure (Bernstein, 1967). Nowhere is this redundancy better epitomized than in the control of the human wrist and hand. The wrist and hand form a complex and versatile system of twenty-seven bones and over thirty extrinsic and intrinsic multi-joint muscles (Gray, 1973), having twenty-two DOFs (Soechting & Flanders, 1997). Much of this versatility can be seen in the hand’s dexterity. Dexterity has been defined as “...the essence of purposeful motor behavior ... [entailing] all the ingredients of goal- and object-oriented actions, particularly manipulations that have been practiced and acquired” (Wiesendanger, 1999). This goal and object-oriented action can be seen in the many grasp patterns that the hand forms. Napier classified all static hand grasps into two general categories: “precision” and “power” (Napier, 1956). Precision grasps are characterized by object contact primarily using the fingertips, and power grasps are characterized by object contact primarily using the palm (Johansson & Cole, 1992). The means by which the CNS coordinates the hand musculature to solve the neuromuscular redundancy problem in producing these static multi-joint precision and power hand grasps at sub-maximal force levels is the focus of the present chapter.

Neuromechanical computer models of the hand and empirical evidence have indicated that maximal force levels of precision grasping are produced by a unique and subject-independent pattern of muscle activation, suggesting that the redundancy of control disappears due to the mechanical requirements of maximal precision grasping (Valero-Cuevas, Zajac & Burgar, 1998). Because of the muscular redundancy associated with finger control (i.e. fingers have more muscles than DOFs to be controlled), however, sub-maximal fingertip forces could potentially be produced by multiple muscle coordination strategies (Valero-Cuevas, 2000). Prior research has proposed potentially conflicting paradigms describing the coordination of intrinsic and extrinsic hand musculature to achieve sub-maximal force levels of grasping. Chao proposed that finger muscles are divided into functional classes (primary, secondary, and tertiary muscle groups), whose activation levels depend on the amount of load applied to the fingers (Chao, 1989). Studies of the contribution of finger muscles to isometric precision grasp force have also suggested functional groups of hand musculature (Maier & Hepp-Reymond, 1995a). Other investigations have proposed that a flexible paradigm of task-specific muscle groupings (i.e. muscle synergies) may govern the coordination of muscles in precision grasping (Macpherson, 1991, Maier & Hepp-Reymond, 1995b). In contrast, three to four muscle synergies (a group of muscles whose relative activation levels are neurally coupled) have been reported to describe the patterns of muscle activity associated with the hand postures required to interact with a large number of everyday objects at user-determined force levels (Weiss & Flanders, 2004). Finally, other researchers have proposed a simpler governing control paradigm for sub-maximal force precision grasping, and have suggested that the patterns of muscle coordination are a simple scaling of that observed at maximal force grasping (Valero-Cuevas, 2000, Valero-Cuevas, 2005).

Several studies have suggested that the EMG patterns associated with a wide variety of automatic and volitional control tasks of the neuromotor system can be decomposed into a dimensionally reduced set of muscle synergies (d'Avella et al., 2006, Ting & Macpherson, 2005, Tresch et al., 1999). However, not all properties of the muscle synergy groups are clear or intuitive. One necessary behavior of muscle synergies in accordance with the neuromotor synergy hypothesis is that they exhibit the property of scaling. Scaling implies that as the activation level of a given synergy is increased, the structure of the synergy remains intact (i.e. muscles retain their relative levels of activation) (Lee, 1984). Furthermore, scaling implies that the set of synergies employed to perform a task stays constant, while the synergy activation levels scale with the increase in the force requirements of the task. Thus, this investigation aims to explore the scaling of muscle synergies in static power and precision hand grasp tasks of sub-maximal isometric force levels. Specifically, it was hypothesized that the coordination patterns (CP) used to produce the same multi-digit grasp at varying isometric force levels are statistically linearly scaled versions of a single characteristic vector. The alternative hypothesis is that statistically different muscle coordination strategies are used to produce the same multi-joint grasp pattern at varying isometric force levels. This hypothesis has been examined in end-point precision grasping as previously described, but not extensively in multi-digit whole hand grasping. The investigator extends this hypothesis to suggest that the muscle synergies underlying the decomposition of these coordination patterns linearly scale with increasing grasp force. Within this hypothesis, the following three questions are examined.

- How well is the *magnitude* of the CP vector linearly correlated with the grasp force level over the investigated force range?
- Is the *direction* of the CP vector, and correspondingly the muscle coordination strategy, invariant to isometric force level for a given grasp?

- Finally, how well are the activation levels of the muscle synergies associated with hand grasping correlated to grasp force? Alternatively, is the correlation poor and/or piecewise, suggesting that different synergies are better suited for different force levels of grasping?

5.2 Methods

5.2.1 Subject Information

Thirteen research subjects (four women, nine men, age 28.6 ± 8.0 yrs), twelve of which were self-described right-hand dominant versus one self-described as left-hand dominant, participated in this study. No subject had known history of any neuromuscular disorders. All subjects gave informed consent to the procedures as approved by the Northwestern University Office for the Protection of Research Subjects (NUOPRS) Institutional Review Board. Subjects are referred to by their Subject ID number (SID₁₋₁₃).

5.2.2 Maximal Voluntary Grasp Strength

The maximal voluntary grasp (MVG) strengths of cylindrical, lateral, palmar, and tip grasping (Figure 5.2) were tested for each subject. Maximal power (cylindrical) grasping strengths were recorded using a standard Sammon's Preston (Bolingbrook, IL) clinical hand dynamometer, instrumented with a Honeywell (Acton, MA) Mediamate pressure transducer. Maximal precision grasping strengths were recorded using an in-house fabricated pinch gauge instrumented using a standard fifty-pound load cell from Load Cell Central (Monroeton, PA). MVGs were recorded both pre and post insertion of the percutaneous (fine-wire) electrodes used for muscle activity recording. While some literature has reported that fine-wire electrodes do not affect maximal

grasp strength (Burgar et al. 1997; Valero-Cuevas 2000), it has been the author's personal experience that, due to the large number of percutaneous electrodes used in the current study, MVGs could potentially be affected. The maximal grasp strengths pre and post fine-wire insertion are reported for all grasp types. In addition, subjects were instructed to perform maximal voluntary movements of finger extension, adduction, and abduction, and general maximal excursion of hand movements. MVG forces recorded post fine-wire insertion were used as reference points during the remainder of the protocol and data analyses, and the associated maximal electromyographic (EMG) activities were used in the analyses to normalize the recorded muscle activities during the experimental tasks.



Figure 5.1. Instrumented gauges for grasp force measurements.

(Left) Power grasp forces were measured using an instrumented clinical hand dynamometer. (Right) Precision grasp forces were measured using an in-house fabricated pinch gauge.

5.2.3 Electromyography

Electromyography recordings were performed as described in section 4.2.2 (Electromyography) of this manuscript. Briefly, EMG signals were recorded using bipolar intramuscular wires from an eleven-muscle set consisting of FDS, FDP, EIP, EDC, EDM, EPL, FPL, APL, FDI, and the thenar (TE) and hypothenar (HTE) eminences, as shown and described in Figure 4.1 and Table 4.1. Signals were recorded at 3000 Hz using a Noraxon (Phoenix, AZ) Telemyo 2400R system, and processed through a 20 – 1000 Hz analog bandpass filter with a gain of 2000. The data were recorded and visualized using an in-house custom built virtual

instrument interface in National Instruments (Austin, TX) LabVIEW Developer's Environment ver 7.2. Raw EMG was saved in a standard ASCII file for further processing.

5.2.4 Tasks and Data Collection

Study participants were seated comfortably in an upright chair with the dominant arm and wrist supported, and were instructed to perform a force-tracking task using each of four hand postures: cylindrical, lateral, palmar, and tip (Figure 5.2A-D). Each subject randomly determined the order of the performed grasps. The force-tracking task consisted of tracking a force curve composed of randomly ordered force plateaus, ranging between 5% and 50% MVG at 5% step intervals (Figure 5.2E). The plateau was three seconds in duration, with a two-second rest period between consecutive plateaus. This rest period served to washout any potential effects the presentation order of force may have had on the coordination strategies chosen by the motor system. An on-screen trace line that corresponded to the current grasp force level was used for visual feedback. Data from the middle two seconds of constant force activity were chosen for further analysis (gray sections of Figure 5.2E). Subjects performed fifteen trials of each of the ten force levels for a total of 150 randomly ordered trials per grasp. Each grasping task took approximately thirteen minutes to complete. Subjects were allowed as much time as desired to rest between grasping tasks to prevent muscle fatigue, and typically took between five and ten minutes.

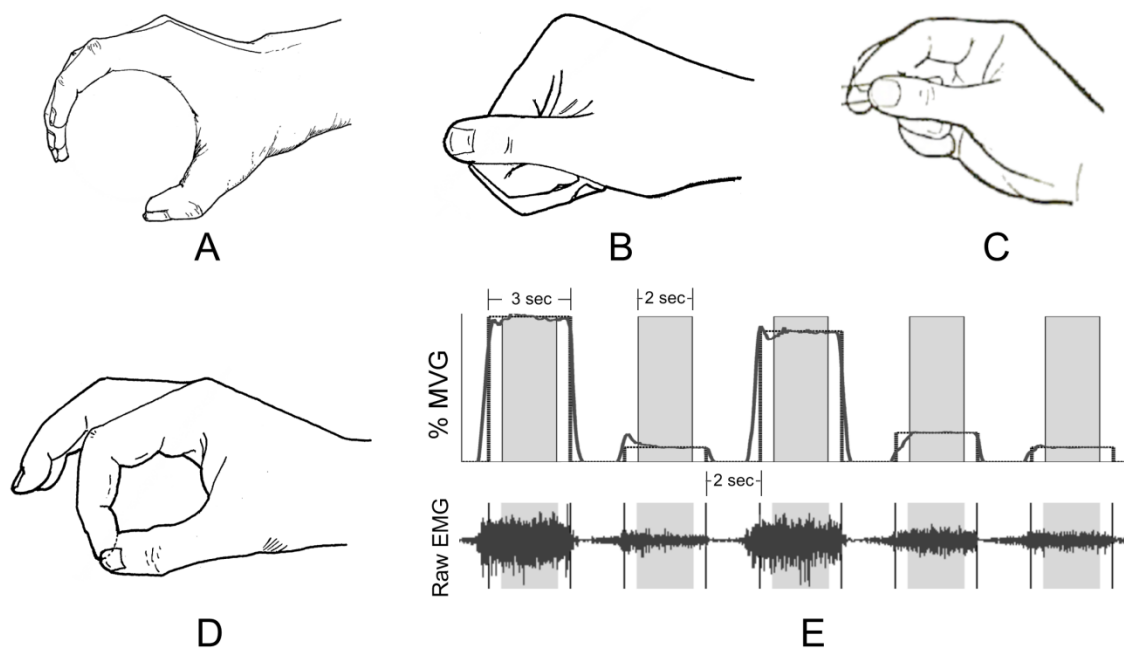


Figure 5.2. Hand postures and force-tracking task.

Subjects shaped their dominant hand into each of four hand postures: A) Cylindrical B) Lateral C) Palmar D) Tip. E) Using each posture, subjects performed a force-tracking task in which they were visually guided to range the grasp strength between 5% and 50% of their maximum voluntary grasp (MVG) strength at 5% intervals, with the order fully randomized. Illustrated is a typical trace of five out of 150 tracking attempts for a given posture. The force-tracking curve (black dotted line) consisted of 60% duty cycle trials of length 5 seconds. Cylindrical grasp force was measured using an instrumented hand dynamometer, and lateral, palmar, and tip grasp forces were measured using an instrument pinch gauge. Only the middle two seconds of steady state force production (gray regions) were further analyzed.

5.2.5 Data Analysis

Before further analysis, all recorded EMGs were first bandpass (30 Hz – 600 Hz) and notch filtered (59.5 Hz – 60.5 Hz). The root-mean-square (RMS) values of the resulting signals were computed over the middle two seconds of constant force grasping. This RMS value was used as the representative EMG activity for each muscle. This value was normalized relative to the resting and maximum activities of the particular muscle observed in all trials of all experimental

tasks, such that the resultant muscle activities ranged between zero and one. Each trial of constant force was represented as an eleven-dimensional vector in normalized muscle space, with each dimension corresponding to one of the investigated muscles. Each data matrix of recorded activity (V_{CYL} , V_{LAT} , V_{PAL} , and V_{TIP}) therefore was of dimension 11 x 150 (muscles x observations). There were a few instances when subjects did not adequately maintain the proper amount of grasp force, and these multivariate outliers were removed from further analysis using the Mahalanobis distance metric (Filzmoser, 2004, Rousseeuw & Vanzomeren, 1990a, Rousseeuw & Vanzomeren, 1990b).

5.2.5.1 Effect of Fine-Wire Electrodes on Maximal Voluntary Grasp (MVG) Strength

For each grasp type, a pair-wise t-test was performed to determine if there was a statistical difference in the pre- versus post- fine-wire maximal voluntary grasp strengths across the subject population. A pair-wise t-test was also performed with pooled data from all grasp types to determine whether insertion of fine-wire electrodes significantly affected general hand grasp strength. Statistical significance was assessed at the $[\alpha, \beta] = [0.05, 0.85]$ significance level. Analyses were performed using SPSS, Inc.'s (Chicago, IL) SPSS version 15.0 statistical software package.

5.2.5.2 Correlation of CP Vector Magnitude to Grasp Force

The relationship between grasp force (GF) and muscle coordination pattern magnitudes was first quantified to determine if the two were linearly proportional. For each grasp, the magnitude of the coordination pattern vectors was calculated for all trials of each desired grasp force level j using the Euclidean norm, given in equation 5.1. A linear regression was performed per grasp type per subject on grasp force versus coordination pattern (CP) magnitude (equation 5.2),

returning a Pearson coefficient (r) to characterize the degree of linear correlation between the two. The population averaged Pearson correlation coefficient is reported for this analysis.

$$\overline{CP}_j = \left\| \langle m_{j1}, m_{j2}, \dots, m_{j11} \rangle \right\| = \sqrt{\sum_{i=1}^{11} (m_{ji})^2} \quad (5.1)$$

$$GF = \beta_0 + \beta_1 \cdot \overline{CP} + \varepsilon \quad (5.2)$$

5.2.5.3 Variance of CP Vector Direction wrt Grasp Force

To systematically assess whether grasp force had a significant effect on the direction of the coordination pattern vector for the subject population, a repeated measure multivariate analysis of variance (RM-MANOVA) was performed on the full thirteen-subject data set, with each subject's response per force level represented by an optimal trial. The optimal trial at each force level was determined to be that in which the subject's average grasp force minimally deviated from the targeted grasp force level. The trial for each force level was represented as a unit normalized eleven-dimensional vector of muscle activity, so that the CP vector magnitude would not affect the results of the statistical test. Hence the only differences in the vector would be attributable to direction, which would signify different coordination patterns. Conceptually similar to a repeated measures analysis of variance (RM-ANOVA), the RM-MANOVA analysis served to test if the systematic variance observed in the CP vector directions due to the effect of grasp force was significantly greater than the unsystematic variance due to expected differences in the subject population. In other words, this analysis tested if the differences observed in the CP vector directions relative to grasp force level were due to chance. The null hypothesis that grasp force had no effect on the coordination pattern vector, and hence the observed differences were due to random chance, was tested at the $[\alpha, \beta] = [0.05, 0.85]$

significance level. If the RM-MANOVA test returned a statistically significant p-value, eleven univariate repeated measure analysis of variance (URM-ANOVA) tests were performed. These tests served to determine if the normalized activity of each individual muscle statistically differed between the investigated force levels, thereby determining the cause(s) of the differences in vector directions, and hence the root of the differences in muscle coordination patterns.

5.2.5.4 Activations of Muscle Synergies wrt to Grasp Force

An analysis of the relationship between grasp force and the activation levels of the underlying synergies composing the EMG patterns of grasping was performed on seven of the thirteen subjects. To perform this synergy analysis, the span of investigated hand postures was increased by including EMG data associated with miming of 33 letters and numbers of the ASL posture set. This EMG data was the same data acquired from the seven subjects in the previous study investigating the predictive power of muscle synergies, described in *Chapter 4: Muscle Synergies as a Predictive Framework for EMG Patterns of Static Hand Postures*. Briefly, subjects performed seven trials of miming each of the 33 ASL postures (Figure 4.2), presented in randomized order. Subjects mimed each posture for eight seconds, with two seconds in between each posture. All eleven EMG signals were filtered using a sixth-order Butterworth bandpass filtered [30, 600] Hz, and notch [59.5, 60.5] Hz. RMS values were calculated on the static portion of the posture mimes ($t = 2.5 \text{ sec}$ to $t = 5 \text{ sec}$), which were then normalized relative to the resting and maximum activities of the respective muscles observed during maximal voluntary contraction (MVC) tests. The full data matrix \mathbf{V}_{ASL} of recorded activity for each subject was thus of dimension 11×231 . Thus the full data matrix $\mathbf{V} = [\mathbf{V}_{ASL} \ \mathbf{V}_{CYL} \ \mathbf{V}_{LAT} \ \mathbf{V}_{PAL} \ \mathbf{V}_{TIP}]$ of both the posture miming and force-tracking tasks was 11×831 .

Non-negative matrix factorization (NMF) (Lee & Seung, 1999, Lee & Seung, 2001) was used to calculate the underlying synergies of the EMG patterns associated with the postures and grasp force levels of the force-tracking task. The data matrix \mathbf{V} was separated into a synergy generation matrix \mathbf{V}_{gen} and a cross-validation matrix \mathbf{V}_{cv} . \mathbf{V}_{cv} (11×180) consisted of 30% of the trials from the force-tracking task of each posture, while \mathbf{V}_{gen} (11×651) consisted of the remaining force-tracking trials and the data from the ASL posture miming task. Synergy and source matrices \mathbf{W}_{gen} and \mathbf{H}_{gen} , respectively, were calculated of \mathbf{V}_{gen} , using the objective function and multiplicative update rules of equations 3.8 – 3.9. The synergies \mathbf{W}_{gen} were validated on \mathbf{V}_{cv} by estimating \mathbf{H}_{cv} while holding constant \mathbf{W}_{gen} . The validity of each estimation was quantified by the amount of variance explained (VE) in the original data matrices \mathbf{V}_{gen} and \mathbf{V}_{cv} by the estimated matrices $\mathbf{V}_{est,gen} = \mathbf{W}_{gen} \times \mathbf{H}_{gen}$, and a cross-validation matrix $\mathbf{V}_{est,cv} = \mathbf{W}_{gen} \times \mathbf{H}_{cv}$, respectively. n synergies were estimated, with n ranging from one to thirteen, and the appropriate number of synergies n was determined to be the knee of the VE vs n curve. The knee was defined to be that point in which adding more synergies did not significantly increase the amount of variance explained by the muscle synergy model. Statistically, this was the smallest n such that a linear fit of the VE curve, from n to 13, had a residual mean square error less than $5e-5$. The determined matrix of synergy activation coefficients \mathbf{H} were plotted versus the grasp force for each grasp type to determine the linear relationship between the two. Reported for each determined synergy is the correlation coefficient of its activation level with grasp force, along with the amount of variance explained by the synergy.

5.3 Results¹

5.3.1 Effect of Fine-Wire Electrodes on Maximal Voluntary Grasp (MVG) Strength

Paired t-test analyses comparing MVG strength pre and post fine-wire insertion revealed that insertion of the fine-wire electrodes had a statistically significant effect ($p < 0.05$) across the subject population. Average MVG values [pre-insertion, post-insertion] in Newtons (mean \pm SD) for cylindrical were [517.1 \pm 95.7, 407.8 \pm 113.4], and for lateral were [103.8 \pm 18.6, 74.7 \pm 13.6]. Significance of the fine-wire effect was observed ($p < 0.05$) for both the cylindrical and lateral grasps. Specific p-values for each grasp are reported in Table 5.1.

Table 5.1. Effect of Fine-Wire Electrodes on MVG Strength: Paired T-test Analysis

Grasp	Pre minus Post MVG Mean \pm SD (N)	t	df	P
<i>Cylindrical</i>	109.4 \pm 87.0	4.4	11	0.001
<i>Lateral</i>	29.1 \pm 17.7	5.7	11	< 0.001

¹ The results for the cylindrical and lateral grasp patterns are reported in this section, while the results for the palmar and tip grasps are reported in Appendix A. The reason for this is extraneous movements of the hand not contributing to the grasp force were generally more restricted in the cylindrical and lateral grasp patterns. In the palmar and tip grasp patterns, non-involved digits were not restricted in the study, thereby negating the isometric nature of the force-tracking task and potentially introducing confounding variables into their results. In hindsight, these extraneous digits should have been restricted for unconfounding and interpretable results. Nevertheless the results for these two grasps (palmar and tip) are reported in Appendix A, but not compared to the results of the isometric force tracking tasks using the cylindrical and lateral grasps.

5.3.2 Correlation of CP Vector Magnitude to Grasp Force

The linear regression of grasp force versus coordination pattern (CP) vector magnitude resulted in average (mean \pm SD) Pearson correlation coefficient (r) values for the cylindrical and lateral grasps of 0.94 ± 0.04 and 0.91 ± 0.08 respectively. The correlation coefficient is the equivalent of the standardized coefficient β_1 in equation 5.2. The corresponding adjusted r^2 values, quantifying how much of the observed variance in grasp force was explained by the CP vector magnitude, were 0.89 ± 0.07 and 0.83 ± 0.13 , respectively. Both correlation values were statistically significantly different from zero ($p < 0.05$). Hence as expected, grasp force was significantly linearly correlated with the magnitude of the muscle coordination pattern vector associated with both the cylindrical and lateral multi-joint grasps.

5.3.3 Variance of CP Vector Direction wrt Grasp Force

The working hypotheses tested were that for each of the hand postures, the force vectors representing each muscle coordination pattern were scaled versions of a single characteristic vector and hence did not statistically differ with respect to direction i.e. the vectors lay in a one-dimensional subspace. The Wilks's Lambda (Λ) and p-values of significance are reported for each grasp. The Λ statistic is a multivariate version of the standard F-statistic and is formulaically transformed such that it has an approximate F-distribution with the appropriate degrees-of-freedom, resulting in a standard p-value (Bock, 1975, Bray & Maxwell, 1985). For the cylindrical grasp, the RM-MANOVA analysis resulted in $\Lambda = 0.342$ and $p = 0.142$. Hence, *the vector representations of the coordination patterns at different force levels of the cylindrical grasp were not statistically different with respect to direction across the subject population.*

Analysis of the lateral grasp resulted in $\Lambda = 0.143$ and $p < 0.001$. Hence, for this precision grasp, the vector representations of the muscle coordination patterns at the varying force levels were statistically different with respect to direction, *thereby implying that across the subject population, statistically different muscle coordination strategies were used with respect to precision lateral grasp force level*. The RM-MANOVA was followed up with a univariate repeated measure ANOVA (URM-ANOVA) for each muscle to determine which muscle(s) caused the significant differences observed in the directions of the muscle coordination vectors of lateral grasping. This analysis reported the activities of TE ($p = 0.003$) and FPL ($p = 0.012$) to be significantly different between the force levels of lateral grasping, and that of EDC ($p = 0.064$) was borderline significant.

5.3.4 Activations of Muscle Synergies wrt to Grasp Force

The activation levels for each estimated synergy relative to cylindrical and lateral grasp forces are plotted in Figure 5.3 for a representative subject. Shown with each plot is the amount of variance explained by the particular synergy-activation level combination for the cylindrical and lateral grasps. A linear regression revealed the extent to which the activation levels of the synergies were correlated with grasp force, along with p-values assessing the significance of the regression slope.

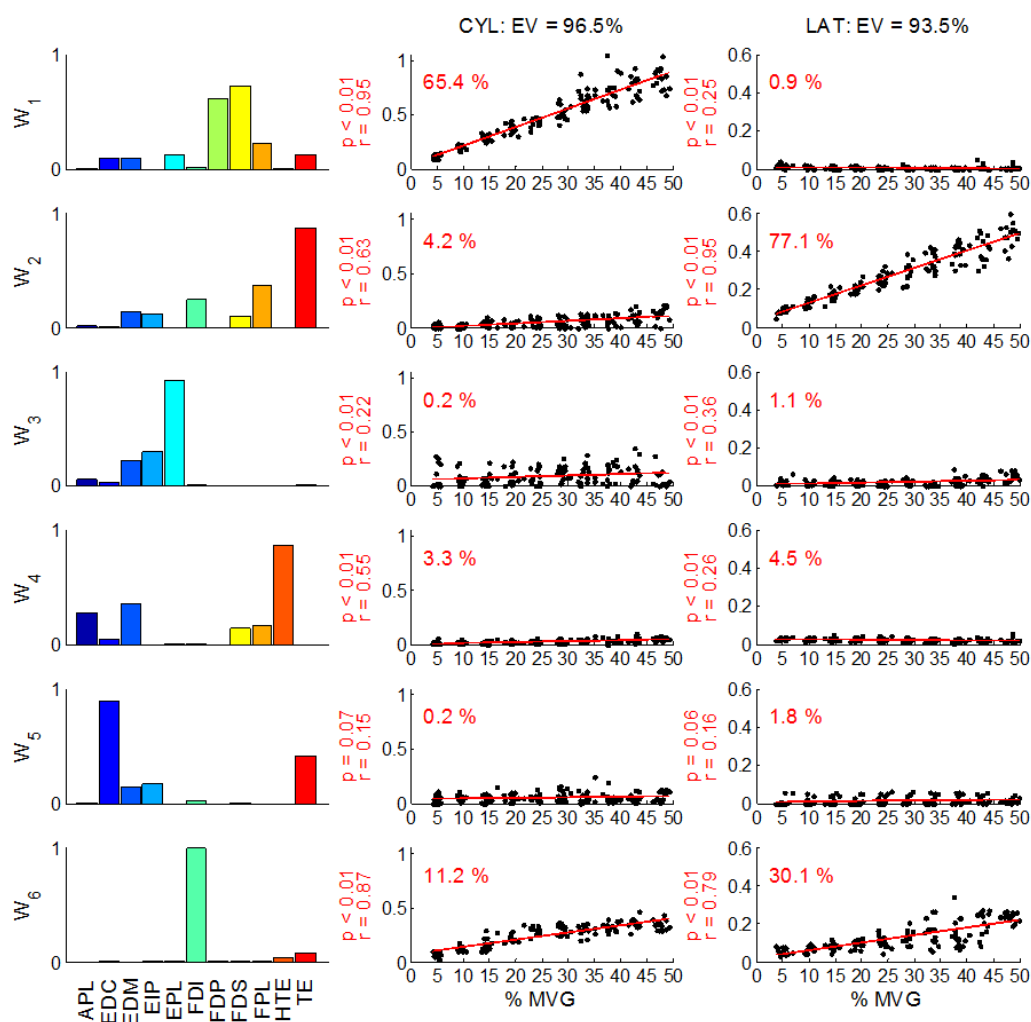


Figure 5.3. Synergy structures and activation levels for a representative subject.

Bar plots in column one show the structure of the synergies extracted from the ASL posture miming and force-tracking tasks. Scatter plots in columns two and three show the activation level of each synergy relative to cylindrical and lateral grasping forces, respectively. The amount of explained variance (EV) of each synergy-activation level combination is shown on each graph as a percentage. A linear regression of activation level versus grasp force revealed the significance of the relationship between the two. Associated correlation (r) and significance (p) values are shown to the left of each plot. In the cylindrical grasp, the first three to four synergies (i.e. most variance explained) were typically highly correlated, while only the first two synergies were highly correlated with lateral grasp force. As the amount of variance explained by successive synergies decreased, the correlation between activation level and grasp force generally decreased.

For this representative subject, the top three to four synergies were moderately to highly significantly correlated with cylindrical grasp force, while the top two synergies were moderately to highly significantly correlated with lateral grasp force. The level of correlation seemed to decrease with a decrease in the amount of variance explained by the synergy. Note that the most important synergies (i.e. those that explained the most variance) were not necessarily the same for the two grasp types. For example, the activation level of synergy W_1 was highly correlated ($r = 0.95$, $EV = 65.4\%$) with cylindrical grasp force, while it was very weakly correlated with lateral grasp force ($r = 0.25$, $EV = 0.9\%$). In contrast, the activation level of synergy W_2 was highly correlated with lateral grasp force ($r = 0.95$, $EV = 77.1\%$), while it was much less correlated with cylindrical grasp force ($r = 0.63$, $EV = 4.2\%$). Figure 5.4 reports the average variance explained across the subject population for the first four synergies of each subject. Figure 5.5 shows the population averaged correlations between these ordered synergies with cylindrical and lateral grasp forces. Again, across the subject population, the correlation of each synergy's activation with grasp force seemed to decrease with decreasing importance of the synergy to the task (i.e. decreased explained variance).

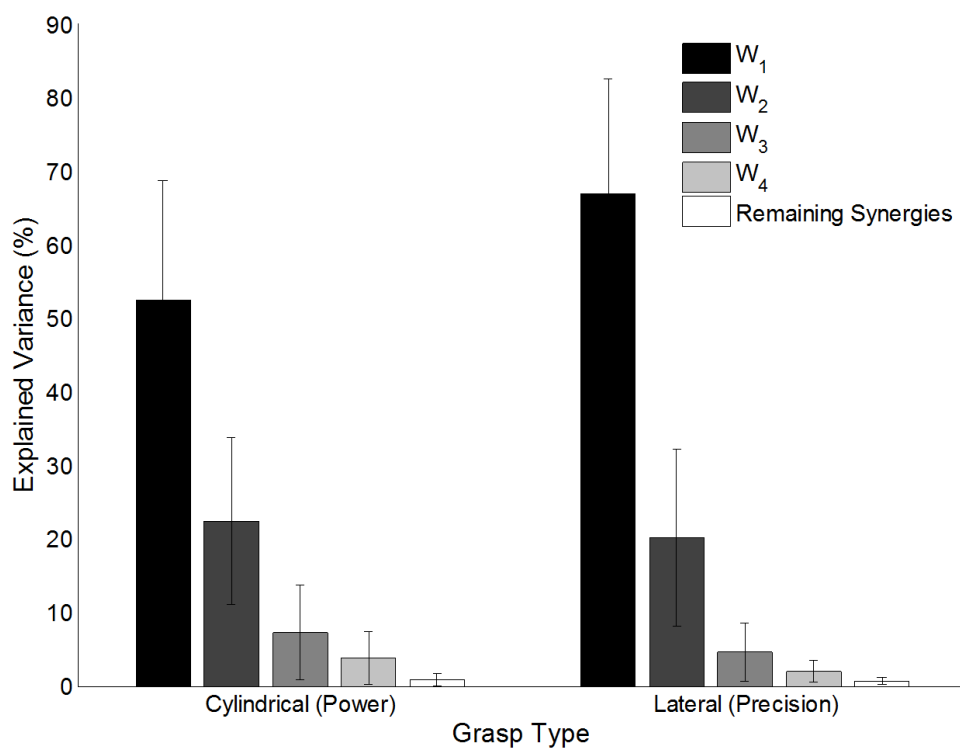


Figure 5.4. Population averaged explained variances of synergies for ASL and force-tracking.

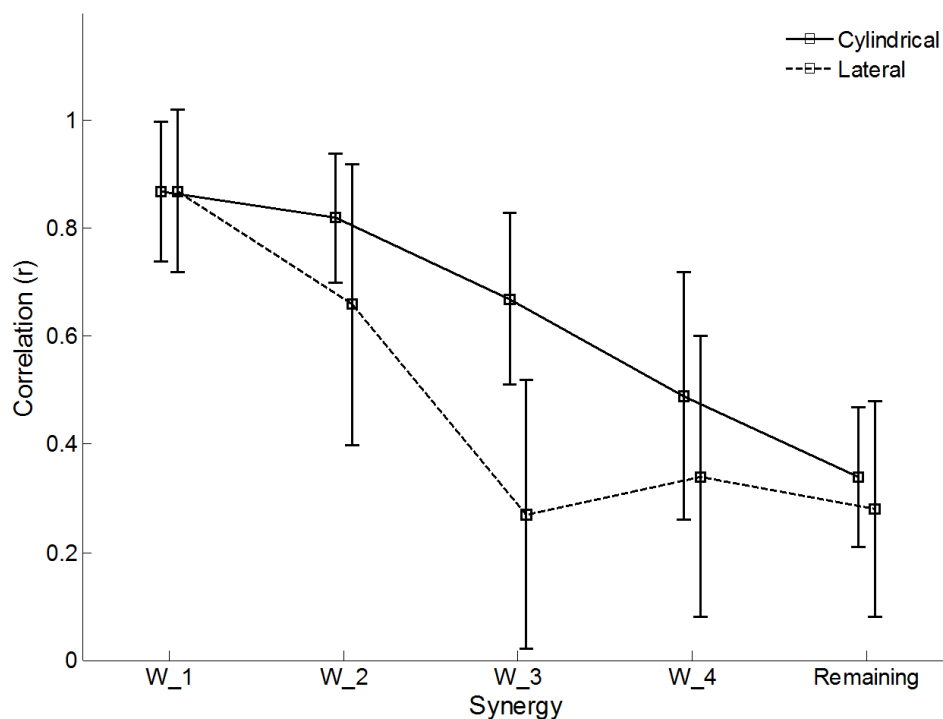


Figure 5.5. Population averaged correlations of synergy activations to exerted grasp force.

Shown are the correlation values for the activation levels of synergies W_1 to W_4 , and the remaining synergies. Synergies are numbered in order of most explained variance of the force-tracking task using each grasp type. As the percentage of variance explained decreases (Figure 5.4), the correlation of activation level also decreases. Nevertheless, the activation levels of the first three to four synergies are moderately to highly correlated with cylindrical grasp force, while the first the activation levels of the first two synergies are moderately to highly correlated with lateral grasp force.

Functionally, the synergies that exhibited the most consistent scaling of activation level with grasp force consist of the muscles that one would expect to be relevant to the specified task. For example, the data of the representative subject illustrated in Figure 5.3 shows that for the cylindrical grasp, the two most dominant and scalable synergies were ones that primarily controlled activation of the finger flexors (FDS and FDP), and one that primarily controlled index finger abduction (FDI). The two most dominant and scalable synergies for the lateral grasp

were ones that primarily controlled intrinsic thumb flexion and abduction adduction (TE), and one that primarily controlled index finger abduction (FDI). Similar dominant synergies were found in other subjects, with some subjects additionally exhibiting dominant and highly scalable synergies involving the extrinsic thumb flexor (FPL) and extensor (EPL) for one or both of the cylindrical and lateral grasps.

5.4 Discussion

5.4.1 Main Findings

This investigation has sought to understand the relationship between muscle coordination patterns, the activation levels of the underlying muscle synergies, and sub-maximal levels of grasping force in multi-joint precision and power hand grasp patterns. Much of the current literature has reported somewhat differing views on the paradigms of control of sub-maximal muscle coordination, particularly concerning control of endpoint index finger forces. This study has expanded the investigation from control of forces of a single endpoint to include whole hand grasp force control in multi-joint grasp patterns. This study is additionally unique because it has examined these muscle coordination patterns incrementally over a wide range of grasp forces. Finally, it has examined these patterns within the context of a muscle synergy paradigm, and specifically sought to understand how the activation of muscle synergies are affected by overall hand grasp force. Perhaps one limitation of the current investigation, and of all investigations that use fine-wire electrodes to record EMG activity, is that due to the large number of percutaneous electrodes, the manner in which the research subjects performed the specified hand tasks may have been adversely affected. It was clear that the full set of inserted

electrodes affected the maximal voluntary grasp (MVG) force for the hand patterns, though no subject reported any significant pain while performing the experimental tasks. Hence, it was assumed that the recorded muscle coordination patterns were indicative of that which the subjects would normally use in whole hand grasping.

The main findings of this investigation are that first, the muscle coordination patterns associated with isometric cylindrical hand grasping at sub-maximal force levels were statistically a simple result of linearly scaling a single coordination pattern, while this was not the case for lateral precision grasping. The magnitudes of the coordination patterns did seem to linearly scale with an increase in exerted force using either grasp. Furthermore, the extracted muscle synergies that serve as the basis vectors (i.e. primitives) for these EMG patterns generally scaled with increasing grasp force. Specifically, the top three to four synergies exhibited linear scaling of activation levels with increasing cylindrical grasp force, while only the first two seemed to exhibit linear scaling of activation levels with increasing lateral grasp force. The degree of correlation of activation level to grasp force level was directly related to the amount of variance explained by the synergy.

5.4.2 Scaling of Activation Coefficients

The observed muscle coordination patterns (CP) were represented as vectors in EMG space, possessing both magnitude and direction. The magnitudes of these vectors were indicative of the overall grasp force levels. It is well established that muscle activity cannot be considered linear over the entire contraction range due to changes in muscle properties resulting from changes in sarcomere length (Basmajian & De Luca, 1985, Valero-Cuevas, 2000, Zajac, 1989). However, the tasks specified in this investigation only required subjects to produce isometric force contractions, where the muscle lengths would be at most insignificantly changing, and

linear relationships could be expected between force and individual muscle activities (Lawrence & Deluca, 1983, Maier & Hepp-Reymond, 1995a). Thus, even given the possibility that the relative lengths between muscle belly and accompanying tendon could slightly vary in the isometric task, it was reasonable to expect that the relationship between grasp force and the CP vector magnitude would be linear.

What was not necessarily clear to expect was that the activation levels of the underlying muscle synergies would linearly scale with grasp force. At least three scenarios could have occurred. The first is that all synergies underlying the EMG patterns of a grasp could simply linearly scale with an increase in the exerted grasp force. This would result in a force invariant EMG pattern, whose overall magnitude would also scale tightly with grasp force. Such a result would be in congruence with what has been reported in some end-point force production tasks (Valero-Cuevas, 2000, Valero-Cuevas, 2005). A second scenario would be that the dominant synergies would scale linearly with grasp force, while the lower-order synergies would maintain a constant level of activation, or be more variable in activation. This would suggest that subjects actively modulate these important synergies for the given hand grasp task, and that the observed variability would be due to these lower-order unmodulated synergies. The well modulated synergies could be considered to comprise a controlled manifold, while the variable synergies could be considered to comprise an uncontrolled manifold (Latash, Scholz, Danion & Schoner, 2001, Latash, Scholz & Schoner, 2002, Shim, Latash & Zatsiorsky, 2003, Zatsiorsky & Latash, 2004). A third scenario would be that due to the potentially different biomechanical requirements of producing a multi-joint grasp at higher force levels, such as joint stabilization, the activation level of synergies could scale in a non-linear manner. They could also scale in a piecewise manner, where different and/or more synergies are recruited at higher force levels, due to an increase in the recruitment of different motor unit pools. This could potentially result

in what some other researchers have suggested to be flexibility in the muscle synergy paradigm, lack of fixed muscle synergies for varying task requirements, and/or load-dependent muscle groupings (Buchanan et al., 1986, Chao, 1989, Macpherson, 1991, Maier & Hepp-Reymond, 1995b, Soechting & Lacquaniti, 1989). The muscle synergies underlying the cylindrical force-tracking task generally followed scenario one. The activation levels of the dominant synergies scaled well with increasing grasp force. This reinforced the results of the RM-MANOVA test, which showed that the overall EMG coordination pattern for cylindrical grasping was invariant to force level. Any variability seen in the data was due to random chance, that is likely attributable to the remaining synergies that explained less than two percent of the variance in the data. The activation levels of only the top two synergies underlying lateral grasping at varying force levels scaled well with force (scenario two). This could thus explain why there was a statistically significant difference in the overall EMG coordination patterns, as determined by the RM-MANOVA test. The non-scaling synergies explain greater than 10% of the data variance, and hence could account for significant variations in the coordination pattern vector direction.

5.4.3 Implications for Myoelectric Control

Scalability of inputs in myoelectric control paradigms is important because it allows for implementation of proportional control. The speed of the motors of the controlled device is directionally proportional to the magnitude of the input signal. The fact that the primary synergies in a power grasp have been shown to scale with increasing grasp force (and hence force of muscle contraction) suggest that the synergy paradigm could be used to implement proportional control for power grasping. However, this is less promising in the precision

grasping case because only the first two synergies scale well with increasing force of muscle contraction.

5.5 Conclusion

As stated in the introduction, scaling of muscle synergies is a necessary property of the neuromotor synergy hypothesis (Lee, 1984). The muscles within a synergy should maintain the same relative activation levels, and the synergies involved within a task should remain consistent with an increase in the task force requirements. The results of this investigation show that the dominant synergies involved in cylindrical and lateral force-tracking tasks do linearly scale with grasp force. This scaling thus possibly allows for implementation of proportional control of myoelectric devices.

6 Independent and Simultaneous Volitional Control of Muscle Synergies

6.1 Introduction

Myoelectric control is a standard of practice for the actuation of electrically powered devices such as upper-limb prostheses and teleoperated robotic arms. The success of myoelectrically controlled devices is largely dependent both on the efficacy of the elicited myoelectric input signals and the paradigm employed for discerning, from the acquired EMG patterns, the desired controlled degree-of-freedom (DOF) and/or function. With regard to signal efficacy, significant work has been done in the development of implantable myoelectric sensors (IMES) which serve to increase the number of myoelectric input control sites and decrease signal compromise via cross-talk (Weir, 2003, Weir, Kuiken & Ajiboye, 2004a, Weir, Kuiken & Ajiboye, 2004b). With regard to the discerning paradigm for control, current commercially available myoelectric prosthetic devices typically employ a single-input-single-output (SISO) algorithm, where the activities of a pair of agonist myoelectric inputs are tied to the control of a single degree-of-freedom. Such a paradigm is in theory functionally limited when the number of controlled DOF becomes large. As a result, much research has gone into developing pattern recognition based systems, which rely on extracting and recognizing consistent spatial and time domain features from global EMG patterns. Several of these methods include the use of basic time domain features, autoregressive coefficients, linear discriminant analyzers, and Gaussian mixture models, used in conjunction with fuzzy logic and artificial neural network architectures (Ajiboye & Weir, 2005, Englehart et al., 2001, Huang et al., 2005, Hudgins et al., 1993). Many of these

methods, though, have not been shown to be successful in a scenario where the user has to simultaneously control two or more degrees-of-freedom. With regard to simultaneous control of myoelectric devices, at least two criteria have been suggested as qualitative measures of success. First, independent control should still exist within the context of simultaneous control i.e. it should be possible to control any function without interfering with the control of other functions. Second, the simultaneous and coordinated control of independent degrees-of-freedom should be subconscious and exert a low mental burden on the user (Childress, 1992).

The study described in this chapter investigates the use of muscle synergies as a viable means of simultaneous myoelectric control of multiple degrees-of-freedom. Muscle coordination for the control of movement has been termed an “ill-posed” problem due to the redundancies of the neuromotor system (Bernstein, 1967). One way that the neuromotor system potentially solves this redundancy is by specifying the activities of muscles through functional groups, termed muscle synergies. Several studies have suggested that the central nervous system uses lower level primitives of muscle coordination (i.e. muscle synergies) to produce more complex automatic and natural motor behaviors, such as arm reaching, standing, and varying methods of locomotion (d'Avella et al., 2006, d'Avella et al., 2003, Torres-Oviedo et al., 2006). Other researchers have shown that a wide variety of hand postures can be described by a paradigm based upon muscle synergies (Weiss & Flanders, 2004). Furthermore the investigations described in previous chapters of this manuscript have shown that the muscle synergy paradigm is robust in that it allows for prediction of the EMG activity patterns of new postures, and generally scales with increasing activity of force. What is not clear is if users can volitionally activate groups of synergies for the purposes of independent and simultaneous control of multiple degrees-of-freedom. Furthermore, the benefit of a synergy based control paradigm versus a SISO based control paradigm is unclear. Hence, the goal of this

investigation is to characterize, through a virtual target reaching task, the volitional independent and simultaneous control of multiple degrees-of-freedom using muscle synergies versus single-muscle inputs. Specifically, it is hypothesized that, due to the underlying neural and biomechanical coupling of muscles into synergy-based groups, users would better and more intuitively achieve independent control of myoelectric inputs using a control paradigm based upon muscle synergies over one based upon single-muscle control. Success of control is quantified by the final end point error, the activation levels of the undesired synergies, the error of path linearity in reaching the virtual target, and the minimization of the activity within the null space of control (i.e. redundant information). Furthermore, it is hypothesized that subjects are able to simultaneously modulate pairs of muscle synergies more successfully than pairs of single muscles to perform the virtual reach task. The alternative hypothesis is therefore that a synergy-based control paradigm would prove more difficult for successful completion of the virtual reach task than a single-muscle based control paradigm.

6.2 Methods

6.2.1 Subject Information

Five healthy research subjects (three men, two women, age 27.6 ± 4.3 yrs), all of which were self-described right-hand dominant, participated in this study. No subject had known history of any neuromuscular disorders. Subjects were obtained from a diverse population at the Rehabilitation Institute of Chicago and Northwestern University, and efforts were made to be consistent with the demographics of the Chicago area. All subjects gave informed consent to the procedures as approved by the Northwestern University Office for the Protection of

Research Subjects (NUOPRS) Institutional Review Board. Subjects are referred to by their Subject ID number (SID₁₋₅).

6.2.2 Electromyography

Electromyography recordings were performed as described in section 4.2.2 (Electromyography) of this manuscript. Briefly, EMG signals were recorded using bipolar intramuscular wires from FDS, FDP, EIP, EDC, EDM, EPL, FPL, APL, FDI, and the thenar (TE) and hypothenar (HTE) eminences, as shown and described in Figure 4.1 and Table 4.1. Signals were recorded at 3000 Hz, and processed through a 20 – 1000 Hz analog bandpass filter with a gain of 2000. The data was recorded and visualized using an in-house custom built virtual instrument interface in National Instruments (Austin, TX) LabVIEW Developer's Environment ver 7.2. Raw EMG was saved in a standard ASCII file for further processing.

6.2.3 Tasks and Data Collection

6.2.3.1 *Posture Miming*

To first define the axes of the control field in which to navigate, subjects first performed five trials of miming letters and numbers of the ASL alphabet, as described in section 4.2.3. Briefly, subjects were seated upright in a comfortable chair with their dominant arms and wrists supported. They were instructed to shape their dominant hand into each of thirty-three static letters and numbers of the American Sign Language (ASL) set (Figure 4.2). Dynamic letters 'J' and 'Z' were omitted, along with the number '0', which was visually the same as the letter 'O'. Subjects were guided by a visual cue to shape their hand into one of the thirty-three ASL hand postures. These static postures were held for eight seconds. At the end of the eight second period, the visual aid was cleared and an audio cue instructed the subjects to return to the rest

position. The next letter was presented after a two second rest period. EMG activities were recorded from the eleven aforementioned muscles during the entire phase of ASL miming.

6.2.3.2 Generation of Synergies and Axes of Control Field

Muscle synergies were generated from the patterns of EMG associated with miming of the static ASL letters. Each set of EMG signals were [30, 600] Hz bandpass and [59.5, 60.5] Hz notch filtered. The RMS of each signal was calculated from the static hold portion of miming ($2.5 \text{ sec} < t < 5 \text{ sec}$), and normalized to the respective EMG values of resting and maximum voluntary contraction. The full 11×165 data matrix \mathbf{V} of recorded activity was then subjected to non-negative matrix factorization (NMF) analysis using equation 6.1 and as described in section 4.2.4.3.

$$V = W \times H, \quad \text{where}$$

$$V_{m \times o} = \begin{bmatrix} \bar{v}_1(t) \\ \bar{v}_2(t) \\ \vdots \\ \bar{v}_m(t) \end{bmatrix}, W_{m \times n} = \begin{bmatrix} w_{11} & w_{21} & \cdots & w_{n1} \\ w_{12} & \ddots & & w_{n2} \\ \vdots & & \ddots & \vdots \\ w_{1m} & \cdots & \cdots & w_{nm} \end{bmatrix}, H_{n \times o} = \begin{bmatrix} \bar{h}_1(t) \\ \bar{h}_2(t) \\ \vdots \\ \bar{h}_n(t) \end{bmatrix} \quad (6.1)$$

All five trials per mimed posture were used in the synergy generation data set. $n = 4$ synergies were estimated from the generation data. The synergies were ranked \mathbf{W}_{1-4} in order of variance explained (\mathbf{W}_1 explained the most variance and \mathbf{W}_4 explained the least variance) of the original generation data set by the estimated data set $\mathbf{V}_{\text{est},i} = \mathbf{W}_i \times \mathbf{H}_i$, where \mathbf{W}_i and \mathbf{H}_i are the i^{th} column and row of \mathbf{W} and \mathbf{H} , respectively. These synergies $\mathbf{W}_{\text{BSP},1-4}$ defined the axes of the *Best Synergy Paradigm (BSP)* for myoelectric control of the virtual reaching task. Additionally, the generation data matrix was estimated by $n = 11$ singular synergies, where each synergy exclusively represented the activation of an individual muscle. Hence \mathbf{W} was fixed to be an $11 \times$

11 identity matrix of singular synergies, and the corresponding matrix of activation coefficients \mathbf{H} was estimated using the objective function and update rules shown in equations 3.8 and 3.9. These singular synergies were then ranked \mathbf{W}_{1-11} in order of variance explained of the original generation data set. The top four singular synergies $\mathbf{W}_{SMP,1-4}$ defined the axes of the *Singular Muscle Paradigm (SMP)* for myoelectric control of the virtual reaching task.

6.2.3.3 Target-Reaching Task

A four degree-of-freedom position-based control field (Figure 6.1) was created as a virtual instrument in National Instruments (Austin, TX) LabVIEW Developer's Environment ver 7.2. The field consisted of four axes, each of which represented the activation coefficient of one of the four synergies of \mathbf{W}_{BSP} or muscles of \mathbf{W}_{SMP} . The targets on each axis were located such that the subject would be able to comfortably reach the end of each axis without significant exertion that would induce fatigue. Specifically, the target was centered at $h = 1.0$ which corresponded to 40% MVC. The goal of the task was, given an $m \times 4$ synergy matrix \mathbf{W}_{1-4} (i.e. \mathbf{W}_{BSP} or \mathbf{W}_{SMP}) which represents a control paradigm, to reach the targets on each axis in this field by controlling each of four bars, with minimal activity on the non-desired bars (off-axes). The bar lengths were the time-varying coefficients $\mathbf{H}_{1-4} = [h_1 \ h_2 \ h_3 \ h_4]^T$ of the corresponding synergies \mathbf{W}_{1-4} . Solving for \mathbf{H}_{1-4} , and hence the bar lengths at a specific point in time t results in equation 6.2, where \mathbf{W}_{1-4}^+ is the Penrose pseudo-inverse matrix of the control paradigm synergy matrix \mathbf{W}_{1-4} (Mosier, Scheidt, Acosta & Mussa-Ivaldi, 2005). The Penrose pseudo-inverse is used rather than the standard matrix inverse because the standard matrix inverse requires a square matrix, and \mathbf{W}_{1-4} is of dimension $m \times 4$, where m is the number of recorded muscles. The EMG data vector \mathbf{V} was obtained by online processing of the EMG patterns recorded during the virtual reach task. EMG signals were recorded at 1000 Hz from the same eleven-muscle set as during the ASL

posture miming phase. The signals were [30 – 500 Hz] bandpass filtered online, and the real-time moving average RMS of the resulting signals were calculated. RMS was calculated on 300 samples at a time (300 ms worth of EMG) for all signals, and the resultant RMS signals formed the data vector \mathbf{V} . The $[h_1 \ h_2 \ h_3 \ h_4]$ bar lengths were calculated from this vector \mathbf{V} and the appropriate synergy matrix \mathbf{W} , and displayed on the screen. The moving average RMS window overlapped 270 samples (270 ms worth of data) between consecutive bar length updates. Hence the bar lengths were recalculated and updated at a rate of 30 Hz.

$$H_{(4 \times 1)} = W_{(4 \times m)}^+ \times V_{(m \times 1)}, \quad \text{where} \quad (6.2)$$

$$H_{(4 \times 1)} = \begin{bmatrix} h_1 \\ h_2 \\ h_3 \\ h_4 \end{bmatrix}, \quad W_{(4 \times m)}^+ = \begin{bmatrix} w_{1,1} & w_{2,1} & w_{3,1} & w_{4,1} \\ w_{1,2} & w_{2,2} & w_{3,2} & w_{4,2} \\ \vdots & \vdots & \vdots & \vdots \\ w_{1,m} & w_{2,m} & w_{3,m} & w_{4,m} \end{bmatrix}^+, \quad V_{(m \times 1)} = \begin{bmatrix} v_1 \\ v_2 \\ \vdots \\ v_m \end{bmatrix}$$

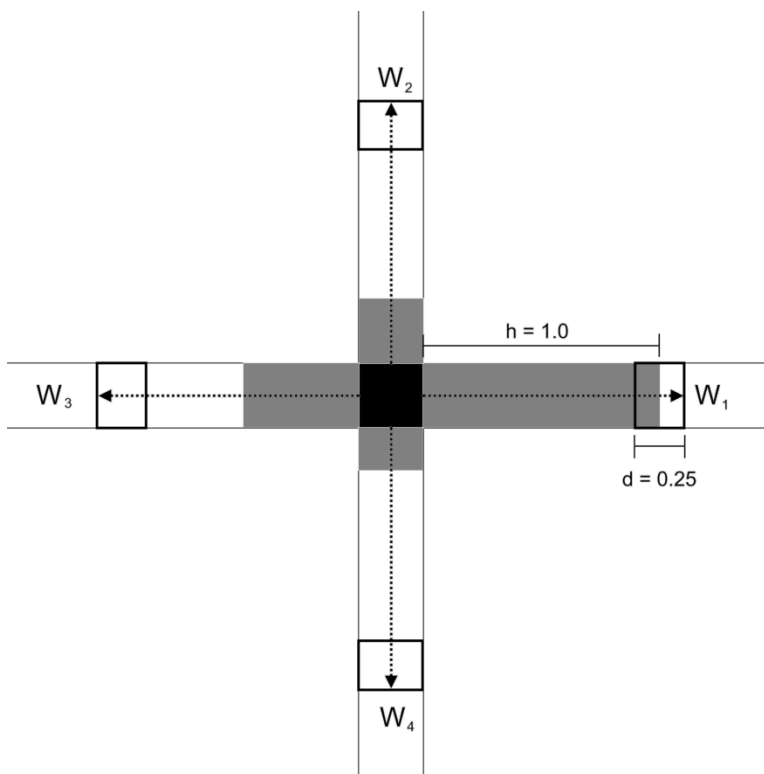


Figure 6.1. Four degree-of-freedom field for virtual target reaching task.

Subjects performed a task in which they were required to reach each of four targets along the axes of a control field. The control field axes were defined by either a *Singular Muscle Paradigm (SMP)* or *Best Synergy Paradigm (BSP)* (see text for details). Subjects were required to activate the instructed synergy, whose activation coefficient was represented by the appropriate bar length, while minimizing all off-axis activation coefficients. Subjects were presented in a random sequence fifteen trials each of targets one through four. Beginning from the home target, subjects were instructed to move to the center of the given target as quickly and accurately as possible, and maintain the final position for 125 ms. A target was considered reached if the subject was within an error of 12.5%. Subjects performed the same reaching task using both paradigms with the addition of a mental loading exercise. Finally subjects performed the same reaching task using both paradigms, but with the goal of simultaneously activating two axes to reach two targets at a time, while keeping the off-axes quiet.

Subjects were seated comfortably in an upright chair with their dominant arm and wrist supported. Hand movement, however, was not restricted. Subjects began the task by first

exploring the targetless four-dimensional space that was defined by the current control paradigm. In this exploration phase, subjects were merely asked to practice and demonstrate that they could reach the extremes of the defined axes. Subjects were allowed to explore the field until they could demonstrate confident control of each axis in the field. Naturally, this resulted in subjects overlearning the control task. Overlearning was desired because ultimately the question of interest is one of controllability and not about the process of learning controllability. Furthermore, if subjects were not allowed to overlearn the control task, they could be at different points on the learning curve during the different paradigms, thereby not allowing for a fair comparison of performance between paradigms. After the exploration phase, subjects performed fifteen trials of reaching per virtual target. Subjects began each reach at rest, with all bars consequently at length zero. When the subject had maintained the rest position for 125 ms, a target would light up, and a simultaneous audio cue initiated the movement. Subjects were instructed to move along the proper axis towards the target, while keeping all other axes inactive. No time limit was placed on the movement, and the bar length was visible throughout the reach (i.e. subjects had visual feedback of the bar lengths). A successful reach was defined as the subject maintaining the bar of interest for 125 ms within an error of 12.5% of the specified target's center. An audio cue signaled the end of a successful reach, upon which subjects were then required to return to rest by relaxing their musculature. The next reach proceeded from the rest once the subject had relaxed for 125 ms. The order of the targets was completely randomized within a session. Ample time was given between sessions and paradigms to reduce the potential effect of fatigue. Target position, bar lengths, and the RMS EMG values were saved for further analysis.

6.2.3.3.1 Effect of Control Paradigm on Virtual Reaching Success

To determine what effect the methodology of control had on task success, all subjects performed the virtual reaching task using both the single-muscle (*SMP*) and best-synergy (*BSP*) paradigms. Subjects were not informed which paradigm they would be using a priori. The *SMP* paradigm defined the field axes such that a single axis was controlled by singular muscle activation, with the activation of the four most important muscles controlling the four axes (i.e. the four muscles which singularly explained the most variance). The *BSP* paradigm defined the field axes such that the four estimated muscle synergy groups controlled each of the four axes. Subjects were given a single target at a time to reach in the target field, and the task proceeded as described above. There were fifteen reaches attempted at each target, for a total of sixty reaches within each paradigm. The order in which each subject performed the two paradigms was randomly determined.

6.2.3.3.2 Effect of Mental Loading on Virtual Reaching Success

To systematically assess which control paradigm was perceived as most natural and least mentally burdensome, all subjects performed a second set of virtual reaches using both the *SMP* and *BSP* paradigms as described above, but with the additional requirement of reverse counting. Subjects were instructed to count backwards from 1000 by 3 during the first control paradigm, and count backwards from 1000 by 4 during the second control paradigm. It was not important that subjects perform the actual counting accurately, although subjects were not told this. The point was to give them another mentally taxing task that would potentially interfere with their performance of the virtual reaching task. The control paradigm which was least affected by the addition of another mental task would be that which was the least mentally burdensome. Subjects again performed fifteen reaches per target for a total of sixty reaches within each paradigm. The paradigm presentation order was again randomly determined by

each subject, such that each paradigm was combined with either mental task over the entire investigated population.

6.2.3.3.3 Virtual Reaching Success during Simultaneous Control of Synergies

Finally the ability of subjects to simultaneously reach two targets using each of the *SMP* and *BSP* control paradigms was investigated. Using the same setup for the single-target reaches, two targets were simultaneously presented, and subjects had to activate the appropriate two axes to reach the targets. Success of the reach trial was determined only when the subject simultaneously held both specified activation levels within the target boxes for 125 ms. Situations where one target was reached but not the other did not complete the trial. Situations where both targets were reached but one of the targets was not maintained for the full 125 ms did not count as a completed trial. Subjects continued until both targets were reached and maintained for the specified time. Fifteen virtual reach trials of each of the six combination pairs were performed for a total of 90 reaches per paradigm. Again, the order of the paradigms was randomized from subject to subject. No mental load exercise was included in this portion of the study.

6.2.4 Data Analysis

The described task can be thought of as reaching a virtual target in four-dimensional Euclidean space. The success of subjects using each control paradigm to do so was quantified by examining the final endpoint error of the virtual reaches, the average activation of all undesired synergies during the full reach phase, the two-dimensional path errors from linearity, the amount of null space activity (i.e. unused information), and the effect of mental loading on each of these measures.

6.2.4.1 End Point Error (EPE)

At any time t the bar lengths can be represented as a four-element vector $\mathbf{h}(t) = [h_1(t) \ h_2(t) \ h_3(t) \ h_4(t)]$. The final endpoint error for each reach was defined as the Euclidean distance between the desired target (also represented as a four-element vector e.g. [1 0 0 0]) and $[\mathbf{h}_1 \ \mathbf{h}_2 \ \mathbf{h}_3 \ \mathbf{h}_4]$ at the completion of the reach. The final endpoint error is a direct practical measure of how well subjects were able to minimize the off-axes activities while maintaining the final position at the specified target(s).

6.2.4.2 Uncontrolled Synergies Error (USE)

In addition to the final endpoint error, the activation of the uncontrolled synergies throughout the entire target reach was determined as the uncontrolled synergies error. At any time t , the activation of the uncontrolled synergies $\mathbf{h}'(t)$ could be represented as a k element vector, where k is the number of uncontrolled synergies. The error of the uncontrolled synergies axes was thus defined as the root-mean-square of the $\mathbf{h}'(t)$ time series, as given in equation 6.3. This error measure gives temporal information of how well subjects minimized undesired synergy / single-muscle activity during the full reaching phase.

$$USE = \sqrt{\frac{\sum_{t=1}^p |h'(t)|}{p}} \quad (6.3)$$

6.2.4.3 Path Linearity Error (PLE)

The two-dimensional deviation from a straight lined path was quantified for each subject as a measure of how well subjects simultaneously activated two synergies. Given any path to two simultaneous axial targets (represented in Figure 6.2 by a single target not located on either synergy axis), the average deviation from linearity (ϵ) was defined as the root-mean-square

(RMS) of the perpendicular distances of all points along that path from the straight line path (equations 6.4 – 6.6).

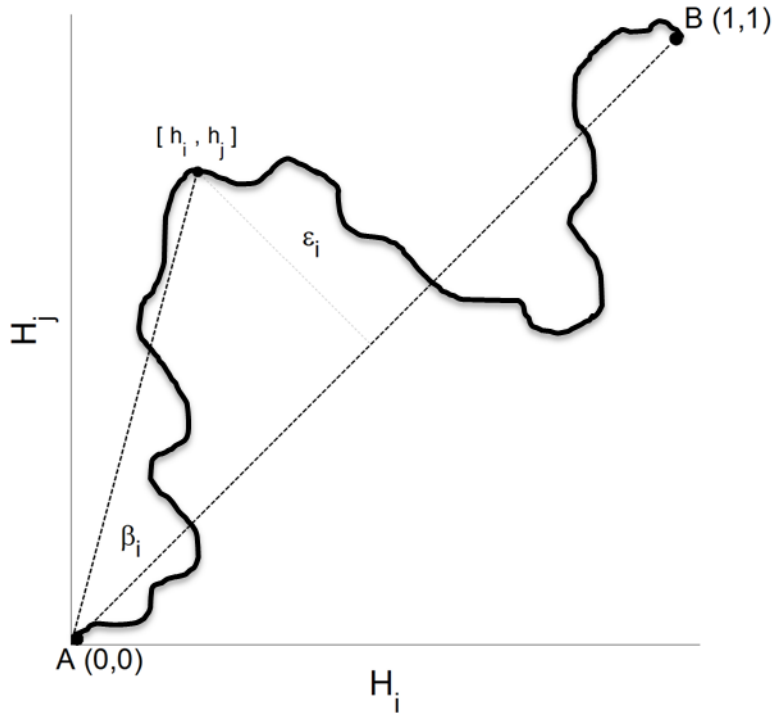


Figure 6.2. Calculation of linearity error for a given path.

Average deviation from the straight line between rest and a given target (representing simultaneous activation of two synergies) was determined by finding the RMS of the perpendicular distances (ϵ_i) between each point $[h_i, h_j]$ and the straight line between A and B . The straight line represents ideal simultaneous activation of the two specified synergies W_i and W_j (whose activation coefficients are H_i and H_j).

$$\beta_i = \cos^{-1} \left(\frac{[h_i, h_j] \cdot [1, 1]}{\|[h_i, h_j]\| \cdot \|[1, 1]\|} \right) \quad (6.4)$$

$$\epsilon_i = \|[h_i, h_j]\| \cdot \sin(\beta_i) \quad (6.5)$$

$$\varepsilon = \sqrt{\frac{\sum_{i=1}^p (\varepsilon_i)^2}{p}} \quad (6.6)$$

6.2.4.4 Null Space Activities

Given that subjects used an eleven-dimensional system to control a cursor in a four-dimensional field, the system is by definition redundant. Hence, subjects may have used extraneous muscle activity in the seven-dimensional null space while performing the virtual reaches in the four-dimensional task space. To assess how much redundant activity in the null space was used, the projections of the data vectors \mathbf{v} into the task space (\mathbf{v}_T) and null space (\mathbf{v}_N) were calculated, where $\mathbf{v} = \mathbf{v}_T + \mathbf{v}_N$ by vector addition. The calculations of these vectors are given in equations 6.7 – 6.8 (Mosier et al., 2005), where I_{11} is the 11×11 identity matrix.

$$\mathbf{v}_T = \mathbf{W}_{ij} \times \mathbf{W}_{ij}^+ \times \mathbf{v} \quad (6.7)$$

$$\mathbf{v}_N = (\mathbf{I}_{11} - \mathbf{W}_{ij} \times \mathbf{W}_{ij}^+) \times \mathbf{v} \quad (6.8)$$

The average magnitude of the null space vectors \mathbf{v}_N as a percentage of the magnitude of the data vector \mathbf{v} across the entire interval of virtual reaching is determined for each control paradigm. This value serves as a quantitative measure of the efficiency rating of each control paradigm. The algorithm which has less null space activity is deemed more efficient.

6.2.4.5 Statistical Analyses

A three-factor repeated measure analysis of variance (RM-ANOVA) was used to systematically assess the effects that the control paradigm (*SMP* vs *BSP*), the target position, and mental loading had on each of the above described error calculations during virtual reaching to a single target in the synergy field (i.e. individuated control). The control paradigm

is a factor because the chosen paradigm could affect the ability of the subjects to reach the desired target. The target position (specifying which synergies to activate) is a potential factor because not all DOF and DOF combinations may be activated with the same success. Mental loading is a factor because the additional mental task could affect subjects' abilities to successfully perform the task. The null hypothesis was simply that subjects were more successful at the virtual reaching task using the *BSP* paradigm for individuated control as would be evidenced by the statistically significantly lower error measures. A two-factor RM-ANOVA was used to systematically assess the effects of the control paradigm and target position on each of the error calculations during virtual reaching to simultaneously presented targets (i.e. simultaneous control). The working hypothesis was that subjects were more successful at the virtual reaching task using the *BSP* paradigm for simultaneous control as would be evidenced by the statistically significantly lower error measures.

6.3 Results

6.3.1 Individuated Muscles and Estimated Synergies for Control

Figure 6.3 shows for a representative subject the individuated muscle set and synergy set of the *SMP* and *BSP* paradigms, respectively. The individual muscles and synergies chosen for each paradigm were subject specific, and the *SMP* and *BSP* paradigms were significantly distinct within a subject. While there were some instances of sparse synergies (i.e. primarily dominated by an individual muscle) which resembled individuated muscle control, many synergies consisted of a balance between two or more muscle activations. Hence the *BSP* and *SMP* paradigms were actually different control methodologies. Many of the estimated synergies were comprised of patterns of the muscles that were estimated for individual control (e.g. *BSP*

W_1 is comprised of *SMP* W_1 and W_2 in Figure 6.3). This allowed for direct comparison of whether or not control was better accomplished using the muscles as individual control inputs or using them as coordinated synergy groups. The individual muscles and synergies in the *SMP* and *BSP* control methods were on average comparable with regard to amount of variance explained of the original ASL EMG data set, as shown in Figure 6.4.

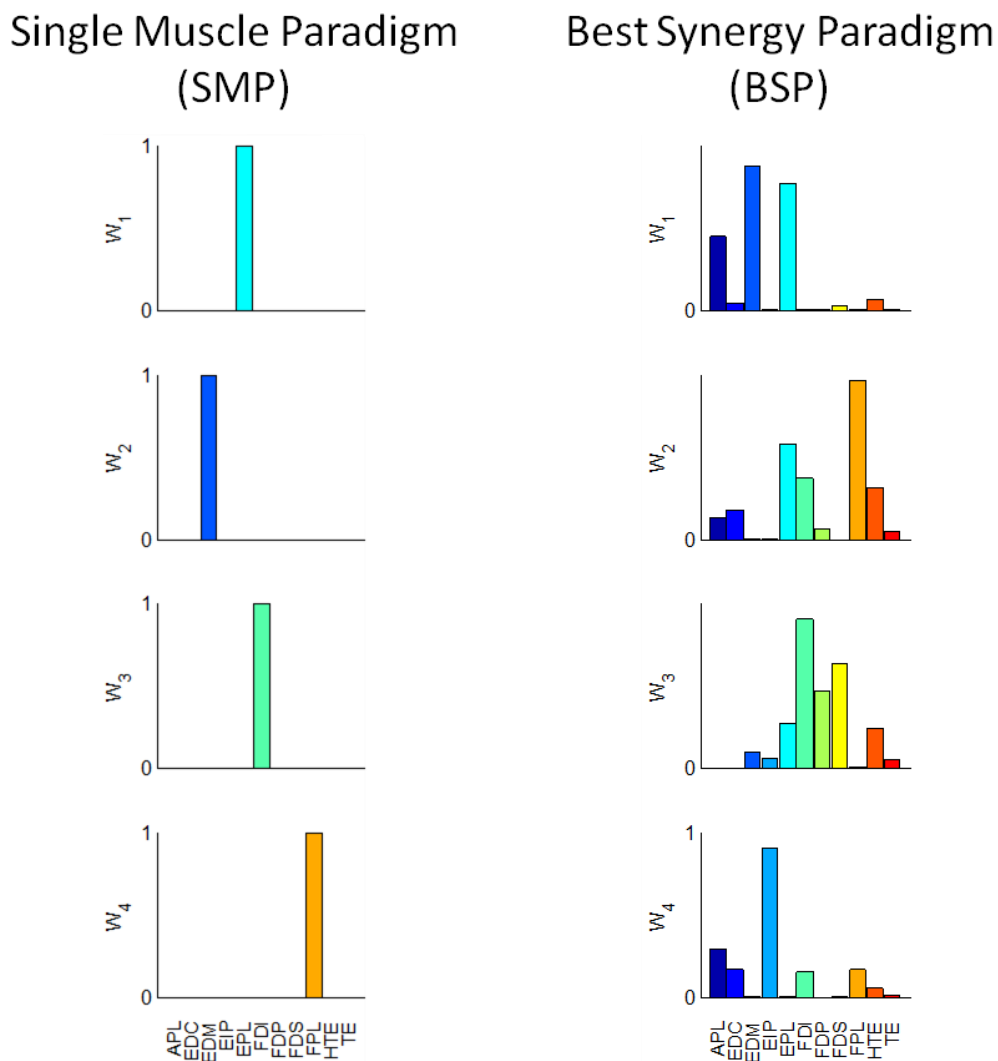


Figure 6.3. Individuated muscles and estimated synergies for a representative subject.

Synergies were estimated from the ASL EMG data set using non-negative matrix factorization, and composed the *Best Synergy Paradigm* (*BSP*, right column). The four synergies were distinct for each subject, but on average explained between 80 – 90% of the ASL EMG data. The four muscles which explained the most variance in the ASL EMG data were also determined and comprised the set of the *Single Muscle Paradigm* (*SMP*, left column). For each subject, the paradigms were distinct i.e. consisted of significantly different muscle groups, though some extracted synergies were sparser than others. Given a paradigm, the activation of each of the four muscle groups formed the axes of the space to be controlled (Figure 6.1).

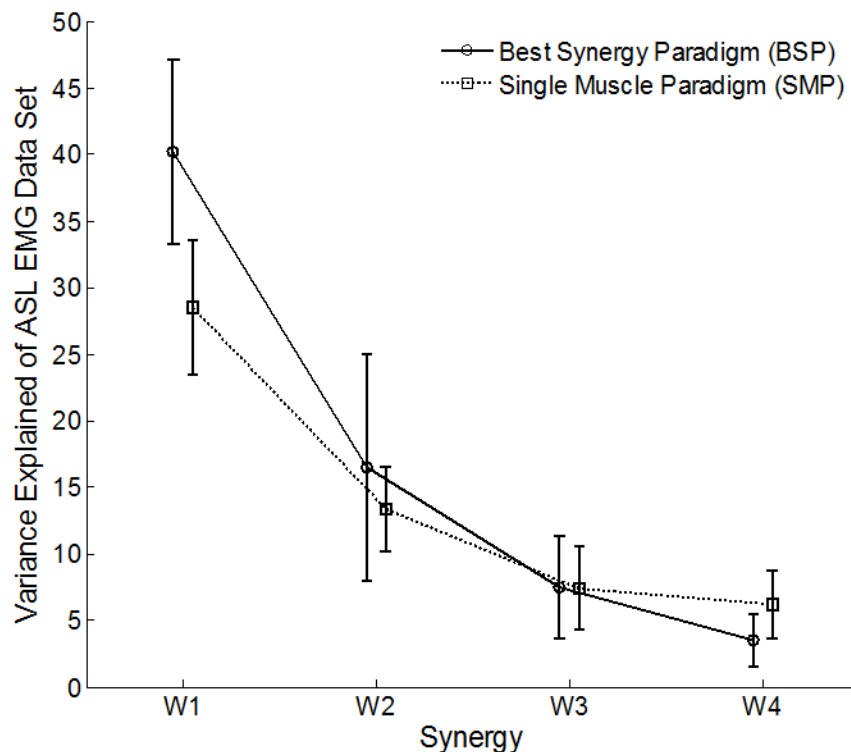


Figure 6.4. Variance explained by SMP and BSP control methods.

The population averages of the variances explained of the original ASL EMG data set were generally comparable between ordered synergies of the *SMP* and *BSP* control methods, with the exception of W_1 .

6.3.2 Independent Control of a Single DOF

Figure 6.5 shows for a representative subject the paths of activation during single DOF control in the four-dimensional space using both the *SMP* and *BSP* paradigms, and with and without the addition of a mental loading exercise. In some instances and for certain DOF, subjects seemed to perform the task more successfully using synergy control over single-muscle control, while for other DOFs subjects seemed to prefer single muscle control over control of synergies.

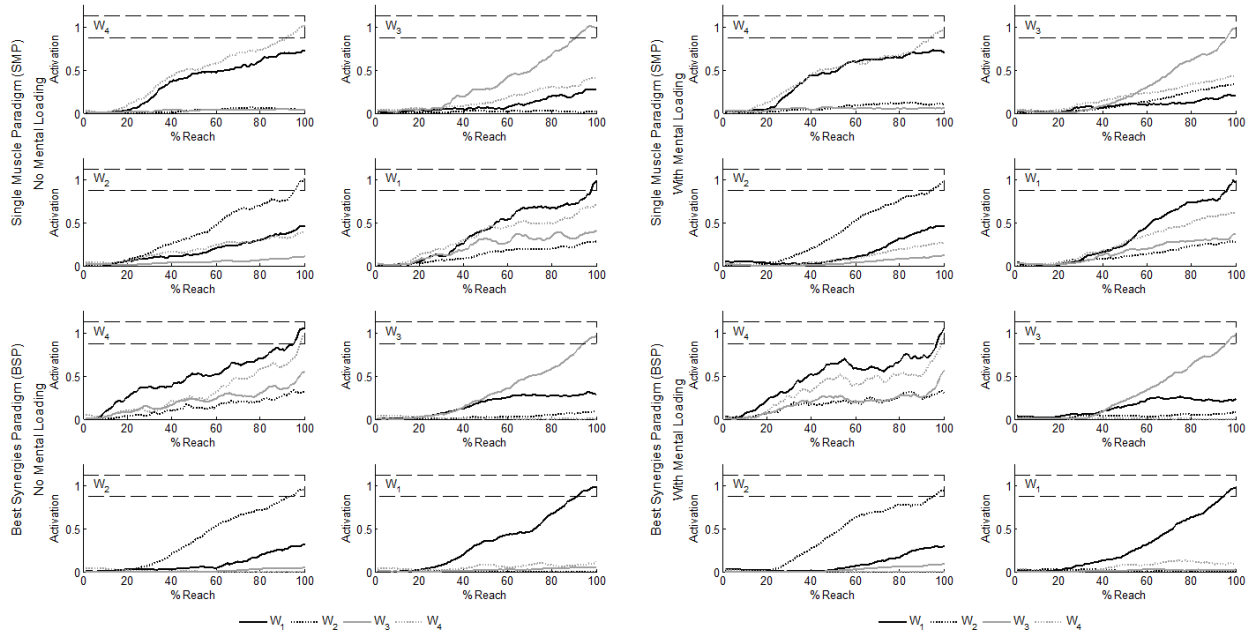


Figure 6.5. Average paths of single target activation for a representative subject.

Subjects attempted to reach a target in the workspace by activating the specified synergy (W) in each plot to a level of $H_i = 1.0 \pm 0.125$, while minimizing all other synergy activations. Subjects performed these virtual target reaches using both the *Single Muscle Paradigm* (SMP, top 8 plots) and *Best Synergy Paradigm* (BSP, bottom 8 plots), and with (right 8 plots) and without (left 8 plots) the addition of a mental loading exercise. Trials were normalized in time and the average activation levels of all four synergies for each target are plotted. For this particular subject, there were clear instances when the SMP paradigm performed better (i.e. less undesired activity) than the BSP paradigm, such as when reaching the target specified exclusively by synergy W_4 . However, reaching of some other targets, such as that of W_1 , was better achieved using the BSP over the SMP paradigm. The addition of a mental loading exercise did not seem to significantly affect the path plots of either the SMP or BSP paradigms.

The end point error (EPE) measure quantified the ability of subjects to successfully keep the desired DOF at the specified final level of activity (i.e. at 100% reach) while inactivating all other DOFs. Figure 6.6 (A) shows the EPE measures for all subjects across all targets using single-muscle and best-synergy paradigms. On average, there were no consistent differences between the end-point errors of the synergy and single muscle paradigms. In addition, the large

standard deviations show that subjects were quite variable in their end point activation levels. A three-factor ANOVA verified that there were no statistically significant differences in final EPEs of the single-muscle and synergy paradigms ($p = 0.348$), showing that subjects were equally successful controlling synergies and individual muscles to perform the task. Also, the target specification was not a significant factor in determining the ability of the subjects to successfully maintain the instructed synergy. In other words, the amount of variance explained by the synergy did not have an effect on relative controllability at the end point over the investigated population ($p = 0.398$). Finally, neither the mental loading nor the interaction between control paradigm and mental loading proved to be significant factors, implying that the mental loading task similarly affected errors associated with either paradigm. This implies that both the *SMP* and *BSP* paradigms seemed to require the same mental attention to perform the target reaching task.

The uncontrolled synergies error (USE) quantified the temporal ability of subjects to successfully inactivate the undesired DOFs while modulating the activity of the desired DOF. The ensemble averages for all subjects are reported in Figure 6.6 (B). There was no general trend with regard to subjects being more successful with one paradigm over the other. Quantitatively, a three-factor ANOVA revealed that the *BSP* control method did not prove to be more advantageous than the *SMP* control method over the time course of the reach ($p = 0.643$). Again, neither mental loading nor the interaction between mental loading and the chosen paradigm proved to be significant.

Finally, the amount of activity in the seven-dimensional null space allowed for a rating of each control paradigm's efficiency. In the *SMP* paradigm, the seven-dimensional null space consists of the activity from the seven muscles which were not specified for control, and as a result, a low efficiency rating would be expected. The null space for the *BSP* paradigm is more abstract

since all muscles are included in the four synergy controllers. As a result of all muscles being included, it would be expected that the null space activity of the *BSP* control method, and hence the inefficiency rating, would be less than that of the *SMP* paradigm. Figure 6.6 (C) reports this inefficiency rating for each subject as a ratio of the average length of the null space EMG vector to the length of the complete 11-dimensional EMG vector. The *BSP* control method algorithm consistently proved to be more efficient for all subjects with respect to single DOF activation (three-way ANOVA $p = 0.023$).

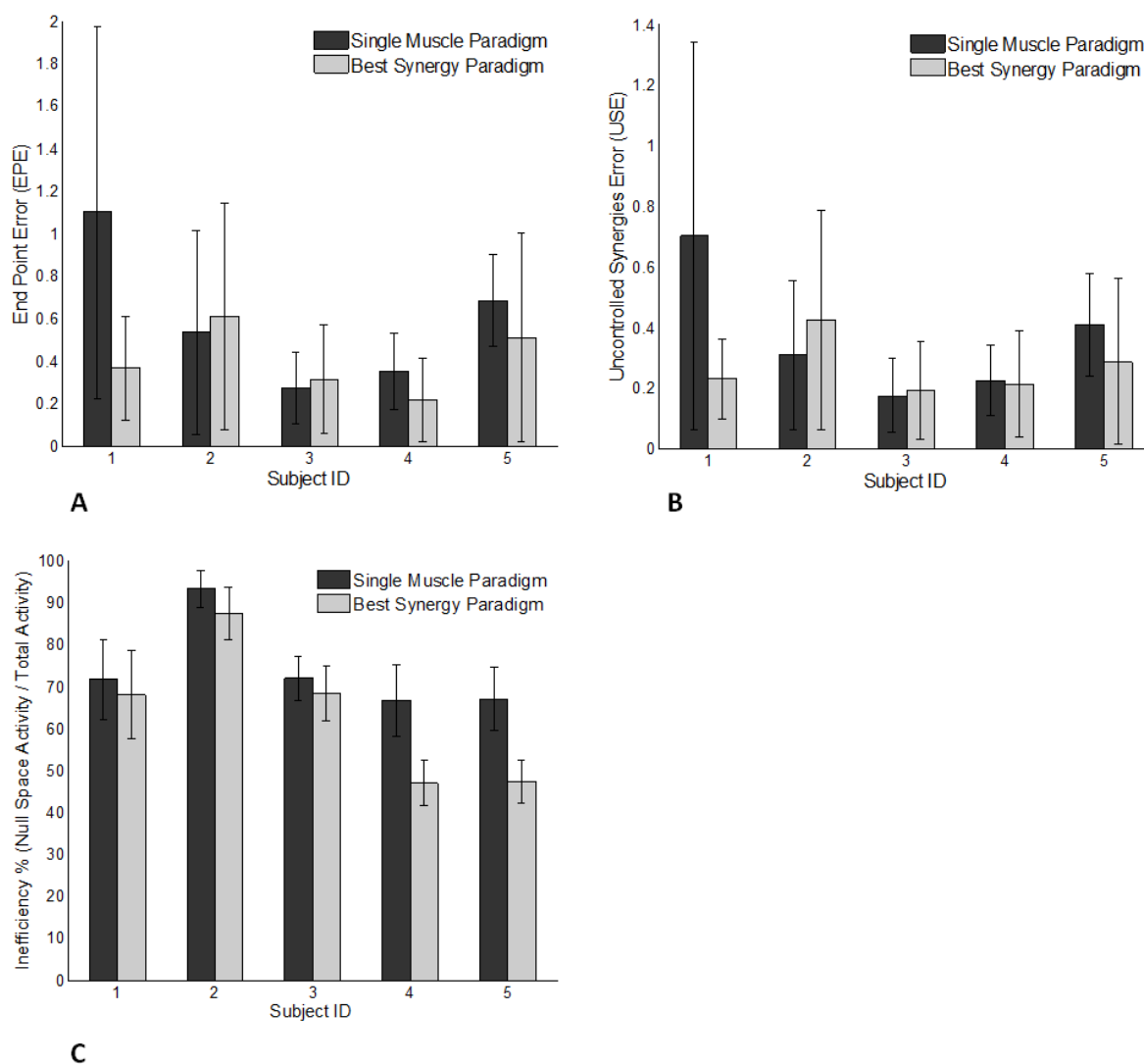


Figure 6.6. Error and inefficiency measures for all subjects during individual DOF control.

Error measures of the final synergy end point activations (A) and uncontrolled temporal synergy activations (B) revealed that subjects showed no difference in maintaining the final activation level of the desired input while minimizing the activation of the undesired inputs using the synergy paradigm over the single muscle paradigm. In addition, the large deviation bars show that subjects were quite variable in their abilities. Also, no general trend and no statistical significance existed between the two paradigms according to the USE error measure. (C) Redundant and extraneous activity within the null space of control contributed to the inefficiency of each paradigm. The *SMP* control method consistently proved less efficient than the *BSP* control method.

6.3.3 Simultaneous Control of Two DOFs

Figure 6.7 shows the average paths of activation during reaching of two targets in the control space (i.e. simultaneous and coordinated activation of two degrees-of-freedom) using both the *SMP* and *BSP* control methods. Subjects were able to perform the simultaneous control task, albeit anecdotally with more difficulty than the single control task. In general subjects attempted to simultaneously activate two degrees-of-freedom rather than activating them sequentially. As with the single degree-of-freedom activation task, subjects did not seem to successfully perform particularly better with one paradigm over the other. The above mentioned error measures quantified this success, and the results of the statistical tests discerning the effects of paradigm and target are described next.

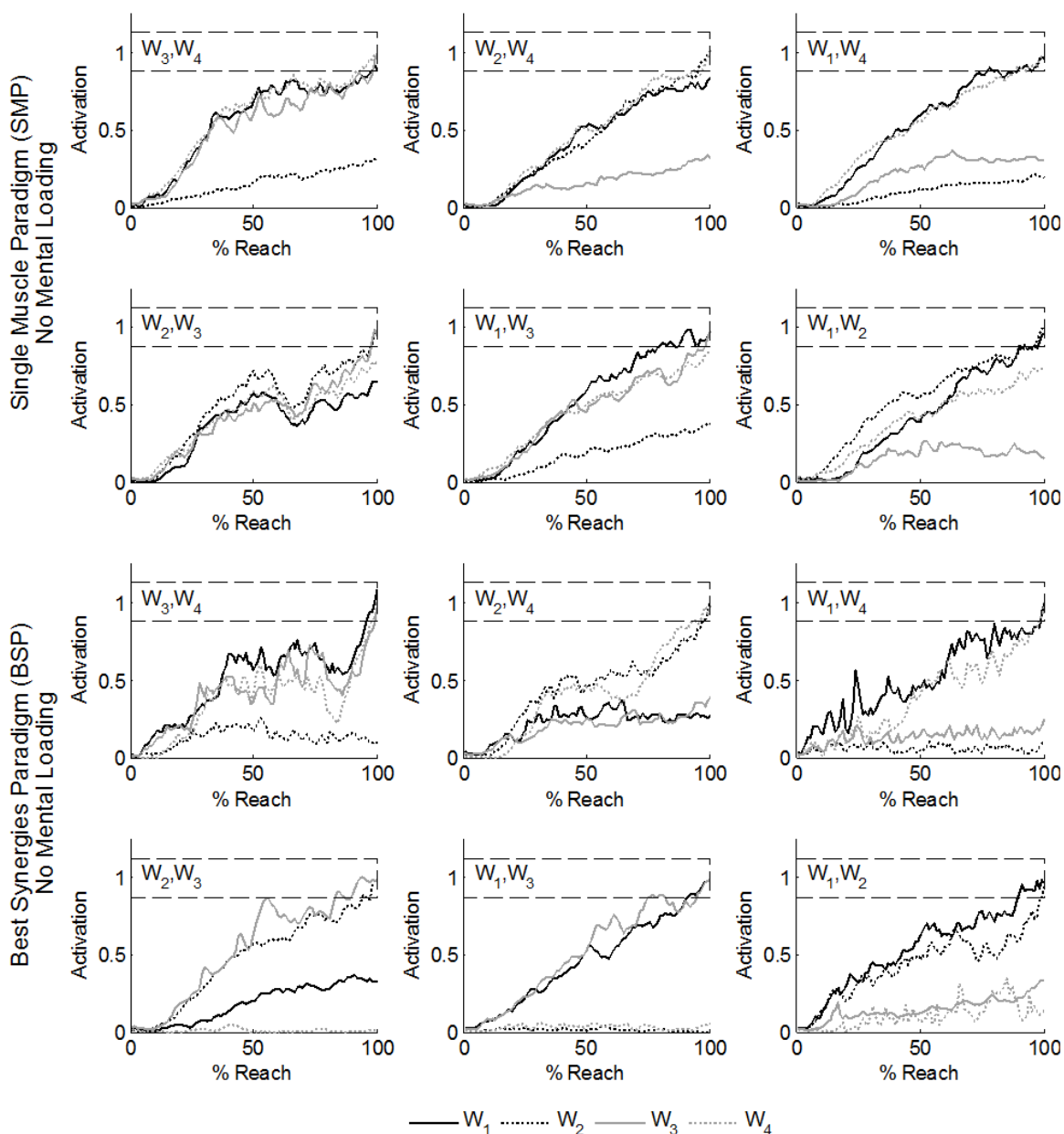


Figure 6.7. Average paths of simultaneous DOF activation for a representative subject.

In general subjects opted to simultaneously activate two degrees-of-freedom rather than sequentially activating individual degrees-of-freedom to perform the task. Subjects did not seem to preferentially perform better with either the single muscle paradigm (top 6 plots) or best synergy paradigm (bottom 6 plots), as evidenced by the non-significant differences in error measures from the ANOVA tests.

Figure 6.8 reports the average error measures for each subject across all targets in the simultaneous activation task. Subjects generally had lower end point errors using the synergy paradigm over the single-muscle paradigm. However, while four of five subjects showed this general trend, the large standard error bars factored into the two-way ANOVA returning statistical non-significance for the effect of paradigm on the EPE measure ($p = 0.095$). The effect of target, and the interaction between target and paradigm, also were found to be statistically insignificant, implying that the the different target combinations, which were composed of synergies explaining different amounts of variance, did not significantly affect subjects' abilities to perform the task.

Unlike the EPE measure, there was no general trend in the temporal ability of subjects to simultaneously activate two degrees-of-freedom more successfully with either paradigm (Figure 6.8 B). Subjects seemed to be able to successfully adapt to either control paradigm without a change in error. The two-factor ANOVA verifies that subjects were equally successful using either paradigm ($p = 0.144$). Thus, it appears that, given either single muscle or synergistic groups of muscles as the control inputs, subjects had the same success in keeping the undesired DOF inactive.

The path linear error (PLE) quantified the simultaneous nature of control, and is in effect a measure of linear correlation. An error of zero would suggest that given the two instructed DOFs, subjects preferentially and perfectly coupled them to obtain the targets in the control space. The greater the deviation from zero, the less simultaneous and hence the more sequential the control. Perfect sequential control without target overshooting or path retracing would have a PLE value of 0.4082 (see Figure 6.9). Instances where subjects had PLE values greater than 0.4082 meant that the subjects overshot the target during the virtual reach.

Subjects seemed to perform simultaneous activation in similar manners, and hence had similar PLE values, using either paradigm (two-factor ANOVA, $p = 0.234$).

Finally, the analysis of the amount of null space activity showed that, as with the task of independent control, the synergy based paradigm proved to be more efficient across the subject population i.e. it had statistically less activity in the null space than the single-muscle paradigm (two-way ANOVA, $p = 0.005$). Again, this was to be expected due to the fact that the activities of more muscles are taken into consideration in the synergy based paradigm.

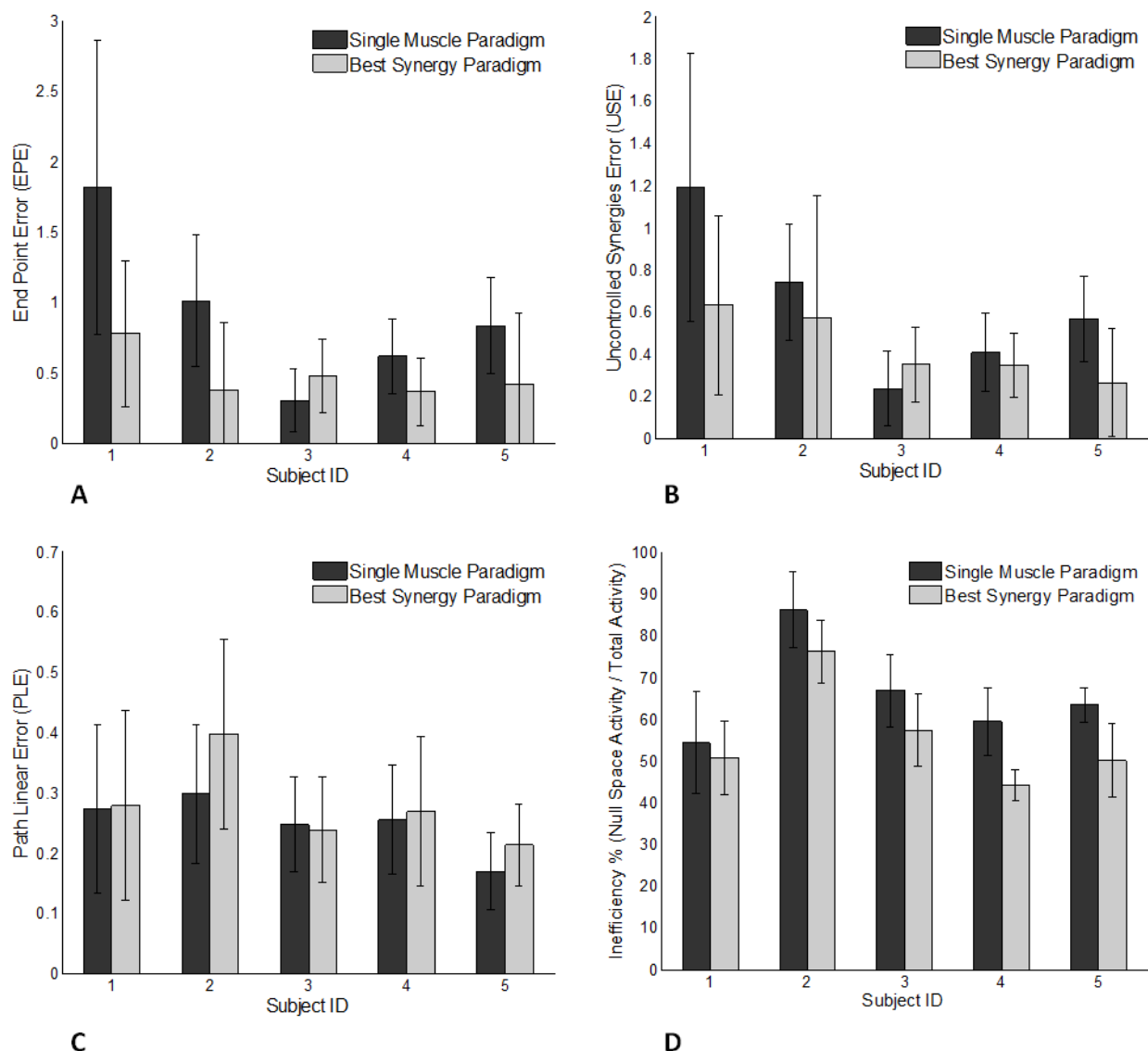


Figure 6.8. Error and inefficiency measures for all subjects during simultaneous DOFs control.

(A) The EPE measure revealed that as a trend, subjects generally had fewer end point errors with the synergy-based control paradigm than with the single-muscle control paradigm. However, these differences were not found to be statistically significant. Significant difference in the *SMP* and *BSP* paradigms were neither found with the (B) USE nor the (C) PLE error measures (see text for details). (D) As with the independent control task, the *BSP* paradigm did prove to be more efficient (i.e. less null space activity) than the *SMP* paradigm.

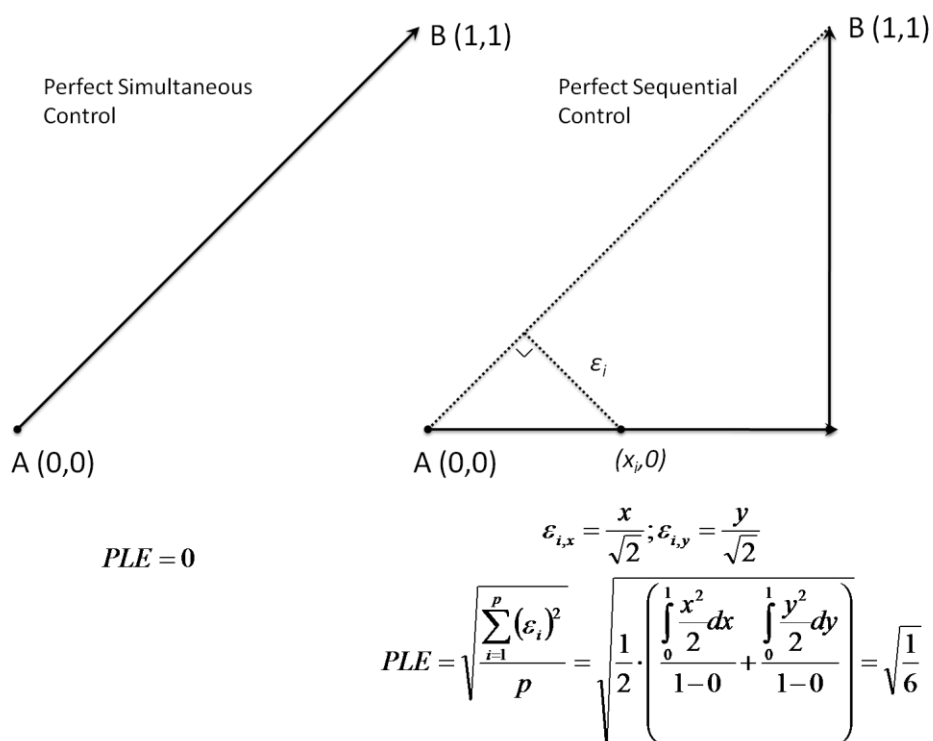


Figure 6.9. PLE calculations for perfect simultaneous control and perfect sequential control.

6.4 Discussion

The ability of subjects to both independently and simultaneously control multiple degrees-of-freedom for myoelectric control is a potentially limiting factor in the development and use of multifunction myoelectric devices. It is unclear whether users have the cognitive and physiological ability to perform simultaneous control of an external device with repeated success. Naturally, the choice of control algorithm potentially has an effect on users' abilities to perform simultaneous control. It is clear that humans everyday successfully coordinate many neuromuscular degrees-of-freedom to perform the most complex of tasks with relative physical

and cognitive ease. The need to address the inherent redundancy in the neuromotor system has led many researchers to posit and suggest evidence that redundancy is addressed through the grouping of muscles into synergistic groups. This model of muscle coordination is articulated in the neuromotor synergy hypothesis, which states that “low-level, neurally based patterns significantly constrain intentional actions” (Lee, 1984). This synergistic model of muscle coordination is potentially advantageous over the single-muscle control paradigm that is currently implemented in the control of myoelectric devices, if in fact synergies do serve as fundamental building blocks of muscle coordination, and they are volitionally controllable.

The synergies extracted for each subject that served as the control inputs for the task were representative of a wide variety of muscle patterns and combinations that were elicited from miming of the ASL set. It cannot be definitively stated that the synergies extracted during the experimental protocol are the four synergies used for all coordination of hand muscles. One reason for this is that it is unclear, even in the large body of motor control literature, how to determine the absolute correct number of synergies to describe a set of tasks. Several methods have been suggested, such as hard thresholds of 80 – 90% explained variance, or finding the point of diminishing returns, where adding more synergies does not significantly add to the explained variance. Another reason why the synergies extracted in this study cannot be seen as definitive is that it has not been shown in the motor control literature that the decomposition algorithms used for synergy extraction result in unique and global solutions. Rather, because they are based on search optimization, it is possible that the returned solution, and hence the extracted synergies, may not be the absolute best descriptors of the given data. Nevertheless, the four synergies extracted per subject explained between 80 – 90% of the variance of the EMG data set and thus were good representations of the muscle coordination patterns involved in the ASL posture miming task.

Users were able to complete the independent control and simultaneous control tasks using both the single-muscle and synergy based paradigms. The chosen error measures were designed to give a practical assessment of how well the users accomplished the task goals of independently activating individual muscles and synergy groups, and achieving true simultaneous control. Although subjects were instructed to minimize the activities of the undesired degrees-of-freedom, the potential existed that, should subjects have been unable to decouple any two degrees of freedom, the EPE and USE errors could have been larger for either the *BSP* or *SMP* paradigm. The fact that there was no difference in subjects' errors using either paradigm in both the independent and simultaneous control problems suggests that it was just as easy to modulate individual muscle activations while inhibiting others, as it was to modulate specific synergy groups while inhibiting others. If synergistic muscle groups were the only means of muscle coordination, as posited by the neuromotor synergy hypothesis, then it would have been expected that subjects would have performed better with the *BSP* paradigm i.e. had smaller errors. Likewise, if singular muscle activation were the only means of muscle coordination, it would have been expected that subjects would have performed better with the *SMP* paradigm. The lack of significant difference between the two paradigms possibly suggests that neither synergies alone nor single muscles alone, at least from the perspective of volitional control, function as the building blocks of muscle coordination. As a result, it seems that either paradigm would be equally adequate for myoelectric control of multiple independent DOFs.

The use of mental loading exercises is a well documented practice to discern the relative cognitive requirements of a set of tasks. It has been used extensively to assess the cognitive requirements of balance control and locomotion in able-bodied subjects, and those who have experienced lower limb amputation or neurological motor disorders (Dault, Geurts, Mulder & Duysens, 2001, Geurts & Mulder, 1994, Geurts, Mulder, Nienhuis & Rijken, 1991, Heller, Datta

& Howitt, 2000). These researchers argue that a task that is unnatural and not well automated requires a significant amount of attention and cognitive resources. This is not an issue if the amount of available cognitive resources exceeds that required by the task. However, if another unnatural and un-automated task with a fixed cognitive demand is simultaneously performed, the performance of the original task will degrade. The degree of degradation gives insight into the cognitive requirement of the original task (Heller et al., 2000). The result of the current virtual reaching study, namely that mental loading seemed to have the same degradation effect on a single-muscle based paradigm as it did on a synergy-based paradigm (i.e. the interaction term between mental loading and paradigm was statistically insignificant) suggests that both paradigms required similar levels of cognitive attention (i.e. were similarly intuitive, or similarly difficult). There does exist the possibility that the required mental loading task was too well automated and hence too easy. However, supervision of each subject, and anecdotal evidence from each subject suggested this to not be the case. Hence from the standpoint of a natural control paradigm, it seems that there is not much of a difference between independent control of synergies versus independent control of single muscles.

Ultimately, it was the use of the *SMP* and *BSP* paradigms in simultaneous volitional control of two DOFs that was the focus of this study. The path linear error (PLE) measure allowed for quantification of the degree of simultaneity, ranging from 0 (perfect simultaneity) to infinity. The result of insignificant differences between the PLE measures of both paradigms suggests that subjects performed simultaneous control in similar manners. One paradigm was not more conducive to sequential or simultaneous control than the other. One possible reason for this observation is that it is unclear whether subjects *subconsciously* think in terms of individual muscles or muscle synergies to shape the hand. Rather, it is clear that subjects *consciously* thought of the task in terms of the kinematic hand postures that would result in the appropriate

EMG patterns to complete the reaching task. While some hand postures may have been easier to form and maintain than others, the hand postures were not formed sequentially using either paradigm. Hence it makes sense that the associated EMG activations also were not sequential using either paradigm. Hence the *BSP* paradigm was no better, but no worse in realizing simultaneous control than the *SMP* paradigm.

The main difference observed between the *SMP* and *BSP* paradigms was in the amount of EMG activity located in their respective null spaces. The null space is practically the extraneous EMG activity that does not contribute to completion of the task. Hence its use as an inefficiency metric is warranted. It was expected that the *BSP* paradigm would have statistically significantly higher efficiency ratings than the *SMP* paradigm, mainly because it takes into account the activity of not just more muscles, but more muscles that were relevant to hand manipulation. The *SMP* method only took into account four individual muscles. Given that more than four muscles are clearly used for hand control, the activities of those unobserved muscles comprise the null space and hence add to the inefficiency rating. From the perspective of completing the experimental tasks of this study, this difference though, was not of major importance because it did not manifest itself in the error measures of success. Had the task been more difficult, such as controlling six or eight muscle degrees-of-freedom, the differences between the two paradigms during independent control could have been realized in the error measures.

6.5 Conclusion

This investigation has sought to compare the benefits of using a muscle synergy based paradigm for independent and simultaneous control of multiple degrees-of-freedom over a single-muscle based paradigm. It was hypothesized that the muscle synergy model would offer a more successful method of achieving multi-DOF myoelectric control due to the posited

existence of muscle groups whose activation levels may be specified together. The error measures used in this study quantified the success of volitional modulation of these synergies in both independent and simultaneous control tasks. The result that there were no differences in these error measures suggests that muscle synergies are not necessarily more beneficial than a single-muscle paradigm for myoelectric control. Furthermore, because users seem to have equal ability in modulating the activation levels of muscle synergies and single muscles, it suggests that neither synergies nor individual muscles serve as the sole building blocks of muscle coordination.

7 Conclusions

This dissertation has described investigations into the use of neuromuscular synergies as a potential paradigm of control for multifunctional myoelectric trans-radial prostheses. This work was motivated by the desire to increase the functionality of current myoelectric devices without increasing the mental demand placed on the user. With the advent of implantable myoelectric sensors, it is now possible to record from a wide variety of muscles for control. However it is not clear the best way to coordinate the newly acquirable control signals. Evidence from anatomical studies, cortical mapping and recording studies, and kinetic and kinematic studies of movement in lower-level vertebrae have all suggested that the neuromotor system organizes coordination of muscles into functional groups termed synergies. It was hypothesized that a muscle synergy based control paradigm for myoelectric control would result in advantageous control by users and a reduced mental burden. A better understanding of properties of muscle synergies was needed in conjunction with the practical motivations for control. Thus within this hypothesis, the specific aims of this research were as follows.

- Assess the predictive power of a muscle synergy paradigm in new and untrained for hand postures.
- Determine if the EMG patterns and underlying muscle synergies associated with sub-maximal multi-joint hand grasping are linearly scaled variants of a single characteristic coordination pattern.
- Assess the success of subjects to modulate activations of muscle synergies in a multi-degree-of-freedom control task, contrasted to their success of modulation of individual muscle activations.

These aims, the experimental protocols, and the investigation conclusions are briefly reviewed next.

7.1 Review of Investigations

7.1.1 Muscle Synergies as a Predictive Framework for EMG Patterns of Static Hand Postures

Muscle synergies have been shown to form an adequate *descriptive* framework for the EMG patterns observed in the neuromotor system's control of a wide variety of automatic response and volitional movements. However it had not been shown that they could form a robust and generalizable *predictive* framework for a wide variety of movements. Robustness and generalizability has been stated as a necessary property of muscle synergies. Such a framework would add credibility to the use of muscle synergies as physiological building blocks of muscle coordination, and would potentially allow them to be used for controlling a highly articulated terminal device without the need to train for all desired states of the device. It was hypothesized that a small number of muscle synergies associated with a small number of hand postures would be robust in predicting the EMG activity of new hand postures.

Subjects mimed static numbers and letters of the American Sign Language set while EMGs were recorded from extrinsic and intrinsic muscles of the hand. Non-negative matrix factorization (NMF) was used to discern the synergies associated with k postures, and these synergies were then used to predict the EMG patterns of $33 - k$ hand postures. k was incrementally increased from 1 to 32, and the predictive power of each synergy set was quantified by the explained variance. It was found that as few as 11 hand postures, accounting for as few as 8 synergies could predict the EMG patterns associated with the full 33 posture set predict with up to 90% accuracy. Furthermore, the estimated synergies were very robust to

differing sets of predictor postures, and even to the addition or removal of postures from the predictor set. Examining the structure of the observed synergies revealed that while several consisted of balanced activity from multiple muscles, many (particularly those generalizable across the subject population) also were sparse and resembled control of individual muscles.

The main conclusion from this investigation is that a small number of muscle synergies can serve as a *predictive* basis set for a wide variety of hand postures, due to their demonstrated robustness and generalizability. Thus they have the potential for use in multifunctional myoelectric control as the building blocks of any set of observed muscle coordination patterns for determining the state of a terminal device. Also, the predictive nature of this synergy framework and the small dimensions of this framework suggests that the estimated synergies were not task specific, but rather generalizable enough for a wide variety of tasks. Finally, the observed sparse structure of many, but not all of these synergies suggests that muscle coordination by the neuromotor system consists of control of both individual muscles and muscle groups, rather than being exclusive to either.

7.1.2 Muscle Synergies Exhibit Scalability with Increasing Grasp Force

This study investigated how the structures of the muscle coordination patterns (CPs) and underlying synergies associated with power and precision grasping were related to grasp force level. There has been little consensus in the literature as to the method by which the neuromotor system handles muscle coordination at different force levels, and even less knowledge about the scalability behavior of muscle synergies with respect to grasp force. Scalability of muscle synergies could potentially allow them to be used in a proportional control scheme in control of myoelectric devices. It was hypothesized that the CPs and the underlying

synergy structures of muscle coordination during hand grasping at sub-maximal force levels were statistically linearly scaled versions of characteristic vectors.

Subjects performed a force-tracking task using precision and power grasps from 0 – 50% maximum voluntary grasp strength while EMG was recorded from extrinsic and intrinsic muscles of the hand. A correlation analysis between grasp force and overall CP magnitude revealed that the CP vector magnitude was strongly linearly related to grasp force in all grasps. An analysis of the CP vector direction revealed that the direction was invariant to grasp force in the power grasp but not in the precision grasps. An analysis of the underlying muscle synergies associated with each grasp revealed that on average the top three to four synergies scaled well with force in the power grasp while the top two scaled well with force in the precision grasps. The degree of correlation was well related to the amounts of variance accounted for by each synergy. In neither case were the synergies activated in a piecewise manner relative to grasp force level.

The main conclusion from this investigation is that the primary muscle synergies involved with hand grasping scale well with increased grasp force, rather than being piecewise and structurally dependent on the force requirement. This scalability behavior thereby allows for implementation of a proportional control scheme in myoelectric control, whereby the activation level of a synergy would determine the velocities of the prosthesis motors.

7.1.3 Independent and Simultaneous Volitional Control of Muscle Synergies

This study investigated the use of muscle synergies as a myoelectric control paradigm in a real-time control task. While the potential for muscle synergies to be used in a control paradigm has been shown in the previous studies as a result of their predictive power and scalability, it was not known whether subjects could volitionally modulate them independently and

simultaneously in a real-time control task. The advantages a synergy paradigm could present towards providing an intuitive means of control, over the control of individual muscles, was also unclear. It was hypothesized that users would be able to better modulate the activations of desired synergies over individuated muscles in independent and simultaneous control tasks, and that the synergy control paradigm would require less mental effort, due to the natural groupings of muscle within the neuromotor system.

Subjects were given targets in a four-degree-freedom field whose axes were defined by either activation of muscle synergies or activation of individuated muscles. In the independent control experiment, subjects attempted to reach the target using only the instructed synergy / muscle. Subjects also attempted to perform the reaching task with the addition of a mental loading exercise. In the simultaneous control condition, subjects attempted to reach two targets using the instructed pairs of synergies / muscles. The results showed that subjects were able to modulate their synergy activation coefficients independently and simultaneously. However there were no differences found in the success measures when subjects used synergy control versus individual muscle control. Also, the mental burden task did not seem to differentiate the successes of the two paradigms.

The main conclusion from this investigation is that while subjects can independently and simultaneously modulate synergy activations for control, they do it no better and no worse than modulating the activations of individual muscles. The fact that subjects can do both equally well, even in the presence of a mental loading exercise, suggests that both paradigms seem to be appropriated for control by the neuromotor system. With regard to myoelectric control, it seems that a synergy based paradigm does not offer significant advantages for simultaneous control, at least in a four degree-of-freedom problem.

7.2 General Conclusions

The overall goal of these three studies was to investigate the possibility of muscle synergies for independent and simultaneous DOF control of a multifunctional myoelectric device. Though it has been shown that synergies are robust and scalable and subjects can adequately use them for control in a multi-DOF task, the overall benefit of muscle synergies for control is tempered by the fact that they seem to do no better than single muscle control in this particular application. Admittedly this result was undesired from the perspective of myoelectric control. However, through this work, it has become evident that muscle synergies as posited in the motor control literature and articulated by the neuromotor synergy hypothesis do not significantly constrain volitional movements. The fact that both synergies and single muscles were found to be part of the predictive framework of hand posture EMG patterns, and both were equally successful for multi-DOF control leads to the conclusion that both are used by the neuromotor system for control of the hand.

Finally, while control of muscle synergies may have not proven beneficial for multifunctional myoelectric control the concept of motor primitives may still be applicable. Since individuals can independently and simultaneously control multiple muscles and synergies, one possibility of control is that the activation levels of these inputs could potentially be used for synergistic control of prosthetic motors. This paradigm of control would be in the vein of the postural synergy primitives that have been suggested in the literature. Thus each myoelectric input could synergistically drive a group of motors to form the hand into various functional states.

References

- Ajiboye, A.B. (2003). Investigation of Fuzzy Logic as a Classification Algorithm of EMG for the Control of Multifunctional Myoelectric Prostheses: A Master's Thesis. *Biomedical Engineering* (p. 145). Evanston: Northwestern University.
- Ajiboye, A.B., & Weir, R.F. (2005). A heuristic fuzzy logic approach to EMG pattern recognition for multifunctional prosthesis control. *IEEE Transactions on Neural Systems and Rehabilitation Engineering*, 13 (3), 280-291.
- Akaho, S., & Kappen, H.J. (2000). Nonmonotonic generalization bias of gaussian mixture models. *Neural Computation*, 12 (6), 1411-1427.
- Balakrishnama, S., & Ganapathiraju, A. Linear Discriminant Analysis - A Brief Tutorial. (p. 8): Institute for Signal and Information Processing, Department of Electrical and Computer Engineering, Mississippi State University.
- Basmajian, J.V., & De Luca, C.J. (1985). *Muscles alive : their functions revealed by electromyography*. (pp. xii, 561 p.). Baltimore: Williams & Wilkins.
- Basmajian, J.V., & Stecko, G. (1962). A New Bipolar Electrode for Electromyography. *Journal of Applied Physiology*, 17 (5), 849-849.
- Bernstein, N. (1967). *The co-ordination and regulation of movement*. (Oxford: Pergamon Press.
- Bernstein, N. (1971). Biodynamics of locomotion. In: T. Whiting (Ed.) *Human motor actions : Bernstein reassessed* (New York: North-Holland.
- Bizzi, E., D'Avella, A., Saltiel, P., & Tresch, M. (2002). Modular organization of spinal motor systems. *Neuroscientist*, 8 (5), 437-442.
- Bizzi, E., Mussa-Ivaldi, F.A., & Giszter, S. (1991). Computations Underlying the Execution of Movement - a Biological Perspective. *Science*, 253 (5017), 287-291.
- Bizzi, E., Tresch, M.C., Saltiel, P., & d'Avella, A. (2000). New perspectives on spinal motor systems. *Nature Reviews Neuroscience*, 1 (2), 101-108.
- Bock, R.D. (1975). *Multivariate statistical methods in behavioral research*. (pp. xiii, 623 p.). New York,: McGraw-Hill.
- Box, G., & Jenkins, G. (1970). *Time Series Analysis, Forecasting and Control*. (San Francisco, CA: Holden Day.
- Bray, J.H., & Maxwell, S.E. (1985). *Multivariate analysis of variance*. (p. 80 p.). Beverly Hills: Sage Publications.

- Brochier, T., Boudreau, M.J., Pare, M., & Smith, A.M. (1999). The effects of muscimol inactivation of small regions of motor and somatosensory cortex on independent finger movements and force control in the precision grip. *Experimental Brain Research*, 128 (1-2), 31-40.
- Buchanan, T.S., Almdale, D.P.J., Lewis, J.L., & Rymer, W.Z. (1986). Characteristics of Synergic Relations during Isometric Contractions of Human Elbow Muscles. *Journal of Neurophysiology*, 56 (5), 1225-1241.
- Chan, A.D.C., & Englehart, K.B. (2003). Continuous classification of myoelectric signals for powered prosthesis using Gaussian mixture models. *25th Engineering in Medicine and Biology Society International Conference* (Cancun, Mexico).
- Chan, F.H.Y., Yang, Y.S., Lam, F.K., Zhang, Y.T., & Parker, P.A. (2000). Fuzzy EMG classification for prosthesis control. *Ieee Transactions on Rehabilitation Engineering*, 8 (3), 305-311.
- Chao, E.Y. (1989). Biomechanics of the hand : a basic research study. (pp. xi, 191 p.). Singapore ; Teaneck, N.J.: World Scientific.
- Cherry, E.C. (1953). Some Experiments on the Recognition of Speech, with One and with Two Ears. *The Journal of the Acoustical Society of America*, 25 (5), 975-979.
- Cheung, V.C.K., d'Avella, A., Tresch, M.C., & Bizzi, E. (2005). Central and sensory contributions to the activation and organization of muscle synergies during natural motor behaviors. *Journal of Neuroscience*, 25 (27), 6419-6434.
- Cheung, V.C.K., & Tresch, M.C. (2005). Non-negative matrix factorization algorithms modeling noise distributions within the exponential family. *27th IEEE Engineering in Medicine and Biology Society Annual International Conference* (Shanghai, China).
- Childress, D. (1992). Control of Limb Prostheses. In: J. Bowker, & J. Michael (Eds.), *Atlas of Limb Prosthetics, Surgical Prosthetic, and Rehabilitation Principles* (pp. 175-199). St. Louis, MS: Mosby-Year Book, Inc.
- Comon, P. (1994). Independent Component Analysis, a New Concept. *Signal Processing*, 36 (3), 287-314.
- d'Avella, A., & Bizzi, E. (1998). Low dimensionality of supraspinally induced force fields. *Proceedings of the National Academy of Sciences of the United States of America*, 95 (13), 7711-7714.
- d'Avella, A., & Bizzi, E. (2005). Shared and specific muscle synergies in natural motor behaviors. *Proceedings of the National Academy of Sciences of the United States of America*, 102 (8), 3076-3081.

- d'Avella, A., Portone, A., Fernandez, L., & Lacquaniti, F. (2006). Control of fast-reaching movements by muscle synergy combinations. *Journal of Neuroscience*, 26 (30), 7791-7810.
- d'Avella, A., Saltiel, P., & Bizzi, E. (2003). Combinations of muscle synergies in the construction of a natural motor behavior. *Nature Neuroscience*, 6 (3), 300-308.
- Dault, M.C., Geurts, A.C.H., Mulder, T.W., & Duysens, J. (2001). Postural control and cognitive task performance in healthy participants while balancing on different support-surface configurations. *Gait & Posture*, 14 (3), 248-255.
- Doerschuk, P.C., Gustafson, D.E., & Willsky, A.S. (1983). Upper Extremity Limb Function Discrimination Using EMG Signal Analysis. *Ieee Transactions on Biomedical Engineering*, 30 (1), 18-29.
- Englehart, K., & Hudgins, B. (2003). A robust, real-time control scheme for multifunction myoelectric control. *Ieee Transactions on Biomedical Engineering*, 50 (7), 848-854.
- Englehart, K., Hudgins, B., & Parker, P.A. (2001). A wavelet-based continuous classification scheme for multifunction myoelectric control. *Ieee Transactions on Biomedical Engineering*, 48 (3), 302-311.
- Farry, K., Fernandez, J., Abramczyk, R., Novy, M., & Atkins, D. (1997). Applying Genetic Programming to the Control of an Artificial Arm. *Myoelectric Controls Conference: Issues in Upper Limb Prosthetics* (pp. 50-55). Fredericton, New Brunswick, Canada: Institute of Biomedical Engineering, University of New Brunswick.
- Farry, K.A., Walker, I.D., & Baraniuk, R.G. (1996). Myoelectric teleoperation of a complex robotic hand. *Ieee Transactions on Robotics and Automation*, 12 (5), 775-788.
- Filzmoser, P. (2004). A multivariate outlier detection method. *Seventh International Conference on Computer Data Analysis and Modeling*, 1 (pp. 18-22). Belarusian State University, Minsk.
- Finley, F., Wirta, R., & Cody, K. (1968). Muscle synergies in motor performance. *Arch Phys Med*, 49 (11), 655-660.
- Gallant, P.J., Morin, E.L., & Peppard, L.E. (1998). Feature-based classification of myoelectric signals using artificial neural networks. *Medical & Biological Engineering & Computing*, 36 (4), 485-489.
- Geurts, A.C.H., & Mulder, T.W. (1994). Attention Demands in Balance Recovery Following Lower-Limb Amputation. *Journal of Motor Behavior*, 26 (2), 162-170.
- Geurts, A.C.H., Mulder, T.W., Nienhuis, B., & Rijken, R.A.J. (1991). Dual-Task Assessment of Reorganization of Postural Control in Persons with Lower-Limb Amputation. *Archives of Physical Medicine and Rehabilitation*, 72 (13), 1059-1064.

- Giszter, S.F., Mussa-Ivaldi, F.A., & Bizzi, E. (1993). Convergent Force-Fields Organized in the Frogs Spinal-Cord. *Journal of Neuroscience*, 13 (2), 467-491.
- Glaser, E.M., & Ruchkin, D.S. (1976). Principles of neurobiological signal analysis. (pp. xii, 471). New York: Academic Press.
- Gould, H.J., Cusick, C.G., Pons, T.P., & Kaas, J.H. (1986). The Relationship of Corpus-Callosum Connections to Electrical-Stimulation Maps of Motor, Supplementary Motor, and the Frontal Eye Fields in Owl Monkeys. *Journal of Comparative Neurology*, 247 (3), 297-325.
- Graupe, D., & Cline, W.K. (1975). Functional Separation of EMG Signals Via Arma Identification Methods for Prosthesis Control Purposes. *Ieee Transactions on Systems Man and Cybernetics*, SMC5 (2), 252-259.
- Gray, H. (1973). Gray's Anatomy. (Philadelphia, PA: Lea & Febiger.
- Hager-Ross, C., & Schieber, M.H. (2000). Quantifying the independence of human finger movements: Comparisons of digits, hands, and movement frequencies. *Journal of Neuroscience*, 20 (22), 8542-8550.
- Haykin, S., & Chen, Z. (2005). The Cocktail Party Problem. *Neural Computation*, 17 (9), 1875-1902.
- Heller, B.W., Datta, D., & Howitt, J. (2000). A pilot study comparing the cognitive demand of walking for transfemoral amputees using the Intelligent Prosthesis with that using conventionally damped knees. *Clinical Rehabilitation*, 14 (5), 518-522.
- Hendler, R.W., & Shrager, R.I. (1994). Deconvolutions Based on Singular-Value Decomposition and the Pseudoinverse - a Guide for Beginners. *Journal of Biochemical and Biophysical Methods*, 28 (1), 1-33.
- Holdefer, R.N., & Miller, L.E. (2002). Primary motor cortical neurons encode functional muscle synergies. *Experimental Brain Research*, 146 (2), 233-243.
- Huang, Y.H., Englehart, K.B., Hudgins, B., & Chan, A.D.C. (2005). A Gaussian mixture model based classification scheme for myoelectric control of powered upper limb prostheses. *Ieee Transactions on Biomedical Engineering*, 52 (11), 1801-1811.
- Hudgins, B., Parker, P., & Scott, R.N. (1993). A New Strategy for Multifunction Myoelectric Control. *Ieee Transactions on Biomedical Engineering*, 40 (1), 82-94.
- Hussein, S.E., & Granat, M.H. (2002). Intention detection using a neuro-fuzzy EMG classifier. *IEEE Eng Med Biol Mag*, 21 (6), 123-129.
- Hyvarinen, A., Karhunen, J., & Oja, E. (2001). Independent component analysis. (pp. xxi, 481 p.). New York: J. Wiley.

- Hyvarinen, A., & Oja, E. (2000). Independent component analysis: algorithms and applications. *Neural Networks*, 13 (4-5), 411-430.
- Jerde, T.E., Soechting, J.F., & Flanders, M. (2003). Biological constraints simplify the recognition of hand shapes. *Ieee Transactions on Biomedical Engineering*, 50 (2), 265-269.
- Johansson, R.S., & Cole, K.J. (1992). Sensory-Motor Coordination during Grasping and Manipulative Actions. *Current Opinion in Neurobiology*, 2 (6), 815-823.
- Johnson, R.A., & Wichern, D.W. (1992). Applied multivariate statistical analysis. (pp. xiv, 642). Englewood Cliffs, N.J.: Prentice Hall.
- Jutten, C., & Herault, J. (1991). Blind Separation of Sources .1. An Adaptive Algorithm Based on Neuromimetic Architecture. *Signal Processing*, 24 (1), 1-10.
- Takei, S., Hoffman, D.S., & Strick, P.L. (1999). Muscle and movement representations in the primary motor cortex. *Science*, 285 (5436), 2136-2139.
- Kargo, W.J., & Giszter, S.F. (2000). Rapid correction of aimed movements by summation of force-field primitives. *Journal of Neuroscience*, 20 (1), 409-426.
- Karlik, B., Tokhi, M.O., & Alci, M. (2003). A fuzzy clustering neural network architecture for multifunction upper-limb prosthesis. *Ieee Transactions on Biomedical Engineering*, 50 (11), 1255-1261.
- Krishnamoorthy, V., Latash, M.L., Scholz, J.P., & Zatsiorsky, V.M. (2003). Muscle synergies during shifts of the center of pressure by standing persons. *Experimental Brain Research*, 152 (3), 281-292.
- Lang, C.E., & Schieber, M.H. (2003). Differential impairment of individuated finger movements in humans after damage to the motor cortex or the corticospinal tract. *Journal of Neurophysiology*, 90 (2), 1160-1170.
- Latash, M.L., Scholz, J.F., Danion, F., & Schoner, G. (2001). Structure of motor variability in marginally redundant multifinger force production tasks. *Experimental Brain Research*, 141 (2), 153-165.
- Latash, M.L., Scholz, J.P., & Schoner, G. (2002). Motor control strategies revealed in the structure of motor variability. *Exercise and Sport Sciences Reviews*, 30 (1), 26-31.
- Lawrence, J.H., & Deluca, C.J. (1983). Myoelectric Signal Versus Force Relationship in Different Human Muscles. *Journal of Applied Physiology*, 54 (6), 1653-1659.
- Lee, D.D., & Seung, H.S. (1999). Learning the parts of objects by non-negative matrix factorization. *Nature*, 401 (6755), 788-791.

- Lee, D.D., & Seung, H.S. (2001). Algorithms for non-negative matrix factorization. *Advances in neural information processing systems*, 13 (pp. 556-562): MIT Press.
- Lee, W.A. (1984). Neuromotor Synergies as a Basis for Coordinated Intentional Action. *Journal of Motor Behavior*, 16 (2), 135-170.
- Lemon, R. (1988). The Output Map of the Primate Motor Cortex. *Trends in Neurosciences*, 11 (11), 501-506.
- Loeb, E.P., Giszter, S.F., Saltiel, P., Bizzi, E., & Mussa-Ivaldi, F.A. (2000). Output units of motor behavior: An experimental and modeling study. *Journal of Cognitive Neuroscience*, 12 (1), 78-97.
- Macpherson, J. (1991). How Flexible are Muscle Synergies. In: D. Humphrey, & H. Freund (Eds.), *Motor Control: Concepts and Issues* (pp. 33-47). New York: John Wiley and Sons Ltd.
- Maier, M.A., & Hepp-Reymond, M.C. (1995a). Emg Activation Patterns during Force Production in Precision Grip .1. Contribution of 15 Finger Muscles to Isometric Force. *Experimental Brain Research*, 103 (1), 108-122.
- Maier, M.A., & Hepp-Reymond, M.C. (1995b). Emg Activation Patterns during Force Production in Precision Grip .2. Muscular Synergies in the Spatial and Temporal Domain. *Experimental Brain Research*, 103 (1), 123-136.
- Mason, C.R., Gomez, J.E., & Ebner, T.J. (2001). Hand synergies during reach-to-grasp. *Journal of Neurophysiology*, 86 (6), 2896-2910.
- Mason, C.R., Theverapperuma, L.S., Hendrix, C.M., & Ebner, T.J. (2004). Monkey hand postural synergies during reach-to-grasp in the absence of vision of the hand and object. *Journal of Neurophysiology*, 91 (6), 2826-2837.
- Micera, S., Sabatini, A.M., Dario, P., & Rossi, B. (1999). A hybrid approach to EMG pattern analysis for classification of arm movements using statistical and fuzzy techniques. *Medical Engineering & Physics*, 21 (5), 303-311.
- Mosier, K.M., Scheidt, R.A., Acosta, S., & Mussa-Ivaldi, F.A. (2005). Remapping hand movements in a novel geometrical environment. *Journal of Neurophysiology*, 94 (6), 4362-4372.
- Muller, K.R., Vigario, R., Meinecke, F., & Ziehe, A. (2004). Blind source separation techniques for decomposing event-related brain signals. *International Journal of Bifurcation and Chaos*, 14 (2), 773-791.
- Mussa-Ivaldi, F.A., Giszter, S.F., & Bizzi, E. (1994). Linear-Combinations of Primitives in Vertebrate Motor Control. *Proceedings of the National Academy of Sciences of the United States of America*, 91 (16), 7534-7538.

- Mussa-Ivaldi, F.A., & Solla, S.A. (2004). Neural primitives for motion control. *Ieee Journal of Oceanic Engineering*, 29 (3), 640-650.
- Napier, J.R. (1956). The Prehensile Movements of the Human Hand. *Journal of Bone and Joint Surgery-British Volume*, 38 (4), 902-913.
- Penfield, W., & Boldrey, E. (1937). Somatic motor and sensory representation in the cerebral cortex of man as studied by electrical stimulation. *Brain*, 37, 398-443.
- Penfield, W., & Rasmussen, T. (1950). The cerebral cortex of man; a clinical study of localization of function. (p. 248). New York,: Macmillan.
- Perotto, A., & Delagi, E.F. (2005). Anatomical guide for the electromyographer : the limbs and trunk. (pp. xv, 345 p.). Springfield, IL: Charles C Thomas.
- Poliakov, A.V., & Schieber, M.H. (1999). Limited functional grouping of neurons in the motor cortex hand area during individuated finger movements: A cluster analysis. *Journal of Neurophysiology*, 82 (6), 3488-3505.
- Reiter, R. (1948). A New Electrohand. *Grenzgebiet der Medizin*, 1 (4), 133-135.
- Rousseeuw, P.J., & Vanzomeren, B.C. (1990a). Unmasking Multivariate Outliers and Leverage Points. *Journal of the American Statistical Association*, 85 (411), 633-639.
- Rousseeuw, P.J., & Vanzomeren, B.C. (1990b). Unmasking Multivariate Outliers and Leverage Points - Rejoinder. *Journal of the American Statistical Association*, 85 (411), 648-651.
- Saltiel, P., Wyler-Duda, K., D'Avella, A., Tresch, M.C., & Bizzi, E. (2001). Muscle synergies encoded within the spinal cord: Evidence from focal intraspinal NMDA iontophoresis in the frog. *Journal of Neurophysiology*, 85 (2), 605-619.
- Santello, M., Flanders, M., & Soechting, J.F. (1998). Postural hand synergies for tool use. *Journal of Neuroscience*, 18 (23), 10105-10115.
- Santello, M., Flanders, M., & Soechting, J.F. (2002). Patterns of hand motion during grasping and the influence of sensory guidance. *Journal of Neuroscience*, 22 (4), 1426-1435.
- Santello, M., & Soechting, J.F. (1998). Gradual molding of the hand to object contours. *Journal of Neurophysiology*, 79 (3), 1307-1320.
- Sato, K.C., & Tanji, J. (1989). Digit-Muscle Responses Evoked from Multiple Intracortical Foci in Monkey Precentral Motor Cortex. *Journal of Neurophysiology*, 62 (4), 959-970.
- Schieber, M.H. (1990). How Might the Motor Cortex Individuate Movements. *Trends in Neurosciences*, 13 (11), 440-445.

- Schieber, M.H. (1991). Individuated Finger Movements of Rhesus-Monkeys - a Means of Quantifying the Independence of the Digits. *Journal of Neurophysiology*, 65 (6), 1381-1391.
- Schieber, M.H. (1999). Somatotopic gradients in the distributed organization of the human primary motor cortex hand area: evidence from small infarcts. *Experimental Brain Research*, 128 (1-2), 139-148.
- Schieber, M.H. (2001). Constraints on somatotopic organization in the primary motor cortex. *Journal of Neurophysiology*, 86 (5), 2125-2143.
- Schieber, M.H., & Hibbard, L.S. (1993). How Somatotopic Is the Motor Cortex Hand Area. *Science*, 261 (5120), 489-492.
- Schieber, M.H., & Poliakov, A.V. (1998). Partial inactivation of the primary motor cortex hand area: Effects on individuated finger movements. *Journal of Neuroscience*, 18 (21), 9038-9054.
- Schieber, M.H., & Santello, M. (2004). Hand function: peripheral and central constraints on performance. *Journal of Applied Physiology*, 96 (6), 2293-2300.
- Sherrington, C.S. (1906). The integrative action of the nervous system. (pp. xvi, 411 p.). New York,: C. Scribner's sons.
- Shim, J.K., Latash, M.L., & Zatsiorsky, V.M. (2003). Prehension synergies: trial-to-trial variability and hierarchical organization of stable performance. *Experimental Brain Research*, 152 (2), 173-184.
- Smith, L. (2002). A Tutorial on Principal Component Analysis. (University of Otago, New Zealand.
- Soechting, J.F., & Flanders, M. (1997). Flexibility and repeatability of finger movements during typing: Analysis of multiple degrees of freedom. *Journal of Computational Neuroscience*, 4 (1), 29-46.
- Soechting, J.F., & Lacquaniti, F. (1989). An Assessment of the Existence of Muscle Synergies during Load Perturbations and Intentional Movements of the Human Arm. *Experimental Brain Research*, 74 (3), 535-548.
- Speeter, T.H. (1990). Control of the Utah-Mit Dexterous Hand - Hardware and Software Hierarchy. *Journal of Robotic Systems*, 7 (5), 759-790.
- Taylor, D., & Finley, F. (1971). Multiple-axis prosthesis control by muscle synergies. *Control of Upper Extremity Prostheses and Orthoses* (pp. 181 - 189). Göteborg, Sweden: Charles C Thomas.
- Ting, L.H., & Macpherson, J.M. (2005). A limited set of muscle synergies for force control during a postural task. *Journal of Neurophysiology*, 93 (1), 609-613.

- Todorov, E., & Ghahramani, Z. (2004). Analysis of the synergies underlying complex hand manipulation. 2 (pp. 4637-4640 Vol.4636).
- Todorov, E., & Jordan, M.I. (2002). Optimal feedback control as a theory of motor coordination. *Nature Neuroscience*, 5 (11), 1226-1235.
- Torres-Oviedo, G., Macpherson, J.M., & Ting, L.H. (2006). Muscle Synergy Organization Is Robust Across a Variety of Postural Perturbations. *J Neurophysiol*, 96 (3), 1530-1546.
- Tresch, M.C., Cheung, V.C.K., & d'Avella, A. (2006). Matrix factorization algorithms for the identification of muscle synergies: evaluation on simulated and experimental data sets. *J Neurophysiol*, 00222.02005.
- Tresch, M.C., Saltiel, P., & Bizzi, E. (1999). The construction of movement by the spinal cord. *Nature Neuroscience*, 2 (2), 162-167.
- Tresch, M.C., Saltiel, P., d'Avella, A., & Bizzi, E. (2002). Coordination and localization in spinal motor systems. *Brain Research Reviews*, 40 (1-3), 66-79.
- Turk, M., & Pentland, A. (1991). Eigenfaces for Recognition. *Journal of Cognitive Neuroscience*, 3 (1), 71-86.
- Valero-Cuevas, F.J. (2000). Predictive modulation of muscle coordination pattern magnitude scales fingertip force magnitude over the voluntary range. *Journal of Neurophysiology*, 83 (3), 1469-1479.
- Valero-Cuevas, F.J. (2005). An integrative approach to the biomechanical function and neuromuscular control of the fingers. *Journal of Biomechanics*, 38 (4), 673-684.
- Valero-Cuevas, F.J., Zajac, F.E., & Bugar, C.G. (1998). Large index-fingertip forces are produced by subject-independent patterns of muscle excitation. *Journal of Biomechanics*, 31 (8), 693-703.
- Weir, R.F.f. (2003). *IEEE IEMBS* (Cancun, Mexico).
- Weir, R.F.f., Kuiken, T., & Ajiboye, A.B. (2004a). Implantable Myoelectric Sensors (IMES) for Upper-Extremity Prosthesis Control – Independence of Multiple Intra-Muscular EMGs. *XVth International Society of Electrophysiology and Kinesiology Conference* (Boston, MA).
- Weir, R.F.f., Kuiken, T., & Ajiboye, A.B. (2004b). Independence of Multiple Intra-Muscular EMGs for Implantable Myoelectric Sensors. *11th World Congress of the International Society for Prosthetics & Orthotics* (Hong Kong, China).
- Weiss, E.J., & Flanders, M. (2004). Muscular and postural synergies of the human hand. *Journal of Neurophysiology*, 92 (1), 523-535.

Wiesendanger, M. (1999). Manual dexterity and the making of tools - an introduction from an evolutionary perspective. *Experimental Brain Research*, 128 (1-2), 1-5.

Woolsey, C.N., Erickson, T.C., & Gilson, W.E. (1979). Localization in Somatic Sensory and Motor Areas of Human Cerebral-Cortex as Determined by Direct Recording of Evoked-Potentials and Electrical-Stimulation. *Journal of Neurosurgery*, 51 (4), 476-506.

Woolsey, C.N., Settlage, P.H., Meyer, D.R., Sencer, W., Hamuy, T.P., & Travis, A.M. (1952). Patterns of localization in precentral and "supplementary" motor areas and their relation to the concept of a premotor area. *Research publications - Association for Research in Nervous and Mental Disease*, 30 (30), 238-264.

Zajac, F.E. (1989). Muscle and Tendon - Properties, Models, Scaling, and Application to Biomechanics and Motor Control. *Critical Reviews in Biomedical Engineering*, 17 (4), 359-411.

Zatsiorsky, V.M., & Latash, M.L. (2004). Prehension synergies. *Exercise and Sport Sciences Reviews*, 32 (2), 75-80.

Appendix A: Muscle Synergy Scalability in Palmar and Tip Hand Grasps

The results of the investigation of muscle synergy activation relative to sub-maximal grasp forces in the palmar and tip hand grasps are reported in this section. The results for these hand postures are reported separate from the cylindrical and lateral grasps (reported in *Chapter 5: Muscle Synergies Exhibit Scalability with Increasing Grasp Force*) because unlike the cylindrical and lateral grasps, the palmar and tip grasp force-tracking tasks allowed for potentially significant extraneous movements of the uninvolved digits. In retrospect, these digits should have been casted in place during the experimental protocol. Not doing so has the potential of confounding the results of the study because the forces produced would be far from isometric, and the changing positions of the uninvolved digits could affect the activity of the involved digits. Nevertheless, the results for the palmar and tip grasps are presented here as a continuation of Chapter 5 for the sake of completeness.

Results

Effect of Fine-Wire Electrodes on Maximal Voluntary Grasp (MVG) Strength

Average MVG values [pre-insertion, post-insertion] in Newtons (mean \pm SD) for palmar were [104.1 \pm 28.1, 87.0 \pm 17.1], and for tip were [60.7 \pm 18.9, 44.6 \pm 10.1]. Significance of the fine-wire effect was observed ($p < 0.05$) for both the palmar ($p = 0.077$) and tip ($p = 0.008$) grasps.

Correlation of CP Vector Magnitude to Grasp Force

The linear regression of grasp force versus coordination pattern (CP) vector magnitude resulted in average (mean \pm SD) Pearson correlation coefficient (r) values for the cylindrical and lateral grasps of 0.91 ± 0.05 and 0.74 ± 0.15 respectively. The corresponding adjusted r^2 values were 0.82 ± 0.08 and 0.57 ± 0.22 , respectively. Both correlation values were found to be statistically significantly different from zero ($p < 0.05$). Hence as expected, grasp force was significantly linearly correlated with the magnitude of the muscle coordination pattern vector associated with both grasps, although to a lesser extent in the tip grasp.

Variance of CP Vector Direction wrt Grasp Force

The null hypotheses tested were that for each of the hand postures, the force vectors representing each muscle coordination pattern were scaled versions of a single characteristic vector and hence did not statistically differ with respect to direction i.e. the vectors lay in a one-dimensional subspace. The Wilks's Lambda (Λ) and p-values of significance are reported for each grasp. Analysis of the palmar grasp resulted in $\Lambda = 0.284$ and $p = 0.011$. Analysis of the tip grasp resulted in $\Lambda = 0.283$ and $p = 0.011$. Hence, for both precision grasps, the vector representations of the muscle coordination patterns at the varying force levels were statistically different with respect to direction, thereby implying that across the subject population, statistically different muscle coordination strategies were used with respect to precision grasp force level.

The RM-MANOVA was followed up with a univariate repeated measure ANOVA (URM-ANOVA) for each muscle to determine which muscle(s) caused the significant differences observed in the directions of the muscle coordination vectors of palmar and tip grasping. For the palmar grasp, the activity of FPL ($p = 0.001$) was significantly different between the grasp

force levels, and that of EPL ($p = 0.051$) was borderline significant. For the tip grasp, only the activity of FPL ($p = 0.011$) was statistically different between grasp force levels.

Activations of Muscle Synergies wrt to Grasp Force

The activation levels for each estimated synergy relative to palmar and tip grasp forces are plotted in Figure A.1 for a representative subject. Shown with each plot is the amount of variance explained by the particular synergy-activation level combination for the palmar and tip grasps. A linear regression revealed the extent to which the activation levels of the synergies were correlated with grasp force, along with p-values assessing the significance of the regression slope.

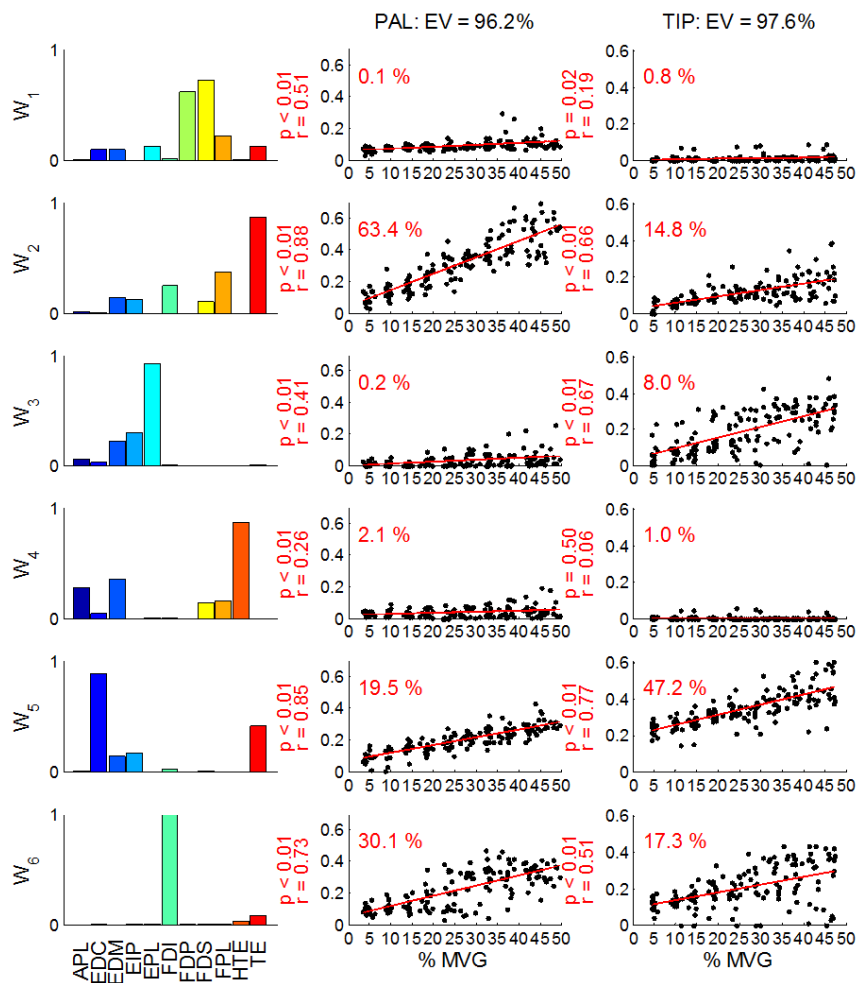


Figure A.1. Synergy structures and activation levels for a representative subject.

Bar plots in column one show the structure of the synergies extracted from the ASL posture miming and force-tracking tasks. Scatter plots in columns two and three show the activation level of each synergy relative to palmar and tip grasping forces, respectively. The amount of explained variance (EV) of each synergy-activation level combination is shown on each graph. A linear regression of activation level versus grasp force revealed the significance of the relationship between the two. Associated correlation (r) and significance (p) values are shown to the left of each plot. In the palmar grasp, the first three synergies (i.e. most variance explained) were typically highly correlated, while only the first four synergies were highly correlated with tip grasp force. As the amount of variance explained by successive synergies decreased, the correlation between activation level and grasp force generally decreased as well.

For this representative subject, the top three synergies were moderately to highly significantly correlated with palmar grasp force, while the top four synergies were moderately to highly significantly correlated with lateral grasp force. Figure A.2 reports the average variance explained across the subject population for the first four synergies of each subject. Figure A.3 shows the population averaged correlations between these ordered synergies with palmar and tip grasp forces. Across the subject population, the correlation of each synergy's activation with grasp force seemed to decrease with decreasing importance of the synergy to the task (i.e. decreased explained variance).

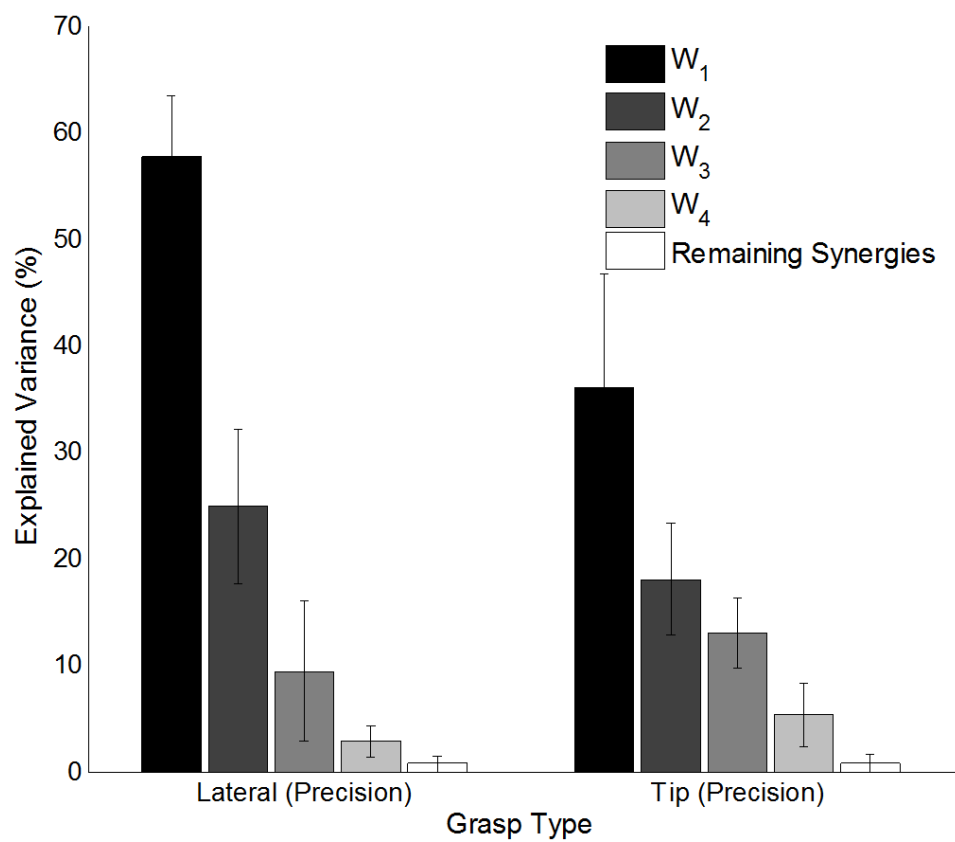


Figure A.2. Population averaged explained variances of synergies for ASL and force-tracking.

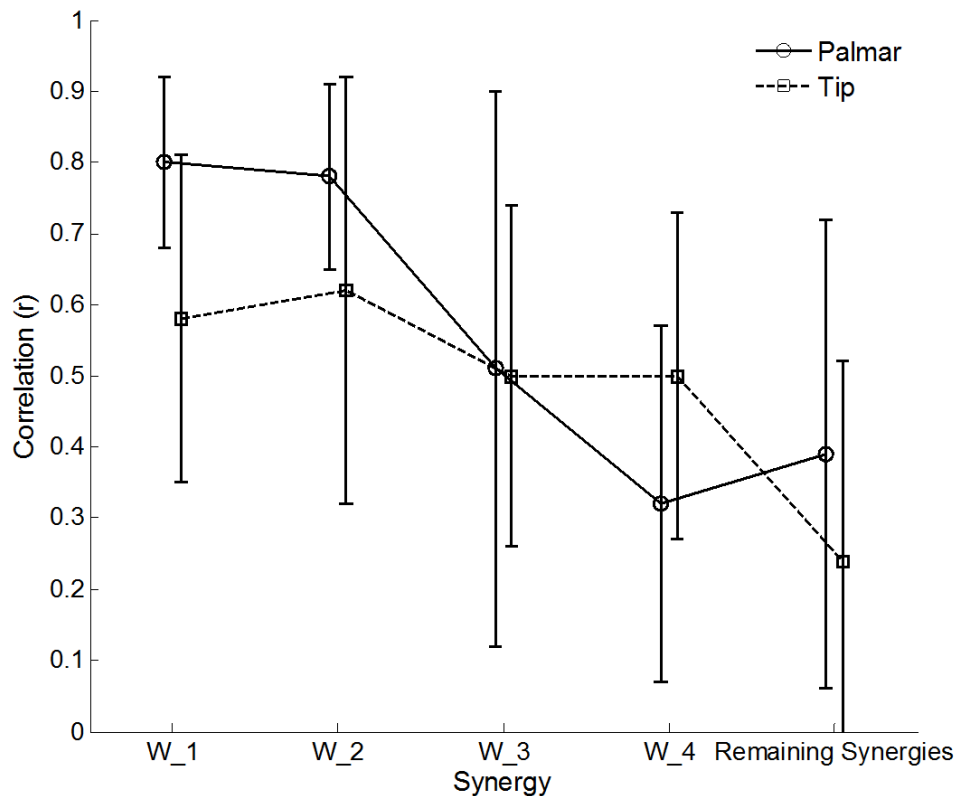


Figure A.3. Correlation of synergy activation to exerted grasp force.

Shown are the correlation values for the activation levels of synergies W_1 to W_4 , and the remaining synergies. Synergies are numbered in order of most explained variance of the force-tracking task using palmar and tip grasp types. As the percentage of variance explained decreases (Figure A.2), the correlation of activation level also generally decreases. On average, the activation levels of the first two synergies are moderately to highly correlated with grasp force in both the palmar and tip grasps, although moreso in the palmar grasp.

Discussion

The synergies whose activation levels were best correlated with force in each grasp consisted of muscles that would be expected to be relevant to the specified grasp type. For example, for the representative subject's synergies illustrated in Figure A.2, the synergies whose activation

levels were most correlated with palmar grasp force consisted of the intrinsic thumb muscle (TE), the index finger abductor (FDI), and the finger extensors (EDC). The tip grasp included these synergies, in addition to one that primarily controlled for thumb extension (EPL), possibly for stabilization. As with the palmar grasp pattern, the two most important synergies scaled fairly well with grasp force, while the remainder did not. For the tip grasp, even the first two synergies were only moderately correlated with grasp force. This lack of high correlation in the synergy space is consistent with the results of the statistical tests in the muscle space, namely that the vector direction of the coordination pattern seemed to change with changes in the required grasp force.

Abidemi Bolu Ajiboye

a-ajiboye@northwestern.edu

EDUCATION

Northwestern University, Evanston, IL

Department of Biomedical Engineering, The Graduate School

Doctor of Philosophy (PhD), Biomedical Engineering – December 2007

Advisor: Richard F. ff. Weir, PhD

Committee: Richard F. ff. Weir, PhD (chair); Lee E. Miller, PhD; Ferdinando (Sandro) Mussa-Ivaldi, PhD; Eric J. Perreault, PhD; Matthew C. Tresch, PhD

GPA: 4.0 on 4.0 scale

Research Focus: Investigation of the central motor control system and its construction of muscle activation patterns in the control of complex movements of the intact hand; Manifestations of this behavior in the electromyographic signal for application to control of myoelectric devices, and specifically wrist and hand prehensors.

Partial Skill Set: Intramuscular (fine-wire) and surface electromyography (EMG), biomedical signal analysis, computational EMG analysis, fuzzy system analysis (data clustering, system generation), digital motion capture and analysis, SIMM (Software for Interactive Musculoskeletal Modeling), MATLAB, LabVIEW, SPSS

Master of Science (MS), Biomedical Engineering – June 2003

Thesis: Investigation of Fuzzy Logic as a Classification Algorithm of EMG for the Control of Multifunctional Myoelectric Prostheses

Advisors: Dudley S. Childress, PhD; Richard F. ff. Weir, PhD

Committee: Dudley S. Childress, PhD (chair); Richard F. ff. Weir, PhD; Joseph T. Walsh, Jr., PhD; Alan V. Sahakian, PhD

GPA: 4.0 on 4.0 scale

Research Focus: Issues involved in the control of myoelectric upper limb prostheses; Investigation of novel intelligent control algorithms, specifically fuzzy logic based pattern recognition and control, to create clinically viable and practical multifunctional hand prostheses

Course Work: Control of Human Limbs and their Artificial Replacements, Biomechanics of Movement, Digital Signal Processing, Geometry of Robotics

Duke University, Durham, NC

Bachelor of Science in Engineering (BSE) – May 2000

Majors: Biomedical and Electrical Engineering

Minor: Computer Science

Designs / Courses: Design of Pitch-Based System for Wheelchair Control for Quadriplegic Individuals, Medical Instrumentation and Design, Linear Control Systems Theory, Computer Organization and Programming, Software Design and Implementation, Numerical Methods and Analysis

PEER – REVIEWED PUBLICATIONS

Ajiboye AB, Weir RF (2007). "Muscle Synergies Form a Generalizable Predictive Framework for Control of Hand Functions". *In preparation*.

Ajiboye AB, Weir RF (2007). "Muscle Synergies in the Scaling of Hand Grasp Forces". *In preparation*.

Ajiboye AB, Weir RF (2005). "A Heuristic Fuzzy Logic Approach to EMG Pattern Recognition for Multifunctional Prosthesis Control". *IEEE Transactions on Neural Systems and Rehabilitation Engineering*, 13(3), 280 – 291.

Ajiboye AB, Weir RF (2005). "Fuzzy C-Means Clustering Analysis of the EMG Patterns of Six Major Hand Grasps". *Proceedings of the IEEE 9th International Conference on Rehabilitation Robotics: Frontiers of the Human-Machine Interface*, Chicago, IL, June 28 - July 1, 2005.

Ajiboye AB, Weir RF, Heckathorne CW, and Childress DS (2002). "Neuro-Fuzzy Logic as a Control Algorithm for an Externally Powered Multifunctional Hand Prosthesis". *Proceedings of the Myoelectric Control Conference (MEC 2002)*, University of New Brunswick, Fredericton, New Brunswick, Canada, August 19-23, 2002.

ABSTRACTS

Ajiboye AB, Weir RF (2006). "Shared and specific muscle synergies in the control of hand postures at varying force levels". *Proceedings of the 2006 Meeting of the Society for Neuroscience*, Atlanta, GA, October 14 – October 18, 2006.

Ajiboye AB, Weir RF (2006). "Shared and specific muscle synergies in the control of hand postures at varying force levels". *Proceedings of the 2006 Biomedical Engineering Society Meeting*, Chicago, IL, October 11 – October 14, 2006.

Ajiboye AB, Weir RF (2006). "Analysis of Shared and Specific Neuromuscular Synergies of Hand Grasp Patterns at Varying Force Levels using Non-negative Matrix Factorization". *Proceedings of the 16th Annual Neural Control of Movement Conference*, Key Biscayne, FL, May 02 - May 07, 2006.

Ajiboye AB, Weir RF (2005). "Two Paradigms for EMG Pattern Recognition for Multifunctional Prosthesis Control: Fuzzy Heuristic Model and Muscle Synergy Component Model". *National Center for Medical Rehabilitation Research (NCMRR) Training and Career Development Workshop*, Rockville, MD, December 4 - December 6, 2005.

Ajiboye AB, Weir RF (2005). "Principal Component (PC) and Fuzzy C-Means (FCM) Cluster Analyses of the EMG of Six Major Grasp Patterns". *Proceedings of the 15th Annual Neural Control of Movement Conference*, Key Biscayne, FL, April 12 - April 17, 2005.

Ajiboye AB, Weir RF, and Heckathorne CW (2004). "EMG Pattern Classification for Controlling Below Elbow Myoelectric Hand Prostheses". *Proceedings of the 11th World Congress of the International Society for Prosthetics & Orthotics (ISPO)*, Hong Kong, Aug 1-6, 2004.

Weir RF, Kuiken T, and **Ajiboye AB** (2004). "Independence of Multiple Intra-Muscular EMGs for Implantable Myoelectric Sensors". *Proceedings of the 11th World Congress of the International Society for Prosthetics & Orthotics (ISPO)*, Hong Kong, Aug 1-6, 2004.

Ajiboye AB and Weir RF (2004). "EMG Pattern Classification for Controlling Below Elbow Myoelectric Hand Prostheses". *Proceedings of the 25th Congress of the International Society of Electrophysiology & Kinesiology (ISEK)*, Boston, MA, Jun 18-21, 2004.

Weir RF, Kuiken T, and **Ajiboye AB** (2004). "Implantable Myoelectric Sensors (IMES) for Upper-Extremity Prosthesis Control – Independence of Multiple Intra-Muscular EMGs". *Proceedings of the 25th Congress of the International Society of Electrophysiology & Kinesiology (ISEK)*, Boston, MA, Jun 18-21, 2004.

Weir RF ff. and **Ajiboye AB** (2003). "A Multifunction Prosthesis Controller based on Fuzzy-Logic Techniques". *Proceedings of the 25th Silver Anniversary International Conference of the IEEE Engineering in Medicine and Biology Society (EMBS)*, Cancun, Mexico, September 17-21, 2003.

INVITED TALKS

"Fuzzy C-Means Clustering Analysis of the EMG Patterns of Six Major Hand Grasps". *IEEE 9th International Conference on Rehabilitation Robotics: Frontiers of the Human-Machine Interface*, Chicago, IL, June 28 - July 1, 2005.

"Implantable Myoelectric Sensors (IMES) for Upper-Extremity Prosthesis Control – Independence of Multiple Intra-Muscular EMGs". *25th Congress of the International Society of Electrophysiology & Kinesiology (ISEK)*, Boston, MA, Jun 18-21, 2004.

"Neuro-Fuzzy Logic as a Control Algorithm for an Externally Powered Multifunctional Hand Prosthesis". *Myoelectric Control Conference (MEC 2002)*, University of New Brunswick, Fredericton, New Brunswick, Canada, August 19-23, 2002.

POSTER PRESENTATIONS

"Shared and specific muscle synergies in the control of hand postures at varying force levels". *2006 Meeting of the Society for Neuroscience*, Atlanta, GA, October 14 – October 18, 2006.

"Shared and specific muscle synergies in the control of hand postures at varying force levels". *2006 Biomedical Engineering Society Meeting*, Chicago, IL, October 11 – October 14, 2006.

"Analysis of Shared and Specific Neuromuscular Synergies of Hand Grasp Patterns at Varying Force Levels using Non-negative Matrix Factorization". *16th Annual Neural Control of Movement Conference*, Key Biscayne, FL, May 02 - May 07, 2006.

"Two Paradigms for EMG Pattern Recognition for Multifunctional Prosthesis Control: Fuzzy Heuristic Model and Muscle Synergy Component Model". *National Center for Medical Rehabilitation Research (NCMRR) Training and Career Development Workshop*, Rockville, MD, December 4 - December 6, 2005.

"Principal Component (PC) and Fuzzy C-Means (FCM) Cluster Analyses of the EMG of Six Major Grasp Patterns". *15th Annual Neural Control of Movement Conference*, Key Biscayne, FL, April 12 - April 17, 2005.

"EMG Pattern Classification for Controlling Below Elbow Myoelectric Hand Prostheses". *25th Congress of the International Society of Electrophysiology & Kinesiology (ISEK)*, Boston, MA, Jun 18-21, 2004.

"EMG Pattern Recognition using Fuzzy Logic for the Control of Multifunctional Myoelectric Prostheses". *Rehabilitation Engineering & Assistive Technology Society of North America (RESNA) 26th International Conference – Technology and Disability: Research, Design, Practice, and Policy*. Atlanta, GA, June 19-23, 2003.

FELLOWSHIPS AND HONORS

National Institute of Health (NIH)	2005 – 2008
National Research Service Award (NRSA) Pre-Doctoral Fellowship (F31):	1F31HD49319
Northwestern University	2002 – 2005
Graduate Research Assistant Tuition Scholarship	
Northwestern University	2001 – 2002
Walter P. Murphy Fellowship for Graduate Research	
Duke University	1999 – 2000
Helga and Erya W. Kehaya Scholarship	

TEACHING EXPERIENCE

Teaching Fellow, Northwestern University EXCEL / MEOP Summer Program (July 2003 – July 2007). Independently created and instructed four-week summer courses for engineering students taking Integral Calculus; **Selected as Most Outstanding Teaching Fellow in 2004** (Evanston, IL)

Teaching Assistant, Biomedical Signals and Imaging (January 2001 – March 2001), Northwestern University Department of Biomedical Engineering (Evanston, IL)

Grader, Analysis and Simulation of Biological Systems (April 2001 – June 2001, April 2002 – June 2002), Northwestern University Department of Biomedical Engineering (Evanston, IL)

MEMBERSHIPS

Society for Neuroscience	2006 – Present
Neural Control of Movement Society	2005 – Present

WORK EXPERIENCE

Procter and Gamble, Hunt Valley, MD

Managed team of vendors and technicians to develop mechanical device for a manufacturing line in operation. Ultimately designed and integrated device myself. Managed separate team of technicians in streamlining manufacturing processes to immediately increase business production. Analyzed and critiqued design specifications, and developed plan to integrate new HVAC (Heating Ventilation Air Conditioning) system. *Internship, May 1999 – August 1999.*

International Business Machines (IBM), Research Triangle Park, NC

Developed application to increase Internet security using Secure Sockets Layer (SSL) Protocol v.2 and v.3. Included learning and developing several algorithms for server and client-side certificate authentication in both Internet Explorer 4.x and Netscape Communicator 4.x. Performed defect fixes on SSL Protocol v.2 and v.3. Languages used include C, C++, Java, JavaScript, and HTML. *Internship, May 1998 – November 1998.*

Analyzed and critiqued C++ code to remedy defects in new release of Personal Communications 4.2™ by IBM, an emulator for personal computers. *Internship, Summer 1997.*

Duke University Trinity Computing, Durham, NC

Performed software and hardware support and maintenance for various departments of Duke University. Installed hardware and software, initialized network PC's for personal and network usage, and oversaw associated troubleshooting. *Work Study, October 1997 – April 1998.*

Duke University Medical Center, Durham, NC

Analyzed patient DNA for blood clotting protein. Involved processes such as gel electrophoresis, polymerase chain reactions, and DNA purification. *Comprehensive Cancer Research Center Program, Summer 1996 – January 1997.*

Cisco Systems, Inc., Research Triangle Park, NC

Learned network protocols (i.e. TCP/IP) and routers; developed networks and web sites. *Internship, September 1995 - May 1996.*

North Carolina State University Food Science Dept., Raleigh, NC

Developed procedure to remove phospholipid proteins from dairy products for the lactose intolerant public. *Minority Research Apprenticeship Program, Summer 1995.*